

---

# Development of functionalized reconstituted HDL as a novel anti-atherosclerotic tool

---

Shifa Jebari Benslaiman

Doctoral Thesis 2022



## Doctoral Thesis

*Development of functionalized reconstituted HDL  
as a novel anti-atherosclerotic tool.*

Shifa Jebari Benslaiman

Supervisor:

Prof. César Martín Plágaro

Leioa, 2022

**TESI ZUZENDARIAREN  
BAIMENA TESIA AURKEZTEKO**

**AUTORIZACIÓN DEL/LA  
DIRECTORA/A DE TESIS PARA  
SU PRESENTACIÓN**

Zuzendariaren izen-abizenak /Nombre y apellidos del/la director/a: César Martín Plágaro

IFZ /NIF: 14608590W

Tesiaren izenburua / Título de la tesis: Development of functionalized reconstituted HDL as a novel anti-atherosclerotic tool

Doktorego programa / Programa de doctorado: Biomedicina y Biología Molecular

Doktoregaiaren izen-abizenak / Nombre y apellidos del/la doctorando/a:  
**Shifa Jebari Benslaiman**

Unibertsitateak horretarako jartzen duen tresnak emandako ANTZEKOTASUN TXOSTENA ikusita, baimena ematen dut goian aipatzen den tesiak aurkez dadin, horretarako baldintza guztiak betetzen baititu.

Visto el INFORME DE SIMILITUD obtenido de la herramienta que a tal efecto pone a disposición la universidad, autorizo la presentación de la tesis doctoral arriba indicada, dado que reúne las condiciones necesarias para su defensa.

Tokia eta data / Lugar y fecha: Leioa 19 de Enero de 2022



Sin. / Fdo.: Tesiaren zuzendaria / El/La director/a de la tesis

César Martín Plágaro

## **AUTORIZACIÓN DE LA COMISIÓN ACADÉMICA DEL PROGRAMA DE DOCTORADO**

La Comisión Académica del Programa de Doctorado en Biología Molecular y Biomedicina en reunión celebrada el día 20 de enero de 2022, ha acordado dar la conformidad a la presentación de la Tesis Doctoral titulada: Development of functionalized reconstituted HDL as a novel anti-atherosclerotic tool dirigida por el Dr Cesar Martín Plagaro y presentada por Dña. Shifa Jebari Benslaiman adscrita al Departamento de Bioquímica y Biología Molecular

En Leioa, a 21 de enero de 2022

LA RESPONSABLE DEL PROGRAMA DE DOCTORADO

Fdo.: Itziar Alcorta Calvo

## AUTORIZACIÓN DEL DEPARTAMENTO

## CONFORMIDAD DEL DEPARTAMENTO

El Consejo del Departamento de Bioquímica y Biología Molecular en reunión celebrada el día 13 de Enero de 2022 ha acordado dar la conformidad a la admisión a trámite de presentación de la Tesis Doctoral titulada:

**Development of functionalized reconstituted HDL as a novel anti-atherosclerotic tool**

dirigida por el Dr César Martín Plágaro y presentada por Doña Shifa Jebari Benslaiman

ante este Departamento.

En Leioa a 13 de Enero de 2022

VºBº DIRECTORA DEL DEPARTAMENTO

Fdo.: Miren Josu Omaetxebarria

SECRETARIO DEL DEPARTAMENTO



Fdo.: César Martín Plágaro

## **ACTA DE GRADO DE DOCTOR O DOCTORA**

## **ACTA DE DEFENSA DE TESIS DOCTORAL**

DOCTORANDA DOÑA Shifa Jebari Benslaiman

TITULO DE LA TESIS:

**Development of functionalized reconstituted HDL as a novel anti-atherosclerotic tool.**

El Tribunal designado por la Comisión de Postgrado de la UPV/EHU para calificar la Tesis Doctoral arriba indicada y reunido en el día de la fecha, una vez efectuada la defensa por el/la doctorando/a y contestadas las objeciones y/o sugerencias que se le han formulado, ha otorgado por \_\_\_\_\_ la calificación de:

*unanimidad ó mayoría*

*SOBRESALIENTE / NOTABLE / APROBADO / NO APTO*

Idioma/s de defensa (en caso de más de un idioma, especificar porcentaje defendido en cada idioma):

Castellano\_\_\_\_\_

Euskera\_\_\_\_\_

Otros Idiomas (especificar cuál/cuales y porcentaje)\_\_\_\_\_

En \_\_\_\_\_ a \_\_\_\_\_ de \_\_\_\_\_ de \_\_\_\_\_

EL/LA PRESIDENTE/A,

EL/LA SECRETARIO/A,

Fdo.: \_\_\_\_\_

Fdo.: \_\_\_\_\_

Dr/a: \_\_\_\_\_

Dr/a: \_\_\_\_\_

VOCAL

Fdo.: \_\_\_\_\_

Dr/a: \_\_\_\_\_

EL/LA DOCTORANDO/A,

Fdo.: \_\_\_\_\_



# TABLE OF CONTENTS

List of tables.....	vi
List of figures.....	vii
<b>1. INTRODUCTION/1. SARRERA.....</b>	<b>1</b>
1. Atherosclerosis .....	3
1.1. Endothelium.....	3
1.2. Atherosclerosis initiation and fatty streak formation .....	5
1.3. Fibrous plaque development .....	16
1.4. Plaque stability and rupture.....	20
2. HDL metabolism.....	23
2.1. HDL remodelling and reverse cholesterol transport. ....	23
2.2. HDLs constitute an heterogeneous lipoprotein group.....	28
2.3. ABCA1 is a lipid transporter .....	30
2.4. ApoA-I structure and lipid solubilisation .....	35
3. RNA interference pathway. MicroRNAs .....	37
3.1. MicroRNAs regulate gene expression .....	37
3.2. MicroRNA circulation by HDLs. ....	39
3.3. miR-33-a, a regulator of RCT .....	40
4. Reconstituted HDLs.....	43
4.1. rHDL as a theranostic tool .....	43
4.2. Clinical trials. Successes and limitations.....	45
<b>2. OBJECTIVES/ 2. HELBURUAK.....</b>	<b>48</b>
Hypothesis and objectives .....	49
Specific Objectives .....	50
<b>3. MATERIALS AND METHODS / 3. MATERIALAK ETA METODOAK.....</b>	<b>52</b>
1. Giza apoA-I proteinaren purifikazioa .....	53
1.1. Bakterio anduiak eta plasmidoa.....	53
1.2. Bakterio hazkuntza selektiboak .....	54

1.3.	Bakterio kimiokonpetenteen garapena .....	54
1.4.	ApoA-I plasmidoaren amplifikazioa eta purifikazioa .....	55
1.5.	Giza apoA-I proteina errekonbinantearen adierazpena eta purifikazioa .....	56
<b>2.</b>	<b>Giza apoA-I rHDL nanodikoen prestakuntza .....</b>	<b>58</b>
2.1.	Kolato hondarren neurketa metodo kalorimetrikoaz .....	62
2.2.	rHDL nanodiskoen purifikazioa .....	63
2.3.	rHDLen karakterizazio biofisikoa.....	64
2.4.	rHDL masa molekularraren azterketa masa-fotometria bidez. ....	70
2.5.	rHDLen markaketa fluoreszentea .....	71
<b>3.</b>	<b>rHDL bidezko miRNAen garraioaren azterketa .....</b>	<b>71</b>
3.1.	miRNA eta rHDL arteko lotura azterketa .....	71
<b>4.</b>	<b>Lipoproteinen purifikazioa .....</b>	<b>74</b>
4.1.	rHDL bidezko miRNAen transfekzioaren optimizazioa .....	75
<b>5.</b>	<b>Azetilatutako LDLak .....</b>	<b>76</b>
5.1.	Azetilazioaren egiaztapena .....	76
5.2.	azLDLen kontserbazioa .....	77
<b>6.</b>	<b>Zelula-hazkuntzak .....</b>	<b>77</b>
6.1.	Monogeruzan egindako esperimentuen zelula-hazkuntzak .....	77
6.2.	Ateroma modeloa eratzeko zelula-hazkuntzak .....	78
6.3.	Hiru lerro-zelularreko ateroma modelo bidimentsionalak .....	79
<b>7.</b>	<b>Zelula apartsuen garapena.....</b>	<b>83</b>
7.1.	Zelula apartsuen eraketaren kuantifikazioa .....	83
<b>8.</b>	<b>Kolesterol kanporaketaren azterketa .....</b>	<b>85</b>
8.1.	<i>Labeling</i> medioaren prestaketa .....	85
8.2.	Kolesterol kanporaketa monogeruza kultiboetan .....	86
<b>9.</b>	<b>Ateroma modeloaren erabilera kolesterol kanporaketaren azterketarako .....</b>	<b>88</b>
9.1.	rHDL bidezko miRNAen transfekzioaren optimizazioa .....	89
9.2.	AntagomiR-33-a-ren barneraketaren efektuaren azterketa .....	92
9.3.	rHDLen administrazio sekuentziala ateroma modeloa, kolesterol kanporaketa induzitzeko.....	97
<b>10.</b>	<b>Analisi estatistikoa .....</b>	<b>99</b>
<b>4.</b>	<b>RESULTS/ 4. EMAITZAK .....</b>	<b>101</b>

<b>Results 1. Development of rHDL: Experimental set up .....</b>	<b>103</b>
1. Human recombinant apoA-I purification .....	103
2. rHDL size and molecular weight determination.....	103
3. Binding of miRNA to rHDLs. ....	106
4. Protein and lipid molar ratio determination in rHDL .....	107
5. Determination of apoA-I number in rHDL by Crosslinking .....	108
6. rHDL conservation.....	109
<b>Results 2. Cholesterol efflux efficiency of reconstituted HDL is affected by nanoparticle lipid composition .....</b>	<b>112</b>
1. Development and Biophysical Characterization of rHDL .....	112
2. J774A.1 macrophages derived foam cells formation .....	116
3. Effect of rHDL Lipid Composition on Cholesterol Efflux In Vitro .....	120
<b>Results 3: Boosting cholesterol efflux from foam cells by sequential administration of rHDL to deliver microRNA and to remove cholesterol in a triple-cell two-dimensional atherosclerosis model.....</b>	<b>124</b>
1. Development and Biophysical Characterization of DPPC:CE:LPC and DPPC rHDL ....	124
2. Delivery of antagomiR-33a by DPPC:CE:LPC rHDL into foam cells in atheroma plaque model .....	126
3. Cholesterol efflux promoted in foam cells within the 2D atheroma model.....	132
<b>5. DISCUSSION /5. EZTABAIDA .....</b>	<b>138</b>
<b>6. CONCLUSIONS /6. ONDORIOAK.....</b>	<b>148</b>
<b>7. REFERENCES / 7. ERREFERENTZIAK.....</b>	<b>151</b>
<b>ANNEX I: Functional characterization of LDLR and PCSK9 variants ..</b>	<b>199</b>
<b>1. Familial Hypercholesterolemia (FH) .....</b>	<b>200</b>
1.1. Genetics of FH .....	200
1.2. LDLR.....	201
1.3 APOB.....	202
1.4. PCSK9.....	202
<b>2. Determining the Pathogenicity of LDLr Variants.....</b>	<b>205</b>
<b>3. Determining the Pathogenicity PCSK9 Variants.....</b>	<b>207</b>
<b>4. Materials and Methods.....</b>	<b>207</b>
4.1. LDLR variant selection .....	207

4.2. Construction of LDLR variants carrying plasmids .....	208
4.3. LDL isolation and labelling.....	208
4.4. Analysis of LDLR expression by FACS .....	209
4.5. Analysis of LDLR activity by FACS .....	209
4.6. Analysis of PCSK9-LDLR EC50 by Solid-Phase Immunoassay.....	210
<b>5. Results.....</b>	<b>210</b>
5.1. Characterization of LDLr variants .....	210
5.2. Characterization of PCSK9 variants .....	212
<b>REFERENCES .....</b>	<b>213</b>
<b>ANNEX II: An atlas of O-linked glycosylation on peptide hormones reveals diverse biological roles.....</b>	<b>216</b>
1. <b>Introduction.....</b>	<b>217</b>
2. <b>Methods .....</b>	<b>217</b>
3. <b>Results .....</b>	<b>217</b>
<b>REFERENCES .....</b>	<b>219</b>
<b>ANNEX III: Design and Validation of a Process Based on Cationic Niosomes for Gene Delivery into Novel Urine-Derived Mesenchymal Stem Cells .....</b>	<b>220</b>
4. <b>Introduction.....</b>	<b>221</b>
5. <b>Methods .....</b>	<b>221</b>
6. <b>Results .....</b>	<b>222</b>
<b>REFERENCES .....</b>	<b>224</b>
<b>ANNEX IV: Statin-induced type 2 diabetes mellitus by upregulation of mir-27b .....</b>	<b>225</b>
1. <b>Type 2 Diabetes Mellitus and liver .....</b>	<b>226</b>
2. <b>Statin Treatment-Induced Development of Type 2 Diabetes.....</b>	<b>228</b>
2.1. Primary Action of Statins: Cholesterol Biosynthetic Pathway .....	229

2.2.	MicroRNAs and Impact of Statin Therapy on microRNA Expression Profile	231
3.	<b>MiR-27b modulates insulin signaling in hepatocytes .....</b>	<b>232</b>
3.1.	MiR-27b Controls the Expression INSR and IRS1 Expression .....	234
4.	<b>Molecular mechanisms of lipotoxicity-induced pancreatic <math>\beta</math>-cell dysfunction .</b>	<b>235</b>
	<b>REFERENCES.....</b>	<b>236</b>

# List of tables

## 3. MATERIALS AND METHODS / 3. MATERIALAK ETA METODOAK |Error!

Marcador no definido.

<b>1. TAULA: BAKTERIOAK HAZTEKO MEDIO SELEKTIBOAK .....</b>	<b>55</b>
<b>2. TAULA. PRESTATURIKO APOA-IEN RHDL KONPOSIZIOAK .....</b>	<b>61</b>
<b>3. TAULA: RHDLAK PRESTATZEKO ERABILITAKO LIPIDO ZERRENDA.....</b>	<b>61</b>
<b>4.TAULA. LANDUTAKO MIRNAEN SEKUENTZIAK.....</b>	<b>89</b>
<b>5. TAULA: RHDL EI KONJUGATUAKO MIRNA KOMERTZIALAK.....</b>	<b>90</b>
<b>6.TAULA. MIRNAEN QRT-PCRAK BURUTZEKO HASLEEN ZERRENDA.....</b>	<b>93</b>
<b>7. TAULA. ZELULA APARTSUETAN QRT-PCRAK BURUTZEKO ERABILITAKO HASLEEN ZERRENDA.....</b>	<b>95</b>
<b>8. TAULA. WESTERN PLAPAKETAN ERABILITAKO ANTIGORPUTZ ZERRENDA.....</b>	<b>96</b>

## 4. RESULTS/ 4. EMAITZAK ..... |Error! Marcador no definido.

<b>TABLE 1. MOLECULAR SIZE STANDARDS USED FOR SUPERDEX 200 10/300 CALIBRATION ...</b>	<b>104</b>
<b>TABLE 2. A-HELICAL CONTENT OF APOA-I AND RHDL DETERMINED BY CD.....</b>	<b>113</b>
<b>TABLE 3. A-HELICAL CONTENT OF APOA-I AND RHDL DETERMINED BY CD.....</b>	<b>126</b>

# List of figures

<b>3. MATERIALS AND METHODS / 3. MATERIALAK ETA METODOAK</b> <small> Error!</small>	
Marcador no definido.	
<b>1. IRUDIA. APOA-I PURIFIKATZEKO PNFXEX BEKTOREA</b> .....	53
<b>2. IRUDIA: GIZA APOA-1EN PRODUKZIOAREN LABURPEN ESKEMATIKOA BAKTERIO SISTEMAN</b> .....	57
<b>3. IRUDIA: RHDL NANODISKOEN PRESTAKUNTZAREN ESKEMA</b> .....	60
<b>4. IRUDIA: DPH FLUOROFOROAREN KOKAPENAREN IRUDI ESKEMATIKOA RHDLEN BIGERUZA LIPIDIKOAN</b> .....	68
<b>5. IRUDIA. LDL ETA HDL PURIFIKAZIOA DENTSITATE ZENTRIFUGAZIO ISOPIKNIKO BIDEZ</b> .....	75
<b>6. IRUDIA: HIRU LERRO-ZELULARREKO ATEROMA MODELO BIDIMENTSIOANALAREN IRUDIA</b> .....	80
<b>7. IRUDIA: HIRU-LERRO ZELULARREKO ATEROMA MODELOAREN GARAPENAREN KRONOLOGIA</b> .....	81
<b>8. IRUDIA: HIRU-LERRO ZELULARREKO ATEROMA MODELOAREN GARAPENAREN LABURPEN BISUALA</b> .....	81
<b>9. IRUDIA. ERRESISTENTZIA ELEKTRIKO TRANSENDOTELIALAREN NEURKETA</b> .....	83
<b>10. IRUDIA. RHDL BIDEZKO MIRNAEN TRANSFEKZIOAREN AZTERKETAREN KRONOLOGIA, ATEROMA MODELOAN</b> .....	92
<b>11. IRUDIA. RHDL ADMINISTRAZIO SEKUENTZIALA ATEROMA MODELOAN ETA KOLESTEROL KANPORAKETAREN AZTERKETA</b> .....	98
<b>4. RESULTS/ 4. EMAITZAK</b> <small> Error!</small> Marcador no definido.	
<b>FIGURE 1. APOA-I PURIFICATION POLYACRYLAMIDE GEL</b> .....	103
<b>FIGURE 2. CALIBRATION CURVE OF SUPERDEX 200 10/300</b> .....	104
<b>FIGURE 3. DPPC RHDL SIZE MEASUREMENT BY MASS PHOTOMETRY</b> .....	106
<b>FIGURE 4. MICRORNA LOADING OF DPPC:CE:LPC RHDL</b> .....	107
<b>FIGURE 5. CROSSLINKED APOA-I OF RHDL SAMPLES.</b> .....	108
<b>FIGURE 6. RHDL STRUCTURAL ANALYSIS WHEN STORED AT 4 °C FOR A MONTH</b> .....	110

<b>FIGURE 7. MASS PHOTOMETER MEASUREMENT OF FROZEN RHDL SAMPLES.....</b>	111
<b>FIGURE 8. DEVELOPMENT AND BIOPHYSICAL CHARACTERIZATION OF RHDL .....</b>	114
<b>FIGURE 9. FLUORESCENCE ANISOTROPY OF DPH IN HDL, DPPC, DPPC:CHOL:LPC AND DPPC:CE:LPC RHDL AS A FUNCTION OF TEMPERATURE .....</b>	116
<b>FIGURE 10. AGAROSE GEL ELECTROPHORESIS OF ACETYLATED LDL .....</b>	117
<b>FIGURE 11. QUANTITATIVE AND QUALITATIVE ANALYSIS OF FOAM CELL FORMATION .....</b>	119
<b>FIGURE 12. EFFECT OF HDL, DPPC, DPPC:CHOL:LPC, DPPC:CE:LPC AND SOY-PC RHDL ON CHOLESTEROL EFFLUX.....</b>	120
<b>FIGURE 15. DEVELOPMENT AND BIOPHYSICAL CHARACTERIZATION OF RHDL .....</b>	125
<b>FIGURE 16. DPPC:CE:LPC RHDL ARE EFFICIENTLY DELIVERED INTO FOAM CELLS IN THE 2D ATHEROMA MODEL.....</b>	128
<b>FIGURE 17. MIRNA TRANSFER CAPACITY, MIR-33A DOWNREGULATION AND ABCA1/ABCG1 UPREGULATION BY MIRNA DELIVERY BY DPPC:CE:LPC RHDL TO FOAM CELLS .....</b>	131
<b>FIGURE 18. MIRNA TRANSFER CAPACITY BY DPPC:CE:LPC RHDL TO FOAM CELLS CULTURED IN MONOLAYER.....</b>	131
<b>FIGURE 19. CHOLESTEROL EFFLUX PROMOTED IN FOAM CELLS BY SEQUENTIAL RHDL ADMINISTRATION IN A TRIPLE CELL 2D ATHEROMA MODEL .....</b>	133
<b>FIGURE 20. COMBINATION OF TO901317 AND ANTAGOMIR-33A-RHDL CAUSED A SYNERGISTIC UPREGULATION OF ABCA1 AND ABCG1 PROTEIN LEVELS IN FOAM CELLS. ....</b>	135
<b>FIGURE 21. INTRACELLULAR CHOLESTEROL LEVELS IN FOAM CELLS AFTER TO901317 TREATMENT, ANTAGOMIR-33A-RHDL DELIVERY OR COMBINED TREATMENT OF TO901317 AND ANTAGOMIR-33A-RHDL IN 1D GROWN FOAM CELLS OR 2D ATHEROMA MODEL FOAM CELLS .....</b>	136
<b>FIGURE 22. CHOLESTEROL EFFLUX PROMOTED IN FOAM CELLS BY SEQUENTIAL RHDL ADMINISTRATION IN A TRIPLE CELL 2D ATHEROMA MODEL .....</b>	137



# 1. INTRODUCTION

## 1. SARRERA

**The results presented in this section have been published at:**

1. Pathophysiology of Atherosclerosis. **Jebari-Benslaiman S**, Galicia-Garcia U, Larrea-Sebal A, Alloza I, Vandenbroucke K, Martín C and Benito-Vicente A. International Journal of Molecular Sciences (*second revision*).

## 1. Atherosclerosis

### 1.1. Endothelium

In a healthy state, the vessel wall is lined with a single endothelial cell (EC) layer called endothelium. This layer together with collagen and elastic fibbers forms the luminal layer of the vessels or the intima. ECs are in intimate contact with tunica media consisting of vascular smooth muscle cells (VSMC) and elastic and collagenous tissue. Finally, surrounding this layer is tunica adventitia, which is composed mainly by a dense matrix of connective tissue. Endothelium is strategically located between circulating blood and tissues, working as a sensor and transductor of signals by the production of biologically active substances. It modulates the tone of underlying vascular smooth muscle, maintains a non-adhesive luminal surface, and mediates hemostasis, cellular proliferation, and inflammatory and immune response in the vascular wall<sup>1</sup>. In fact, endothelium releases both agonists and antagonists in order to balance the effect in both directions. For instance, ECs are able to produce both coagulants or anti-coagulants, vasodilators or vasoconstrictors and pro-inflammatory or anti-inflammatory molecules.<sup>1,2</sup> Thus, the endothelium plays an important role regulating vascular homeostasis under physiological conditions<sup>3</sup> but, if compromised, it can also contribute significantly to the pathophysiology of several cardiovascular diseases<sup>1</sup>.

As endothelium lines the arterial vasculature, it is directly affected by the hydrodynamic forces of blood flow: wall shear stress, hydrostatic pressure and cyclic strains<sup>4,5</sup>. Indeed, it is accepted that hydrodynamic forces modulate the endothelium biology<sup>5</sup>. For example, shear stress induces a characteristic endothelial cell alignment<sup>6–9</sup> (**Figure 1**). In tubular or straight regions of arteries, where the blood flow and therefore, shear stress is increased, endothelial cells show a flattened shape and an elongated alignment in the direction of the flow<sup>4</sup>. In

addition, the nucleus of ECs are oriented to the lumen of the blood vessel as a response to hemodynamic shear stress<sup>10,11</sup>. However, when blood flow and therefore, shear stress decreases, ECs augment their volume showing a cobblestone appearance<sup>12</sup>. Moreover, hemodynamic forces determine the early development of localized atherosclerotic plaques that are not randomly distributed, neither in experimental animal models nor in humans<sup>5,13</sup>. Straight areas of the vasculature, where the blood flow is laminar (a lineal and uniform movement), are fairly protected from atherogenesis, at least at the early stages of disease<sup>14,15</sup>. However, in branched areas of the vessels (bifurcations or arches), this rectilinear flow is disrupted and changes to a turbulent flow during the cardiac cycle<sup>4</sup> (**Figure 1**). These recircularization regions, where shear stress is lower, are more susceptible to atheroma plaque formation<sup>5</sup> emphasizing the importance of arterial branches to make a diagnosis.

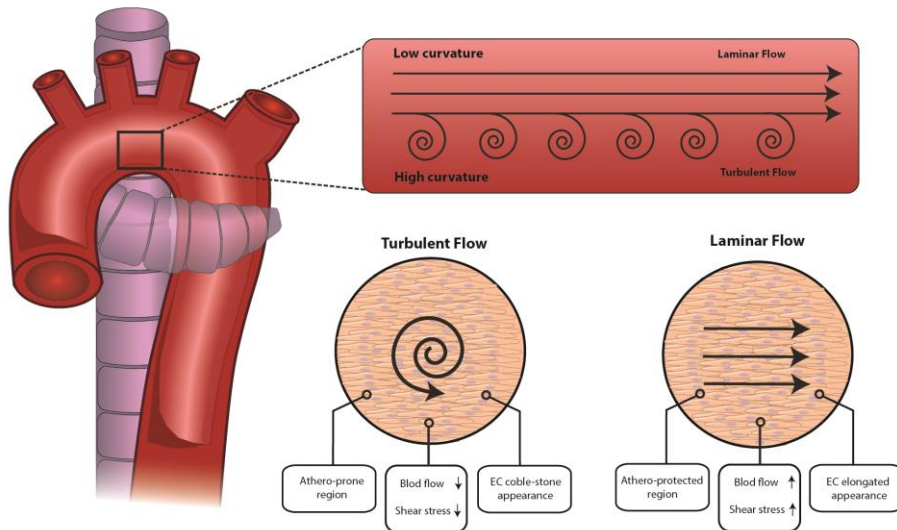


**Figure 1:** Effect of blood flow on atherosclerosis development. Turbulent flow occurs at bifurcations and branch points where the arterial curvature is higher. Disturbed laminar flow or turbulent flow reduces shear stress and promotes endothelial dysfunction and LDL infiltration that constitute the first step for atheroma plaque formation. On the contrary, low curvature areas of the vascular system subjected to higher shear stress are athero-protected.

## 1.2. Atherosclerosis initiation and fatty streak formation

Atherosclerosis initiates upon endothelial dysfunction accompanied by low density lipoprotein (LDL) retention and its modification in the intima<sup>16</sup>. Modified LDLs together with additional atherogenic factors promote the activation of endothelial cells that leads to monocyte recruitment within the intima. Modified LDLs are avidly captured by differentiated monocytes and VSMC, which promotes foam cell formation<sup>17,18</sup>. In addition, several inflammatory signalling pathways are activated allowing fatty streak formation. Fatty streak is the first sign of atherosclerosis, which is visible to the naked eye and is characterized by a huge accumulation of lipids both within the cells (macrophages and VSMC) and the extracellular media<sup>19</sup>.

### 1.2.1. *Endothelial dysfunction in atherosclerosis development*

Endothelial dysfunction can be described as a disruption of the mechanisms involved in vascular homeostasis regulation<sup>20,12,9</sup>. Briefly, when endothelial cells lose their ability of maintaining homeostasis, vessel walls are predisposed to vasoconstriction, lipid infiltration, leukocyte adhesion, platelet activation and oxidative stress, among others<sup>21,22</sup>. All together induce an inflammatory response that is considered the first step of atheromatous plaque formation: the fatty streak<sup>12</sup>. In addition, endothelial dysfunction also plays a remarkable role in subsequent steps of atherosclerosis by participating in plaque development and in its rupture in the last steps of atherosclerosis<sup>23</sup>. Therefore, an increased endothelial dysfunction is considered an early indicator of atherogenesis<sup>3</sup>.

#### 1.2.1.1. Hemodynamic forces and endothelial dysfunction

Hemodynamic forces constitute a local risk factor of atherogenesis as they promote endothelial dysfunction<sup>24</sup>. As indicated above, lesion prone regions are mainly located in areas where the laminar flow is disturbed due to flow separation, recircularization or reattachment<sup>25</sup>. This turbulent flow creates temporal and spatial gradients, which result in a higher oscillatory index and a lower shear stress<sup>4,15</sup>. In addition, a disturbed flow also favours lipoprotein infiltration into the vessel intima, firstly because LDLs remain longer periods of time in those areas; and secondly, because turbulent flow induces physical disruption of endothelial integrity<sup>26</sup>, which facilitates lipoprotein infiltration<sup>26,27</sup>. In addition, another fundamental link between hemodynamic forces and atherogenesis relies on the expression of diverse endothelial genes regulated by blood mechanical stimulus<sup>29–33</sup>.

The effect of shear stress over endothelial gene expression has been studied during the last 20 years and since that, more than 40 genes implicated in the process have been discovered so far<sup>34–39</sup>. Among them, the activation in endothelial cells of several atherogenic genes such as monocyte chemoattractant protein 1 (MCP-1) that induces monocyte permeation into the arterial wall<sup>40–42</sup> and platelet-derived growth factors (PDGF) that enhances VSMC migration<sup>43–45</sup>. Interestingly, research evidence revealed shear stress response elements (SSRE) in the promoters of these genes and others, such as eNOS or platelet adhesion molecule-1 (PECAM-1) that contribute to plaque development<sup>46–49</sup>. Moreover, the combination of two or more SSRE in the same promoter could have a synergistic effect that enhances the expression of those genes<sup>50</sup>. On the other hand, in straight regions of the vasculature, blood shows a laminar flow, which drives high shear stress in the endothelium, thus downregulating atherogenic genes and upregulating antioxidant and cell cycle growth-arrest genes. Indeed, it has been demonstrated that long exposure of endothelial cells to undisturbed laminar flow

promotes the upregulation of endothelial nitric oxide synthases (eNOS), thus increasing their nitric oxide (NO) synthesis capacity<sup>46,51</sup>.

These findings suggest a differential molecular response in endothelium depending on the blood flow pattern, highlighting the role of hemodynamic forces in endothelial dysfunction. In conclusion, branched areas and curvatures are the preferential location for atherosclerotic lesions development<sup>52</sup>.

#### 1.2.1.2. Role of nitric oxide in endothelial dysfunction

Endothelial dysfunction is also explained through a reduction in NO bioavailability<sup>23</sup>. NO is synthesized from L-arginine in endothelial cells in a reaction catalysed by eNOS and diffuses across cell membranes, reaching the smooth muscle tissue of the artery wall. NO promotes smooth muscle fiber relaxation, known as endothelium-dependent vasodilatation<sup>53,54</sup>. NO is considered an athero-protective molecule because it counteracts atherogenesis and its complications. Specifically, NO is involved in reduction of platelet aggregation, tissue oxidation and inflammation, activation of thrombogenic factors, cell growth, proliferation and migration, among others<sup>55–57</sup>. Moreover, it maintains metabolic homeostasis as it reduces triglyceride content and steatosis and increases insulin synthesise, glucose clearance and mitochondrial efficiency<sup>58</sup>. However, in the presence of cardiovascular risk, factors such as hyperlipidemia, hypertension, smoking or diabetes, NO production is reduced as a consequence of an increased oxidative stress, which is commonly associated to those pathologies<sup>12,20,25</sup>. Oxidative stress stimulates NF- $\kappa$ B activation directly or through heat shock proteins (HSP-60). NF- $\kappa$ B in turn, promotes synthesis of pro-atherogenic cytokines (TNF- $\alpha$ , interleukins IL-1 and IL-6), adhesion molecules (VCAM-I and ICAM-I) and chemokines (MCP-1) that inhibit eNOS activity and consequently, NO production<sup>12</sup>. The latter also favours angiotensin II synthesis and its activity, an antagonist of NO<sup>59–63</sup>, hence leading to

an inflammatory response<sup>64</sup>. In fact, studies carried out in hypercholesterolemic patients demonstrated an impaired endothelium-dependent vasodilatation due to a defect in the bioactivity of NO<sup>65</sup>. Hypertensive patients also show a defect in the endothelium-derived NO system that may explain the abnormal endothelium-dependent vasodilatation<sup>66,67</sup>.

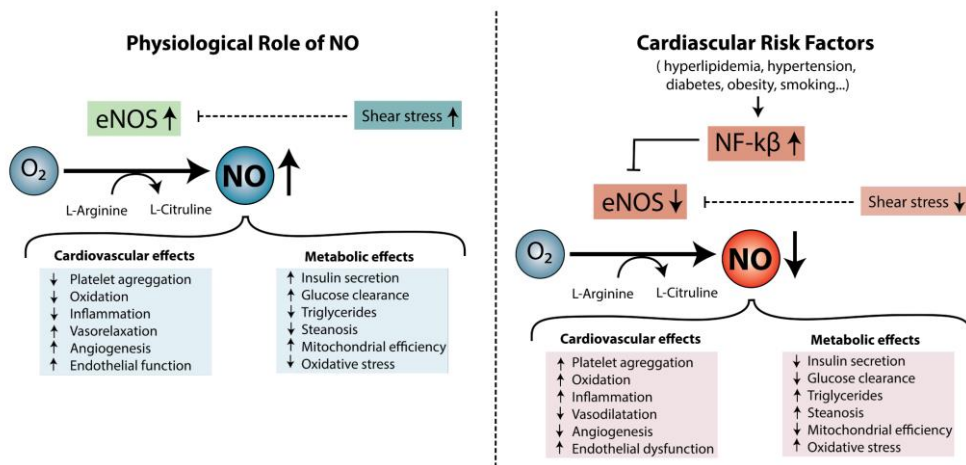


**Figure 2:** Nitric oxygen regulates cardiovascular metabolism and is compromised in the presence of cardiovascular risk factors. eNOS catalyses the production of NO from L-Arginine. NO is an essential metabolite that inhibits the progression of atherosclerosis improving vasorelaxation, angiogenesis, endothelial function, insulin secretion and glucose clearance and mitochondrial efficiency. On the other hand, it reduces oxidative stress, inflammation, plasma lipid levels and steanos. Cardiovascular risk factors such as hyperlipidemia, hypertension or diabetes inhibit eNOS activity upon NF-κβ induction reducing NO and promoting atherosclerosis development.

### 1.2.2. *LDL infiltration*

Accumulation of LDL in plasma favours transendothelial migration of circulating LDLs to the intima, which occurs mainly in athero-prone regions. Although it has been traditionally accepted that LDLs cross the endothelium by diffusion or paracellularly<sup>68-71</sup>, nowadays it is accepted that transcytosis plays an important role

in transendothelial transport of LDLs<sup>72,73</sup>. More specifically, it has been shown that LDL transcytosis is mediated by scavenger receptor B1 (SR-B1) and activin A receptor like type 1 (ALK1) receptor of the endothelium, which differs from the classical LDL endocytosis pathway mediated by LDLR<sup>74</sup>.

It has been shown that ALK1 mediates LDL transcytosis independently of its kinase activity<sup>75</sup>. Similarly, SR-B1 mediates LDL transport across the endothelial barrier as demonstrated in studies where SR-B1 silencing significantly reduces LDL transcytosis, both in human coronary ECs and SR-B1-deficient mice<sup>76,77</sup>. However, the exact mechanism is still under study. In the case of LDLR mediated transcytosis, it has only been described in blood brain barrier ECs<sup>78</sup>. In addition, SR-B1 and ALK1 receptors co-localize with caveolae indicating that LDL transcytosis by SRB1 and ALK1 is mediated by caveolae-dependent mechanism<sup>79,80</sup>. Moreover, it has been demonstrated that the absence of caveolin-1, the major structural protein of *caveolae* in ECs<sup>81</sup>, significantly impairs LDL transport and retention within the arterial wall<sup>82,83</sup>. In addition, caveolin-1 expression is increased in atherosclerotic lesions compared to healthy vessels<sup>84</sup>. Although additional experiments are needed to elucidate the specific transport mechanism of both receptors, these findings suggest that caveolae dependent LDL uptake plays an important role in LDL transcytosis<sup>85,86</sup>.

Although, this review only summarizes the role of ECs in LDL infiltration, it is important to note that other factors such as the glycocalyx<sup>87</sup>, pericytes<sup>88</sup>, the subendothelial extracellular matrix<sup>89</sup> and the role of shear stress<sup>90</sup> should be considered.

#### 1.2.2.1. LDL modifications in the intima

Once in the subendothelial space, trapped LDL particles are oxidized, a process facilitated by the absence of protective plasma antioxidants such as tocopherol, ascorbate, urate, apolipoproteins or serum albumin<sup>91,92</sup>. Oxidized LDLs are a key inflammatory components that promote atherosclerotic plaque development, as they contain oxidized lipids and products derived from their degradation that contribute to the physiopathology of the disease<sup>93,94</sup>.

There are several mechanisms that explain how LDL oxidation initiates in the subendothelial space and different cell types are involved in the process, including ECs, macrophages and VSMCs<sup>95–99</sup>. LDLs can be oxidized by free radicals present in the extracellular media like superoxide, hydroxil radicals<sup>100</sup> or other radicals such as HClO produced by the surrounding cells<sup>101</sup>. Additionally, LDLs can be directly oxidized by enzymatic activity of phospholipases and lipoxygenases<sup>102,103</sup>. In fact, the lipoxygenase pathway has been highlighted to explain initiation of LDL oxidation<sup>104</sup>. Interestingly, LDL receptor related-protein (LRP) is involved in LDL recruitment and 12/15 lipoxygenase is translocated to the membrane where oxidation of LDL cholesterol esters take place<sup>103</sup>.

Independently of the mechanism involved in the initiation of the LDL oxidation, the process follows the same phases<sup>105</sup>. The first step is characterized by the loss of the antioxidants carried by LDLs including alpha-tocopherol and carotenoids<sup>106,107</sup>, and a small degradation of polyunsaturated fatty acids (PUFA). Afterwards, PUFAs, mostly arachidonic and linoleic acids, are oxidized to hydroperoxides, which leads to the formation of conjugated dienes and subsequent short chain aldehydes upon further oxidation<sup>105</sup>.

On the other hand, apoB-100, the major protein of the LDL, also suffers different modifications as a consequence of oxidative environment. For instance, aldehydes generated from lipid oxidation form adducts with lysine residues of apoB-100. Instead, apoB-100 can be directly modified predominantly at tyrosine residues by oxidizing agents<sup>108</sup>. These modifications in the apolipoprotein inhibit LDL-LDLR

recognition and increases the uptake of LDL particles through non-regulated receptors<sup>92</sup>.

Depending on LDL oxidation level, oxidized-LDLs are classified as minimally modified LDL (mm-LDL) or extensively oxidized LDL (oxLDL). Mm-LDLs differ chemically from unmodified LDLs but are still recognizable by the LDLR and therefore, are internalized through regulated pathways. However, modified lipids within these particles act as bioactive molecules conferring other biological activities not shown in unmodified LDLs<sup>109</sup>. These bioactive lipids might induce pro-inflammatory response in endothelial cells and macrophages<sup>110</sup>. On the other hand, when LDLs are extensively modified, they become unrecognizable by the LDLR, while allowing being recognizable by a range of scavenger receptors<sup>111–113</sup>. Oxidative modifications of apoB-100 underlie this lack of affinity toward LDLR and the increased affinity for the scavenger receptors. Therefore, it is important to undergo a complete oxidation process to acquire the epitopes that make oxLDLs recognizable for *scavenger* receptors<sup>100</sup>. Moreover, oxLDLs are able to escape from proteoglycan retention hence favouring their non-regulated uptake by *scavenger* receptors<sup>89,114</sup>. Once internalized, products derived from oxLDL trigger the expression of inflammatory molecules in macrophages, as outlined later in this review.

It is important to note that even being LDL oxidation the most common modification, a range of LDL modifications contributing to atherosclerosis development has been well-described in other works including glycosylation, acetylation and aggregation<sup>113,115–117</sup>.

### 1.2.3. *Endothelial activation*

Endothelial stimulation, also known as endothelial type I activation, occurs when inflammatory agents induce a response such as a change in microvascular tone, permeability or leukocyte diapedesis<sup>118</sup>. This phenomenon is an acute response with short-term functional and morphological changes that does not require *de novo* protein synthesis or gene upregulation<sup>119</sup>. However, in response to certain proinflammatory agents such as IL-1, TNF, endotoxins, modified lipoproteins and advanced glycosylation end products (AGE), as well as disturbed flow derived biomechanical stimulation, the endothelium can undergo a sustained phenotypic modulation, known as endothelium type II activation<sup>118,120,121</sup>. This activation leads to a complex inflammatory response that starts with an increased NF- $\kappa$ B production within the endothelial cells, in response to the aforementioned stimulus. As it happens with NO in endothelial dysfunction, NF- $\kappa$ B upregulates the expression of leucocytes adhesion molecules like VCAM-1 and ICAM-1, secreted chemokines like MCP-1 and IL-8<sup>122–124</sup>, and prothrombotic mediators like plasminogen activator inhibitor or tissue factor.

#### *1.2.4. Monocyte recruitment and foam cell formation*

Activated endothelial cells induce selective monocyte recruitment into the intima. This process has not been directly visualized<sup>125</sup>; however, according to experimental evidence it can be summarized in rolling, adhesion, activation and transmigration of monocytes<sup>126–128</sup>.

Briefly, monocyte recruitment starts with monocyte capture and rolling over the endothelium, which is mainly mediated by P-selectin<sup>128,129</sup>. Then, monocyte-rolling is reduced and they remain firmly attached to the endothelium<sup>130</sup>, a process mediated by the binding of monocytes integrins to VCAM-I and ICAM-I of endothelial cells<sup>129,131,132</sup>. In addition, as they roll over the endothelium, monocytes are activated by endothelial surface-bound chemokines<sup>125</sup> like CXCL1, CXCL2,

CXCL4, CCL5 which increases monocyte adhesiveness<sup>130</sup>. Afterwards, monocytes transmigrate into the intima space. This movement comprises the crossing throughout endothelial-cell barrier, its basement membrane and the pericyte layer<sup>129,133</sup>. The migration process is hold by chemokines, which have been previously secreted in response to proinflammatory signals. Chemokines recruit leucocytes and leucocytes expressing specific receptors migrate towards chemokine higher concentration areas<sup>134</sup>.

Regarding monocyte recruitment, MCP-1 (also named as CCL2) is the most frequent chemokine mediating monocyte transmigration, although the effect of other chemokines such as CCL3, CCL4 and CCL5 has been also studied<sup>135,136</sup>. MCP-1 is produced mainly by endothelial cells, smooth muscle cells, monocytes and macrophages of the intima; and its expression level is upregulated after proinflammatory stimulus or tissue injury favouring the transendothelial migration of circulating monocytes from the plasma to the intima<sup>137</sup>. This process is mediated by two different routes, the paracellular and transcellular routes<sup>129</sup>. In the paracellular route, monocyte migration is favoured through endothelial-cell junctions, due to the redistribution of junctional molecules in the inflamed endothelium<sup>138,139</sup>. In addition, some endothelial junction molecules actively mediate this type of migration<sup>140,141</sup>. On the other hand, in the transcellular route, cells migrate through endothelial cells, however, this type of transmigration takes place specially in central nervous-system, where endothelial cells are connected by complex tight junctions<sup>142</sup>. Finally, monocytes cross endothelial-cell basement membrane, which is composed by a network of laminin and collagen, and the pericyte sheath, which is found in most venules<sup>143</sup>.

Once in the intima, monocytes are differentiated into macrophages that can be polarized to M1 (pro-inflammatory) or M2 (anti-inflammatory) phenotypes<sup>144</sup>. Nonetheless, macrophages show sensitivity to the changes in inflammatory environment, and in response to new signals are able to drive their phenotype from

pro-inflammatory phenotype to the anti-inflammatory phenotype<sup>145–147</sup>. This macrophage plasticity is fundamental for a successful response with M1 predominating in disease progression and M2 in regression<sup>148</sup>. These M1 macrophages release inflammatory cytokines and chemokines, produce NO and reactive oxygen species (ROS), which promote more monocyte recruitment and inflammatory response propagation<sup>147</sup>. In addition, macrophages express a battery of receptors that mediates the internalization of modified and non-modified LDLs. As previously mentioned, retained lipoproteins in the intima are prone to suffer modifications due to the inflammatory environment allowing their internalization through CD36, SRA-I and LOX-I<sup>111–113</sup> scavenger receptors. It is important to underline that the expression of those receptors is not downregulated by cholesterol uptake. Thus, in an atherosclerotic context, where oxLDL content is significantly enhanced, cells internalize higher amounts of oxLDLs. Within the cells, oxLDLs are degraded in the lysosomes and the lipoprotein-contained cholesterol is esterified by acyl CoA:cholesterol acyltransferase (ACAT) in the endoplasmic reticulum (ER). Cholesterol esters are stored as lipid droplets located both in the cytoplasm or linked to the ER<sup>149,150</sup>. Hydrolysis of this packed cholesterol esters mediated by neutral cholesterol ester hydrolases, like nCEH and NCEH1, generates free cholesterol that is transferred from macrophages to apoA-I or HDLs (High Density Lipoprotein), an important step for removal of cholesterol excess from peripheral tissues<sup>111</sup>. This process is mediated by ABCA1 and ABCG1 ATP-binding cassettes and SR-B1, cholesterol transporters that play an important role mediating cholesterol efflux from the cells and preventing foam cell formation<sup>111</sup>. However, the pro-inflammatory microenvironment of atherosclerotic lesions impairs ABCA1 efflux system both in M1 and M2 macrophages and promotes foam cell accumulation, as it has been shown in experiments with murine macrophages contributing to plaque development<sup>151,152</sup>.

In addition, the excess of lipid uptake by macrophages perpetuates the inflammatory response. oxLDLs induce signalling cascades that activate NF- $\kappa$ B targets<sup>153–156</sup>, which maintain endothelial cell activation, monocyte recruitment, and foam cell formation<sup>148</sup>. Actually, uptake of oxLDLs by macrophages could be considered a protective mechanism, as they remove cytotoxic elements from the intima. However, the increased migration of monocyte to the intima and the subsequent differentiation onto macrophages leads to a large number of foam cells that induces the growth of the atherosclerotic lesion<sup>149</sup>. Therefore, cholesterol accumulation is considered a hallmark of atherosclerotic lesions<sup>157,158</sup>.

Accumulation of cholesterol in the subendothelial compartment also promotes formation of cholesterol crystals both inside and outside the cells and contributes to the development of atherosclerotic plaques<sup>159–161</sup>. This process has been monitored both outside and inside the cells, in macrophages incubated with oxLDLs<sup>162</sup>. Although cholesterol crystals are a common feature of advanced atherosclerotic lesions they are present also in early plaques and can be used as a marker of early atherosclerosis development<sup>163</sup>. Cholesterol crystals within the plaque activate NLRP3 inflammasome in macrophages, leading to activation of pro-inflammatory pathways. Inflammasomes are cytosolic multiprotein complexes of the innate immune system responsible for the activation of inflammatory pathways<sup>164</sup>. Although NLRP3 activation and assembly is not fully understood, it is known that its activation leads to caspase-1 activation. Caspase-1 subsequently cleaves the proinflammatory IL-1 family of cytokines into their bioactive forms, IL-1 $\beta$  and IL-18 contributing to inflammation<sup>93</sup>. It has been suggested that uptake of oxLDLs mediated by CD36 receptor is responsible of NLRP3 activation<sup>93</sup>. Apparently, CD36 scavenger receptor along with TLR4-TLR6, take up oxLDL, which results in intracellular cholesterol crystals. Those crystals cause lysosomal destabilization<sup>165</sup>, inducing the release of lysosomal contents such as cathepsins

or reactive oxygen species<sup>166</sup>, which finally results in NLRP3 inflammasome assembly and the subsequent activation of caspase-1.

#### *1.2.5. Contribution of VSMC to foam cell population*

VSMC located in the intima are also able to internalize oxLDL in a non-regulated way through different scavenger receptors such as scavenger receptor A (SR-A), CD36 and LOX-1<sup>167–171</sup>. Indeed, it has been shown that their contribution to the sum of foam cell population within the plaque is significant<sup>18</sup>. In addition, a study published in 2009 showed that VSMCs of the intima express less ABCA1 transporter than the ones of the tunica media<sup>172</sup>; therefore, the balance between cholesterol input and output is tilted in favour of cholesterol accumulation and foam cell formation. They also concluded that at least a 50% of the foam cell in human coronary intima are VSMC-derived rather than monocyte-derived, underlying the importance of VSMC in atherosclerosis development<sup>172</sup>. This finding was also confirmed in ApoE deficient atherosclerosis mice model<sup>173</sup>.

Briefly, endothelial dysfunction along with LDL retention and modification in the intima promote endothelial cell activation leading to monocyte recruitment within the intima<sup>16</sup>. Non-regulated internalization of modified LDLs by monocytes and VSMC leads to foam cell formation<sup>17,18</sup>, which together with the activation of inflammatory pathways perpetuate the formation of fatty streak.

### *1.3. Fibrous plaque development*

During fibrous plaque development, atheroma plaques undergo a transition from fatty streak to intimal growing, a step characterized by the presence of a cell-free and lipid rich area known as necrotic core. To stabilize the plaque, the necrotic core is covered by fibrous and the fibrous cap develops. Necrotic core along with fibrous

cap are the hallmarks of advanced atherosclerosis<sup>174</sup>. It is accepted, that at this stage, atheroma plaque regression is unlikely to happen<sup>175,176</sup>.

### *1.3.1. Fibrous cap*

The fibrous cap is the subendothelial barrier between the lumen of the vessel and the atherosclerotic necrotic core. It mainly consist in VSMCs that have migrated to the luminal side of the artery and VSMC-derived extracellular matrix (ECM)<sup>177</sup>. The role of the fibrous cap is serving as a structural support to avoid the exposure of prothrombotic material of the core that would trigger thrombosis<sup>177</sup>.

At physiological situation, differentiated VSMCs of the tunica media show a contractile phenotype that regulates blood vessel diameter and blood flow<sup>178–180</sup>. However, in response to injury, VSMCs switch their phenotype to the synthetic one in which migratory and proliferation activities prevail<sup>181</sup>. For that purpose, neighbouring cells activate the healing process by producing several growth factors, which include epidermal growth factor, fibroblast growth factor, insulin like growth factor, platelet-derived growth factor (PDGF), transforming growth factor-β (TGF-β) and vascular endothelial growth factor (VEGF)<sup>181</sup>. In atherosclerosis, in response to the growth factors produced by foam cells (VSMC- or macrophage-derived) or ECs of the intima, VSMCs from the tunica media migrate to the intima<sup>16,182,183</sup>. Moreover, IL-1 produced by macrophages enhance the endogenous production of PDGF by VSMC, which once in the intima autocrinically leads to their proliferation<sup>184</sup>. In addition to migration and subsequent proliferation, VSMCs with synthetic phenotype also increase the production of ECM components like interstitial collagen, elastin and proteoglycans<sup>16,185,186</sup>. These proliferating VSMCs along with ECM production generate the fibrous cap that will cover the developing atherosclerotic plaque surrounding the lesion and preventing its rupture<sup>187</sup>. Interestingly, if the mitogens production does not cease, VSMC do not switch back

to the contractile phenotype<sup>178,179,188</sup>, thus facilitating lesion development. Fibrous cap features such as thickness, cellularity, matrix composition, and collagen content are important determinants of plaque stability<sup>189</sup>.

### 1.3.2. *Necrotic core*

The necrotic core constitutes the nucleus of the atherosclerotic plaques. Covered by the fibrous cap, the necrotic core consists of a lipid laden hypocellular region with reduced supporting collagen<sup>190–192</sup>. While atherosclerotic plaque develops, necrotic core increases its size mainly as a consequence of two factors, macrophage death and impaired efferocytosis. Both events contribute to inflammatory microenvironment, oxidative stress, thrombogenicity and promote the death of the neighbouring cells such as VSMCs increasing plaque vulnerability<sup>193</sup>.

In early stages of atherosclerosis, macrophage apoptosis is programmed through the coordinated caspase system leading to cell death and subsequent removal of apoptotic cell by phagocytes, a process known as efferocytosis<sup>194</sup>. Efferocytosis is carried out also by macrophages of the plaque and in a physiological context or in early stages of atherosclerosis, where the balance between healthy and apoptotic macrophages is tilted toward the first ones, it inhibits plaque development<sup>195</sup>.

However, when atherosclerosis develops, macrophage and VSMC death is enhanced due to increased oxidative stress, death receptors activation, inhibition of survival pathways and nutrient deprivation promoting apoptotic cell accumulation<sup>196</sup>. At this step, the phagocytic activity of the macrophages is not able to handle the accumulation of apoptotic cells that undergo secondary necrotic death and release intracellular oxidative and inflammatory components, which then propagate more inflammation and enhances the death in neighboring cells<sup>197</sup>. Efferocytosis also become defective in advanced atherosclerosis. For instance, the

activity of several receptors that mediate efferocytosis such as MerTK, LRP1, CD36 and SR-B1 is impaired. Moreover, oxidized phospholipids and oxLDLs present in advanced atherosclerotic plaques inhibit the recognition of apoptotic cells by efferocytotic receptors<sup>197-201</sup>. Efferocytosis impairment in advance plaques also favors the accumulation of cholesterol crystal coming out from apoptotic cells. Under physiological conditions, small cholesterol crystals are rapidly sequestered from interstitial space by phagocytic cells; however, while the lesion advances phagocytic-cells are unable to take up the excess of crystals, that finally increase in size and remain in the subendothelial space<sup>202</sup>. This process activates the complement and increases the proinflammatory state of the plaque. Moreover, as phagocytic cells are unable to internalize big cholesterol crystals by scavenger receptors, their lysosomal content is directly secreted to the interstitial promoting a more intense immune response<sup>203,204</sup>. These events promote the accumulation of death cells and the growing of the necrotic core. Furthermore, the metalloproteinases liberated after death will reduce the size of the fibrous cap and increase plaque vulnerability<sup>205,206</sup>. Finally, apoptotic and necrotic cells liberate tissue factor (TF), which along with oxidized lipids, increase the thrombogenicity of the necrotic core<sup>207,208</sup>.

### *1.3.3. Plaque calcification*

Atheroma plaque calcification is another hallmark of advanced atherosclerosis. It consist in bone-like formation within the plaque and it is initiated in inflammatory regions where there is a local decrease in collagen fibers<sup>209,210</sup>. It has been suggested that nucleation sites that leads to calcium crystalization are provided by membrane vesicles<sup>211,212</sup>. In the particular case of atherome plaques, matrix vesicles, released upon macrophage and synthetic VSMC death, which are specially abundant in acellular areas, initiate the calcification process of the plaque<sup>213-216</sup>.

The nucleation sites accumulate calcium orthophosphate, which is then converted to amorphous calcium phosphate and finally to a crystalline structures<sup>209</sup>. In addition, other factors including a reduction in mineralization inhibitors or increased osteogenic transdifferentiation contribute to the calcification process<sup>209</sup>. In particular, pericytes<sup>217</sup> and VCMC<sup>218,219</sup> transdifferentiate into osteoblast-like phenotype during atherosclerosis development obtaining the capacity to generate a mineralized matrix, leading to calcium deposits as it happens in bone tissue<sup>220–222</sup>.

All together contribute to microcalcifications, the early stage of the vascular calcification cascade in both intima and media<sup>209,223</sup>. Microcalcifications then evolve into a larger calcifications which extend from the bottom of the necrotic core to the surrounding matrix<sup>219</sup>. Although it is clear that calcification is a hallmark of advanced atherosclerosis (it correlates very well with plaque size), there are not strong evidences that correlate calcification rate and plaque vulnerability. Indeed, recent works discuss deeply this question and they concluded that the amount and size of calcium deposits do not reflect plaque vulnerability and that it would rather be linked to other features such as location, calcification type or the surrounding environment<sup>209,210,224</sup>.

#### 1.4. Plaque stability and rupture

##### 1.4.1. *Vulnerable plaque*

As mentioned above, atheroma plaques usually develop in branched areas where the shear stress is lower. Low shear stress allows not only plaque formation but also its progression<sup>225,226</sup>. In the first instance, lumen narrowing is prevented due to plaque remodelling. However, when it is unavoidable, plaque growth provoke reorganization of hemodynamic forces, which results in an increased shear stress<sup>227</sup>. Consequently, the new condition transforms the lesion into a rupture-prone plaque. A plaque is considered vulnerable when the lesion shows a large

necrotic core, a thin fibrous cap and an increased inflammatory response<sup>228,229</sup> due to the continuous exposure to the pro-atherogenic milieu.

Fibrous cap separates the thrombogenic necrotic core from the circulating coagulation factors and platelets and its thickness correlates with the vulnerability of the plaque<sup>187</sup>. As a result of VSMC cell death, ECM production is reduced and the presence of liberated matrix metalloproteinases (MMP) increases, making the fibrous cap weaker<sup>230</sup>.

As mentioned before, inflammation contributes to plaque development in all the steps from the initiation to plaque rupture. Indeed, in this last stage, its relevance is remarkable as it promotes the instability of the fibrous cap<sup>231</sup>. Certain pro-inflammatory cytokines such as IFN-γ might inhibit collagen production in VSMC. In addition, inflammatory mediators usually found in atheroma such as IL-1β, TNF-α and CD40 ligand (CD154) may increase MMP expression in VSMC as observed *in vitro*<sup>232,233</sup>. This inflammatory stage is commonly observed in the cap and shoulders of the plaque instead of a generalized inflammation<sup>187,234</sup>. All together, the data show that when inflammation prevails, the maintenance of the strong and rigid fibrous cap decreases, making the cap unstable and susceptible to rupture when exposed to hemodynamic forces, the most common mechanism of plaque rupture<sup>187,231</sup>.

#### 1.4.2. Plaque rupture and thrombus formation

When the plaque fissures or ruptures, the subendothelial space is exposed to blood, triggering a coagulation process to cover the wound<sup>235,236</sup>. Initially, platelets adhere to the subendothelial collagen and get activated, then more platelets are recruited and aggregate in the region in order to initiate wound healing<sup>237</sup>. Simultaneously, pro-thrombotic elements of the lipid core are released and come into contact with coagulating factors of plasma. More specifically, tissue factor of the core reacts with

factor VII of plasma, activating the coagulation cascade that leads to thrombin production, an essential intermediate for fibrin formation<sup>187,238</sup>. Fibrin is an insoluble protein that forms networks of fibrin threads; and along with platelets, covers the lesion forming a stable and well-arranged structure. This structure is known as the thrombus<sup>231,239</sup>.

Although the aim of this process is twound healing, triggering of the biochemical cascade promotes the expansion of the intima to the luminal side. For instance, activated platelets release TGF-β, which as indicated earlier, promotes the production of interstitial collagen, and therefore, fibrous cap thickening<sup>240</sup>. Consequently, the atherosclerotic lesion expands, leading to lumen constriction. All together, supposes the hall of clinical complication.

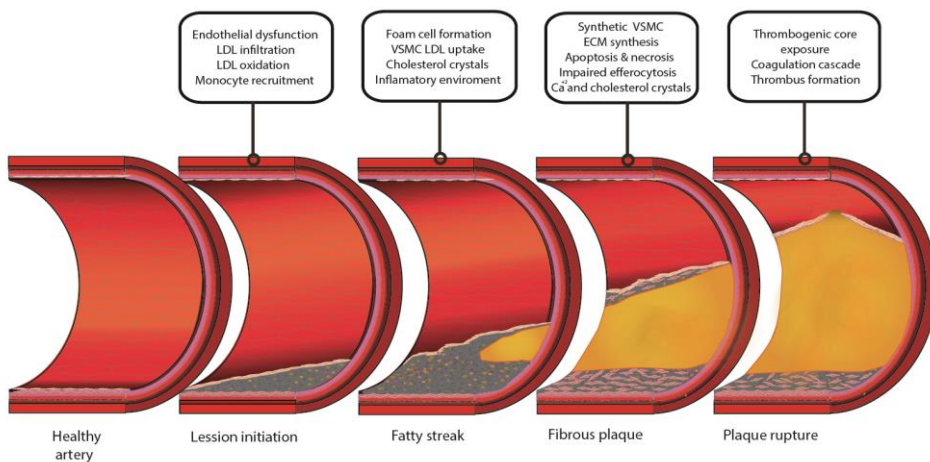


**Figure 3:** Schematic representation of atheroma plaque formation from health artery to plaque rupture underlaying the most important events that contribute to its development in each stage.

#### 1.4.3. *Clinical complications*

Thrombus development triggers a range of reactions that makes the lesion more fibrous and stable and therefore, less prone to rupture. However, due to plaque growth, the risk of vessel obstruction increases. Consequently, blood flow in coronary arteries is reduced, generating isquemic cardiopathies, such as cardiac insufficiency or angina pectoris<sup>231,241,242</sup>. Moreover, if the obstruction is complete or almost complete it leads to myocardial infarction or stroke<sup>243</sup>.

Detachment of the thrombus from the arterial wall would produce a clot, known as embolus that circulates within the cardiovascular system. Eventually, the embolus lodges in distal arteries where it obstructs blood flow leading to local ischemia, organ dysfunction or potential infarction<sup>244</sup>.

However, if the inflammatory response ceases in time, for example, due to a lipid lowering treatment,, a stable plaque with enough lumen for correct blood circulation would be acquired<sup>231</sup>.

## 2. HDL metabolism

### 2.1. HDL remodelling and reverse cholesterol transport.

#### *2.1.1. Reverse cholesterol transport*

Although mammalian cells are not able to degrade cholesterol, several mechanisms avoid its accumulation within peripheral tissues thus preventing cardiovascular disorders. Therefore, the excess of cholesterol must be transported from extrahepatic tissues to the liver where it can be reutilized or converted into bile acids<sup>245</sup>. This process is known as reverse cholesterol transport (RCT) and apoA-I containing lipoproteins are key mediators of RCT. To do so, esterified cholesterol packed within lipid droplets is hydrolysed by ER cholesterol hydrolases like nCEH or NCEH1<sup>246</sup> and then, free cholesterol is delivered to plasma membrane and transferred to circulating apoA-I or HDLs. Cholesterol efflux is performed by ABCA1 and ABCG1 ATP-binding cassettes and SR-BI transporters<sup>247</sup>. In so doing, cholesterol

efflux plays an important role preventing foam cell formation in the intima<sup>245</sup>, the hallmark of atherosclerosis.

### *2.1.2. HDL biogenesis*

In the first instance, liver and intestine release lipid poor apoA-I into the circulation<sup>245,248</sup>, which interacts with ABCA1 transporter within the cell membrane of peripheral tissues. This is thought to occur through interaction of apoA-I and extracellular domains of the transporter<sup>249,250</sup>, which additionally stabilizes the transporter and increases its activity<sup>251</sup>. Lipid efflux occurs by translocation of phospholipids (mostly phosphatidylcholines) and free cholesterol from the inner leaflet of the membrane to the outer leaflet, with ATP hydrolysis<sup>250</sup>. Lipid translocation promotes an unequal lipid accumulation in the membrane that leads to the formation of extra-vesicles rich in phospholipids and cholesterol<sup>252</sup>. Then, apoA-I solubilizes these vesicles by taking spontaneously both phospholipids and free cholesterol<sup>252–254</sup>. Combination of apoA-I with these lipids results in a discoidal shape particles known as nascent HDL or pre-β-HDL. Interestingly, this process requires the presence of amphipathic alpha helical segments of apoA-I to penetrate the plasma membrane and solubilized the lipids<sup>254,255</sup>.

Several mechanisms have been proposed to explain how this phospholipid and cholesterol transfer may occur (see ABCA1 transporter section).

### *2.1.3. Enzymes and lipid transporters act together in HDL remodelling*

During maturation process HDLs shift from a discoidal shape to a bigger and spherical morphology<sup>256</sup>. Several enzymes and proteins from the plasma participate in the HDL remodelling process<sup>245</sup>. Moreover, HDL may interact with other

lipoproteins present in plasma, which promote not only lipids but also apolipoproteins exchange.

HDL remodelling starts with lecithin-cholesterol acyltransferase (LCAT) that associates to discoidal HDLs in plasma and induces cholesterol esterification<sup>257</sup>. ApoA-I of nascent HDLs is essential for LCAT activation<sup>258</sup>, which catalyses phospholipids transfer from phosphatidylcholines to free cholesterol in the discoidal nascent HDLs. LCAT activity results in formation of cholesterol esters (CE) and lysophosphatidylcholine (LysoPC). As discoidal HDLs can accept more cholesterol from cells, LCAT can continuously esterify cholesterol in the HDL surface. Being cholesterol esters insoluble molecules, they migrate from the surface of the particles to the core leading to more spherical morphology change of HDL particles<sup>259,260</sup>. As the particles get bigger, LCAT can also mediate incorporation of another apoA-I into the particle surface, hence leading to particles with three apoA-I molecules<sup>245</sup>.

These spherical HDL particles are able to acquire more cholesterol from cells<sup>245</sup>. Although ABCA1 transporter is the main transporter involved in cholesterol efflux, due to the morphological changes, spherical HDLs are inclined to interact with other transporters than ABCA1, like ABCG1 and SRB1<sup>261–263</sup>. This demonstrates the importance of HDLs promoting cholesterol efflux as they have the ability to incorporate cholesterol in all the maturation process.

Although the mechanism of cholesterol transference mediated by ABCG1 to HDLs is still controversial, it is not completely unknown, as several pathways have been suggested<sup>264</sup>.

On the other side, SRB1 also promotes cholesterol efflux when HDLs are anchored to this receptor. It has been reported that the extracellular domain of SRB1 forms a hydrophobic channel to transport cholesterol esters<sup>265</sup>. However, HDL should present certain maturation level to allow this interaction (HDL<sub>2</sub>), because

free apoA-I can bind to SRB1 but it cannot promote cholesterol efflux<sup>266</sup>. SRB1 mediates bidirectional flux of cholesterol and the net flux depends on the cholesterol gradient between HDL and cell membrane<sup>261,262</sup>. In this way, SRB1 mediates cholesterol efflux primarily in macrophages and foam cells and delivers cholesterol selectively to liver and steroidogenic tissues<sup>267</sup>.

It has been described in mice that the absence or defects in any of three receptors are related with an increase in atherogenesis<sup>268-270</sup>.

Continuing with HDL maturation process, CE within HDLs can be transferred to other lipoproteins (VLDL, IDL or LDL) by cholesteryl transfer protein (CETP). CETP is a lipid transfer protein, which also mediates triglycerides (TG) transference in the opposite direction<sup>271,272</sup>. As a result of CETP mediated lipid exchange, the HDL net content in TG increases while CE content decreases. In addition, as TG molecule size is greater than that of CE, HDL size increases<sup>272</sup>.

CETP contributes to atherogenesis as it participates in the maturation of atherogenic apoB containing lipoproteins by CE transference. However, on the other side, it can be understood as a protective mechanism, since CE rich LDLs are transported back to the liver. Therefore, CETP role in atherosclerosis is still controversial<sup>273</sup>.

In addition to CETP, phospholipid transfer protein (PLTP) transfers phospholipids from triglyceride rich lipoproteins to HDLs<sup>274</sup> which also regulates HDL size.

Finally, HDLs are remodelled also by lipases such as hepatic lipase (HL) or endothelial lipase (EL). HL is released to plasma primarily from the liver and due to its triglyceridase and phospholipase activities transforms HDL<sub>2</sub> particles into HDL<sub>3</sub> particles, thus generating smaller species<sup>275,276</sup>. Endothelial lipase also has phospholipase activity that participates in HDL remodelling, but it is primarily located in vascular endothelial cells<sup>277</sup>. Due to HDL hydrolysis, some apoA-I can

dissociate from the particle and can be reincorporated into other still-growing HDL<sup>245</sup>, or additionally, it can be filtered by kidney and degraded<sup>278</sup>.

#### *2.1.4. HDL catabolism in liver*

As mentioned before, HDL delivers cholesterol to the steroidogenic tissues and liver through SRB1 receptor. In the first case, cholesterol is used for sexual hormones production, while in the second, if not reutilized, cholesterol is converted into bile acids<sup>279</sup>. The latter is a liver exclusive process, because only hepatocytes express high levels of CYP7A1, the enzyme responsible of starting this complex conversion<sup>280</sup>. Finally, bile acids are conjugated with taurine or glycine derivatives to form bile salts which are transported by ABCB11 to bile ducts<sup>281</sup>. Unlike cholesterol, bile salts are amphipathic molecules, which facilitates the formation of micelles.

Although bile salts comprise 80% of the bile, cholesterol can be directly transported into the bile through ABCG5/G8 transporter<sup>282</sup>. In addition, it has been reported that this process requires phospholipid transport mediated by ABCB4<sup>283</sup>, which leads to mixed micelles formation. Finally, the bile containing the micelles and other components such as bilirubin (end product of heme-group metabolism) or heavy metals (like iron and copper), keeps stored in the gallbladder for its secretion during food digestion<sup>284</sup>.

Cholesterol excretion through bile is considered the final step of reverse cholesterol transport and, in other words, this is how cholesterol from foam cells within the vessel wall is eliminated. Therefore, it is reasonable to think that defects in this complex circuit may lead to atherosclerosis related complications<sup>285</sup>.

## 2.2. HDLs constitute an heterogeneous lipoprotein group

High-density lipoproteins are the smallest and densest lipoproteins in plasma that were first described in 1960 after plasma isolation by ultracentrifugation. HDLs are particles with a hydrophobic core of CE and TG surrounded by a monolayer of phospholipids, free cholesterol and apolipoproteins<sup>286</sup>. Due to the high ratio of proteins to lipids, HDLs are the densest lipoproteins (1.063 - 1.21 g/mL) in plasma.

Newly formed HDLs show a discoidal shape, but as they accumulate lipids (esterified cholesterol and triglycerides) in the core they become spherical. In the whole remodelling process, HDL size can vary from 5 to 17 nm<sup>286</sup>. When HDLs are fully matured and cannot store more lipids they go back to the liver as a final step of RCT to be degraded<sup>287</sup>. However, because of the activity of lipolytic enzymes, they can be degraded in plasma, releasing apolipoproteins that can form new HDLs. For instance, apoA-I released from HDL due to HL activity can serve as a scaffold for a new HDL<sup>271,272,275</sup>.

Classification of HDL subpopulations depends on the isolation technique<sup>288</sup>. Ultracentrifugation distinguishes HDL<sub>2</sub> (1.063 < density < 1.125 g/mL) and HDL<sub>3</sub> (1.126 < density < 1.210 g/mL). With gradient gel electrophoresis, HDL<sub>2</sub> and HDL<sub>3</sub> can be classified by their mean diameter: HDL<sub>2a</sub>: 10.6 nm, HDL<sub>2b</sub>: 9.2 nm, HDL<sub>3a</sub>: 8.4 nm, HDL<sub>3b</sub>: 8 nm and HDL<sub>3c</sub>: 7.6 nm<sup>289</sup>. They can also be classified depending if they contain apoA-II along with apoA-I, or apoA-I alone, using immunoaffinity chromatography<sup>290</sup>. Finally, HDLs can be classified according to surface charge. Hence, analysing electrophoretic mobility (agarose electrophoresis) separates, pre- $\alpha$ -HDLs,  $\alpha$ -HDLs and pre- $\beta$ -HDLs<sup>290</sup>.

### 2.2.1. HDL proteome

Proteins constitute the 50% of total HDLs weight. The major apolipoprotein component in HDLs is apoA-I which accounts for approximately 70% of total HDL

protein<sup>291</sup>. The role of this protein is crucial for HDL assembly and proper function. ApoA-II is the second major apolipoprotein in HDLs, which represents approximately 15–20% of total HDL protein<sup>292</sup>. The most abundant ones after these two, are apoA-IV, apoC, apoD and apoE. These proteins can freely exchange between lipoproteins. For instance, HDLs can acquire apoE and apoC proteins from circulating VLDL<sup>293</sup>.

In addition to structural apolipoproteins, HDLs contain several enzymes and lipid transfer proteins associated to the surface that play a major role in converting HDL from one sub-specie to another, such as LCAT, CETP or PLTP, which are not uniformly distributed across HDL subtypes<sup>286</sup>. Mass spectrometry studies revealed that approximately 80 proteins could be associated to HDLs<sup>294</sup>. However, the specific role of all these proteins is still under study.

#### *2.2.2. HDL lipidome*

Regarding to HDL lipid composition, lipidomic studies in healthy normolipemic patients have shown that the most abundant lipids in HDL are phospholipids (phosphatidylcholine 32–35%; lysophosphatidylcholine 1.4–8.1%), sphingolipids (sphingomyelin 5.6–6.6%) and neutral lipids (cholesteryl esters 35–37%; free cholesterol 8.7–13.5%; triglycerides 2.8–3.2%)<sup>288,295</sup>.

#### **Phospholipids**

- Phosphatidylcholine (PC) is a structural lipid and its distribution is consistent across HDL subpopulations. The most common PC species are 16:0/18:2, 18:0/18:2 and 16:0/20:4 species<sup>296</sup>. Interestingly, HDLs are enriched with polyunsaturated fatty acids PCs<sup>297</sup>.
- Lysophosphatidylcholines (lysoPC) formation result from the degradation of PCs by the activity of phospholipases such as LCAT<sup>298</sup>. Moreover, LCAT is

associated manly with small dense HDL particles, which are two times enriched in lysoPC compared to large HDLs<sup>299</sup>.

### **Neutral lipids**

- Cholesterol is the dominant lipid among unesterified free sterols. Free cholesterol (FC) is located in the surface of HDL and regulates monolayer fluidity<sup>300</sup>.
- Cholesteryl esters are formed also by the activity of LCAT, when it mediates trans-esterification of PL and cholesterol. CEs are highly hydrophobic thus they accumulate inside the HDL, forming the lipid core. They account for up to 36 mol % of total HDL lipid<sup>297,301,302</sup>. In addition, the most abundant CE of the HDL is cholesteryl linoleate<sup>296</sup>.
- Triglycerides in the HDLs mostly contain oleic, palmitic and linoleic acid moieties<sup>296</sup> and like CE, they are within the lipid core.

Consequently, HDL consist of a group of heterogeneous particles with different structural and physicochemical properties, which translate in significant differences in their biological activities<sup>303</sup>.

### **2.3. ABCA1 is a lipid transporter**

In 1999, the role of ABCA1 transporter in HDL metabolism was revealed when loss of function mutations in the ABCA1 gene were found in Tangier disease patients<sup>304–306</sup>. As expected, deficiency in ABCA1 leads to intracellular CE accumulation, deficient pre-β-HDL formation and therefore, significant reduction in circulating HDLs<sup>307</sup>. However, Tangier disease is often, but not always, associated with an increased cardiovascular risk<sup>308</sup>.

ABCA1 belongs to the ABC superfamily membrane proteins that transport several substrates across cell membrane, using the energy of ATP hydrolysis. There are 7

subfamilies: from the member A (ABCA) to the member G (ABCG) depending on the phylogenetic distance<sup>309,310</sup>. ABCA subfamily is involved in lipid transport across membranes and ABCA1 specially mediates transference of phospholipids and free unesterified cholesterol to lipid poor apoA-I in the extracellular media. This process is considered as the rate-limiting step in HDL biogenesis<sup>311–313</sup>. It has been shown that ABCA1 highest expression occurs in hepatocytes followed by macrophages and foam cells<sup>264</sup>.

ABCA1 is a glycoprotein of a single polypeptide chain of 2,261 residues, organized in two transmembrane domains (TMD) two nucleotide-binding domains (NBD) and two extracellular domains (ECD) that are glycosylated<sup>249,250</sup>.

It is suggested that ECDs are responsible of apoA-I binding to ABCA1 as binding is sensitive to mutations in this domains<sup>314</sup>. In addition, monoclonal antibodies against ECD1 and ECD2 regions inhibit apoA-I binding, consistent with the proposed key role for this domains<sup>315</sup>.

Although ABCA1 function is well established, the mechanism of PL and FC translocation across the membrane remains unclear. In fact, in a recently published review, six possible mechanisms are taken under consideration<sup>264</sup>. However, we describe here the most expanded version based in mutagenesis studies and structure of the transporter<sup>249,250</sup>.

### *2.3.1 Functional ABCA1*

Human ABCA1 is distributed mainly in plasma membrane of cells and its localization depends in the transporter palmitoylation<sup>316</sup>. ABCA1 is palmitoylated at four cysteine residues and reduction of palmitoylation has been conversely related with the transporter availability in the membrane. In addition, ABCA1 in the plasma

membrane self-associates and should be forming dimers or tetramers to be functional<sup>317–319</sup> and promotes apoA-I binding to the cell surface.

It has been suggested that two apoA-I molecules should bind to ABCA1 dimers to generate nascent HDL; and in fact, it has been reported that apoA-I cannot bind to monomeric ABCA1<sup>317,318</sup>. A fact more than reasonable because to generate a discoidal HDL, two apoA-I proteins must be surrounding the lipid bilayer.

ApoA-I binding to the ABCA1 stabilizes the transporter and inhibits its proteolysis<sup>251</sup>. Apparently, this inhibition is due to dephosphorylation of two amino acids, that when phosphorylated, induce ABCA1 degradation<sup>320</sup>. However, it is remarkable that only a 10% of the apoA-I is bound to the transporter and most of the protein binds to membrane lipid domains generated by ABCA1 action<sup>250</sup>.

### *2.3.2. Mechanism of lipid translocation and transference to apoA-I*

Active ABCA1 leads to lipid reorganization, which relies on PL and FC translocation from the inner to the outer leaflet of the membrane<sup>321</sup>.

The “alternating access” model is the generally accepted mechanism for ABC transporters to translocate substrates<sup>250</sup>. For ABCA1 transporters it seems that this is the most suitable mechanism based in the structure<sup>249</sup>. Translocation relies in the cavity formed by the TMD. This substrate-binding cavity can open to either the cytoplasmic side or the extracellular side of the plasma membrane. In the absence of ATP, the cavity faces to the cytoplasm (open conformation), leading to substrate incorporation. Along with this, two ATP molecules bind to the NBDs, which results in NBD dimer formation with ATP molecules in the interface (close conformation). This event induces a conformational change from TMD inward-facing cavity to an

outward-facing cavity, which result in substrate translocation to the outer leaflet of the membrane<sup>250,322</sup>.

Subsequent hydrolysis of ATP and dissociation of ADP make NBD to separate, which drives to the open conformation, allowing another translocation cycle<sup>250,322</sup>.

In this way, the lipid incorporates to the transporter in the inward facing cavity and then is transported to the outer membrane after reaching the outward-facing position. Human ABCA1 can transport several classes of PL, but it shows more preference to PC than to PS or SM when reconstituted into liposomes<sup>323</sup>.

Then, PL and FC are transferred to cell-associated apoA-I. Whatever the apoA-I is bound to the ABCA1 or not, apoA-I interaction with plasma membrane is essential for HDL formation. Here we explain two possible mechanisms that may integrate this issue.

The early model proposed to explain HDL biogenesis suggests a direct interaction between apoA-I and ABCA1. According to this model, translocated lipids accumulate in the ECDs space, forming a reservoir where apoA-I could take lipids from it<sup>250</sup>. As it has been shown that apoA-I/ABCA1 interaction ratio is 1:1 and that ABCA1 should form a dimer to be active as indicated above<sup>319</sup>, this model could explain the formation of nascent HDLs containing two apoA-I molecules<sup>324</sup>.

Interestingly, the high-resolution structure resolved in 2017<sup>249</sup> revealed that ECDs enclose a hydrophobic tunnel that may serve as a temporary storage or a delivery passage for lipids, accompanied by pronounced conformational changes. In addition, it has been suggested that PL efflux normally precedes the binding of FC<sup>325</sup>

However, according to reservoir model, all the apoA-I bound to the cell when ABCA1 is active should be interacting with the transporter. However, as explained earlier, most of the apoA-I binds directly to the plasma membrane instead to the transporter<sup>326,327</sup>. More specifically, apoA-I interacts with membrane regions that have been created by the activity of ABCA1. It has been shown that these regions protrude to the extracellular space<sup>252,328,329</sup>. According to this mechanism, ABCA1 mediated lipid translocation promotes an imbalanced accumulation of lipids which results in “packing defects” around ABCA1<sup>253</sup>. These microdomains rich in PL and FC are thought to be the sites of HDL assembly: apoA-I deeply inserts to extract PL and FC from these vesicles forming nascent HDL<sup>253</sup>.

It is suggested, anyway, that apoA-I must interact first with ABCA1, before interacting with membrane<sup>330</sup>, although some authors have shown that apoA-I is able to solubilized lipids without any activation<sup>255</sup>.

### *2.3.3. ABCA1 transcriptional regulation.*

ABCA1 along with ABCG1 are oxysterol-regulated genes, which means that *de novo* transcription and translation are sensitive to cell sterol levels.

Liver X receptors (LXR) are the most important transcription factors regulating ABCA1 transcription<sup>331,332</sup>. LXR $\alpha$  and LXR $\beta$  form heterodimers with the retinoic X receptor (RXR), which leads to the transcriptional activation of both ABC transporters after binding of the dimer to response elements in the target genes<sup>333</sup>. Both LXR $\alpha$  and LXR $\beta$  are activated by physiological concentrations of oxysterols resulting of cholesterol metabolism<sup>334</sup>. In addition to ABC transporters, LXRs promote the expression of other RCT related genes such as SRB1, SREBP1c or CETP<sup>335–337</sup>.

## 2.4. ApoA-I structure and lipid solubilisation

ApoA-I is synthesized in the liver and small intestine and is secreted to plasma as many other apolipoproteins<sup>245,248</sup>. The lipid-free form of apoA-I or the poor lipidated apoA-I (containing up to four phospholipid molecules)<sup>338</sup> contributes to the 5-10 % of total apoA-I in plasma<sup>339,340</sup>. In addition to the secreted one, plasma apoA-I can be released from circulating HDLs. This lipid free/poor lipidated apoA-I is the preferred substrate of the ABCA1 membrane transporter in macrophages<sup>341-343</sup> and is the main cholesterol and phospholipid acceptor. In addition to structural and functional contribution in HDLs, apoA-I is also an activator of LCAT<sup>258</sup>.

ApoA-I is a 28 kDa, 243-aminoacid protein. When apoA-I sequence was reported in 1970, it was rapidly noted the presence of amphipathic alpha helices<sup>344-346</sup>. The C-terminal domain (CTD), which constitutes almost all the protein (CTD: 44-243 a.a.), contains two 11-aminoacid and eight 22-aminoacid tandem repeats<sup>347</sup>. Each of these repeats has an amphipathic  $\alpha$ -helix. These helices confer detergent-like properties to the protein and facilitates PL and FC solubilisation within cell membrane domains<sup>348</sup>. The N-terminal domain (NTD: 1-43 a.a.) also contains  $\alpha$ -helices, but they belong to an amphipathic  $\alpha$ -helix class that rarely participates in lipid binding<sup>348</sup>. NTD instead is known to affect both the stability and conformation of the lipid free form. When apoA-I associates to lipids, NTD changes its conformation<sup>349-351</sup>.

It has been estimated by circular dichroism that helicity of monomeric apoA-I ranges from 45-58%, a 12% is estimated to be  $\beta$ -sheets, while the rest is organized in random coils<sup>352,353</sup>. Interestingly, apoA-I lacks a defined tertiary structure but it shows a molten globular state in plasma, which means that apoA-I has a compact folding with a hydrophobic core<sup>354,355</sup>. This core is composed of the  $\alpha$ -helices organized in bundles via hydrophobic interactions.

In a cellular context where ABCA1 has already formed lipid exovesicles (see ABCA1 section), apoA-I binding to lipids initiates with the interaction of the highly hydrophobic CTD and the lipid exovesicles. This contact increases protein helicity, as random coils within the CTD form  $\alpha$ -helices. In addition, the stability of the N-terminal helix bundle decreases, which promotes an open conformation and more interaction with lipids in the particle<sup>356</sup>. In other words, helix-helix interactions change to helix-lipid interactions<sup>357</sup>.

Overall, the major determinants of apoA-I lipid solubilizing and lipid binding properties are the hydrophobicity of CTD and the stability of the NTD.

When apoA-I is inserted into the vesicle, it extracts lipids from the outer and the inner leaflet simultaneously<sup>253</sup>. And, when the  $\alpha$ -helical content of the proteins reaches a critical value, the bilayer begins to destabilize, resulting in membrane fragmentation and the formation of discoidal phospholipid particles<sup>358</sup>. ApoA-I conformational changes involves 100 a.a in total, increasing the helicity by 40%<sup>291</sup>. In other words, the whole apoA-I is involved in lipid binding except for a stretch of six and seven residues of the NTD and the CTD, respectively<sup>352</sup>. It is important to note that although discoidal HDL formation is a spontaneous process, it is triggered by ABCA1<sup>253</sup>. As mentioned in the ABCA1 section, ABCA1 creates this lipid microdomains where apoA-I can be deeply inserted.

Nascent discoidal HDLs (7-17 nm) contain 2-4 apoA-I per particle depending on the size<sup>338</sup>. A nascent HDL with two apoA-I consists in a phospholipid bilayer surrounded by both apoA-I molecules forming a double belt with an antiparallel orientation. Indeed cross-linking experiments showed that central helical portion (a.a. 121-142) of one apoA-I molecule is adjacent to the similar region of its counterpart<sup>359</sup>. In this disposition, the hydrophobic part of amphipathic helices are faced to the acyl

chains of the bilayer, while the hydrophilic part are exposed to the aqueous solution<sup>324</sup>. The N-terminal region of the protein can fold back on itself, which allows particle size modulation. Bigger HDL discs accommodate one or two more apoA-I<sup>360</sup>. However, apoA-I disposition in these cases is still controversial.

Finally, it is interesting to mention that apoA-I amphipathic  $\alpha$ -helices are unstable within the particle and can dynamically change the conformation in presence of phospholipids<sup>361</sup>. For instance, in smaller particles (7.8 nm) some regions of apoA-I lose their helical structure and become unfolded<sup>361</sup>. This conformation flexibility of the lipid bound apoA-I facilitates HDL remodelling during maturation and metabolism<sup>362</sup>.

### 3. RNA interference pathway. MicroRNAs

#### 3.1. MicroRNAs regulate gene expression

MicroRNAs (miRNA) are short non-coding RNAs (18-25 nucleotides) that regulate certain gene expression by inhibiting target messenger RNA (mRNA) translation<sup>363,364</sup>. To do so, miRNAs bind mostly to the 3'-untranslated region (3'-UTR) of the mRNA which result in translational repression and/or mRNA degradation<sup>365,366</sup>.

To date, more than 2,300 miRNAs have been discovered in the human genome and it has been estimated that more than a half of total mRNAs are targets of miRNAs, which highlight the relevance of these small molecules<sup>367</sup>. A miRNA often regulates multiple genes, but the targets are usually involved in the same pathway or cellular mechanism<sup>368</sup>.

Almost half of identified human miRNAs are coexpressed with their host genes and are produced mainly from the introns during the splicing of the primary mRNA transcript<sup>369,370</sup>. The remaining miRNAs are produced from intergenic regions that contain their own promoters<sup>370</sup>. Specifically, they are originated in self-

complimentary regions, therefore in the first instance, miRNAs show a hairpin structure, known as primary-miRNA (pri-miRNA).

In the canonical miRNA production pathway, pri-miRNAs are cleaved by Drosha, an RNase III enzyme. This enzyme directed by DGCR8 protein (also known as Pasha) cleaves pri-miRNA from the edges, removing the non-complemented regions<sup>371,372</sup>. This results in a stem loop precursor-miRNA (pre-miRNA) which is exported to the cytoplasm by Exportin-5, located in the nuclear membrane<sup>373</sup>. Once in the cytoplasm, Dicer, another RNase III enzyme, removes the loop, releasing a double stranded miRNA (miR/miR\*) of ~22 nucleotides length, considered the mature miRNA<sup>374</sup>.

In the miR/miR\* duplex, the one referred as miR incorporates into the RNA-induced silencing (RISC) complex to perform target mRNA silencing, known as guide-strand. The other strand, passenger strand, herein referred as miR\* is quickly degraded<sup>375,376</sup>. However, in some cases, both strands could be functional. In that case, 5p (from the 5' arm of the hairpin) or 3p (from the 3' arm) termination should be indicated in matured miRNA name, and these should be treated as independent miRNAs<sup>375</sup>. Nevertheless, in some cases there is no sufficient data to determine which of the strands is the dominant one. miRbase is the data base providing this information.

The miRNA associates to argonaute (AGO) protein guiding to its specific targets by sequence complementarity (base pairing) within the 3'-UTR. These interaction regions are known as miRNA response elements (MRE). If miRNA-MRE complementarity is total, AGO2 endonuclease triggers the cleavage of target mRNA<sup>377</sup>. However, in animal cells, most of the miRNA-MRE interactions are not perfect<sup>378</sup>. In that case, AGO2 acts as a mediator and repression of mRNA translation will occur by other RISC proteins contribution, which consists in poly-A tail deadenylation and subsequent degradation of the mRNA<sup>379</sup>.

### 3.2. MicroRNA circulation by HDLs.

miRNAs are exported to extracellular media and can be transported associated to proteins (e.g. argonaute), extracellular vesicles, or lipoproteins, which increase RNAs stability in circulation and protects them from ribonuclease activity<sup>380,381</sup>.

HDLs continuously load and unload cargos to cells or exchange them with other lipoproteins. In addition to lipids and proteins, HDLs also transport small non-coding RNAs, suggesting that HDL participates in extracellular miRNAs signalling<sup>382,383</sup>. The most studied ones are miRNAs since their discovery in 2011<sup>381,382</sup>. HDLs accept miRNAs from multiple cells and deliver them to recipient cells<sup>384,385</sup>. It has been shown that macrophages, neutrophils, hepatocytes, beta cells and even neurons export miRNAs to HDLs<sup>382,386–388</sup>.

Plasma purified HDLs transport a vast amount of miRNAs such as miR-223, miR-92a, miR-126, miR-150, miR-146a, miR-30c, miR-378, miR-145<sup>383</sup>. Interestingly, HDLs also transport miR-33 which downregulates the expression of cholesterol exporter ABCA1. In addition miR-122-5p and miR-375-3p are also in the top of the most abundant miRNAs in HDLs and they have been reported to be expressed specifically in hepatocytes and beta cells respectively<sup>381,389</sup>. This gives the idea that in a specific situation, cells export miRNAs to HDLs in order to have an impact in other tissues.

The specific mechanism by which HDLs deliver miRNAs to recipient cells is not well understood. However, several studies show that scavenger receptors are involved, such as SCARB-1 and SRB1 in some cell lines<sup>382,387,390</sup>. However, more studies are required and it has been suggested that other mechanisms could be involved<sup>382</sup>. Regarding to HDL loaded miRNAs, different options are under consideration such as, transporter mediated transference to HDLs, or HDL binding to exported miRNAs without any kind of cell interaction<sup>389</sup>.

Since the discovery, it has been proposed that HDL may participate in intercellular communication. However, it has recently been suggested that HDL

mediated regulation in long distances is unlikely to occur, and that is more reasonable to happen in space-confined regions, such as atheroma plaque<sup>389</sup>. These spaces would provide the environment where HDL-miRNA may accumulate reaching sufficient levels to regulate gene expression and contribute to a notable change in the target tissue. This means that HDL could show a paracrine regulation more than the endocrine one, although more studies are required<sup>389</sup>.

In atherosclerosis environment, it is expected that circulating HDLs may interact extensively with endothelial cells of blood vessels. It has been demonstrated that HDLs deliver miRNAs (miR-223-3p) to recipient endothelial cells and inhibit endothelial cell adhesion molecule ICAM-1 and cytokine expression<sup>385</sup>. In addition, it has been demonstrated that miRNA extracellular signalling between ECs and VSMC in the artery wall mediate atheroprotection (through exovesicles communication)<sup>391</sup>. However, HDL-miRNA intercellular communication in atherosclerosis has not yet been studied. It has been suggested that the confined microenvironment formed in the subendothelial space in atheroma situation, could favour HDL-miRNA communication, as HDL particle and their miRNA cargos may accumulate reaching an effective concentration to impact gene expression<sup>389</sup>.

Finally, it is important to state that miRNA concentration and identity have shown to be altered in various diseases including familial hypercholesterolemia<sup>390,392</sup> or CVD<sup>393-395</sup>. And because of these variations in disease, it has been suggested that atheroprotective role of HDLs (anti-inflammatory, antioxidant and anti-thrombotic, in addition to RCT) could rely on miRNA pattern of HDLs<sup>380</sup>.

### 3.3. miR-33-a, a regulator of RCT

#### *SREBP*

Sterol-response element-binding proteins (SREBP) are transcription factors that regulate the expression of genes involved in cholesterol synthesis and uptake, and

fatty acids biosynthesis<sup>396,397</sup>. In mammals, SREBPs are encoded in *SREBF1* and *SREBF2* genes located in chromosomes 17 and 22, respectively<sup>398</sup>. These proteins act as a sensor and help boosting cellular cholesterol and fatty acid levels when required.

*SREBF1* gene encodes two isoforms of SREBP, SREBP1a and SREBP1c. SREBP1a regulates genes that control cholesterol metabolism and fatty acid synthesis. SREBP1c upregulates the expression of genes regulating fatty acid synthesis and is activated in response to insulin.

*SREBF2* only generates SREBP2 protein and acts as a cholesterol sensor in the cell. This transcription factor regulates cholesterol synthesis and cellular uptake, by overexpressing genes related with those pathways such as HMG-CoA reductase, the key enzyme in cholesterol synthesis pathway, or LDLR receptor, which permits obtaining cholesterol from circulating LDLs<sup>399,400</sup>.

#### *miR-33*

miR-33 is a highly conserved miRNA family within the intronic sequences of SREBP genes. In humans, two isoforms of miR-33 exist: miR-33-a, which is present in the intron 16 of *SREBF2* and miR-33-b, which is encoded in the intron 17 of *SREBF1*<sup>401</sup>.

As both miR-33 share the same seed sequence (they differ only in 2 nucleotides), they are predicted to share same targets<sup>402</sup>. However, the activity of each isoform is related with the corresponding SREBP protein and the stimulatory situation. Both miRNAs are co-expressed with SREBPs proteins, and they act in concert with their respective host genes<sup>402</sup>.

In cholesterol depletion situation SREBP2 and miR-33-a will be highly expressed and coordinated to boost intracellular levels of cholesterol<sup>401,403,404</sup>. While SREBP2 induces genes involved in cholesterol uptake and synthesis, mir-33a targets genes

to reduce cholesterol export<sup>405</sup>. Interestingly, LXR<sub>s</sub> are also activated in this state and acts coordinately with the SREBP2/miR-33 system in order to increase cholesterol efflux by activating the expression of ABCA1<sup>406</sup>.

ABCA1 is the most predicted and conserved target of mir-33a. It suppresses ABCA1 expression by targeting the miRNA responsive elements in the 3'-UTR<sup>401,407</sup>. This results in reduced cholesterol efflux to apoA-I and therefore, HDL-C production<sup>408</sup>. In addition, miR-33-a also plays an important role in the liver, not only targeting ABCA1, but also genes related with bile acid synthesis (CYP7A1) and secretion (via ATP8B1 and ABCB11)<sup>409</sup>. This reveals the important role of miR-33a in cholesterol homeostasis as it regulates multiple steps of RCT<sup>406</sup>.

Interestingly, unlike mir-33b, mir-33a is highly expressed in macrophages and is related with lipid accumulation and plaque formation, revealing the impact of this isoform in atherosclerosis development<sup>410</sup>.

Inhibition or deletion of miR-33a in atherosclerotic mice models (LDLR-/- or ApoE-/-) has resulted in reduced atherosclerotic plaque size and promoted atherosclerosis regression<sup>408,410-412</sup>. It was demonstrated that global inhibition of miR-33 enhances ABCA1 expression in macrophages and liver (and also ABCG1 in rodents), and enhances RCT, leading to a dramatic reduction in lipid accumulation. All the mentioned leads to atherosclerotic plaque reduction and HDL-C increase in mice and non-human primates<sup>411,413,414</sup>. Indeed, it has been shown that the loss of mir-33-a in macrophages is sufficient to reduce plaque size<sup>410</sup>. In liver-specific miR-33 knockout mouse model, it has been shown an increased circulating HDL-C and RCT improvement without any impact on the atherosclerosis plaque size<sup>415</sup>.

All these findings suggest that both liver and macrophages play important roles mediating the effects of miR-33 in atherosclerosis<sup>406</sup>.

On the other hand, some studies have demonstrated that inhibition of miR-33 in western diet-fed LDLR<sup>-/-</sup> mice is atheroprotective with no significant changes in circulating HDLs<sup>410,412</sup>. These findings indicate that miR-33 is involved in regulating other processes related to CVD that are distinct from its HDL raising capabilities<sup>406</sup>. For instance, mir-33 inhibition has been shown to reduce inflammatory response by reducing macrophage inflammation<sup>410–412</sup> or inducing macrophages M2 polarization (anti-inflammatory phenotype)<sup>416</sup>.

## 4. Reconstituted HDLs

### 4.1. rHDL as a theranostic tool

In addition to the aforementioned ability to promote cholesterol efflux from cells, HDLs have shown to possess other anti-atherosclerotic properties such as antioxidative, anti-inflammatory and even anti-thrombotic properties<sup>293,417–419</sup>.

Epidemiological studies show an inverse correlation between HDL-C concentration and cardiovascular risk, suggesting that the more HDLs the more protection you have<sup>420,421</sup>. However, genetic studies concluded that there is no cause-effect relationship between HDL concentration and cardiovascular risk<sup>422–425</sup>. Consequently, the focus of attention has changed from HDL quantity to quality, which could explain the beneficial effects of HDLs in cardiovascular system. This also arose the relevance of HDL specific composition to increased anti-atherogenic functions of rHDLs<sup>426</sup>.

The first *in vitro* HDL particles, known as reconstituted HDLs or rHDLs, were produced in the early 80s by Matz and Jonas<sup>427</sup>. To synthesize them, the main HDL protein, apoA-I and various lipid mixtures were used, obtaining nanoscale discoidal particles that resembled the same as natural pre-β-HDL. The method used by them, the sodium cholate method is nowadays the most common method to form rHDL.

Briefly, a non-denaturing detergent (sodium cholate) is added to the lipid suspension, in order to facilitate apoA-I protein insertion into the lipid vesicles and form the nanodiscs. Variations in this method, initial lipid composition and protein/lipid ratio, allows customizing rHDL composition and size<sup>288</sup>.

In addition to that, other methodologies have been developed for rHDL production such as sonication, thermal cycling, microfluidics or high-pressure homogenization<sup>427–430</sup>. The last two methodologies allows scaling up the production.

The common feature in all the protocols is a step in which the lipid surface of the vesicles is somehow destabilized to facilitate discontinuous appearance in the vesicle surface. This decrease the activation barrier and facilitates apoA-I insertion into the vesicles and consequent nanoparticle formation<sup>288</sup>.

Being the main goal of rHDL to resemble natural HDLs, the most abundant lipids in natural HDLs (phospholipids or sphingolipids with different acyl chain length and saturation, phosphatidylcholine lipid extracts) are used, alone or within lipid mixtures<sup>427,428,431–435</sup>.

Regarding rHDL protein composition, apoA-I is the principal protein used for this nanoparticle production. The source of apoA-I can be from human plasma or produced in bacterial or mammalian systems. Alternatively, apoA-I mimetic peptides have been used to reduce costs. These peptides resemble class A amphipathic  $\alpha$ -helices, that by containing specific charges, allow lipid insertion and HDL reconstitution.

rHDL has been used mainly for cardiovascular treatment to promote cholesterol efflux and reduce atheroma plaque burden with interesting results in clinical trials. However, there are many pre-clinical studies in progress with further

objectives. In the last years, the use of rHDLs as carriers of therapeutic molecules have spread out. Thus, rHDLs have been associated with different cargos such as, statins<sup>436,437</sup> LXR agonists<sup>438,439</sup> bioactive lipids<sup>440</sup>, immunomodulators<sup>441</sup> siRNA and miRNA molecules<sup>387,442,443</sup> as well as preparations where more than one active component is combined<sup>437,444</sup>.

In addition, several attempts have been made to assess the role of both protein components (apoA-I, apoA-I mutants, and mimetic peptides) and different phospholipid compositions in the efficiency of cholesterol efflux induced by rHDL<sup>445-452</sup>. On the other hand, rHDLs have been used as a tool for imaging-diagnosis<sup>453</sup>. For imaging applications, the appropriate tracers have been introduced in rHDL preparations such as fluorescent dyes or quantum dots for optical imaging, contrast agents as iron oxide or gadolinium for magnetic resonance imaging, radionuclides as zirconium-89 (<sup>89</sup>Zr) for PET, or gold based rHDL for CT, among others<sup>429,438,453,454</sup>.

## 4.2. Clinical trials. Successes and limitations

The interaction of HDLs with membrane cholesterol transporters is especially relevant in reducing the intracellular cholesterol content of macrophages that interact with the atheroma plaque. Reducing macrophage intracellular cholesterol content can avoid macrophage conversion into foam cells, a process that normally promotes atherosclerosis development<sup>455</sup>.

The inversely associated relationship between low HDL cholesterol levels and CVD risk in epidemiologic studies<sup>456,457</sup> has focused attention on HDL mimetics as a potential therapeutic tool and as an inspirational source for biomedical engineering. Several nanoparticles mimicking nascent HDL features have been

designed and used in several clinical trials for CVD therapy<sup>458,459</sup>. These include the following:

1. ETC216 (Esperion Therapeutics-Pfizer) or MDCO216 (The Medicines company-Novartis): rHDL containing apoA-I Milano, an apoA-I variant related with low cardiovascular risk and 1-palmitoyl-2-oleoyl-glycero-3-phosphocholine (POPC). ApoA-I is produced in bacteria. Protein to lipid molar ratio was 1:40<sup>460,461</sup>.
2. CER-001 (Cerenis Therapeutics)<sup>433</sup>: recombinant human apoA-I produced in eukaryotic cells and a lipid mixture composed of sphingomyelin (SM) and 1,2-dipalmitoyl-sn-glycero-3-phospho-(1'-rac-glycerol) (DPPG). The final molar ratio of apoA-I:SM:DPPG was 1:103:3.
3. CSL-111 (CSL Limited) and CSL-112 (CSL Behring)<sup>431,432</sup>. These formulations were prepared with human plasma derived apoA-I and soybean phosphatidylcholine (SoyPC). They differ in the molar ratio of protein to lipids. CSL-111 the first produced is 1:150, while CSL-112 was produced at 1:55 molar ratio.

These formulations designed to optimize cholesterol efflux by ABCA1, are the most studied nascent HDL mimicking nanoparticles. However, these nanoparticles have yielded markedly different results when tested *in vivo*. Initially, infusion of apoA-I Milano, a naturally occurring mutation of apoA-I associated with low prevalence of CVD<sup>462,463</sup>, showed regression of coronary atherosclerosis in a Phase II trial (The ApoA-I Milano Trial)<sup>445</sup>. Accordingly, apoA-I Milano was considered as a novel therapeutic strategy to favour reverse-cholesterol transport. However, failure to induce plaque regression in subsequent clinical trials led to discarding this formulation as a therapeutic drug<sup>464</sup>.

The next HDL mimetic to be tested as a cellular-sterol efflux inducer was CER-001. This nanoparticle showed the ability to rapidly mobilize large amounts of cholesterol into the HDL fraction; however, the mimetic did not cause any significant reduction in coronary atherosclerosis as evaluated in the CHI-SQUARE study<sup>433</sup>. Interestingly, posterior analyses showed an *U*-shaped CER-001 dose-response curve with the greatest atheroma regression occurring at a low concentration, while higher concentrations were inefficient in removing cholesterol due to the strong down regulation of the ABCA1 transporter<sup>465</sup>.

Finally, the CSL-112 reconstituted HDLs arose as an improvement upon their predecessor, CSL-111. CSL-111 initially showed a potential therapeutic effect<sup>446</sup>, but was disfavoured due to its hepatotoxicity. On the contrary, CSL-112 was well-tolerated and not associated with any significant alterations in liver or kidney function<sup>459</sup>. Moreover, CSL-112 has been found to enhance cholesterol efflux very efficiently. However, its beneficial potential in reducing major adverse cardiovascular events in a group of high-risk patients will be assessed in the on-going large Phase III clinical trial<sup>459</sup>, the AEGIS-II study (NCT03473223).

## **2. OBJECTIVES**

## **2. HELBURUAK**

## Hypothesis and objectives

High cholesterol levels, atherosclerosis and increased risk of cardiovascular events are a dangerous, directly interrelated triad leading to CVD, which has become the main cause of mortality in industrially developed countries. Finding new ways to reverse lipid build-up in the plaques is thus a task increasingly demanded by society of the scientific community.

The use of well-formulated apoA-I nanoparticles constitutes a significant advance towards clinical application because at therapeutic doses they neither present toxicity nor immunogenicity, making them appropriate for therapeutic application. Based on their biocompatibility, rHDL can be considered ideal carriers for the delivery of drugs and other therapeutic agents, as it has been shown for DNA and synthetic RNA, when incorporating cationic or zwitterionic lipids within rHDLs.

The discovery that multiple miRNAs participate in the progression of atherosclerosis and in the regulation of RCT by directly targeting ABCA1, has opened new opportunities in the use of nanotechnology-based miRNAs therapeutic platforms.

One of the most studied and well-known “target” of ABCA1 is miR-33a. As an intronic miRNA, miR-33a expression is linked to that of SREBP2 and both coordinately participate in the regulation of intracellular cholesterol levels. Among the multiple roles in the regulation of cholesterol metabolism, miR-33a functionally regulates the activity of ABCA1 interfering with the protein expression. Both therapeutic and macrophage-specific miR-33 knockdown intervention to reduce miR-33 levels provided promising results in the past. The advantages of using miRNAs rely both on their small repressive capacity on any single target gene, which is usually less than 2-fold and on their inherent ability to target multiple genes in the same biological pathway. It has been shown that the inhibition of miRNAs using antisense oligonucleotides promotes RCT through upregulation of the *ABCA1* gene. Therefore, some studies have used cationic lipid/polymer-based nanoparticles for

miRNA delivery in preclinical models. Given the huge complexity of atherosclerotic disease, the use of co-culture systems reflecting the cellular complexity of atherosclerosis has been identified as an advantageous approach to in vitro research. The importance of these in vitro studies relies on (i) the demand to overcome the translational gap, (ii) provide a suitable model to understand the physiological mechanisms underlying RCT and (iii) improve the efficiency of the nanoparticles in promoting cholesterol efflux, functional pathways that are central to the development of atherosclerosis.

In this context, and on the basis of the theoretical framework described in the introduction, **the general objective** of the present project has been, **to develop a novel anti-atherosclerotic therapeutic strategy, based on specifically targeted and functionalized nanoparticles, to increase reverse cholesterol transport (RCT) from foam cells.** This strategy will reduce the risk of the formation of new atheroma plaques, and revert the existing atherosclerotic lesions.

## Specific Objectives

1. Setting up the methodology to reconstitute HDL containing recombinant human apoA-I: design, development, and characterization of the nanoparticles.
2. To determine the efficiency of rHDL mimicking different physiologic maturation stages on promoting cholesterol efflux. The effect on cholesterol efflux efficiency of soybean PC (Soy-PC), 1,2-dipalmitoyl-sn-glycero-3-phosphocholine (DPPC), DPPC:Chol:1-palmitoyl-2-hydroxy-sn-glycero-3-phosphocholine (LPC) and DPPC:CE:LPC rHDL with similar sizes will be determined in THP-1 and J774A.1 macrophages, J774A.1 derived

foam cells and vascular smooth foam cells obtained from human carotid endarterectomy.

3. To investigate the contribution of lipid composition to the effectiveness of the nanoparticles in cholesterol removal.
4. Design, development, functionalization and characterisation of antagomiR-33-containing rHDL nanoparticles.
5. Development of 2D cell culture atheroma models as an experimental approach to understand the mechanisms of nanoparticle transport, their interactions with cells and efficacy to improve the translation of basic research into developing and bringing novel nanomedical tools.
6. Development of a therapeutic strategy to improve RCT and cholesterol efflux based in a two-step administration of rHDL. In a first nanodisc administration, antagomiR-33a-loaded DPPC:CE:LPC rHDLs will be used to induce the overexpression of ABCA1 transporter, and in a second step, DPPC rHDLs will be used to remove more efficiently cholesterol from foam cells.

## **3. MATERIALS AND METHODS**

## **3. MATERIALAK ETA METODOAK**

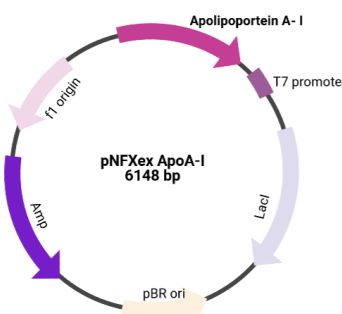
## 1. Giza apoA-I proteinaren purifikazioa

### 1.1. Bakterio anduiak eta plasmidoa

*Escherichia coli* (*E.coli*) DH5 $\alpha$  bakterio andua erabili zen apoA-I kodifikatzen duen plasmidoa amplifikatzeko. DH5 $\alpha$  bakterio andua azido nalidixikoa antibiotikoarekiko erresistentzia dute eta horren presentzian (25  $\mu$ g/mL) hazi ziren.

*E.coli* BL21 (DE3) pLysS bakterio andua aldiz, apoA-I proteina adierazteko eta purifikatzeko erabili zen. Andui honek T7 polimerasa du, proteina errekonbinanteen adierazpen efizientea ahalbidetzen duena eta IPTG (Isopropil- $\beta$ -D-1-tiogalactopiranosido) bidez aktibatzen dena. Andui hau 25  $\mu$ g/mL kloranfenikol antibiotikoaren presentzian hazi ziren.

Giza apoA-I purifikatzeko Oda irakasleak (Children's Hospital Oakland Research Institute, Oakland, CA, EEEB) adeitasunez emandako pNFXex bektorea erabili zen (**1. irudia**). Bektore honek giza apoA-I proteina osoa kodifikatzen du, N-terminalean histidina isatsa duena<sup>466</sup>.



**1. Irudia. ApoA-I purifikatzeko pNFXex bektorea.** Bektoreak anpizilinarekiko erresistentzia erakusten duen genea du, T7 polimerasaz gain.

## 1.2. Bakterio hazkuntza selektiboak

Bakterio anduiak LB (ingelesetik, *Luria Broth*) (Condalab, Spainia) medio likidoan hazi ziren, bakterioak hazteko mantenugaietan aberatsa den ohiko medioa. LB medio likidoa 20 g/L kontzentrazioan prestatu eta autoklabatu zen. Ondoren, medio likido honi intereseko bakterioak gehitzen zaizkio eta dagozkion antibiotikoak proportzio egokian. Gehituriko bakterioak izoztutako lagin batetik, kolonia batetik, edo bolumen txikiko beste hazkuntzatik eratorritakoa izan zitekeen.

Bakterio koloniak lortzeko unean, medio solidoko plakak behar zirenez, 20 g/L LB medioa 15 g/L agar-agarrekin (VWR International, EEBB) nahasi zen. Behin autoklabatuta, intereseko antibiotikoak gehitu eta nahastura plastikozko Petri plaketara jariatu ziren (10 mL/plaka). Behin solidotzean plakak 4 °C-tan kontserbatu ziren bakterioak transformatu unerarte.

## 1.3. Bakterio kimiokonpetenteen garapena

Bakterio kimiokonpetenteak, material genetikoa integratzeko gai diren bakterioak dira eta bakterio andui bat transformatzeko lehendabiziko pausua da. Hasteko, bakterioak (DH5 $\alpha$  edo BL21) LB medio bolumen txikian hazi ziren, dagokien antibiotikoarekin, OD<sub>600</sub> = 0,6 dentsitatea heldu arte. Jarraian, zelulen suspensioaren 2 mL zentrifugatu ziren (4.300 g-tan eta 1 minutuz). Jalkina 100 mM CaCl<sub>2</sub> esterilaren mililitro batean berreseki eta 30 minutuz izotzetan utzi zen berriro zentrifugatu arte (4.300 g, 10 minutuz, 4 °C). Ondoren, 900  $\mu$ L gainjalkina kendu eta jalkina berreseki zen. Lortutako bakterio kimiokonpetenteak kontserbatzeko, glizerola % 10ean (b/b) gehitu eta - 80 °C-tan mantendu ziren.

**1. Taula: Bakterioak hazteko medio selektiboak.**

Bakterio anduia + plasmidoa	Medio hazkuntza selektiboa
DH5α	LB + azido nalidixikoa (25 µg/mL)
DH5α + pNFXex	LB + azido nalidixikoa (25 µg/mL) + anpizilina (100 µg/mL)
BL21 (DE3)	LB + kloranfenikola (25 µg/mL)
BL21 (DE3) + pNFXex	LB + kloranfenikola (25 µg/mL) + anpizilina (100 µg/mL)

**1.4. ApoA-I plasmidoaren amplifikazioa eta purifikazioa**

ApoA-I plasmidoa amplifikatzeko *E.coli* DH5α bakterio kimiokonpetenteak transformatu ziren. Plasmidoak anpizilinarekiko erresistentzia eskaintzen duenez, bakterioak 100 µg/mL anpizilinaren presentzian kultibatu ziren, 25 µg/mL azido nalidixikoaz gain.

1 µg plasmido bakterio kimiokonpetenteen laginari (50 µL) gehitu zitzzion. 1 min eta 30 segundotan zehar 42 °C-tan berotu ostean, LB medioa gehitu zitzzion; jarraian, 37 °C-tan 45 minutuz inkubatzuz. Ondoren, lagina zentrifugatu (1.700 g, 5 min, giro tenperatura), gainjalkineko 450 µL kendu, eta jalkina geratzen zenarekin berresekiz. Transformatutako bakterioak anpizilina eta azido nalidixiko LB agar Petri plaketan erein ziren; eta gau osoan zehar 37 °C-tan inkubatu ziren.

Hurrengo egunean, lortutako kolonietako bat anpizilina eta azido nalidixikoa zeraman LB medio likidora transferitu zen 20 orduz, 37 °C-tan eta agitazioan inkubatzen utzi zelarik. Horren ostean, plasmidoen erauzketarako Qiagen® Plasmid Midi (QIAGEN, Alemania) kit komertziala erabili zen eta kontzentrazioa

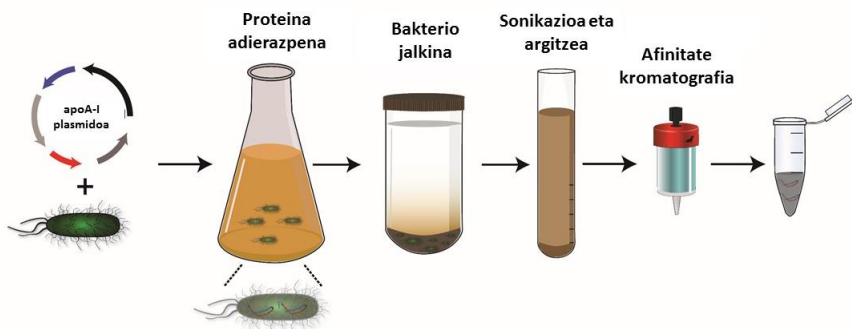
NanoDrop<sup>TM</sup> 2000 (Thermo Fisher Scientific, EEEB) bidez neurtu zen. Plasmidoa - 20 °C-tan kontserbatu zen.

### 1.5. Giza apoA-I proteina errekonbinantearen adierazpena eta purifikazioa

*E.coli* BL21 (DE3) pLysS bakterio anduia giza apoA-I plasmidoaz transformatu zen, *E.coli* DH5α bakterioekin egin zen modu berdinean (ikusi aurreko atala). Kasu honetan baina, LB agar plakak anpizilina eta kloranfenikola zeramatzan. Plakako kolonia bat antibiotikodun LB medioan (25 mL) txertatu eta gau osoan zehar hazten utzi zen, agitazioan 37 °C-tan. Hazkuntza asetua 750 mL LB-ra pasatu eta OD<sub>600</sub> = 0,6 dentsitatea lortu arte hazi ziren. Gero, proteinaren adierazpena 0,4 mM IPTGaz induzitu eta 3 orduz inkubatu ziren, 37 °C-tan. Ondoren, zelulak 6.000 g-tan, 10 minutuz zentrifugatu ziren, 4 °C-tan; eta lortutako jalkina proteina erauzteko disoluzioan ondo berreseki zen (20 mM Tris-HCl pH 8, % 0,1 Igepal (b/b), *Complete EDTA-free cocktail* (Roche, pastilla bat 50 ml-ko) eta PMSF 1:100 (b/b) proteasa inhibitzaileak. Zelulak sonikazio bidez apurtu ziren (10 ziklo: 10 segundu piztu, 10 segundu itzali, 6 mikrako anplitude batekin) Soniprep 150 sonikatzalean (MSE, Erresuma Batua) eta zelula-hondarrak kentzeko lagina zentrifugatu zen (10.000 g, 4 °C, 30 min). Gainjalkina 0,2 µm-tako filtroekin filtratu eta 1:1 (b/b) proportzioan karga-indargetzaileaz diluitu zen (40 mM NaPO<sub>4</sub>, 1 M NaCl eta 4 M guanidinio hidrokloruroa, pH 7,4). Ondoren, karga-indargetzaileaz orekatutako HisTrap<sup>TM</sup> TALON® Crude (5 mL, GE Healthcare, EEEB) nikelozko erretxinadun zutabeen kargatu zen, zirkuito itxian, ordu batez eta 4 °C-tan. ApoA-I proteina errekonbinanteak histidina isats bat du amino terminalean, purifikazioan nikelozko zutabeari lotzeko. Horren ostean, nahasketa zutabeen pasarazten utzi zen eta jarraian, garbitzeko soluzioa (20 mM NaPO<sub>4</sub>, 0,5 M NaCl, 20 mM imidazola, pH 7,4) pasarazi zen. Azkenik, eluzio-indargetzaileaz (20 mM NaPO<sub>4</sub>, 0,5 M NaCl, 0,5 M imidazola, pH 7,4) proteina eluitu zen, 0,5 mL-ko frakzioak jasoz. Proteinaren

presentzia Bradford bidez detektatu zen<sup>467</sup>; eta purutasuna % 15eko sodio dodezil sulfatozko poliakrilamidazko (SDS-PAGE) elekroforesi geletan aztertu zen. SDS-PAGE elektroforesia burutzeko 20 µL lagin, 5µL karga-indargetzaileaz (0,5 M Tris-HCl, 0,2 g/mL glizerol, 77,15 mg/mL DTT, 0,2 g/mL SDS, 1 mg/mL bromofenol urdina, pH 6,8) nahastu eta 100 °C, 5 minutuz berotu ziren. Gela *Coomassie Brilliant Blue* tindagaiaz tindatu zen eta markatzaile moduan SDS-PAGE Standards Broad Range erabili zen (Bio-Rad, EEBB).

Gelan positibo eman zuten frakzioak batu eta 24 orduz dialisatu ziren (20 mM Tris-HCl, 150 mM NaCl, 1 mM benzamidina, 1 mM EDTA, pH 8), 4 °C-tan, 14 kDa-eko porotako mintzean (5 litrotako 3 aldaketekin). Agregatuak kentzeko proteina soluzioa zentrifugatu zen (14.000 g, 15 min, 4 °C). Proteinari glizerola % 10ean (b/b) gehitu eta -80 °C-tan kontserbatu zen, 1 mililitroko alikuotetan (100 µM). Proteina kontzentrazioa 280 nm-tan absorbantzia neurtuz kalkulatu zen NanoDrop™ 2000 (Thermo Scientific, EEBB) aparatuaren eta apoA-ien iraungitze-koefiziente molarra erabiliz ( $\varepsilon = 32.430 \text{ M}^{-1} \cdot \text{cm}^{-1}$ , [ExPasy](#), SIB). Giza apoA-ien purifikazioaren laburpena **2. irudian** agertzen da.



**2. Irudia:** Giza apoA-ien produkzioaren laburpen eskematikoa bakterio sistemean.

## **Giza apoA-I purifikaziorako erabilitako indargetzaileak**

*(Mili-Q uretan prestaturikoak)*

### **Karga-indargetzailea (2X) pH 7,4**

- 40 mM NaPO<sub>4</sub> (Merck, Alemania)
- 1 M NaCl (Merck, Alemania)
- 6 M Guanidinio-HCl (VWR, EEBB)
- 

### **Garbiketa-indargetzailea pH 7,4**

- 20 mM NaPO<sub>4</sub>
- 500 mM NaCl
- 20 mM Imidazol (Merck, Alemania)
- 

### **Eluzio-indargetzailea pH 7,4**

- 20 mM NaPO<sub>4</sub>
- 500 mM NaCl
- 500 mM Imidazola
- 

### **Dialisu-indargetzailea pH 8**

- 20 mM Tris-HCl
- 150 mM NaCl
- 1 mM benzamidina (Santa Cruz Biotechnology, EEBB)
- 1 mM EDTA (Sigma-Aldrich, EEBB)
- 

### **Izozte-indargetzailea**

Dialisu indargetzailea + % 10 glizerola (b/b) (Sigma-Aldrich, EEBB)

## **2. Giza apoA-I rHDL nanodikoen prestakuntza**

rHDLak eratzeko, apoA-I intereseko lipido nahasturarekin nahasten da 1:125 erlazio molarrean (proteina lipidoarekiko). Erlazio horrekin 9-10 nm tarteko

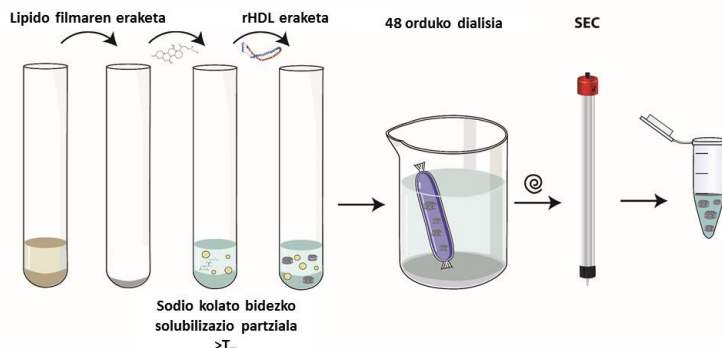
nanopartikulak eratu daitezke itsura diskoidal dutenak, nanodiskoak alegia. Adibide gisa, apoA-I/DPPC rHDLak eratzeko prozedura azalduko da. DPPC lipidoa kloroformo-metanolean (2:1, b/b) disolbatuta dago eta alikuotak -20 °C-tan kontserbatzen dira. Erabiltzeko unean, lipido tutua giro temperaturara hartu arte mantendu zen. Ondoren, lipido kantitate egokia beirazko tutu batera pasa eta N<sub>2</sub> gasa erabiliz lipidoa sikatu zen, tutua biraka eta eskuekin bero ematen, tutu hondoan lipido film siku bat lortu arte. Ondoren, hutsezko ponpan, ilunpetan utzi zen ordu eta erdiz, gutxienez, kloroformo hondarrak guztiz kentzeko.

Behin hutsezko ponpan sikatuta tutuari nanodiskoien prestakuntzarako indargetzailea, TEN indargetzailea, gehitu zitzaison (10 mM Tris-HCl, 150 mM NaCl, 1 mM EDTA, pH 8), lipido kontzentrazioa 12,5 mM izan zedin. Gomendagarria da TEN indargetzailea aurretik berotu izana, lipidoen disoluzioa bizkortzeko. Lipidoak disolbatzeko indarrez *vortex*-an nahastu ziren, 42 °C-ra dagoen ur bainuan tarteka berotuz (DPPCaren trantsizio temperaturan alegia, T<sub>m</sub>), MLV besikulen eraketa baimentzeko (ingelesetik, *multilamellar vesicle*). Jarraian, sodio kolato detergentea (Sigma-Aldrich, EEBB) gehitu zen lipido eta kolato proportzioa 1:1,4 (M/M) izateko doitu egin zelarik TEN indargetzaileaz. Pausu honetan sodio kolatoaren disoluzio kontzentratua prestatu zen, lipidoari gehitzerakoan ahalik eta gutxien diluitzeko. Kolatoa gehitu bezain laster, tutua *vortexeatu* egiten da. Jarrian tutua ur-bainuan T<sub>m</sub>-an uzten da eta 5 minuturo *vortexeatu* behar da, 3 ziklo amaitu arte (15 min totalean).

Denbora tarte horretan proteina prestatzen da. Beharrezko apoA-I alikuotak desizoztu eta 100 µM lortu arte TEN indargetzailearekin diluitu ziren, alikuotak kontzentrazio horretan jada ez bazeuden. Proteina bolumena, lipido bolumenaren berdina izan behar da, modu horretan, lipido eta proteina nahasterakoan, 1:125 (mol/mol) erlazioa beti mantenduko da (**3. irudia**). Proteina gehitzeko unean

vortexeatu eta lortutako nahasketa 12 orduz gutxinez, 42 °C eta 800 rpm-tan inkubatu zen, *Thermomixer*-ean (Eppendorf, Alemania).

Inkubazioa amaitzean, nanodisko soluzioa zelulosazko dialisi mintzera pasa (14 KDa-eko poroak, Sigma-Aldrich, EEBB) eta TEN indargetzailearen 5 litro aurka dialisatu zen kolato hondarrak kentzeko, 42 °C -tan eta 48 orduz, 24 orduro aldaketa bat eginez. Behin dialisia amaituta, nanodiskoak dialisi mintzetik jaso eta agregatuak kentzeko 13.100 g-tan zentrifugatu ziren 30 minututan, ondoren, 0,2 µm-ko filtratik pasaraziz (Sarsted, Alemania). Hemendik aurrera nanodiskoak 4 °C -tan mantendu ziren.



**3. Irudia: rHDL nanodiskoen prestakuntzaren eskema.** Lipido nahasketa sikitzean tutuak lipidoen  $T_{man}$  berotu ziren, tarteka nahastuz, horrekin MLVak lortu zirelarik. Sodio kolatoarekin mintzak partzialki disolbatu ziren eta apoA-I gehikuntzarekin, rHDLak sortu ziren. Gau osoko inkubazio ostean, rHDLak dialisatu eta SEC bidez purifikatu ziren.

rHDLen prestakuntza beste lipido konposizio batekin egiteko, lipidoak sikitzeko unean lipido nahastura presatzen da, intereseko erlazioan baina kontuan izanda, lipido totala 12,5 mM izan behar dela. Horrez gain, lipidoen kurbadura aintzat hartu beharra dago, izan ere rHDLak nanodiskoak dira eta edozein lipido ez da gai horrelako mintz egiturak eratzeko. Hala, kurbadura positibo eta negatiboa duten lipidoak ezingo dira portzentaje altu batean erabili, lipido mota horiek nanodiskoak bezalako egitura zurrunak baino, mizelak bezalako mintz egitera sortzeko joera

baitute<sup>468</sup>. Nolanahi ere, rHDLen sorreran lipido bakoitzaren kontzentrazio maximoa zehaztu daiteke frogak eginez.

Lan honetan zehar, rHDL konposizio desberdinak erabili ziren, **2 . taulan** agertzen den moduan.

### 2. Taula. prestaturiko apoA-1en rHDL konposizioak

rHDL izena	Lipidoak	Lipidoen arteko erlazio molarra (%)
DPPC	Dipalmitoil-fosfatidilkolina fosfolipidoa	100
DPPC:CE:LPC	<ul style="list-style-type: none"> <li>- DPPC fosfolipidoa.</li> <li>- CE: kolesterol esterifikatua, konkretuki, kolesterol linoleatoa.</li> <li>- LPC: 16:0 lisofosfatidilkolina lisofosfatidilcholina</li> </ul>	75:20:5
DPPC:Chol:LPC	<ul style="list-style-type: none"> <li>- DPPC fosfolipidoa.</li> <li>- Chol: kolesterol askea.</li> <li>- LPC: 16:0 lisofosfatidilkolina</li> </ul>	85:10:5
Soy-PC	Sojatik erauzitako fosfatidilkolinen nahastura	100

### 3. Taula: rHDLak prestatzeko erabilitako lipido zerrenda.

Lipidoa	Izen komertziala	Erreferentzia	Etxe komertziala
DPPC, fosfolipidoa	16:0 PC (DPPC) <i>1,2-dipalmitoyl-sn-glycero-3-phosphocholine</i>	850355	Avanti Polar Lipids
CE, kolesterol esterifikatua	Cholesteryl linoleate ≥98% (HPLC; detection at 205 nm)	C0289	Sigma-Aldrich

<b>Chol, kolesterol askea</b>	Cholesterol (plant)	700100	Avanti Polar Lipids
<b>LPC, lisofosfatidikolina</b>	16:0 Lyso PC 1-palmitoyl-2-hydroxy- sn-glycero-3- phosphocholine	855675	Avanti Polar Lipids
<b>Soy-PC, sojazko fosfatidikolinak</b>	Soy-PC L- $\alpha$ -phosphatidylcholine (Soy)	840054	Avanti Polar Lipids

## 2.1. Kolato hondarren neurketa metodo kalorimetrikoaz

rHDL amaierako soluzioan sodio kolatoaren hondarrik ez zegoela frogatzeko honen neurketa egin zen. Kolatoa behazun gatzetan oinarritutako detergentea da eta hura azido sulfurikoarekin tratatzean lortzen den produktua metodo kalorimetrikoaz neurtu daiteke<sup>469</sup>. Azido sulfuriko kontzentratua kolatoaren eratzunaren talde hidroxiloarekin erreakzionatzen du eta lortutako produktuaren absorbantzia 389 nm-tan neurtu daiteke.

Hala, lehendabizi, TEN indargetzailean disolbatutako sodio kolatoaren zuzen patroia prestatu zen 0-0,4 mg/mL bitartekoa. Jarraian, lagin bakoitzaren 50  $\mu$ L (bai zuzen patroia eta bai rHDLak), azido sulfuriko puruaren ( $\geq 98\%$ , VWR, EEBB) 800  $\mu$ L-rekin nahastu ziren 2 mL-tako tutuetan (segurtasun-itxitura zutenak, Eppendorf, Almeania) eta kanpainen. Nahasturak erreakzio exotermikoa eragiten duenez, tutuak kontu handiz itxi eta *vortexeatu* ziren. Behin hoztean, lagin bakoitzaren absorbantzia 389 nm-tan neurtu zen, plastikozko kubetetan. Zuria egiteko TEN indargetzailea erabili zen. Gure laborategian erabilitako protokoloa jarraituta ez zen kolato hondarrik detektatu prestaturiko rHDL laginetan.

## 2.2. rHDL nanodiskoen purifikazioa

rHDLen purifikazioa tamaina baztertzeko kromatografia (ingelesez, *size exclusion chromatography* edo *SEC*) bidez egin zen, Superdex 200 10/300 GL (GE Healthcare) gel filtraziozko zutabea erabiliz.

Gel filtraziozko zutabeak porotasun espezifiko duten erretxinaz eratuta daude lagineko molekulak tamainaren arabera banatzea ahalbidetzen duena. Izan ere, molekula txikienak erretxinaren poroetatik sartzen direnez, denbora gehiago beharko dute zutabe osoa zeharkatzeko. Molekula handiak aldiz, poro txikietatik ezingo dira sartu eta bizkorrago eluituko dira. Hala, gel filtrazio kromatografian zutabe bakoitzak tamaina tarte batean aurkitzen diren molekulak banatzeko ahalmena dute. Superdex 200 10/300 GL 10.000-600.000 Dalton bitarteko molekulak edota partikulak banatzeko gai da eta rHDLak tarte horretan aurkitzen dira. Hala ere, aipatu beharra dago Superosa 6 Increase 10/300 GL (GE Healthcare, EEBB) zutabea ere erabili zela rHDLak purifikatzeko.

Hala, kromatografia egiteko lehendabizi, zutabea kalibratu egin zen molekula tamaina estandarrak erabiliz (Amersham Biosciences, Erresuma Batua). TEN indargetzailea fase mugikor moduan erabili zen eta kromatografia 4 °C-tan egin zen, 0,2 mL/min fluxu abiadura erabiliz. Eluzio profilak erretentzio bolumen gisa adierazi ziren. Zutabe bakoitzaren parametro maximoak [etxe komertzialaren web orrialdean](#) kontsultatu daitezke.

rHDLen purifikazioa ere, 4 °C-tan egin zen, TEN indargetzailea erabiliz eta 0,2 mL/min fluxu-abiadurarekin. 500 µl-tako *loop*-a erabiliz, 500 µl lagina zutabean txertatu zen, 1 mL-ko xiringa erabilz, eta 0,5 mL-tako frakzioak jaso ziren. Txertaketa zikloak modu berdinean errepikatuz ziren rHDL lagin guztia purifikatu arte. Purifikazioak GE AKTA Purifier 10 FPLC System w/ UPC-900 (GE Healthcare, EEBB) burutu ziren.

## 2.3. rHDLen karakterizazio biofisikoa

### 2.3.1. ApoA-I-en egituraren azterketa Dikroismo Zirkularraren (DZ) bidez

Dikroismo zirkularra (DZ) absorbantzian oinarritutako teknika espektroskopikoa da, makromolekula biologikoen egitura sekundarioei eta tertziarioei buruzko informazioa eskaintzen duena, beste erabileren artean. Leginak zirkularki polarizatutako argi destrogiro (eskumatara) eta lebogiroaren (ezkerretara) aurrean erakusten duen absorbantzien arteko differentzia neurten da, eliptizitate [ $\theta$ ] moduan ezagutzen dena. Differentzia horren balio positibo batek, argi destrogiroaren xurgapen handiago bat esan nahi du; eta balio negatibo batek, argi lebogiroarena. Proteina baten egitura sekundaria lortzeko, eliptizitatea 190-260 nm tarteko uhin luzeratan ( $\lambda$ ) neurten da eta lortutako espektroaren arabera estruktura sekundaria ondorioztatu daiteke<sup>470</sup>.

$\alpha$ -helizeak dira apoA-I proteinan agertzen diren estruktura nagusienak.  $\alpha$ -helize baten DZ espektroak bi minimo aurkezten ditu:  $\lambda_{222}$  eta  $\lambda_{208}$ -tan, eta maximo bat  $\lambda\lambda_{190}$  inguruan. Banda hauen intentsitateek, aztertzen ari garen proteinaren eliptizitate proportzioa adierazten dute eta  $\lambda_{222}$  balioarekin  $\alpha$ -helize ehunekoa kalkulatu daiteke.

Lan honetan apoA-I proteinaren estruktura sekundaria aztertu zen, izan ere rHDLak osatzean proteinak bere alfa helizitatea emendatzen du. Neurketa hau rHDLen formakuntza egokia baiezatzeko erabili zen.

ApoA-ien estruktura sekundaria termostatizatuko JASCO J-810 Spectropolarimeter dikrografoan neurtu zen. Neurketak 0,1 cm-ko pasu-optikoa duen kuartzozko kubeta batean egin ziren eta 25 °C, 1 segundoko erantzun denbora, 1 nm-ko banda zabalera eta 50 nm/scan-eko abiadura erabili zen. Espektro bakoitza 15 akumulaziokin lortu zen eta TEN indargetzailearen

espektroaren kenketa eginez zuzendu zen uhin-luzera bakoitzean. Lortutako balioa DEG esango diogu. Jarraian, uhin luzera bakoitzeko  $\theta_{\text{MRE}}$  (ingelesetik, *mean residue ellipticity*) kalkulatu ziren hurrengo formula erabiliz:

$$\theta_{\text{MRE}} = \frac{\text{MRW}_{\text{DEG}}/1000}{10 * [\text{apoA-I}] * \text{pasu-optikoa}}$$

$$\text{Non MRW} = \frac{PM}{aa-1} \text{ den}$$

*[apoA-I]: proteina kontzentrazioa, g/mL-tan; pasu-optiko luzera, cm-tan; PM: pisu molekularra; aa: aminoazido kopurua.*

Dikroismo espektroak  $\lambda$  vs. MRE irudikatuz adierazi ziren. Proteinaren  $\alpha$ -helizitatea rHDL konposizio bakoitzerako hurrengo formula erabiliz kalkulatu zen, 222 nm-tako  $\theta_{\text{MRE}}$  balioa erabiliz: %  $\alpha$ -helix =  $((\theta_{\text{MRE}/222} + 3000)/(36000 + 3000) \times 100$ .

### 2.3.2. Tamainaren determinazioa Dynamic Light Scattering (DLS) bidez

Metodo hau lagineko partikulek eragiten duten argiaren dispersioan oinarritzen da, zehazki argiaren dispersioak denboran zehar duen aldakortasuna neurtzen du puntu zehatz batean ( $173^\circ$ ). Aldakortasun hura radio hidrodinamikoarekin erlazionatzen du. Aldakortasuna handiagoa izango da partikulak txikiagoak direnean hauen mugimendua handiagoa baita. Horri esker, suspentsioan dauden partikulen tamainaren araberako banaketa-profila zehazten du.

rHDLen radio hidrodinamikoa DLS bidez neurtu zen,  $10 \mu\text{m}$  eta  $0,3 \text{ nm}$  bitarteko diametroko partikulak neur ditzakeen *Nano-S Zetasizer* (Malvern Instruments, Erresuma Batua) aparatuan.

Neurketak 3 ziklo berdineta egin ziren 37 °C-tan. Ziklo bakoitzean 15 neurketa egin ziren, bakoitza 10 segundokoa. Biskositatea eta errefrakzio indizeak TEN tanpoira doitu ziren eta datuak *Zetasizer software* bidez aztertu ziren.

### *2.3.3. Nanodiskoen tamaina eta itxuraren azterketa Transmisiozko Mikroskopio Elektronikoaz (TME)*

rHDLen tamaina eta morfologia mikroskopia elektroniko bidez analizatu ziren. Euskarriaren eta partikulen arteko kontrastea hobetzeko, partikulen tindaketa negatibo deritzon teknika erabili zen. Lehendabizi rHDLak kobrezko saretxo batean (Cu-300CN; Pacific Grid-Tech, EEBB) immobilizatu ziren. Gehiegizko disoluzioa kendu eta sarea hiru aldiz garbitu zen ur desionizatuan. Ondoren, uranil azetatozko (pH 4,6) disoluzioaren tanta bat (~30 µL) aplikatu zen % 1ean (p/b) eta 1-3 minutuz ilunpean utzi zen, soberazko tindatzailea kendu aurretik. Azkenik, ur desionizatuarekin garbitu eta lehortzen utzi ziren. Laginen prestaketa eta irudien lorpena *SGIker* zerbitzuetan egin zen (EHU/UPV, Leioa).

Partikulen tamaina zehazteko Feret-en diametroa erabili zen, automatikoki partikula individualak hautatuz (Image J software erabilita) eta gero, gainjarritako edo kaltetutako partikulak kendu ziren. Horrela, tamainaren banaketaren analisi estatistikoa egiteko, rHDL laginen mikrografia bakoitzeko 1.600 partikula neurtu ziren .

### *2.3.4. rHDLen trantsizio tenperatura: anisotropia fluoreszentearen neurketa*

Anisotropia fluoreszentea erabilita rHDL bakoitzaren trantsizio tenperatura ( $T_m$ ) aztertu zen. Anisotropiak bigeruza lipidikoen ordena-maila jakitea ahalbidetzen du, aukeratutako fluoroforoaren orientazio aldaketek eragiten duten polarizazio aldakuntzak erabiliz<sup>471</sup>. Laburki, teknika honetan bai kitzikatutako zein emititutako argia polarizatu egiten da, hau da, orientazio

jakin bat dute. Konkretuki bi orientazio filtratzen dira: horizontala eta bertikala. Fluorimetroak, argi kitzikatu eta emititutakoaren arteko argiaren erlazioaren intentsitatea neurten du (I). Zehazki, beti bertikalki polarizatzen den kitzikatu argiarekiko, paraleloa (<sub>V</sub>) edo perpendikularra (<sub>H</sub>) den fluoreszentzia neurten du. Eta hurrengo formula jarraituz, polarizazio balioa kalkulatu daiteke:

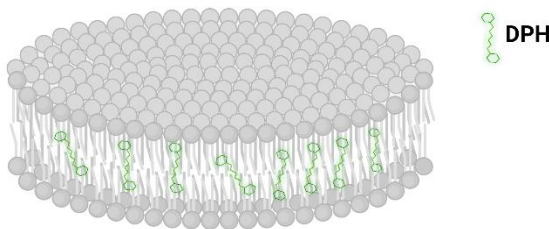
$$P = \frac{I_{VV} - G \cdot I_{VH}}{I_{VV} + G \cdot I_{VH}}$$

Non G, aparatu bakoitzaren zuzenketa balio bat den.

$$G = \frac{I_{HV}}{I_{HH}}$$

Lipido mintz batean dagoen fluoroforo baten emisioaren despolarizazio-mailak, kitzikatu den fluoroforo populazioaren hasierako orientazioaren galera adierazten du. Gainera, fluoroforoen errotazio gradua lipido paketatze molekularragatik mugatuta dagoela erakutsi dute ikerketek<sup>472,473</sup>.

Lan honetan DPH zunda fluoreszentea erabili zen, rHDLen bigeruza lipidikoan tartekatzen dena (**4. irudia**). Temperaturaren igoerarekin batera, rHDLen lipido geruzaren jariakortasuna emendatzen da eta, horrekin batera, DPHaren errotazio gradua. Hala, DPHaren errotazio mugimendua polarizaio balioarekiko alderantziz proportzionala izanik, temperaturaren igoerarekin polarizazio jaitsiera kurbak lortzen dira. Jaitsiera horren inflexio puntu trantsizio tenperatura moduan ezagutzen da ( $T_m$ ).  $T_m$  balioa nanopartikula konposizio bakoitzak duen zurruntasunari buruzko informazioa eskaintzen du: zenbat eta  $T_m$  balio txikiagoa, orduan eta estruktura zurrunagoa duela esan nahi du.



**4. Irudia: DPH fluoroforoaren kokapenaren irudi eskematikoa rHDLen bigeruza lipidikoan.** rHDL eskema honetan apoA-I proteina ezabatu da DPHaren kokapena ikusi ahal izateko. rHDLak DPHarekin inkubatzean, DPHa molekula hidrofobikoa izanda bigeruza lipidikoan tartekatzen da, konkretuki fosfolipidoen alde apolarrean. Temperatura igo ahala DPHaren errotazio gradua emendatzen joango da, lipido bigeruzaren jariakortasunarekin batera.

Horretarako, laginen 2 µg/mL diluzioak DPHarekin inkubatu ziren. Metanolean disolbatuta dagoen DPHa lagin bakoitzari gehitu zitzaion 1:75 erlazio molarrean (zunda lipidoarekiko), eta ordu batez 25 °C-tan agitazioan inkubatu ziren, DPHa nanopartikulen bigeruza lipidikoan txertatzeko helburuarekin. rHDL konposizio ezberdinez gain, giza plasmatik purifikatutako HDLak kontrol moduan erabili ziren.

DPHaren polarizazio fluoreszentzia neurtu zen ( $\lambda_{\text{ex}}$ : 360 nm,  $\lambda_{\text{em}}$ : 428 nm) SFM25 espektrofluorimetroan (Kontron Instruments, Suitza). Laginen neurketak 25 °C eta 60 °C bitartean egin ziren, argi fluoreszentiza balioak  $I_{\text{VV}}$  eta  $I_{\text{VH}}$  2 graduro jaso zirelarik.

### 2.3.5. rHDLen lipido eta proteina ratioaren determinazioa

Nanodiskoetako fosfolipido kantitatea neurtzeko asmotan, Fiske-Subbarow metodo kolorimetrikoa erabili zen, laginean aurkitzen den fosforo inorganikoa neurten duena, hain zuzen ere<sup>474</sup>. Lan honetan baina, horren bertsio erreduzitua erabili zen, espero ziren kontzentrazioak txikiagoak zirelako<sup>475</sup>. Horretarako, 12-hidrato-Na<sub>2</sub>HPO<sub>4</sub>·12H<sub>2</sub>O disoluzioaren 0-25 mM bitarteko zuzen patroia egin zen. Gero, bai zuzen patroia eta bai lagunei azido perklorikoa (% 70, b/b) gehitu zitzaien eta nahastu ostean 205 °C-tan zegoen plakan sartu ziren, 45 minutuz. Perklorikoak molekulak liseritzen ditu, fosforo atomoak askatuz horien neurketarako. Ondoren, laginak atera eta hoztu ostean, molibdato erreaktiboa eta azido askorbikoa (% 10, p/b) gehitu zitzaien, ondo vortexeatu eta ur-bainuan 6 minutuz berotu ziren (120 °C). Horren ostean, fosforo kantitatea, eta beraz, lipido kontzentrazioa, laginen absorbantzia 830 nm-tan neurtzean ondorioztatu zen.

rHDL proteina kontzentrazioa aldiz, 280 nm-tan absorbantzia neurtuz kalkulatu zen NanoDrop™ 2000 erabiliz ( $\epsilon = 32.430 \text{ M}^{-1} \cdot \text{cm}^{-1}$ ).

Balio hauetatik lipido eta proteina erlazio molarra ondorioztatu zen.

#### 2.3.6. rHDLen apoA-I kantitatearen determinazioa

rHDLetara inkorporatutako apoA-I molekulak kuantifikatzeko, dimetil suberimidatoa (DMS, Thermo Scientific, EEBB) erabili zen. DMS molekula gurutzatzaire bat da (ingelesez, *crosslinker*) hau da, oso hurbil dauden proteinak lotzeko balio du proteinen arteko interakzioak detektatzeko balio duena. DMSa, mintzarekiko iragazkorra da, 8 atomo ditu (11 Å) eta bi muturretan aminekiko erreaktiboa den imidoester talde bat du. Hala, purifikatutako rHDLetan zenbat apoA-I molekula barneratzen diren jakiteko DMSa erabili zen. Konposatura lisina-hondakinen ε-amino taldeekiko eta N-terminalaren α-aminekiko erreaktiboa da 7 eta 10 arteko pH-eremuan (pH 8-9 optimoa). Horregatik lehendabizi, rHDLei pHa aldatu zitzaien, 100 µL rHDLei 1 µL NaOH 1M gehituz. Ondoren, rHDLei DMS 1:200

erlazio molarrean gehitu zitzaien. DMS stocka (10 mM) aurretik 0,2 M trietanolamina indargetzailean prestatu zen (pH 8). Nahasketa ordu batez 25 °C-tan inkubatu zen agitazioan. DMSak eragindako loturak kobalenteak direnez, laginak %12,5eko SDS-PAGE batean aztertu ziren.

#### 2.4. rHDL masa molekulararen azterketa masa-fotometria bidez.

Masa-fotometria (ingelesez, *mass photometry*) molekula bakarren masa-neurketa aztertzeko metodo berri bat da<sup>476</sup>. Partikula batek sakabanatzen duen argi kantitatea partikularen bolumenarekin eta erreifrakzio-indizearekin linealki eskalatzen da. Sakabanatze-seinalea molekularen masarekiko zuzenki proporcionala denez, teknika hau molekula baten masa molekularra, argiarekin neurtzea ahalbidetzen du. Hala, sakabanatze-seinaleak masarekin duen korrelazioari esker, masa-fotometria biomolekulen azterketarako analisi-tresna unibertsala bihurtu da.

Masa fotometroa (Refeyn Ltd., Erresuma Batua) rHDLen masa molekularra neurtzeko erabili zen, nire estantzia bitartean, *Copenhagen Center for Glycomics* (Kopenhage, Danimarka) ikerketa zentroan.

Horretarako, laginak neurtzeko mutaia prestatu behar da: beirazko porta garbi batean 4 zulo dituen silikonazko sare bat kokatzen da (ingelesez, *gasket*). Mutaia masa fotometroaren laserraren gainean kokatzen, olio-tanta baten gainean. Silikonazko sareen zuloetan laginak kokatzen dira, banan-bana, neurtzeko unean (20 µL maximo). Neurketak egiterako unean ingurune garbia (hauts partikulak eta olio-orbanak saihestu) eta lasaia (bibrazio gabekoa) mantentzea garrantzitsua izango da.

Hala, lehendabizи, masa fotometroa TEN indargetzailean prestaturiko, pisu molekular ezaguna duten molekula estandarren soluzioaz kalibratu zen (Refeyn Ltd., Erresuma Batua). Kalibrazio egokia lortutakoan rHDLak TEN indargetzailean

diluitu ziren (40 nM). Teknika honetan, laginaren kontzentrazioak garrantzi handia du. Izan ere, lagineko molekula edo partikulak bata besterengandik banatuta egon behar dira, *single-molecule* edo banakako neurketak egiteko. rHDL laginak neurtzerako unean bi aldiz gehiago diluitu ziren.

### 2.5. rHDLen markaketa fluoreszentea

rHDLak fluoreszenteki markatzeko Dil (Vybrant™ Dil, Invitrogen) zunda fluoreszentearekin egin zen. Dil zunda lipofilikoa denez, lipidoen artean tartekatzeko gaitasuna du, kasu honetan, rHDLen mintz bikoitzan.

rHDLak markatzeko erabilitako erlazoa hurrengoa izan zen: 0,1 mg/mL-ra dagoen 1 mL rHDLei 10 µL Dil soluzioa gehitu zitzzion eta 2 orduz 37 °C-tan inkubatuz, agitazioan eta ilunpetan. Jarraian, aurretik TEN indargetzailean orekatutako Sephadex G25 gel iragazpen zutabetik (PD-10 desalting column, GE Healthcare, EEBB) pasarazi ziren Dil soberakina kentzeko. Markaketa ostean rHDL kontzentrazioa berriro neurtu zen, proteina neurtuz NanoDrop™ 2000 erabiliz.

## 3. rHDL bidezko miRNAen garraioaren azterketa

### 3.1. miRNA eta rHDL arteko lotura azterketa

Jakina da HDLak azido nukleikoak garraitzeko ahalmena dutela. Aurretik deskribatu den moduan azido nukleiko eta HDLen lipidoen lotura, erakarpen elektrostatikoetan oinarritzen da<sup>477,478</sup>. izan ere, azido nukleikoen karga negatiboak lipidoen karga positiboengandik erakartzen dira. Horretarako beraz, HDLen azalean karga positiboko lipidoak egon beharko lirateke edota momentu dipolarra erakusten duten lipido *zwitterionikoak*, DPPCa bezala. DPPCa karga neutroa duen lipidoa izan arren, PC buru polarrean agertzen diren karga positibo eta negatiboak

direla eta, momentu dipolarra eratzen da<sup>479</sup>. Hori dela eta karga positiboko gunea rHDLen azalean ikusgai geratzen dira, azido nukleikoekin lotzeko aproposa dena.

Gure laborategian rHDLak miRNAk garraiatzeko helburuarekin eratu ziren. Gure laborategiko aurreko emaitzen oinarrituz, miRNAk garraiatzeko DPPC:CE:LPC aukeratu ziren.

Horrela, lehendabizi rHDL:miRNA erlazio egokia zehaztu behar zen. Horretarako, saturazio kurbak egin ziren, cel-miR-67 rHDLekin 0,001:1-10:1 bitarteko erlazio molarretan inkubatuz (miRNA:rHDL, non rHDL kontzentrazioa proteina kontzentrazioari dagokion). Laginak ordu batez 30 °C-tan agitazioan inkubatu ziren izan ere, lipido eta azido nukleikoen arteko lotura, lipidoa gel fasean dagoenean faboratuta dago hau da, lipidoen  $T_m$  balioaren azpian<sup>480</sup>. rHDLei batu ez zen soberazko miRNA kentzeko, TEN indargetzailearekin 4 garbiketa egin ziren Amicon™ Ultra-4 Centrifugal Filter Units zentrifugazio tutuak erabiliz (100.000 Daltoneko poroak, Merck, Alemania) eta lagin bakoitza 200  $\mu\text{L}$  arte kontzentratu ziren.

### *3.1.1. rHDLtik miRNAren erauzketa*

rHDLetara lotutako miRNA kantitatea neurtzeko alderantzizko transkripzio-polimerasaren kate-errereakzio kuantitatiboa (qRT-PCR, ingelesetik *quantitative reverse transcriptase polymerase chain reaction*) egin zen. Teknika honekin laginetan agertzen den intereseko azido nukleikoen amplifikazioa eta aldi berean kuantifikazioa egin daiteke.

Horretarako, lotutako miRNAren erauzketa egin zen. Lagin bakoitzari 1  $\mu\text{L}$  (20 pmol) UniSp6 spike-in RNA (QIAGEN, Alemania) gehitu zen, erauzketa kontrol moduan eta kuantifikazioa egitean horrekiko erlatibizatzeko. Ondoren, laginei NZYol (NZYTech) soluziotik 1 mL gehitu zen. NZYol fenola eta bestelako konposatuak dituen soluzio komertziala da, zeluletatik eta ehunetatik ARN totala isolatzeko balio duena. Gero,

200 µL kloroformo gehitu eta 15 segundoz *vortexeatu* ziren, jarraian 15 minutuz zentrifugatu zirelarik (12.000 g, 4°C). Pausu horrekin, rHDLei lotutako miRNAk beste konponenteetatik banatu ziren. Hala, laginetako goiko fase akuosoa jaso eta etxe komertzialaren protokoloa jarraituz, miRNAREN purifikazioa egin zen.

### 3.1.2. miRNAREN kuantifikazioa

Aurretik erauzitako miRNAREN DNA osagarria sintetizatzeko (cDNA, ingelesetik *complementary DNA*) miRCURY LNA miRNA PCR System (QIAGEN, Alemania) kit-a erabili zen fabrikatzailerentzat argibideak jarraituta. Kit honek hasle unibertsalak erabiltzen ditu eta RT-PCRa C1000 Thermal Cycler CFX96 Real-Time System (Bio-Rad Laboratories Inc, CA, AEB.) termoziklatzailea erabilita egin zen.

Behin cDNA eskuratutakoan, qRT-PCR bidez lagin bakoitzaren miRNAREN adierazpen maila aztertu zen. MiRNA kuantifikatzeko, 4 µL cDNA laginari, 5 µL SYBR Green (NZYTECH) eta 1 hasle nahasketa gehitu zitzaien (**6.taula**). qRT-PCRa 96 putzutako PCR plaka batean egin da (Bio-Rad Laboratories Inc., CA, AEB) C1000 Thermal Cycler CFX96 Real-Time System termoziklatzailean (Bio-Rad Laboratories Inc., CA, AEB). Polimerasaren aktibazioa 95°C-tan gertatzen denez, erreakzioa tenperatura horretan hasten da eta 10 minutuz mantentzen da, cDNA osatzen duten harizpi biak desnaturatzen daitezten. Ondoren, 60 °C-tara jaisten da minutu batez, haslek cDNAra lotu eta Taq polimerasa aktibatu dadin. Honi esker, anplifikazioa gertatzen da. Termoziklatzaileak SYBR Green fluoroforoak askatutako fluoreszentzia neurtzen du eta, horretarako, lagina 488 nm-ko uhin luzeran kitzikatzen da eta 522 nm-ko uhin luzeran jasotzen da seinalea.

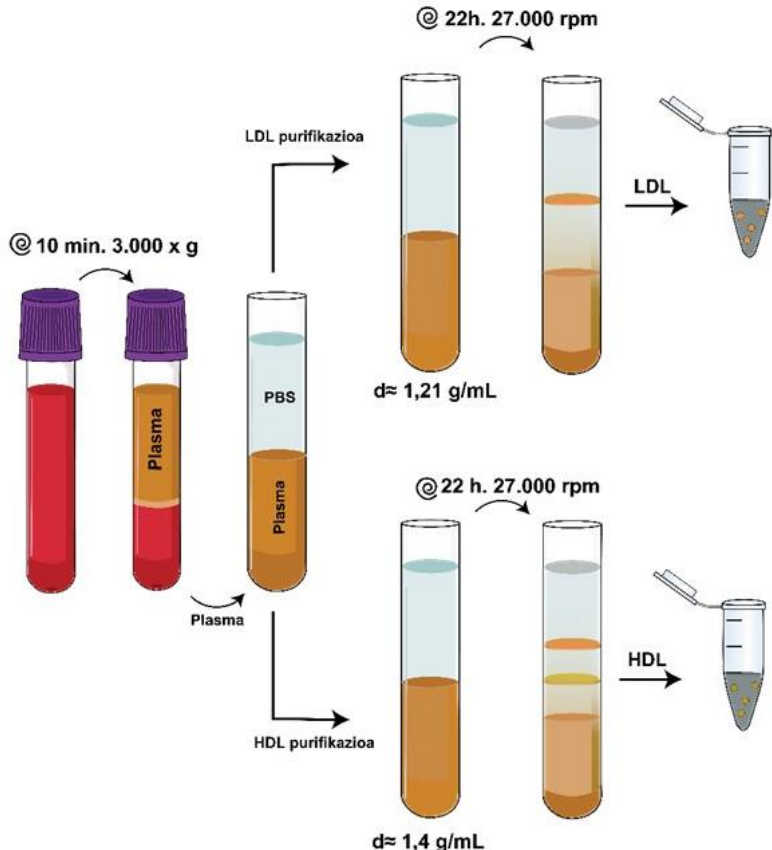
Neurketarekin bukatutakoan, tenperatura berriz ere 95°C-tara bueltatzen da 10 segundoz, prozesua berriz hasteko. Honelako 40 ziklo errepikatu dira, cDNA molekula guztiak anplifikatu direla bermatzeko.

#### 4. Lipoproteinen purifikazioa

Dentsitate baxuko lipoproteinak (LDL) eta dentsitate altuko lipoproteinak (HDL) boluntarioei ateratako odoletik erauzi ziren. Horretarako, EDTA zuten hodietan ateratako odola 10 minutuz,  $3.000 \times g$ -tan eta  $4^{\circ}\text{C}$ -tan zentrifugatu zen, odoleko plasma eta zelulak banatu ahal izateko. Odol plasma  $-80^{\circ}\text{C}$ -tan kontserbatu daiteke. Odol plasmatik, lipoproteinak erauzteko eta gainontzeko proteinetik banatzeko gradientezko ultrazentrifugazio isopiknikoa egin zen. Horren arabera, dentsitate gradiente bat eratzen da, kasu honetan, KBra erabiliz (Sigma-Aldrich, EEBB) eta zentrifugazio bidez nahasketaren partikulak dentsitatearen arabera banatzen dira<sup>481</sup>. Horretarako lehendabizi bi fase prestatu ziren ultrazentrifugazioarako tutuetan. Tutuen beheko fasea plasmari dagokio. Honi KBr-a gehitu zitzaion dentsitate jakin bat iritsi arte. LDLak purifikatzeko 1,21 g/mL-ko dentsitatea heldu arte gehitu zen; aldiz, HDLak purifikatzeko 1,4 g/mL-ko dentsitatea heldu arte. KBr-a disolbatu eta plasmaren gainean, PBS tanpoi hotza gehitu zen emeki-emeki, bi faseak nahas ez zitezen. Laginak 27.000 rpm abiaduran zentrifugatu ziren 22 orduz eta  $4^{\circ}\text{C}$ -tan, SW 28.1 errotorea erabilita. Amaitzeko, LDL eta HDL bandak jaso ziren beirazko punta erabiliz (**5. irudia**).

Purifikatutako lipoproteinak, aurretik orekatutako Sephadex G25 gel iragazpen zutabetik (PD-10 desalting column, GE Healthcare, EEBB) pasarazi ziren, intereseko indargetzailean jartzeko eta KBr hondarrak kentzeko.

Lipoproteinen kontzentrazioa DC Protein Asssay (Bio-Rad, EEBB) kit-a erabiliz neurtu zen. DLS bidez tamaina neurtu eta polidispersioa aztertu zen. Laginak  $4^{\circ}\text{C}$ -tan 2 astez gehienez mantentzen ziren.



## 5. Irudia. LDL eta HDL purifikazioa dentsitate zentrifugazio isopikniko bidez.

### 4.1. rHDL bidezko miRNAen transfekzioaren optimizazioa

rHDL bidezko miRNAen transfekzioa burutzeko, aurretik garatutako rHDL miRNA konplexuen kontzentrazio egokia aukeratu behar zen. Hala, transfekzioaren optimizaziorako rHDL konjugatuak 1:1 miRNA:proteina mol ratioan erabili ziren eta cel-miR67 miRNA kontrola erabili zen.

Horrela, analisi honetan J774A.1 zeluletan eratorritako zelula apartsuak erabili ziren (ikusi [zelula hazkuntzak](#) atala) eta rHDL:miRNA konplexuen 0-20  $\mu\text{g/mL}$  tarteko kontzentrazioak erabili ziren OptiMEM medioan. Inkubazioa 24 orduz egin

zen eta jarraian qRT-PCR burutu zen aurretik azaldu den moduan (ikusi [miRNAREN erauzketa](#) eta [kuantifikazioa](#) atala). Kasu honetan zelula putzu bakoitzari 500 µL NZYol gehitu zitzzion. Eta kuantifikaziorako U6 snRNA erabili zen barne-kontrol moduan, normalizaziorako.

## 5. Azetilatutako LDLak

LDLak azetilatzeko aurretik deskribatutako protokoloa jarraitu zen<sup>482</sup>. Hasteko, aurretik purifikatutako giza LDLak 16 mg/mL-ko 1 mL soluzioa lortu arte kontzentratu ziren, ziren Amicon™ Ultra-4 Centrifugal Filter Units zentrifugazio tutuak erabiliz (100.000 Daltoneko poroak, Merck, Alemania). LDL mililitroa, saturatutako sodio azetato (36,2 g/100 mL)<sup>483</sup> 1 mL-kin nahastu zen. Ondoren, 4°C-tan eta etengabe irabiatur (*Thermomixer*, 850 rpm), anhidrido azetiko puruaren tantak (2 µL) gehitu ziren, ordu batean zehar, anhidrido azetikoaren molartasuna LDLen lisinena baino 40 aldiz handiagoa izan arte. Jarraian, lagina 30 minuto gehiago utzi zen baldintza berdinatan. Lagina jaso eta dialisatu zen PBS + 0,3 mM EDTA (pH 7,4) indargetzailearen 12 litroren aurka, 24 orduz eta 4 °C-tan.

Azetilatutako LDLak (azLDL), 15 minutuz, 13.100 g-tan zentrifugatu ziren, agregatuak kentzeko. Ondoren, DC Protein Assay kit-a erabiliz (Bio-Rad, EEBB) kontzentrazioa kalkulatu zen.

### 5.1. Azetilazioaren egiaztapena

azLDLak LDL normalak baion mobilitate elektroforetiko handiagoa dute, izan ere, azetilazioek lisinen karga positiboa karga neutroagatik ordezkatzen dute. Hori dela eta, LDLen azetilazioa mobilitate elektroforetikoa aztertuz konfirmatu daiteke, agarosazko elektroforesi bidez.

Horretarako, agarosa gela % 0,7 (p/b) elektroforesi indargetzailean prestatu zen (90 mM Tris-HCl, 80 mM azido borikoa, pH 8,2). LDL normal (kontrol moduan) eta

azLDLei glizerola % 10ean gehitu eta gelan kargatu zen. Elektroforeisia 80 minutuz, 90 V-tan eta 4 °C-tan burutu zen. Ondoren, agarosa gela 30 minutuz, giro tenperaturan fixatu zen (% 5 azido azetiko glaziala, % 75 etanola, b/b). Fixapen soluzioa kendu, hondarrak filtrozko paper batekin sikatu eta gela 80 °C-tan ordu batez sikatu zen. Jarraian *Coomassie* tindagaiaz tindatu zen.

## 5.2. azLDLen kontserbazioa

azLDLak - 80 °C-tan kontserbatu ziren erabiltzeko unerarte. Horretarako, sakarosa % 10ean (b/b) gehitu zitzaien, % 50ean (p/b) PBSan prestaturiko stock batetik. Kontzentrazioa neurtu eta aliquotatu zen.

# 6. Zelula-hazkuntzak

## 6.1. Monogeruzan egindako esperimentuen zelula-hazkuntzak

THP-1 monozito giza zelula-lerroa, J774A.1 makrofago sagu zelula-lerroa ATCC-tik (American Type Culture Collection, Manassas, Virginia, EEBB) lortu ziren. Suspentsioan hazten diren zelulak T75 Flasketan kultibatu ziren (Sarsted, Alemania), 37 °C-tan eta % 5-ko CO<sub>2</sub>-ko atmosferan.

THP-1 zelulak RPMI 1640 medioan kultibatu ziren, % 10 FBS (b/b), 100 µg/mL estreptomizina, 100 U/mL penizilina, L-glutamina and MycoZap™ profilaktikoarekin osatuta. Makrofagoetara diferentziatzeko 100 nM PMA induktorea gehitu zitzaien (ingelesetik, *phorbol 12-myristate 13-acetate*), zelulak 24 putzuko plakara pasa ( $2,5 \cdot 10^5$  zelula/putzu) eta 24 orduz inkubatu ziren, plakara itsasteko. Hurrengo egunean medio berria jarri eta 72 orduz diferentziatzetan jarraitu zuten.

J774A.1 makrofagoak Dulbecco's modified Eagles Medium (DMEM, glukosa baxua) (+ % 10 FBS (b/b), 100 µg/mL estreptomizina, 100 U/mL penizilina eta MycoZap™ profilaktikoa gaineratuta) medioan hazi ziren. J774A.1 makrofagoetatik

zelula apartsuak garatzeko, zelulak 24 putzuko plakan erein ( $10^5$  zelula/putzu) eta 24 ordura 125  $\mu\text{g}/\text{mL}$  azLDLak gehitu ziren OptiMEM medioan (Gibco, Thermo Scientific, EEBB). 24 orduz azLDLekin inkubatu eta medio berrian ipini ziren.

Giza VSMC (ingelesetik, *vascular smooth muscle cells*) karotida arterietako ehun aterosklerotiko laginetatik isolatu ziren. Zelula horiek muskulu leuneko zelulak dira, zeinak zelula apartsu fenotipoa erakusten duten. Zelula hauek Medium-231 medio selektiboan (Gibco, Thermo Scientific, EEBB) hazi ziren (2  $\text{ng}/\text{mL}$  FGFb, 20  $\text{ng}/\text{mL}$  IGF-1, 0,5  $\text{ng}/\text{mL}$  EGF, 5  $\text{ng}/\text{mL}$  Heparin, 5% NCS, 0,2  $\mu\text{g}/\text{mL}$  BSA, 2 mM L-glutamina, 100  $\mu\text{g}/\text{mL}$  estreptomizina eta 100 U/mL penizilina)

Karotidako ateroma plaka laginak endarterektomiaz lortu ziren. Laginak izotzetan jarri eta berehala prozesatu ziren.

VSMC ehun aterosklerotikotik isolatzeko bi digestio entzimatiko burutu ziren. Lehenik, ehuna 3 orduz liseritu zen 300 U/mL Kolagenasa I-ekin, % 5 CO<sub>2</sub> eta 37 °C atmosferan. Jarraian, gau-osoko liseriketa egin zen 220 U/mL kolagenasa berdinarekin. Liseritutako ehuna 100  $\mu\text{m}$ -tako nylonezko Falcon™ Cell Strainer erabilita (CLS431752-50EA, Sigma-Aldrich, EEBB) filtratu zen liseritu gabeko ehuna kentzeko eta gero, zelulak plakeatu ziren Medium-231 medioan, VSMCen hazkuntza selektiboa sustatzen duena. Lerro zelular honekin egindako esperimentu guztiak 0 pasean burutu ziren zelulak % 70eko konfluentzian, errerealitatetik ahalik eta gertuen egoteko.

## 6.2. Ateroma modeloa eratzeko zelula-hazkuntzak

HUVEC giza zilbor-hesteko zelula endotelialak (ingelesetik, *human umbilical vein endothelial cells*), Alicia Rodriguez doktoreak (Euskal Herriko Unibertsitatea) adeitasunez emandakoa eta VSMC muskulu leuneko lerro hilezkorra (Coriell Cell Repositories, AG11545, Camden, NJ, EEBB) 6-9 bitarteko paseetan erabili ziren

esperimentu guzietan. Zelulak 37 °C-tan eta % 5-ko CO<sub>2</sub>-ko atmosferan hazi ziren. Bi lerro zelularrak Medium-199 medioan (Gibco, Thermo Scientific, Erresuma Batua) hazi ziren (FBS % 10ean (ez-inaktibatua), 0,02 mg/mL ECGS, 0,05 mg/mL heparina eta 2mM L-glutamina zeramana).

Zelula hauek T75 Flask-etan hazteko, gelatinazko oinarri bate behar zuten. Horretarako, Flask ontzietara, lehendabizi Gelatina soluzioa (% 0,1 gelatina (p/b) + % 0,09 NaCl (p/b)) gehitu eta 40 minutuz utzi ziren, 37 °C-tan eta % 5-ko CO<sub>2</sub>-ko atmosferan. Ondoren, gelatina kendu eta Medium-199 medioa gehitu zen Flask-a estali arte, 30 minutuz gutxienez. Pausu horrek, medioaren konponenteak gelatinan tartekatzea ahalbidetzen du, zelulen hazkuntzarako giro egokia sortuz. Horren ostean zelulak Flask horietan kultibatu ziren.

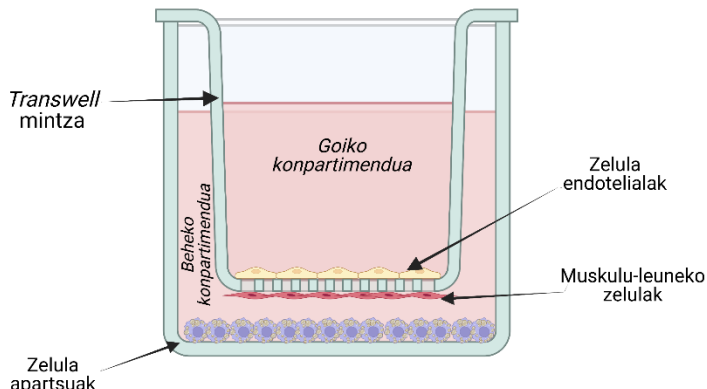
Bi lerro horiek kultibo bidimentsionalak eraikitzeko erabili ziren.

### 6.3. Hiru lerro-zelularreko ateroma modelo bidimentsionalak

Ateroma plakaren fase aurreratuetan tunika mediaren VSMCak arteriaren lumenera migratzen dute, zelula endotelialen azpian kokatuz eta matrize extrazelularra jariatz. Sortzen den egitura horri geruza fibrotsua esaten zaio (ingelesez, *fibrous cap*) eta gero eta handiagoa den lesio aterosklerotikoa estaltzen du. Lan honetan erabiltzen diren rHDLak geruza hori zeharkatzeko gaitasuna dutela eta, horren azpian aurkitzen diren zelula apartsuetara miR-33-a transferitzeko gaitasuna dutela frogatzeko, hiru lerro-zelularreko ateroma modelo bidimentsionalak garatu ziren.

Sistema modular honekin, zelula endotelialak, VSMCak eta makrofagoetatik eratorritako zelula apartsuak elkar kultibatzea ahalbidetzen du. Horrela, konpartimentu baskularra imitatuz, zelula apartsuen eta rHDLen arteko interakzioa eta dinamika aztertu daiteke. Ilustrazio eskematikoa **6. irudian** azaltzen da. 0,4 µm-

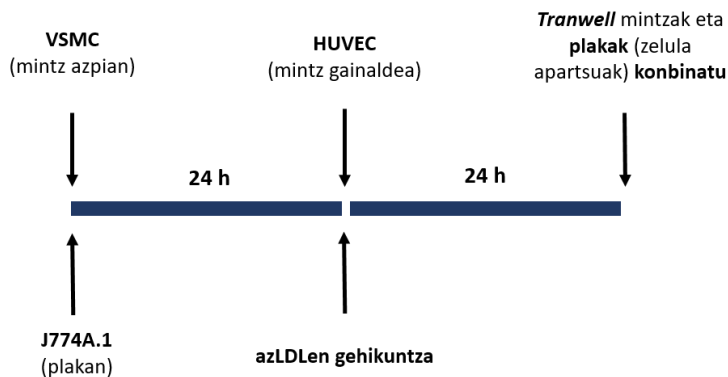
tako poroak dituen *Transwell* mintzek (Corning, EEBB), zelula geruza bakoitza isolatzea ahalbidetzen du, zelulen arteko kontaminazioa saihestuz.



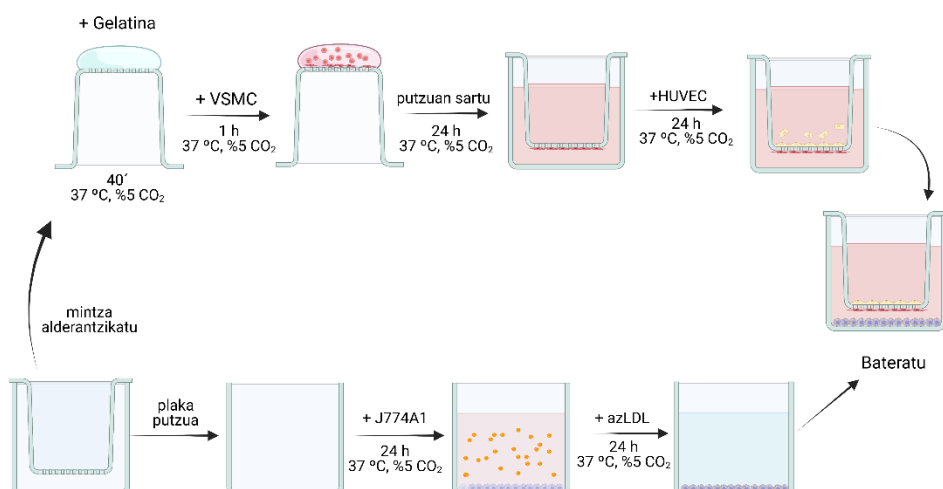
**6. Irudia: hiru lerro-zelularreko ateroma modelo bidimentsioanalaren irudia.** Ateroma modeloa garatu den plaka putzuaren itxura. Zelula apartsuak plakaren hondoan garatzen dira. VSMC zelulak *Transwell* mintzaren azpian eta HUVEC zelulak mintz berdinaren goialdean.

Zelula horiek hazteko, *Transwell* mintzaren behoko aldean gelatina soluzioaren tanta bat ipini zen eta horiek 30 minutuz, 37 °C-tan eta % 5-ko CO<sub>2</sub>-ko atmosferan mantendu ziren, buruz-behera eta baldintza aseptikoetan. Ondoren, gelatina kendumendi eta mintzak Medium-199 medioan murgildu ziren, beste 30 minutuz. Jarraian, berriro buruz-behera jarri eta mintz bakoitzean VSMC  $8 \cdot 10^4$  zelula erein ziren 50 µL-ko tanta batean. Zelulak mintzera eransteko ordu batez 37 °C-tan eta % 5-ko CO<sub>2</sub>-ko atmosferan inkubatu ziren. Gero, *Transwell* mintzak orientatu eta plakako putzuetan sartu ziren, 500 µL medio zeramana. Horrez gain, *Transwell*-aren gainaldean beste 200 µL medio jarri ziren. Egun berdinean beste putzu batzuetan J774A.1 zelulak DMEM medioan erein ziren eta zelula apartsuak garatu ziren (ikusi Zelula apartsuen garapena atala). Hurrengo egunean, HUVEC zelulak konfluentzian ( $8 \times 10^4$  zelula) erein ziren, *Transwell* mintzaren gainaldean eta beste 24 orduz inkubatu ziren. Egun berdinean, J774A.1 zelulei azLDLak gehitu ziren.

Hurrengo egunean, J774A.1 zelulak Meidum-199 medio garbia gehitu zitzaien eta VSMC eta HUVEC zelulak zeramatzen *Transwell* mintzak zelula apartsuen putzuetan sartu ziren (**7 eta 8. irudia**).



**7. Irudia: hiru-lerro zelularreko ateroma modeloaren garapenaren kronologia.**



**8. Irudia: hiru-lerro zelularreko ateroma modeloaren garapenaren laburpen bisuala.** Transwell mintzaren behoko aldean VSMC zelulak erein ziren, gelatinazko geruza baten gainean. Hurrengo egunean HUVEC zelulak mintzaren goiko aldean erein ziren 24 orduz. Aurretik beste plaka batean, J774A.1 zeluletatik eratorritako

zelula apartsuak garatu ziren. Azkenik, transwell mintzak zelula apartsuen putzuetan sartu ziren.

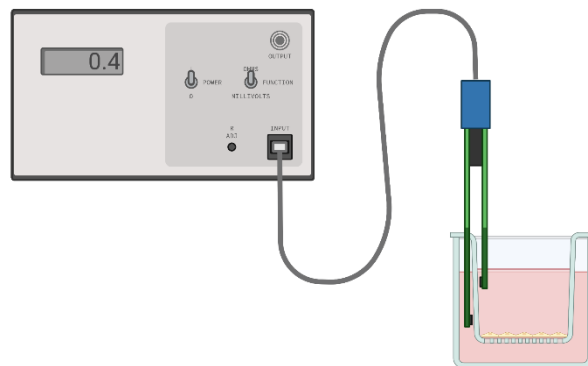
### 6.3.1. Erresistentzia elektriko transendoteliararen neurketa (TEER).

TEER neurketa (ingelesetik, *Transendothelial Electrical Resistance*) teknika ez-inbasiboa da endotelio zelulen lotura estuen integritatea modu zeharrean aztertzeko balio duena, zelula geruzaren erresistentzia elektrikoa neurtuz<sup>484</sup>. Horretarako, TEER neurketarako ekipamendua erabili zen (Millicell ERS-2 VoltOhmmeter, Merck, Alemania). TEER neurgailu honen elektrodoak zilar/zilar kloruro (Ag/AgCl) jalkina muturrean duten elektrodoak dira eta boltaia edo potentzial diferentzia neurtzeko balio dute. Ateroma modeloaren kasu konkretuan, elektrodo bat *transwell* mintzaren goiko konpartimentuan sartzen da eta bestea, beheko konpartimentuan, medioan murgilduta (**9. irudia**). Zelula geruza baten TEER balioa lortzeko, egoera horren erresistentzia neurtu zen ( $R_{NEURTUA}$ ) eta neurketen zuzenketarako, zelula gabeko *transwell* mintzaren erresistentzia neurtu zen ( $R_{ZURIA}$ ). Horrela, endotelio monogeruzaren erresistentzia espezifikoa ( $R_{MONOGERUZA}$ ) lortzen da, zeina mintzaren azalerarekin batera TEER balioa eskaintzen duen:

$$\text{TEER } (\Omega \cdot \text{cm}^2) = R_{\text{MONOGERUZA}} (\Omega) \times \text{Azalera } (\text{cm}^2),$$

Non  $R_{\text{MONOGERUZA}} = (R_{\text{TOTALA}} - R_{\text{ZURIA}})$  den.

Lan honetan erabilitako mintzen azaleraren balioa  $0.33 \text{ cm}^2$  izan zen. *Transwell* mintz hutsaren TEER balioak, zein endotelio zelulen geruzarenak, hiru aldiz neurtu ziren.



#### **9. Irudia. Erresistentzia elektriko transendotelialaren neurketa.**

Elektrodoak transwell mintzaren alde bietan sartzen dira eta horren erresistentzia ohmikoa neurgailuan jasotzen da.

### **7. Zelula apartsuuen garapena**

Zelula apartsuak eratzeko hainbat metodologia daude<sup>485-488</sup>. Lan honetan, giza (THP-1) eta sagu (J774A.1) makrofagoak azLDLekin inkubatuz garatu ziren.

Aurretik 24 putzuko plaketan ereindako makrofagoak ( $10^5$  zelula/putzu) PBSarekin behin garbitu eta ondoren, azLDL kontzentrazio desberdinak gehitu zitzaiak (0-200  $\mu\text{g/mL}$ ) optiMEM medioan (0,5 mL putzuko), 24 orduz inkubatu zirelarik azLDLak barneratzeko. Ondoren, mediao kendu eta DMEM medio osoa gehitu zitzaien beste 24 orduz zelula apartsuak garatzeko. Hala, azLDLak gehitu eta 48 ordura zelula apartsuuen formazioaren azterketak burutu ziren.

#### **7.1. Zelula apartsuuen eraketaren kuantifikazioa**

##### **7.1.1. Zelula apartsuuen kuantifikazio kuantitatiboa ORO eta Kristal Bioleta bidez.**

Zelula apartsuen sorreraren azterketa kuantitatiboa Oil-Red-O (ORO) tindatzailearekin egin zen (Sigma-Aldrich, EEBB). ORO tindatzailea lipido neutroei batzen denez, zelula apartsuetan lipido tantak tindatzeko erabili daiteke<sup>489</sup>.

ORO soluzioa tindatzeko momentuan prestatu zen, % 0,5ean (p/b, isopropanolean) dagoen disoluzioa ur destilatuaren 1,5 aldiz diluituz. Hala, lehendabizi zelulak 3 aldiz PBSarekin garbitu eta gero 10 minutuz paraformaldehidoaz (% 4 p/b) fixatu ziren. PBS garbiketak errepikatu eta jarraian % 60 isopropanola (b/b) 5 minutuz inkubatu zen. Jarraian, prestaturiko ORO soluzioa 12 minutuz inkubatu zen. Mili-Q urarekin 3 garbiketa egin eta tindaketa mikroskopio optikoan konprobatu zen.

Kuantifikaziorako ORO tindatzailea zeluletatik erauzi behar zen. Horretarako, erauzketarako, isopropanol % 60 (b/b) 200 µL gehitu eta 30 minutuz agitazioan utzi ziren. ORO tindatzailea isopropanolera pasa zen, 510 nm-tan absorbantzia neurtu zitekeelarik.

Ondoren, Kristal Bioleta tindatzaileaz (Sigma-Aldrich, EEBB) zelulen nukleoak tindatu ziren, zelula zenbakia kalkulatzeko eta amaieran ORO sinalea erlatibizatzeko balio zuena.

Horretarako Kristal Bioletaren stocka % 0,5 (p/b) mili-Q uretan prestatu zen eta tindatzeko, stock hori PBSan diluitu zen (% 0,1, b/b). Hala, zelula plakatik isopropanola kendu eta garbiketak egin ziren, 2 ur destilatuarekin eta 1 PBSarekin. Jarraian Kristal Bioleta soluzio diluitua gehitu zen 30 minutuz. PBS 4 garbiketa egin, mikroskopioan tindaketa konprobatu eta Kristal Bioletaren erauzketarako % 75 etanol (b/b) 200 µL gehitu zen, agitazioan eta 15 minutuz. Etanolera transferitutako Kristal Bioletaren absorbantzia 580 nm-tan neurtu zen.

#### *7.1.2. Zelula apartsuen kuantifikazio kualitatiboa mikroskopia optiko bidez.*

Zelula apartsuen formazioaren behaketa mikroskopia optiko bidez burutu zen. Horretarako, lipido tanta ORO bidez tindatu ziren aurreko atalean azaldu den modu berdinean. Nukleoak tindatzeko aldiz, kasu honetan Hematoxilina-Eosina (Sigma-Aldrich, EEBB) ohiko tindatzailea erabili ziren.

Horretarako, ORO tindaketa ostean, behin putzuak Mili-Q uretan zeudela, Hematoxilina-Eosina (Sigma-Aldrich, EEBB) soluzioaren 300 µL zuzenean gehitu zen 6 minutuz. Jarrian, PBSarekin 3 garbiketa egin ziren eta Mili-Q urarekin beste hainbat garbiketa. Zelulen argazkiak Nikon ECLIPSE TS100 mikroskopio alderantzkatuan ateria ziren (Nikon, Japonia).

## 8. Kolesterol kanporaketaren azterketa

rHDLen konposizio lipidiko desberdinek kolesterol kanpora-fluxuan duten eragina aztertu zen. Kolesterol fluxuak aztertzeko BODIPY talde fluoreszentea daraman kolesterola erabili zen, Top-Fluor<sup>®</sup> Cholesterol (Avanti Polar Lipids).

BODIPY-kolesterol, bestelako lipidoak bezala, kloroformo/metanol (2:1, b/b) soluzioan prestatu eta -20 °C-tan kontserbatzen da. Zelulei gehitzeko, metil-β-ziklodextrinarekin (Sigma-Aldrich, EEBB) inkubatu behar da, mintz zelularra zeharkatzeko gai diren konplexuak eratu daitezen. Soluzio horri “labeling medioa” deituko zaio.

### 8.1. *Labeling* medioaren prestaketa

“Labeling medioa”, kolesterola (kolesterol normala eta BODIPY-kolesterol) metil-β-ziklodextrinarekin (16 mM) nahastuz prestatu zen, 1:80 erlazio molarrean (kolesterol:ziklodextrina). Horretarako, kolesterol normala eta BODIPY-kolesterola

(3:1, M:M) nahastu eta beirazko tutu batean sikatu ziren N<sub>2</sub> gasa erabiliz. Ondoren, 1,5 orduz hutsezko ponpa batean utzi ziren, ilunpetan. Kolesterol filmari,  $\beta$ -ziklodextrina disolbatuta zuen MEM-Hepes medioa (Minimum Essential Medium Eagle, Hepes 25 mM, pH 7,4) gehitu zen. kolesterola, kolesterol-BODIPY eta ziklodextrina zeramatzan tutua ur bainu batean sonikatu zen 40 °C-tan 30 minutuz, kolesterola berresekiteko, jarrian agitazioan 3 ordutan zehar inkubatu zirelarik, 37 °C-tan. “*Labeling* medioa”, zelula putzu bakoitzari 125  $\mu$ L gehituko zitzaiak kontuan izanda prestatu zen. Erabiltzeko unean fluxu laminarreko kanpaian, 0,2  $\mu$ m-tako filtroak erabiliz filtratu zen.

## 8.2. Kolesterol kanporaketa monogeruza kultiboetan

Zelulak 24 putzuko plaketan erein eta diferentziatu ziren, [Monogeruzan egindako experimentuen zelula-hazkuntzak](#) atalean azaltzen den moduan. Hala, diferentziatutako zelulei “*labeling* medioa” gehitu zitzaien, RPMI-1640 medioan aurretik diluitu zena (1:1, v:v). Medioak % 2 FBS, % 4 BSA eta 4  $\mu$ g/mL ACAT inhibitzailea zeramatzen eta zelulekin 45 minutuz inkubatu zen (37 °C, 5 % CO<sub>2</sub>). ACAT entzima inhibitzailea garrantzitsua da, zeluletan barneratutako kolesterola esterifikatu ez dadin eta erabilgarria egon dadin. Zelulen markaketa ondo joan zela, mikroskopio optikoan behatu zen.

Ondoren, zelulak MEM-Hepes medioarekin bi aldiz kontuz garbitu ziren eta zelulak hurengo medioan 15 orduz utzi ziren: RPMI-1640 medioa + % 2 BSA eta 2  $\mu$ g/mL ACAT inhibitzailea. Medio hau gehitzerako unean TO901317 edo TO90 (3  $\mu$ M) gehitu daiteke. TO90 LXRen agonista da eta horren aktibazioa induitzituz, ABCA1 kolesterol garraiatzailearen adierazpena emendatzeko gehitzen da, kolesterol kanporaketan egongo diren desberdintasunak handiagoak eta beraz, bisualagoak izan daitezzen<sup>490</sup>.

Atseden denbora honen ostean kolesterol hartzaleak gehitu ziren MEM-Hepes 25 mM (pH 7,4) medioan prestaturikoak, 2 µg/mL ACAT inhibitzaileaz. Erabilitako rHDL lipido konposizioak:

- DPPC
- Sojazko PC
- DPPC:CE:LPC (7,5:2:0,5)
- DPPC:Chol:LPC (8,5:1:0,5)

Erabilitako barne-kontrolak:

- BSA (10 µg/mL): gantz-azido gabeko BSA rHDLen kontzentrazio berdinean prestatu zne, kolesterol kanporaketa inespezifikoa neurtzeko.
- FBS % 20an (b/b): FBS kontzentrazio honekin kolesterol kanporaketa maximoa neurtzeko erabili zen, serumean kolesterol hartzale desberdinak baitaude<sup>491</sup>.

Kontrol positiboak:

- ApoA-I (10 µg/mL): kolesterol kanporaketa espezifikoa neurten da, izan ere, ABCA1en hartziale nagusia da apoA-I.
- HDL (10 µg/mL): giza plasmatik purifikatutakoak, rHDL kolesterol efluxua honekiko erlatibizatu zen.

Horiez gain, kontrol negatiboak sartu ziren, hartzale gabeko medioa alegia. Kolesterol hartzaleak 6 orduz inkubatu ziren. Ondoren, medioak jaso eta zelula hondarrak kentzeko 2.900 g-tan zentrifugatu ziren, 15 minutuz. Putzuetako zelulak MEM-Hepes 25 mM medioarekin kontuz bi aldiz garbitu ziren. Ondoren, zelulak lisi indargetzailearekin apurtu ziren (50 mM Tris–HCl, pH 7,5, % 0,1 SDS, % 0,1 azido deoxikolikoa, 0,1 mM EDTA, 0,1 mM EGTA, % 1 NP-40, 5,3 mM NaF eta 1,5 mM NaP), 30 minutuz plaka irabiagailuan eta giro-temperaturan. Liseritutako zelulak eta

medioak 96 putzuko fluoreszentzia plakara pasa ziren eta fluoreszentzia Synergy HTX Multi-Mode (BioTek, EEBB) irakurgailuan neurtu ziren ( $\lambda_{\text{ex}}: 485 \pm 20$  nm,  $\lambda_{\text{em}}: 528 \pm 20$  nm). Fluoreszentzia intentsitateak (FI) kolesterolaren kanporaketa baldintza bakoitzean neurtzeko erabili ziren, hurrengo formula jarraituz :

$$\text{Kolesterol kanporaketa \%} = \frac{\text{zelula medioaren FI}}{\text{zelula medioaren FI} + \text{zelula lisatuen FI}} \cdot 100$$

Zelula medioen FI balioari hartzaile gabeko medioaren fluoreszentziaren balioa kendu zitzaison aurretik. Kolesterol kanporaketa espezifikoa BSArekiko kanporaketaren balioa (ez-espezifikoa) kenduz lortu zen.

Esperimentu hau monogeruza zelularretan egin zen, presaturiko rHDLek kolesterol kanporaketa induitzeko duten efizientzia aztertzeko. Hurrengo 1erro zelularretan burutu zen: THP-1, J774A.1, J774A.1-etik eratorritako zelula apartsuak eta pazienteen plakako VSMC.

## 9. Ateroma modeloaren erabilera kolesterol kanporaketaren azterketarako

Hiru 1erro zeluletako kultibo bidimentsionala ateroma plakaren *in vitro* modelo bat da, aterosklerosiaren fase garatuetan gertatzen den egoera imitatzen duena, zelulen lokalizazioari dagokionez. Modelo horrekin egindako esperimentuetan rHDL erabili ziren. Lehendabizi, antagomiR-33-a garraiatzeko DPPC:CE:LPC rHDLak erabili ziren, aurretik gure laborategian egindako analisietan miRNAk batzeko konposizio egokiena zela ondorioztatu baitzen. Bestalde, DPPC rHDLak kolesterol kanporaketa induitzeko erabili ziren lan honetan kolesterol fluxua induitzeko efizienteenak zirela ondorioztatu zelako.

Horrela, lehendabizi, miRNA zeramaten rHDLen HUVEC eta VSMC bidez sortutako kultibo bidimentsionala zeharkatzeko eta J774A.1 zeluletatik eratorritako zelula apartsueta barneratzeko baldintzak optimizatu behar ziren. Ondoren,

aukeratutako baldintzetan antagomiR-33-a-ren efektua aztertu zen, hau da, mir-33-a-ren isilpena eta horren itu geneak diren ABCA1 eta ABCG1en gainadierazpena. Amaitzeko, sistema optimizatu ostean, DPPC rHDLek induzitutako kolesterol efluxua aztertu zen, J774A.1-etik eratorritako zelula apartsuetan.

### 9.1. rHDL bidezko miRNAen transfekzioaren optimizazioa

Entseguaren optimizaziorako DPPC:CE:LPC rHDLak erabili ziren. Ateroma modeloaren kultibo bidimentsionalak zeharkatzeko eta plakan dauden J774A.1-etik eratorritako zelula apartsuetan barneratzeko kontzentrazio egokia jakiteko 0-100 µg/mL tarteko kontzentrazioak erabili ziren (rHDLen proteina kontzentrazioa). Bestalde rHDL horien eta miRNAren konjugazioa 1:1 mol ratioan (miRNA:proteina) egitea erabaki zen. Optimizazio probetarako, *C.elegans* nematodoaren cel-miR-67 microRNA kontrola erabili zen,

Inkubazio denbora, laborategian aurretik egindako probak kontuan hartuta, 24 orduko inkubazioa izatea erabaki zen. Ondoren rHDL eta miRNAren transferentzia zelula apartsuera eman zela aztertu zen.

Esperimentu honen kronologia hurrengoa izan zen: zelulen ateroma modeloa behin garatuta (ikusi [Zelula-hazkuntzak](#) atala), goiko konpartimentuan rHDL konjugatuak gehitu ziren 150 µL OptiMEM medioan (Gibco, Thermo Scientific, EBBB) eta beheko konpartimentuan medio berdinaren 400 µL ipini ziren. rHDL kontzentrazioak bolumen totalerako kalkulatu ziren (550 µL). rHDLak 24 orduz inkubatu ziren 37 °C eta % 5 CO<sub>2</sub>-ko atmosferan. 24 orduko inkubazio horren ostean rHDLen eta miRNAren barneraketa fisikoa aztertu zen. Atal honen kronologia **10. irudian** agertzen da laburtuta.

#### 4.Taula. Landutako miRNAen sekuentziak.

<b>miRNA</b>	<b>Espeziea</b>	<b>Kodea</b>	<b>Sekuentzia</b>
MiR-33-a-5p	<i>Homo sapiens</i>	<a href="#">MIMAT0000091</a>	5'-GUGCAUUGUAGUUGCAUUGCA-3'
Cel-miR67-3p	<i>C.elegans</i>	<a href="#">MIMAT0000039</a>	5'-UCACAACCUCCUAGAAAGAGUAGA-3'

### 5. Taula: rHDLei konjugatuako miRNA komertzialak.

<b>miRNA</b>	<b>Espeziea</b>	<b>Erreferentzia</b>	<b>Etxe komertziala</b>
AntagomiR-33-a-5p	<i>Homo sapiens</i>	<a href="#">IH-300509-08</a>	Horizon Discovery (Erresuma Batua)
Cel-miR67-3p	<i>C.elegans</i>	<a href="#">IN-001005-01</a>	

#### 9.1.1. rHDLen barneraketaren azterketa

##### 9.1.1.1. Mikroskopia fluoreszentea

rHDLen barneraketa azterzeko, Dil-rekin markaturiko DPPC:CE:LPC rHDLak erabili ziren aurretik azaldu den moduan (ikusi [rHDLen markaketa fluoreszentea](#) atala), 0-100 µg/mL bitarteko kontzentrazioetan. rHDL horiek cel-miR67 miRNA zeramaten konjugatua 1:1 erlazio molarrean. rHDLen 24 orduko inkubazioa amaitzean, hiru leerroen hazkuntzak PBSaz ondo garbitu ziren eta laginen argazkiak ZOETM Fluorescent Cell Imager (Bio-Rad Laboratories, Inc., Spainia) mikroskopioarekin atera ziren.

##### 9.1.1.2. rHDLen fluxu-zitometria

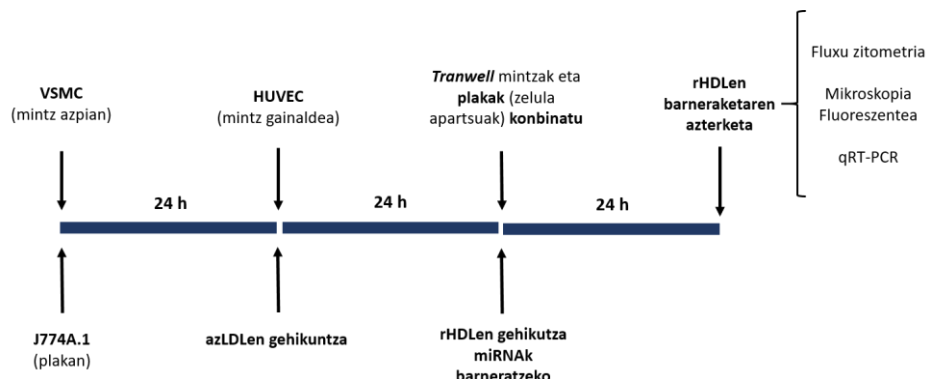
Argazkiak atera ostean, Dil-rekin markaturiko DPPC:CE:LPC rHDLen barnerapena fluxu-zitometriaz ere aztertu zen, 0-100 µg/mL bitarteko kontzentrazioetan ere. Fluxu-zitometria zelulen analisirako parametro anitzeko teknika da. Bertan, aztertu behar diren partikulen suspentsioa (gehienetan zelulak) banan bana lerrokatuta laser batetik pasarazten dira. Laserrak zelulekin talka egitean informazioa ematen duten seinale desberdinak igortzen dira, argiaren dispersioarengatik eta fluoreszentzia igorpenarengatik. Zelula bakoitzetik detektatzen diren parametroak hauek dira:

- Argiaren aurreranzko dispersioa (ingelesez, *forward-scatter* edo FSC), zelulen tamainarekiko proportzionala den parametroa da.
- Angelu zuzeneko dispersioa (ingelesez, *Side-Scatter* edo SSC), zelulek duten barne konplexutasunarekiko proportzionala dena.
- Fluoreszentzia intentsitatea uhin luzera desberdinatan, zelulek saioan jasan duen markaketa edo fluorokromoaren araberakoa izango dena, kasu honetan Dil.

Horrela, Dil rHDLak ateroma modeloan 24 orduz inkubatu ostean, zelulak PBS bidez garbitu eta hazkuntza guziak (HUVEC, VSMC eta zelula apartsuak) *Transwell* mintzetik edo plakatik banatu ziren tripsina gehituz. Askatutako zelulen erdia fluxu zitometriazko analisia burutzeko erabili ziren. Beste erdia [urrengo atalerako](#). Hala, 10.000 gertaeren fluoreszentzia neurtu zen CytoFLEX (Beckman Coulter, EEBB) zitometroan. Saio guziak hiru bider errepikatu ziren zitometroak ekarritako argibideak jarraituz aurretiaz deskribatu zen moduan<sup>492</sup>. Zitometroa kalibratzeko, etxe berdineko bihiak erabili ziren (CytoFLEX Daily QC Fluorospheres) eta datuak analizatzeko CytExpert softwarea erabili zen (Beckman Coulter, v. 2.3.0.84, EEBB).

#### *9.1.2. Cel-miR-67 miRNAREN barneraketaren azterketa*

rHDL bidezko miRNAREN barneraketa zeluletan aztertzeko, garaiatzen zuten cel-miR67-a-ren identifikazioa egin zen. Horretarako, aurretik PBS + 5 mM EDTAz askatutako zelulen beste erditik miRNA erauzi eta kuantifikatu zen qRT-PCR bidez. Aurretik azaldu den moduan rHDL goranzko kontzentrazioak erabili ziren (0-100 µg/mL) eta beraz, cel-miR67-a-ren kontzentrazioa gorakorra izan zen ere. Kasu honetan, ateroma modeloaren zelula apartsuetan soilik aztertu zen miRNAREN barneraketa erabilitako rHDL kontzentrazio bakoitzean. Zelula apartsuen PBS bidezko garbiketen ostean NZYol (NZYTech) soluziotik 500 µL gehitu zitzaien eta fabrikatzailaren argibideak jarraituz miRNAREN purifikazioa egin zen. Ondoren, miRNAREN amplifikazio eta kuantifikaziorako miRCURY LNA miRNA PCR System (QIAGEN, Alemania) erabili zen, argibideak jarraituz. Barne kontrol moduan adierazpen egonkorreko U6 snRNA erabili, kuantifikazioaren datuak erlatibizatzeko (ikusi [miRNAREN kuantifikazioa](#) atala).



**10. Irudia. rHDL bidezko miRNAen transfekzioaren azterketaren kronologia, ateroma modeloan.**

## 9.2. AntagomiR-33-a-ren barneraketaren efektuaren azterketa

AntagomiR-33-a tratamendua ateroma modeloan zuen eragina frogatzeko lehendabizi, mir-33-a-ren isilpena aztertu zen eta ondoren, mir-33-a-ren ituak diren geneen adierazpen maila aztertu zen.

#### *9.2.1. miR-33-a-ren isilpenaren azterketa*

zelula apartsuetan adierazten den miR-33-a isilarazteko rHDLak antagomiR-33-a-rekin konjugatu zen 1: 1 erlazio molarrean eta ateroma modeloan inkubatzeko 50 µg/mL-ko kontzentrazioa erabili zen. Kontrol moduan, cel-miR67 miRNA kontrola konjugatutako rHDLak erabili ziren. Inkubazioa 24 orduz egin zen eta jarraian qRT-PCR burutu zen aurretik azaldu den moduan (ikusi [miRNAren erauzketa](#) eta [kuantifikazioa](#) atala). Kasu honetan bian zelula putzu bakoitzari 500 µL NZYol gehitu zitzaion. MiRNA kuantifikatzeko, miRCURY LNA miRNA PCR System (QIAGEN, Alemania) kit-a erabili zen Hasle moduan cbr-miR-67 miRCURY LNA miRNA PCR Assay (QIAGEN, Alemania) erabili zen, cel-miR-67-3p sekuentziarekin bat zetorrena. Eta miR-33-a-ren kuantifikazioa egiteko, etxe berdineko hasleak erabili ziren. Kuantifikaziorako barne-kontrol moduan U6 snRNA erabili zen, datuen normalizaziorako. Hasleak miRCURY LNA™ PCR primers set, Qiagen etxe komertzialek erosi ziren.

#### **6.Taula. miRNAen qRT-PCRAk burutzeko hasleen zerrenda**

<b>miRNA</b>	<b>Erreferentzia</b>	<b>Etxe-komertziala</b>
MiR-33a-5p	YP00205690	Qiagen
Cbr-miR67-3p	YP02114865	Qiagen
U6 snRNA	203907	Metabion international
UniSp6 spike	YP00203954	Qiagen

### 9.2.2. ABCA1en eta ABCG1en gainadierazpenaren azterketa

AntagomiR-33-a tratamenduak zuen eragina frogatzeko mir-33-a-ren ituak diren geneen adierazpen maila aztertu zen. Esperimentu honen kronologia hurrengoa izan zen. Zelulen ateroma modeloa behin garatuta (ikusi [Zelula-hazkuntzak](#) atala), goiko konpartimentuan 50 µg/mL rHDL gehitu ziren (antagomiR-33-a, 1:1 ratio molarrean, aurretik konjugatu zitzaina) 150 µL OptiMEM medioan eta beheko konpartimentuan medio berdinaren 400 µL ipini ziren. rHDL kontzentrazioa bolumen totalerako kalkulatu zen (550 µL). rHDLak 24 orduz inkubatu ziren eta atal honen kontrol moduan miRNA kontrola zeramatzen rHDLak erabili ziren. 24 orduko inkubazio horren ostean, zelulei DMEM bolumen berdina gehitu zitzaien % 20 FBSarekin, eta beste 24 orduz inkubatu ziren, anitimir-33-a-ren efektuak mRNA eta proteina mailetan islatu ahal izateko.

#### 9.2.2.1. qRT-PCR

ABCA1 eta ABCG1 proteinen RNA mezulari maila neurtzeko, qRT-PCR erabili zen. NZYol erreaktiboa (NZYTech, Portugal) erabiliz, zelula apartsuetatik RNA erauzi zen, fabrikatzalearen argibideak jarraituta. Ondoren, One Step SYBR PrimeScript RT-PCR Kit (Perfect Real Time) (Takara, Japan) erabili zen, RNA totalaren DNA osagarria sintetizatzeko (cDNA, ingelesetik *complementary DNA*) eta lortutako cDNAren PCRa jarraian burutzeko, dena aldi berean. Hala, gene bakoitzeko 3 neurketa burutu ziren. Intereseko genearen cDNAa kantitatea jatorrizko cDNA kantitate totalarekiko normalizatzeko, adierazpen egonkorreko *GAPDH* genea erabili zen, honen hasleak ABCA1 eta ABCG1en hasleekin hasieran gehitu zirelarik.

qRT-PCR erreakzioak CFX96 Touch™ Real-Time PCR Detection System (Bio-Rad, EEBB) aparatuaren egin ziren. Erabil zen programaren arabera laginak lehendabizi 50 °C-tan 20 minutuz berotu ziren eta gero 95 °C-tan 10 minutuz. Ondoren, 40 ziklo burutu ziren, horietan laginak 95 °C arte berotzen ziren 15 segundoz, segituan 60 °C-tan ipintzeko, minutu batez. Gene bakoitza amplifikatzeko erabili diren hasleak

**7. taulan** ageri dira, Metabion international (Alemania) etxe komertzialetik lortutakoak.

**7. Taula. Zelula apartsueta qRT-PCRak burutzeko erabilitako hasleen zerrenda**

GENEA	Aurreranzko hasle sekuentzia (5' -> 3')	Alderantzizko hasle sekuentzia (5' -> 3')
ABCA1	ACCCACCCATGAACAAACATGA	GAGTCGGGTAACGGAAACAGG
ABCG1	ATTCAAGGCACCTTCCTATT CGG	CTCACCACTATTGAACTTCCCG
GAPDH	GGAGCGAGATCCCTCCAAAAT	GGCTGTTGTCATACTTCATGG

**9.2.2.2. Western plapaketa**

Zeluletatik eratorritako ABCA1 eta ABCG1en detekzioa Western plapaketa bidez aztertu zen. Horretarako, esperimentua amaitu ostean J774A.1-etik eratorritako zelula apartsuetatik zelulen medioa kendu, PBS garbiketak egin eta 100 µl liseriketa medioda gehitu zen (50 mM Tris-HCl, pH 7,5, 125 mM NaCl, 1% Nonidet P-40, 5,3 mM NaF, 1,5 mM NaP, 1 mM ortonanadato, 1 mg/mL *protease inhibitor cocktail* (Roche), eta 0,25 mg/mL Pefabloc, 4-(2-aminoetil)-benzenosulfonil fluorido hidrokloruroa (AEBSF; Roche). Zelulak frekuentzia baxuan sonikatu ziren Soniprep 150 sonikatzailean (MSE, Erresuma Batua) ondoren, laginak errotazioan utzi zirelarik, 30 minutuz, 4 °C-tan. Liseriketa ostean, laginak 12.000 g-tan 10 minutuz zentrifugatu ziren, 4 °C-tan eta laginen jalkinak Western plapaketa bidezko analisi erdi-kuantitatiboa burutzeko prestatu ziren. Horretarako, proteinen kontzentrazioa DC Protein Assay (bio-Rad, EEBB) kit-a erabiliz neurtu zen eta pisu molekularraren arabera, % 8,5eko SDS-PAGE bidez banatu ziren. Proteinen transferentzia ostean nitrozelulosazko mintzak (Protran BA 83, Whatman™, GE Healthcare, Alemania) ordubetez inkubatu ziren blokeo soluzioan (TBST + % 5 BSA, p/b) antigorputzen lotura inespezifikoak ekiditeko eta ondoren, antiABCA1 (sagu) eta antiABCG1

(untxia) antigorputzkin inkubatu ziren 16 orduz 4°C-tan. 3 TBST garbiketa egin ostean, HRP entzima kojugatutako antigorputz sekundarioarekin inkubatu zen, ordu batez giro temperaturan. TBST garbiketak errepikatu eta mintza Luminata™ Forte Western HRP Substrate (Merck Millipore, EEBB) HRParen substratu kimioluminiscentearekin inkubatu zen eta proteinen detekzioa ChemiDoc XRS (Bio-Rad, EEBB) aparatuaren bitartez egin zen.

Glyceraldehyde 3-phosphate dehydrogenase (GAPDH) proteina barne kontrol moduan erabili zen. Kasu honetan, elementu infragorria duen antigorputz sekundarioarekin inkubatu zen ordu batez giro temperaturan. GAPDH banden detekzioa ChemiDoc XRS (Bio-Rad, EEBB) aparatuaren zen.

Irudien analisi dentsitometrikoak [NIH ImageJ softwarea](#) erabiliz egin zen (<https://imagej.nih.gov/>) eta proteina kuantifikazioa GAPDH seinalearekiko erlatibizatu zen.

#### **8. Taula. Western plapaketan erabilitako antigorputz zerrenda**

Antigorputza	Etxe-komertziala	Erreferentzia	Diluzioa	inkubazioa	jatorria
Anti ABCA1 polyclonal	Abcam	ab18180	1:500	16 h, 4°C	sagua
ABCG1 polyclonal antibody	Novus Biologicals	NB400-132SS	1:500	16 h, 4°C	untxia
Anti GAPDH	Santa Cruz Biotech	sc-47724	1:1000	16 h, 4°C	sagua
Anti-Rabbit IgG, HRP linked antibody	Cell signaling	7074	1:5000	1 h, RT	
Anti-mouse IgG, HRP linked antibody	Cel signaling	7076	1:5000	1 h, RT	
IRDye® 800CW Goat anti-Rabbit IgG	LI-COR	926-32211	1:5000	1 h, RT, ilunpetan	ahuntza

### 9.3. rHDLen administrazio sekuentziala ateroma modeloa, kolesterol kanporaketa induitzeko

Behin sistema optimizatuta, kolesterol kanporaketa ateroma modeloa aztertu zen. Hau da, DPPC:CE:LPC rHDLak antagomiR-33-a kultibo bidimentsionala zeharkatzeko, zelula apartsu eta barneratzeko (bai rHDLak eta bai horri lotutako miRNA) eta horietan itu genen gainadierazpena induitzeko gai dela ikusi ostan.

Horrela, esperimentu honen kronologia hurrengoa izan zen (**11. irudia**): zelulen ateroma modeloa behin garatuta (ikusi [Zelula-hazkuntzak](#) atala), goiko konpartimentuan 50 µg/mL rHDL gehitu ziren (antagomiR-33-a, 1:1 ratio molarrean aurretik inkubatuta) 150 µL OptiMEM medioan eta beheko konpartimentuan medio berdinaren 400 µL ipini ziren. rHDL kontzentrazioa bolumen totalerako kalkulatu zen (550 µL). rHDLak 24 orduz inkubatu ziren eta atal honen kontrol moduan rHDL hutsak erabili ziren, hau da, miRNA gabeko rHDLak. 24 orduko inkubazio horren ostan, *transwell* mintza kendu eta zelula apartsu *labeling* medioa gehitu zitzaien ([8.2 atalean](#) agertzen den modu berdinen) 45 minutuz 37 °C eta % 5 CO<sub>2</sub>-an.

Ondoren, zelulak MEM-Hepes medioarekin bi aldiz kontuz garbitu ziren eta zelulak hurengo medioan 15 orduz utzi ziren: RPMI-1640 medioa + % 2 BSA eta 2 µg/mL ACAT inhibitzailea. Medio hau gehitzerako unean laginen erdiari TO90 LXR agonista (3 µM) gehitu zen.

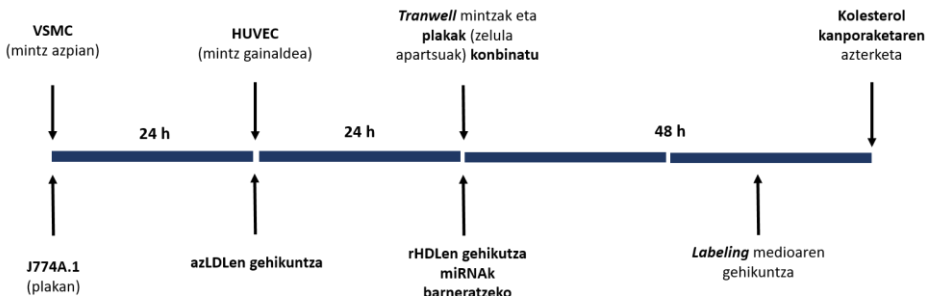
Atseden denbora honen ostan kolesterol hartzaileak gehitu ziren MEM-Hepes 25 mM (pH 7,4) medioan prestatuikoak, 2 µg/mL ACAT inhibitzaileaz. Hartzaileak

gehitzeko unean, DPPC:CE:LPC rHDLak gehitu eta 48 ordu ondoren izango litzateke, antagoniR-33-a ABCA1en gainadierazpena eragin ostean alegia.

Koletserol kanporaketa entsegu honetan erabilitako rHDL bakarra DPPC rHDLak izan ziren. Horrez gain hurrengo kontrolak gehitu ziren:

- Barne kontrol moduan gantz-azido gabeko BSA (10 µg/mL) erabili zen (Sigma Aldrich, EEBB). Honekin, kolesterol kanporaketa inespezifikoa neurtu zen.
- Kontrol positibo moduan, giza plasmatik purifikatutako HDLak (10 µg/mL). DPPC rHDLak induzitutako kolesterol kanporaketa honekiko erlatibizatu zen.
- Horiez gain, kontrol negatiboak sartu ziren, hartzaile gabeko medioa alegia.

Kolesterol hartzaleak 6 orduz inkubatu ziren 37 °C eta % 5 CO<sub>2</sub>-an. Laginen tratamendua [8.2 atalean](#) agertzen den modu berdinean egin zen.



**11. Irudia. rHDL administrazio sekuentziala ateroma modeloan eta kolesterol kanporaketaren azterketa.**

## 10. Analisi estatistikoa

Neurketa guztiak gutxienez hiru aldiz egin ziren, kontrakoa adierazi ezean, eta emaitzak batez besteko  $\pm$  SD gisa aurkezten dira (desbiderapen estandarra, ingelesetik *standard deviation*). Shapiro-Wilk proba bat egin zen datuen banaketa normala zela baieztatzeko. Hipotesi nulua egiaztago zen, datuak normal banatuta zeudela adieraziz.

Banaketa normala duten aldagaien analisi estatistikorako, Student t-testa edo ANOVA erabili zen. Aldagai kategorikoak Chi karratuaren proba edo Fisherren proba zehatza erabiliz alderatu ziren. p balioa  $<0,05$  esanguratsutzat jo zen. Analisi

estatistiko guztiak SPSS 25-rekin egin ziren (SPSS, Inc., Chicago, IL, AEB).



# **4. RESULTS**

## **4. EMAITZAK**

**The results presented in this section have been published at:**

1. Cholesterol Efflux Efficiency of Reconstituted HDL Is Affected by Nanoparticle Lipid Composition. Jebari-Benslaiman S, Uribe KB, Benito-Vicente A, Galicia-Garcia U, Larrea-Sebal A, Alloza I, Vandenbroeck K, Ostolaza H, Martín C. *Biomedicines*. 2020 Sep 23;8(10):373. doi: 10.3390/biomedicines8100373.
2. Boosting Cholesterol Efflux from Foam Cells by Sequential Administration of rHDL to Deliver MicroRNA and to Remove Cholesterol in a Triple-Cell Two-Dimensional Atherosclerosis Model. **Jebari-Benslaiman S**, Uribe KB, Benito-Vicente A, Galicia-Garcia U, Larrea-Sebal A, Santin I, Alloza I, Vandenbroeck K, Ostolaza H, Martín C. *Small*. 2022 (*in press*, DOI: 10.1002/smll.202105915).

## Results 1. Development of rHDL: Experimental set up

### 1. Human recombinant apoA-I purification

Human apoA-I was purified from *E. coli* BL21 (DE3) pLysS transformed with recombinant hapoA-I (rhapoA-I) vector kindly provided by Prof. Oda, (Children's Hospital Oakland Research Institute, Oakland, USA) as described before<sup>493</sup>. ApoA-I vector contains 6-histidine tag and was purified in one step using HiTrap TALON® crude 5 mL (GE Healthcare, USA) and purity was analyzed in a 12,5% SDS-PAGE electrophoresis (**Figure 12**).

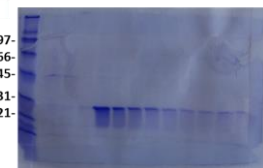


**Figure 12. ApoA-I purification polyacrylamide gel. Purification purity was analyzed with SDS-PAGE.** Marker bands size: 200, 116.3, 97.4, 66.2, 45, 31, 21.5, 14.4 and 6.5 kDa. ApoA-I bands correspond to its size of ~ 28 kDa.

### 2. rHDL size and molecular weight determination

#### 2.1. rHDL molecular weight by size exclusion chromatography

Size exclusion chromatography (SEC) was used for rHDL purification and this technique, with the adequate calibration, can be used to calculate the molecular weight of the interest molecule<sup>494</sup>. Superdex 200 10/300 gel filtration column was first calibrated with molecular size standards (Amersham Biosciences, UK). The buffer used for rHDL formation, TEN buffer (Tris 10 mM, EDTA 1 mM, NaCl 150 mM, pH 8), was used as mobile phase. Chromatography was performed at 4 °C using a flow rate of 0.2 mL/min and elution profiles were expressed as retention volume

( $V_e$ ). The molecular size standards with their retention volume and molecular weights (MW) are shown in **Table 1**. In addition,  $K_{av}$  value is also indicated.  $K_{av} = \frac{V_e - V_0}{V_T - V_0}$ , where  $V_e$  is the retention volume for each molecule.  $V_0$  is the void volume which corresponds to  $V_e$  of Blue Dextran.  $V_T$  is the total volume of the column.

**Table 1. Molecular size standards used for Superdex 200 10/300 calibration**

Molecule	$V_e$ (mL)	Mw (kDa)	$K_{av}$
<b>Blue dextran 2000</b>	7.43	2000	---
<b>Thyroglobulin</b>	10.8	669	0.272
<b>Ferritin</b>	12.4	440	0.402
<b>Catalase</b>	13.24	232	0.47
<b>Aldolase</b>	14.6	158	0.58
<b>Ovalbumin</b>	17	44	0.773
<b>Ribonuclease A</b>	18.7	13.7	0.911

There is a linear relationship between the  $K_{av}$  of molecules and the logarithms of their molecular weights over a considerable size range. This calibration curve (**Figure 13**) was used to determine the molecular weight of purified rHDLs from retention volume.

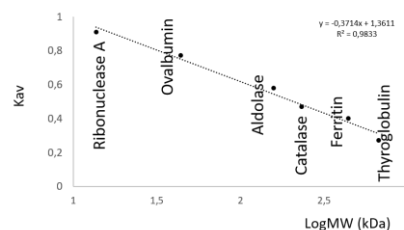


**Figure 13. Calibration curve of Superdex 200 10/300.** Molecular size standards  $K_{av}$  and logarithm of their molecular weight. This linear regression can be used to calculate molecular weight from  $K_{av}$  of the molecule of interest.

rHDL retention volume peak was ~ 12 mL in Superdex 200 10/300 and using the standard curve of **Figure 13**, the molecular weight calculated was 450 kDa. However, it is interesting to note that small variations in retention volume suppose significant changes in molecular weight, which do not agree with DLS hydrodynamic diameter measurements.

## *2.2. rHDL molecular weight by mass photometry*

Mass photometry is a novel method for analysing mass measurement of single molecules<sup>476</sup>. The amount of light scattered by a particle scales linearly with the particle's volume and refractive index. As the scattering signal is directly proportional to the molecule's mass, it is possible to weigh single molecules with light. The correlation of scattering signal with mass makes mass photometry a universal analysis tool for biomolecules in solution. Mass photometer (Refeyn Ltd, UK) was used to measure molecular size of rHDL during my stay in Copenhagen Centre for Glycomics (Copenhagen, Denmark). As shown in **Figure 14** DPPC rHDL of apoA-I weighs  $182 \pm 28$  kDa, a size that differs from the one measured by SEC.

According to Sigma-Aldrich MWGF1000 bulletin, gel filtration chromatography is an established method to determine protein molecular weight. However, size standard molecules for the calibration curve, should have similar shape of the unknown protein. This is because, although molecular weight has been correlated with retention volume, gel filtration column actually separates proteins not on their molecular weight but on their Stokes radius, a parameter that is affected by the shape of the unknown molecule<sup>495</sup>. In addition, according to Erickson, if the molecule at study is elongated, it can easily elute at a position twice the molecular weight of a globular protein<sup>495</sup>. The standards for calibration are globular proteins and TEM micrographs have shown that rHDL are elongated due to its discoidal morphology. Therefore, this could explain why rHDLs have an elution profile of 450 kDa molecule and not of 180 kDa, which is obtained from mass

photometry measurements. Therefore, it is reasonable to assume that SEC is not an accurate technique to measure rHDL molecular weight in an accurate manner.

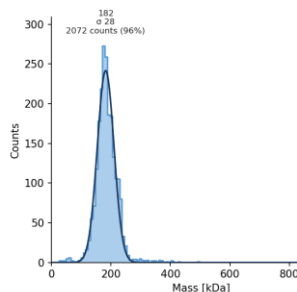


**Figure 14. DPPC rHDL size measurement by mass photometry.** Almost all the sample in solution (96 %) shows the same molecular weight of 182 kDa.

### 3. Binding of miRNA to rHDLs.

Previous work in our Lab demonstrate (data not shown) that DPPC:CE:LPC (7.5:2:0.5) rHDLs were the most efficient in binding microRNA. In addition, we considered that this lipid composition resembles HDL in their mature forms where cholesterol is already esterified.

In this way, DPPC:CE:LPC rHDL particles were loaded with a control miRNA as illustrated in **Figure 15A**. Binding efficiency of miRNA was assessed at different miRNA:apoA-I ratios. As shown in **Figure 15B**, maximum miRNA binding was obtained at 1:1 mol:mol ratio.

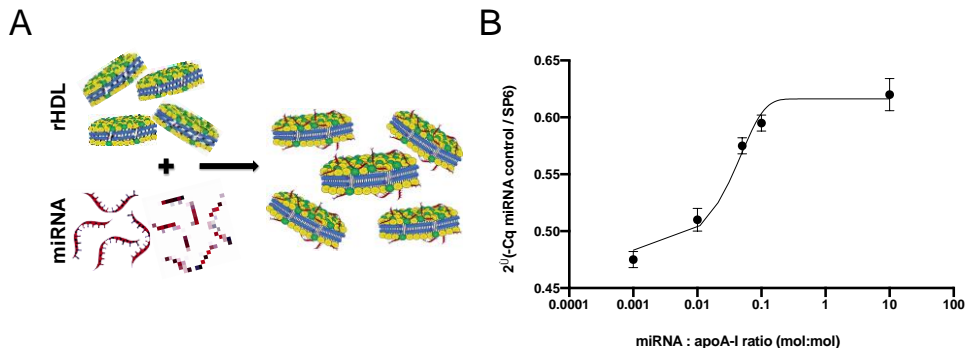


**Figure 15. MicroRNA loading of DPPC:CE:LPC rHDL** **A.** Schematic representation of rHDL loading with microRNA. **B.** Efficiency of miRNA binding to rHDL determined by qRT-PCR. A mimic control (cel-miR-67 mature sequence) was used at miRNA:protein mol ratios ranging 0.001-10:1. Binding efficiency was calculated as described in Methods. Data represent the mean  $\pm$  S.D. of at least three independent measurements.

#### 4. Protein and lipid molar ratio determination in rHDL

For rHDL production, lipids were added in a 125 molar excess respect to apoA-I concentration. This relationship was used to get nanoparticles of  $\sim$ 10 nm, based in data from previous work of our Lab, were it was demonstrated that increasing or decreasing the molar ratio of lipid to protein, produces bigger or smaller particles.

ApoA-I and lipid ratio after rHDL formation was characterized in this work. rHDL protein concentration, was determined by absorbance at 280 nm using NanoDropTM 2000 ( $\epsilon = 32,430 \text{ M}^{-1} \cdot \text{cm}^{-1}$ ). For lipid concentration Fiske-Subbarow colorimetric method was used as explained in methods<sup>474</sup>. According to measurements, when apoA-I is mixed with lipids in 1:125 molar ration, nanodiscs are reconstituted in 1: 80-1:100 molar ratio.

## 5. Determination of apoA-I number in rHDL by Crosslinking

Crosslinking is the use of a probe to link proteins that are at a known distance that serves to check protein interactions. In this work crosslinking was used to check the number of apoA-I molecules within each rHDL particle.

Dimethyl suberimidate (DMS) is a spacer arm of 8 atoms (11 Å) that contains a group of amine-reactive imidoesters in each end. DMS was incubated with rHDL sample as explained before and, after reaction, samples were analyzed by SDS-PAGE. DMS links proteins covalently, which makes possible to analyze the oligomers in a denaturing gel. As shown in **Figure 16**, DMS linked two and three apoA-I molecules, which means that apoA-I is organized in two by two or three by three in rHDL. The monomer band corresponds to the apoA-I that did not interact with DMS, which serves as a control of specific crosslinking.

Therefore, it can be concluded that two or three apoA-I molecules incorporate to rHDLs, similar as in nascent HDL<sup>338</sup>.

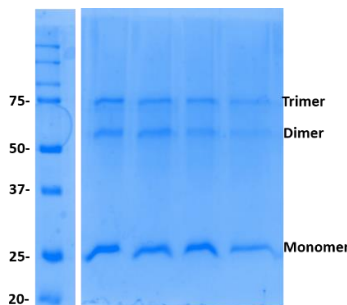


**Figure 16. Crosslinked apoA-I of rHDL samples.** DPPC rHDL samples were incubated with DMS and analyzed by SDS-PAGE. Each sample corresponds to a fraction of the rHDL peak resolved by SEC (~ 12 mL). Monomer band is the apoA-I that does not interact with DMS (~ 28 kDa). Second and third bands correspond to apoA-I dimers (56 kDa) and trimers (~ 80 kDa), respectively.

## 6. rHDL conservation

rHDL preparation is a laborious process that takes one week, therefore, it was interesting to analyse rHDL conservation when kept at 4 °C and when frozen. rHDL samples were analyzed freshly purified and after a month kept at 4 °C. Structural techniques such as DLS and circular dichroism were used to determine rHDL degradation. In addition, recently, mass photometer was used to analyse molecular size of frozen rHDLs.

As shown in **Figure 17**, apoA-I has the same secondary structure after a month from purification conserved at 4 °C. rHDL size was also maintained as shown in DLS measurements. In addition, mass photometer, shows that a month at 4 °C, do not affect the molecular weight of rHDL sample. Moreover, degradation or residual products could not be observed with mass photometry (a second peak) nor aggregation products.

However, studies about lipids or protein chemical modifications should be assessed (e.g. oxidation) for a comprehensive analysis.

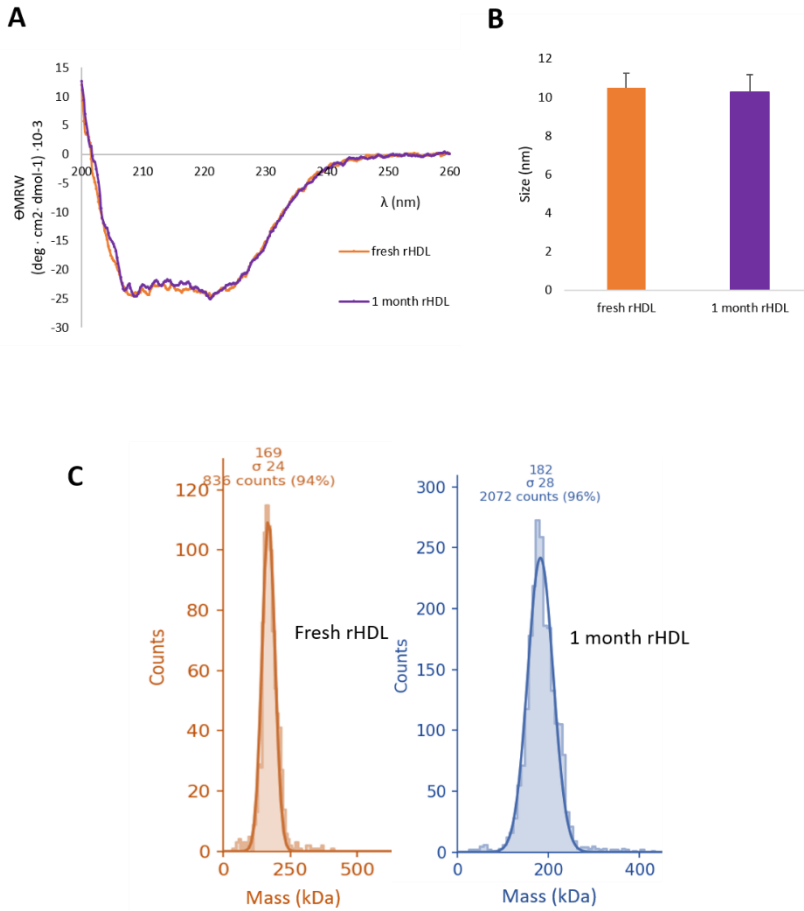


**Figure 17. rHDL structural analysis when stored at 4 °C for a month. A.** Circular dichroism spectra of fresh rHDL and rHDL kept at 4 °C for one month. ApoA-I secondary structure was preserved when conserved the samples at 4 °C for one month. **B.** Hydrodynamic diameter of fresh rHDL and samples stored for one month at 4 °C . No changes in size were observed. **C.**

On the other hand, recently and using mass photometer, rHDL cryopreservation was analyzed. Mass photometer lower limit is 30 kDa, which makes possible to measure apoA-I shedding due to rHDL degradation.

Sucrose is a cryopreserving composite that is already used to conserve lipoproteins for longer periods at -20 or -80 °C<sup>496,497</sup>. DPPC rHDL were frozen at different sucrose percentages both at -20 °C and -80 °C for three weeks, after thawing the samples, rHDL samples were diluted in TEN buffer to 40 nM. Mass photometer calibration was done with TEN buffer and samples were diluted two more times for the measurement. As shown in **Figure 18** rHDL molecular sizes did not change when rHDL were frozen either at -20 or at -80. However, a second smaller peak (~ 10% of the total) was detected during the freeze-thaw process, which suggests particle damage during this period. Functional analysis such as cholesterol efflux experiments should be done with frozen rHDLs to conclude that cryopreservation is a good method for rHDL storage, as concluded with plasma HDLs<sup>497</sup>.

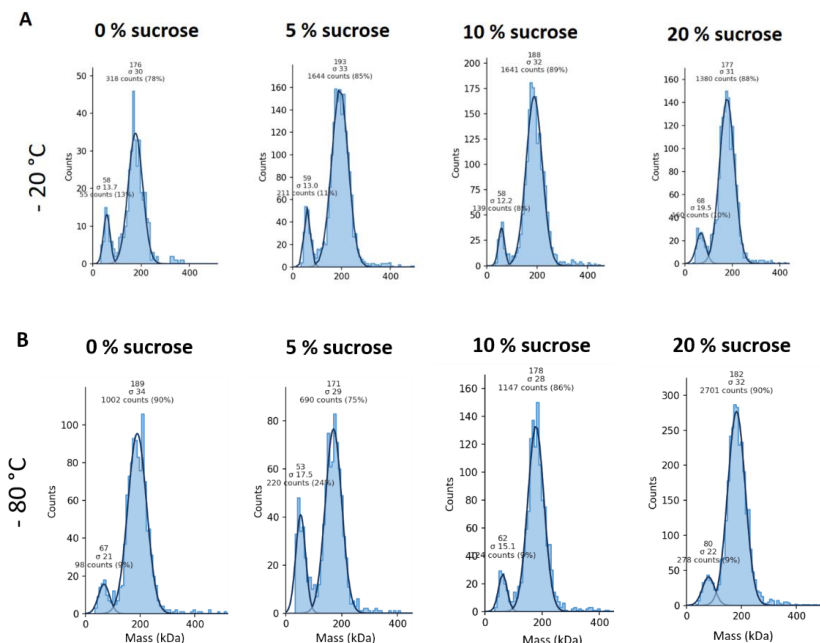


**Figure 18. Mass photometer measurement of frozen rHDL samples.** rHDL samples were stored at **A.** -20 °C or **B.** -80 °C with different sucrose concentration (0-20%, v/v).

## Results 2. Cholesterol efflux efficiency of reconstituted HDL is affected by nanoparticle lipid composition

### 1. Development and Biophysical Characterization of rHDL

HDL were reconstituted with different phospholipid mixtures (Soy-PC, DPPC, DPPC:Chol:LPC (85:10:5 mol%) and DPPC:CE:LPC (75:20:5 mol%) as indicated in Methods section. The reconstitution ratio of apoA-I:lipid was optimized to 1:125. The rHDLs, aggregates, and free apoA-I were detected and separated by size exclusion chromatography on a Superdex 200 column as shown in **Figure 19A**. When applying the rHDLs samples, the aggregates were present in the void volume of the size exclusion column at 7–9 mL, and a rHDL homogenous peak was centered at 11–13 mL, preceding free apoA-I at 15 mL (**Figure 19A**).

DLS was used to characterize rHDL size (hydrodynamic diameter) and homogeneity. The size distribution of nanodiscs indicated that rHDLs have an average diameter of ~10 nm (**Figure 19B**).

We next evaluated, by circular dichroism (CD) measurements,  $\alpha$ -helical structure in the purified rHDL and apoA-I (**Figure 19C**). The higher  $\alpha$ -helical content of rHDL shown by rHDL compared to free apoA-I ( $\approx$ 2.2–2.5 times,

*Table 2*) indicates a correct protein conformation and well-structured protein within the nanodisc (**Figure 19C**).

**Table 2.  $\alpha$ -helical content of apoA-I and rHDL determined by CD.**

	$\alpha$ -helical Content	$\alpha$ -helicity ratio rHDL/apoA-I
ApoA-I	$30.7 \pm 2.3$	-
DPPC	$70.0 \pm 2.8 *$	$2.3 \pm 0.3 *$
DPPC:Chol:LPC	$77.4 \pm 6.6 *$	$2.5 \pm 0.02 *$
DPPC:CE:LPC	$64.7 \pm 3.8 *$	$2.2 \pm 0.04 *$
Soy-PC	$70.3 \pm 3.5 *$	$2.5 \pm 0.3 *$

$\alpha$ -helical content calculated from ellipticity values at 222 nm. R is the ratio of alpha helicities between nanoparticles and free protein. Once incorporated into rHDL, apoA-I increases its helicoidal structure 2 times in each composition of rHDL, with no differences among them. Data represent the mean  $\pm$  S.D. ( $n = 3$ ). All measurements were performed independently 3 times and levels of significance were determined by a two-tailed Student's *t*-test. \* $p < 0.01$  compared to apoA-I. rHDL: reconstituted HDL; DPPC: 1,2-dipalmitoyl-sn-glycero-3-phosphocholine; LPC: 1-palmitoyl-2-hydroxy-sn-glycero-3-phosphocholine. Chol: free unesterified cholesterol; CE: esterified cholesterol; Soy-PC: soy phosphatidylcholine.

Negative stain electron microscopy (NS-EM) was also used to qualitatively examine homogeneity of the rHDLs and to measure particle diameter (**Figure 19D** and **E**). The peak population of the selected 1600 particles was in the diameter range of 8–10 nm, confirming the values obtained by DLS (**Figure 19D**). The determined diameters for the rHDLs were: DPPC  $9.0 \pm 1.6$ , DPPC:Chol:LPC  $9.2 \pm 2.4$ , DPPC:CE:LPC  $10.8 \pm 2.2$  and Soy-PC  $8.7 \pm 2.3$ . Mostly, all nanodiscs appeared as

single particles oriented randomly on the staining grid (**Figure 19E**). The characteristic stacked nanoparticles were also observed by NS-EM but they appeared in a non-significant number. rHDL morphology was approximately circular, consistent with a discoidal shape (**Figure 19E**).

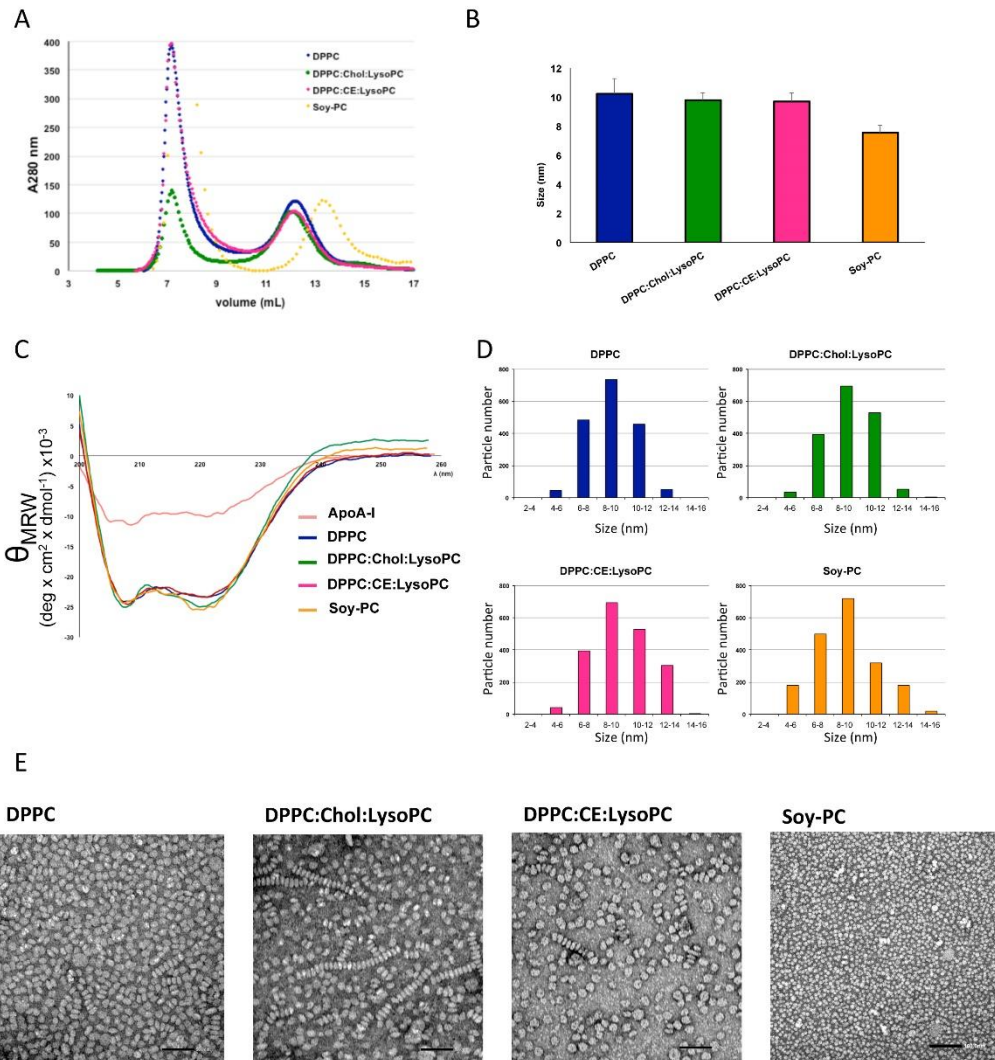


**Figure 19. Development and biophysical characterization of rHDL. A.** Gel filtration profiles of rHDL reconstituted with different lipids and apoA-I. Nanoparticles were analyzed by gel filtration chromatography on a Superdex 200 column eluted at 4 °C.

The profiles were monitored using absorbance at 280 nm. **B.** rHDL size (hydrodynamic diameter) determination by dynamic light scattering (DLS). Each rHDL preparation present 9–10 nm diameter when analyzed trough DLS. No significant differences between different compositions. **C.** Circular dichroism of rHDL preparations and apoA-I protein in solution at 25 °C in buffer TEN (pH 8).  $\theta_{\text{MRW}}$ : mean residue ellipticity. **D.** Frequency histograms showing particle size distribution of rHDL determined from NS-EM images. rHDL size distribution was measured as Feret diameter calculated from 1600 particles. **E.** Representative rHDL transmission electron microscopy images. DPPC, DPPC:Chol:LPC (8.5:1:0.5), DPPC:CE:LPC (7.5:2:0.5) and Soy-PC. Magnification 100 ×. Scale bar of 50 nm. Soy-PC scale bar of 100 nm.

Transition temperature of the rHDLs lipid moiety was assessed by steady state fluorescence anisotropy using DPH, which localizes to the hydrocarbon core of the lipid bilayer<sup>498</sup>. The temperature-dependent fluorescence anisotropy changes of DPH allows determining phase transition temperature of the different lipid mixtures in rHDLs<sup>499</sup>. As shown in **Figure 20**, the phase transition temperature of DPPC rHDL obtained from our measurement is  $42.9 \pm 0.3$  °C, which is similar to the literature value-range of phase transition temperature of DPPC nanodiscs<sup>500</sup>. The addition of Chol/LPC or CE:LPC to the nanodiscs increases the phase transition temperature by 1.7 and 4.1 °C compared to DPPC alone, respectively (**Figure 20**). As shown in the **Figure 20** inset, DPPC:Chol:LPC and DPPC:CE:LPC  $T_m$  are  $44.6 \pm 0.6$  and  $47.0 \pm 0.5$  °C, respectively. As expected due to its lipid composition, HDL  $T_m$  was  $32.0 \pm 0.3$  °C in the range of the previously described transition temperature of lipoproteins (27–34 °C)<sup>501</sup>. Fluorescence anisotropy changes of DPH Soy-PC nanodisc were not assessed because they are already at liquid-crystalline state below 0 °C<sup>502</sup>.

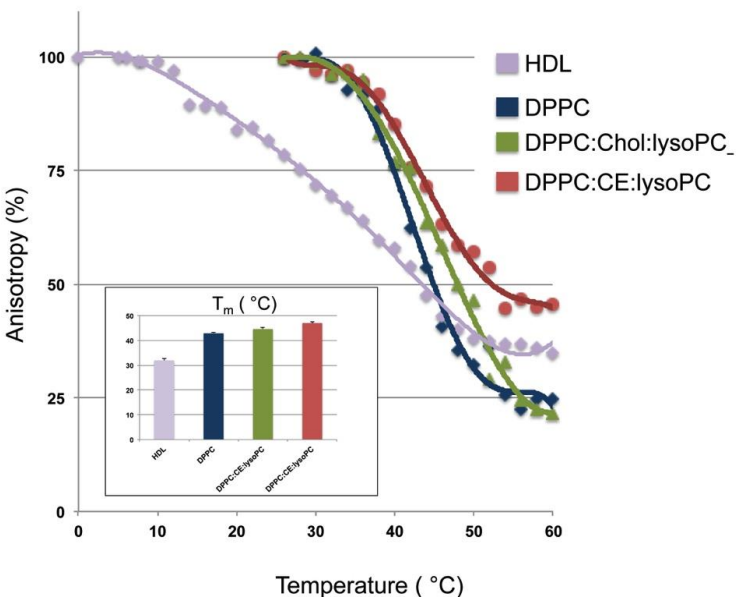


**Figure 20. Fluorescence anisotropy of DPH in HDL, DPPC, DPPC:Chol:LPC and DPPC:CE:LPC rHDLs as a function of temperature.** The inflection point of the plot gives the phase transition temperature of high-density lipoproteins (HDL) and rHDLs. Insert shows the phase transition temperatures. DPH was excited at 360 nm and fluorescence anisotropy was measured at 428 nm. All measurements were carried out in TEN buffer, pH 8. Concentration of HDL and rHDL was kept constant at apoA-I 2  $\mu$ M for all measurements. Data points shown are means  $\pm$  S.D. of at least three independent measurements. DPH: 1,6-diphenyl-1,3,5-hexatriene.

## 2. J774A.1 macrophages derived foam cells formation

### 2.1. Confirmation of LDL Acetylation by Agarose Gel Electrophoresis

Acetylated LDL electrophoretic mobility was assessed in a 0.7% (w/v) agarose gel prepared in running buffer (90 mM Tris-HCl, 80 mM Boric acid, pH 8.2). Due to lysine acetylation, LDLac show a higher electrophoretic mobility than normal LDL (**Figure 21**). Electrophoresis was performed at 4 °C and 90 V for 80 minutes. Gel was

dried at 80 °C for 1 hour, after incubating it for 30 minutes in fixing buffer (75% ethanol, 5% glacial acetic acid) at room temperature. Then, gel was stained with Coomassie Brilliant Blue.

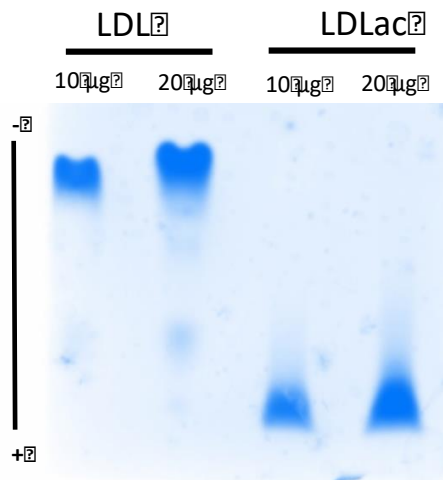


**Figure 21. Agarose gel electrophoresis of acetylated LDL (LDLac).**

Electrophoretic pattern of LDL and acetylated LDL in agarose gel. LDLac show a higher electrophoretic mobility than normal LDL due to lysine acetylation.

## *2.2. Quantitative and qualitative analysis of foam cell formation*

Foam cell formation is a complex process where macrophages internalize modified lipoproteins. This process can be measured by analysing lipid accumulation in the cytoplasm in form of lipid droplets<sup>503</sup>.

J774A.1 cells were incubated with acetylated LDL in a dose response manner and foam cell formation was assessed quantitatively and qualitatively. For quantitative analysis, Oil-Red-O (ORO) dye was used (Sigma-Aldrich, USA) to measure the lipid accumulated within lipid droplets. For ORO data normalization cell nucleus were

labelled with Violet crystal (Sigma-Aldrich, USA). After labelling of each dye, both ORO and Crystal violet were extracted from cells, and their absorbance was measured at 510 nm and 580 nm, respectively.

For qualitative analysis, foam cell formation was assessed by optical microscopy. Cells lipid droplets were labelled again with ORO, whereas the nucleus were labelled with Meyer's Hematoxylin (Sigma-Aldrich, USA). After the required washing steps, pictures of the cells were taken in a Nikon ECLIPSE TS100 inverted microscope (Nikon, Japan) (**Figure 22B**).

As seen in **Figure 22A**, lipid accumulation within cells increases with LDLac incubation, reaching a *plateau* phase at 100 µg/mL. Concentration of 125 µg/mL was chosen for next experiments.

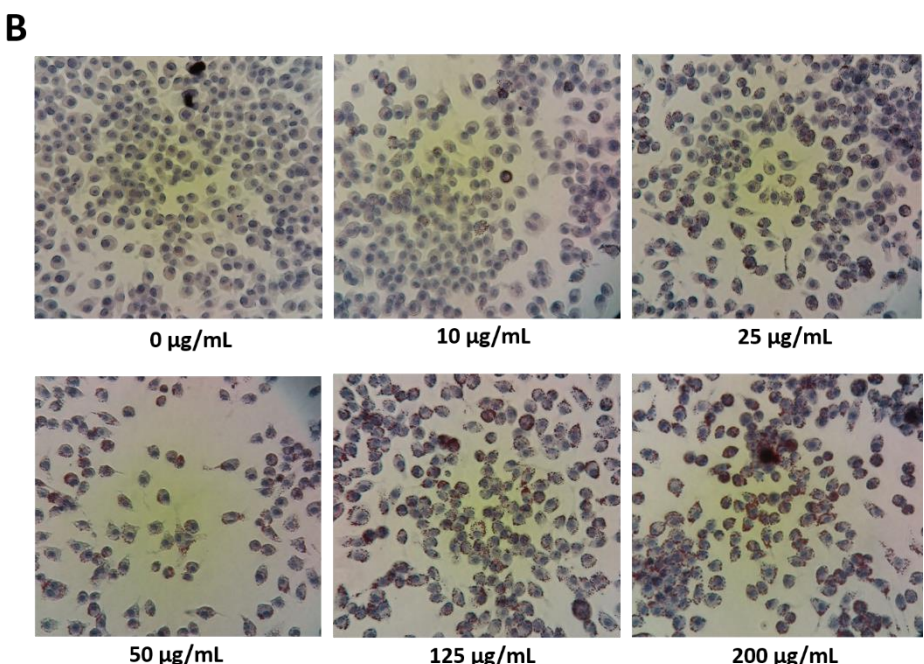
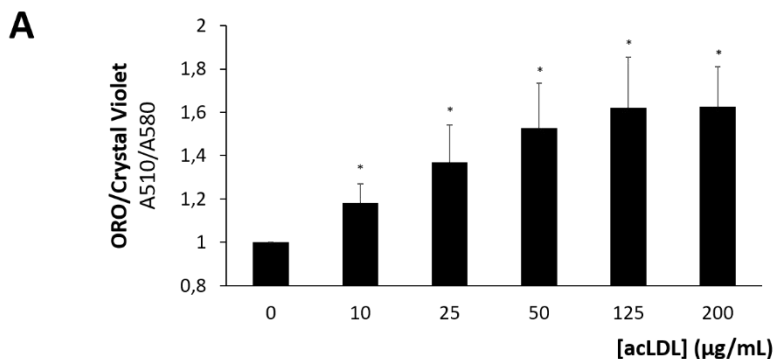


**Figure 22. Quantitative and qualitative analysis of foam cell formation.** **A.** Quantitative analysis of the formation of foam cells was performed with Oil-Red-O (ORO) dye and with Crystal Violet as described in Methods. **B.** Qualitative analysis of foam cells was performed by optical microscopy by staining lipid droplets with ORO and nuclei with Mayer's Hematoxylin. Images were captured in a Nikon ECLIPSE TS100 inverted microscope (Nikon, Japan). The data in (A) represent the mean  $\pm$  S.D. of at least three independent measurements. Levels of significance were determined by a two-tailed Student's t-test. \* $p<0.005$  compared to no addition of acetylated LDLs.

### 3. Effect of rHDL Lipid Composition on Cholesterol Efflux In Vitro

#### 3.1. Cholesterol Efflux Promoted in Human and Murine Macrophages

The effect of rHDL lipid composition on promoting cholesterol efflux was assessed both in human THP-1 and murine J774A.1 macrophages, and in human VSMC-derived foam cells (**Figure 23**, **Figure 13**, **Figure 14**, respectively). Cells were loaded with TopFluor® cholesterol and cholesterol efflux was determined following incubation with rHDL of different lipid compositions.

As shown in **Figure 23A**, incubation of THP-1 derived macrophages with DPPC and DPPC:Chol:LPC rHDLs showed a significantly higher cholesterol efflux than those incubated with human HDL; in fact, DPPC rHDL particles were a 51% more efficient than HDLs and, DPPC:Chol:LPC rHDLs showed a 34% increased efficiency compared to HDLs. In contrast, DPPC:CE:LPC and Soy-PC rHDLs showed a similar cholesterol efflux compared to HDLs.

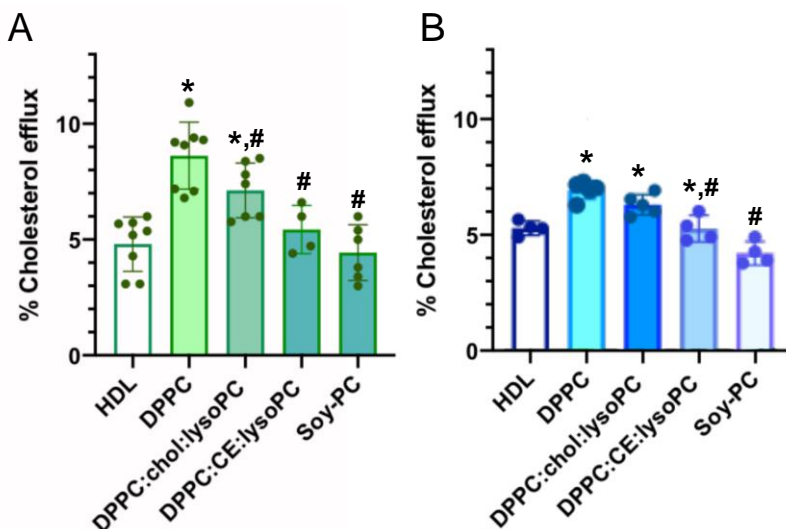


**Figure 23.** Effect of HDL, DPPC, DPPC:Chol:LPC, DPPC:CE:LPC and Soy-PC rHDLs on cholesterol efflux in **A.** human THP-1 and **B.** murine J774A.1 derived macrophages. rHDLs

were added to the cells in MEM-Hepes 25 mM (pH 7.4) containing 2 µg/mL ACAT inhibitor and incubated during 6 h to promote cholesterol efflux. Cholesterol efflux was calculated as described in Methods. The data represent the means ± S.D. of at least three independent measurements. Levels of significance were determined by a two-tailed Student's *t*-test. \* *p* < 0.01 compared to HDL and # *p* < 0.01 compared to DPPC.

Similar results, but to a lesser extent, were obtained in J774A.1 macrophages. As shown in **Figure 23B**, DPPC and DPPC:Chol:LPC rHDLs induced a significantly higher cholesterol efflux from the cells than those incubated with human HDL; in this case, DPPC rHDL particles were 35% more efficient than HDLs and, DPPC:Chol:LPC rHDLs showed increased efficiency by 24% compared to HDLs. In contrast, DPPC:CE:LPC and Soy-PC rHDLs showed similar cholesterol efflux compared to HDLs.

Cholesterol efflux induced by rHDLs in J774A.1 macrophage-derived foam cells showed similar results to those determined in THP-1 and J774A.1 cells (**Figure 1313A**). Incubation with DPPC rHDL induced a significantly higher cholesterol efflux when compared with HDL. Although the cholesterol efflux induced by HDL was lower when compared to non-foam J774A.1 cells, the efficiency of DPPC nanodiscs resulted in a higher efficiency when compared to that determined with DPPC rHDL in non-foam cells (57% vs. 35%, respectively). DPPC:Chol:LPC, DPPC:CE:LPC also showed a higher cholesterol efflux compared to HDL (~20%, ~25%, respectively) while Soy-PC rHDLs showed a similar cholesterol efflux than that determined for HDL. Next, the effect of ABCA1 overexpression on cholesterol efflux induced by rHDLs was examined. ABCA1 mRNA expression was stimulated by incubating J774A.1 foam cells with TO901317 and cholesterol efflux was determined in similar conditions as before. As shown in **Figure 13A**, upregulation of the ABCA1 transporter significantly enhanced the cholesterol efflux induced by rHDL, with the cholesterol efflux induced by DPPC being 140% more effective than that induced by HDL. The effect of DPPC:Chol:LPC and DPPC:CE:LPC rHDLs on cholesterol efflux was 100% higher than HDL. On the other hand, Soy-PC rHDL induced cholesterol efflux

was similar to that induced by HDL. As shown in **Figure 13B** and **C**, TO901317 almost induced twice the upregulation of ABCA1 transporter, indicating that cholesterol efflux induced by DPPC, DPPC:Chol:LPC and DPPC:CE:LPC rHDLs is efficiently enhanced by upregulating the transporter (**Figure 13**).

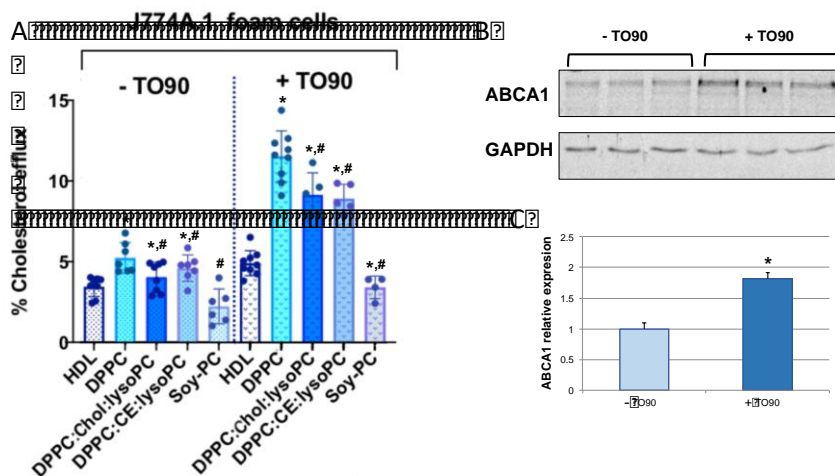


**Figure 13.** Effect of HDL, DPPC, DPPC:Chol:LPC, DPPC:CE:LPC and Soy-PC rHDLs on cholesterol efflux in **A.** murine J774A.1 derived foam cells and murine J774A.1 derived foam cells stimulated with TO901317. **B.** ABCA1 levels in both TO901317 stimulated and non-stimulated foam cells. **C.** Expression levels of ABCA1 determined by optical density. rHDLs were added to the stimulated and non-stimulated cells in MEM-Hepes 25 mM (pH 7.4) containing 2 µg/mL ACAT inhibitor and incubated during 6 h to promote cholesterol efflux. Cholesterol efflux was calculated as described in Methods. The data in A and C, represent the means ± S.D. of at least three independent measurements. Figure B correspond to a representative western blot of  $n = 3$ . Levels of significance were determined by a two-tailed Student's *t*-test. \*  $p < 0.01$  compared to HDL and #  $p < 0.01$  compared to DPPC.

### 3.2. Cholesterol Efflux Promoted in Human VSMC-Foam Cells

VSMCs extracted from carotid arterial atherosclerotic tissue samples showing foam cell phenotype obtained from carotid endarterectomy were used to determine the ability of rHDL to induce cholesterol efflux<sup>504</sup>. As shown in **Figure 14**, upon incubation with rHDLs, only DPPC nanodiscs induced a slight but significant increase in cholesterol efflux (22%) when compared with HDL. DPPC:Chol:LPC and DPPC:CE:LPC rHDLs showed similar cholesterol efflux to HDL. Upregulation of ABCA1 in VSMC by TO901317 increases cholesterol efflux to HDL significantly when compared to non-stimulated cells (**Figure 14**). In addition, cholesterol efflux to DPPC rHDL was also significantly increased compared to HDL upon TO901317 treatment (**Figure 14**). The effect of DPPC:Chol:LPC and DPPC:CE:LP CrHDLs in TO901317 stimulated cells was similar to HDL (**Figure 14**).

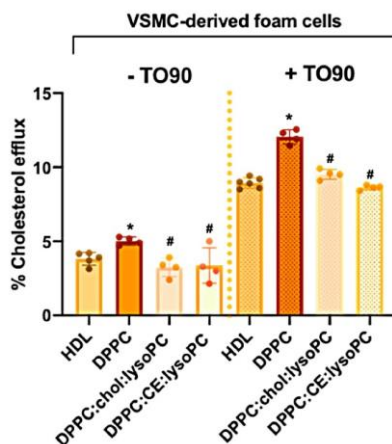


**Figure 14.** Effect of HDL, DPPC, DPPC:Chol:LPC and DPPC:CE:LPC rHDLs on cholesterol efflux in vascular smooth muscle cells (VSMC) derived foam cells stimulated or not with TO901317. rHDLs were added to the stimulated and non-stimulated cells in MEM-Hepes 25 mM (pH 7.4) containing 2 µg/mL ACAT inhibitor and incubated during 6 h to promote cholesterol efflux. Cholesterol efflux was calculated as described in Methods. Data represent the means ± S.D. of at least three independent measurements. Levels of significance were determined by a

two-tailed Student's *t*-test. \* *p* < 0.01 compared to HDL and # *p* < 0.01 compared to DPPC.

## **Results 3: Boosting cholesterol efflux from foam cells by sequential administration of rHDL to deliver microRNA and to remove cholesterol in a triple-cell two-dimensional atherosclerosis model**

### **1. Development and Biophysical Characterization of DPPC:CE:LPC and DPPC rHDL**

HDL were reconstituted with DPPC:CE:LPC (75:20:5 mol%) for antagomiR-33a delivery or DPPC alone for cholesterol efflux as indicated in the Methods section. ApoA-I:lipid ratio was optimized to 1:125 mol:mol in both compositions. Nanoparticle formation is illustrated in **Figure 24A**. Once reconstituted, rHDLs were purified by size exclusion chromatography. As shown in **Figure 24B**, rHDL showed a homogeneous peak centred at 11–13 mL, preceding the elution of free apoA-I at 15 mL. Size distribution of nanodiscs determined by dynamic light scattering (DLS) showed an average diameter of the particles of ~10 nm (**Figure 24C** and F). Finally,  $\alpha$ -helical structure content determined by circular dichroism (CD) showed higher  $\alpha$ -helical content in rHDLs compared to free apoA-I (~2.2–2.5 times, **Figure 24D**; **Table 3**). These results indicate a correct reconstitution of rHDLs (**Figure 24B-D**). Size and morphology of nanoparticles were determined by negative stain electron microscopy (NS-EM) (**Figure 24E**), which showed a circular morphology, consistent with a discoid shape as shown by typically stacked nanoparticles resembling a “rouleaux” formation and, circular shapes presented by nanodiscs viewed from the top (**Figure 24E**). Longitudinal and transverse axes were  $10.6 \pm 0.8$  and  $3.9 \pm 0.4$  nm, respectively. The longitudinal axis was similar to the diameter range (8–10 nm) determined by both DLS and NS-EM (**Figure 24F**).

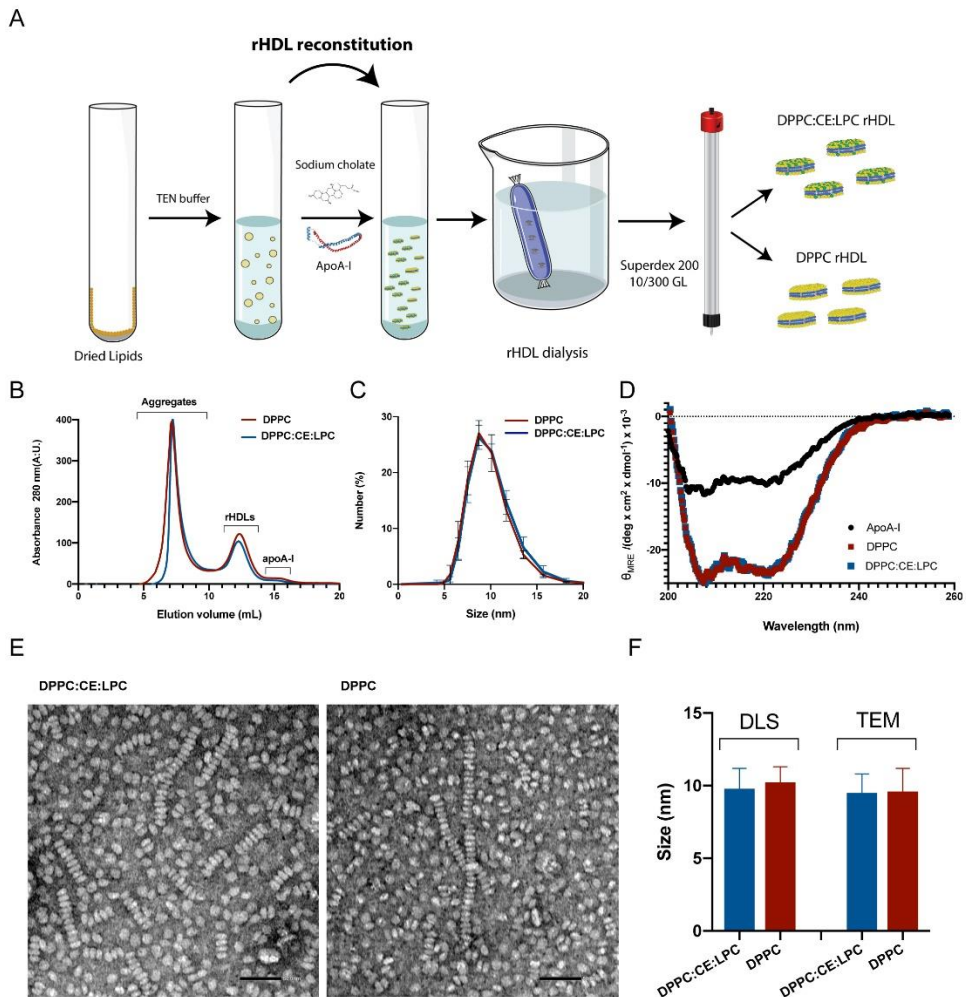


**Figure 24. Development and biophysical characterization of rHDL.** **A.** Schematic representation of rHDL reconstitution and purification by gel filtration chromatography on a Superdex 200 column. **B.** Gel filtration profiles of DPPC and DPPC:CE:LPC rHDLs, profiles were monitored by absorbance at 280 nm. **C.** rHDL size profiles determined by DLS. No significant differences between the different rHDL compositions were determined. **D.** Circular dichroism of DPPC and DPPC:CE:LPC rHDLs and apoA-I protein in solution.  $\theta_{MRE}$ : mean residue ellipticity. **E.** Representative rHDL transmission electron microscopy images. Magnification 100 $\times$ . Scale bar of 50 nm. **F.** rHDL diameter determined

from DLS (hydrodynamic diameter) and NS-EM images. Size of rHDL was measured as Feret diameter calculated from 1600 particles.

**Table 3.  $\alpha$ -helical content of apoA-I and rHDL determined by CD.**

	$\alpha$ -Helical Content	$\alpha$ -Helicity Ratio rHDL/apoA-I
apoA-I	$31.1 \pm 2.0$	-
DPPC	$71.3 \pm 2.5 *$	$2.3 \pm 0.2 *$
DPPC:CE:LPC	$67.4 \pm 3.4 *$	$2.2 \pm 0.1 *$

$\alpha$ -helical content calculated from ellipticity values measured at 222 nm. R is the ratio of  $\alpha$ -helicities between rHDLs and free protein. Data represent the mean  $\pm$  S.D. ( $n = 3$ ). All measurements were performed independently three times and levels of significance were determined by a two-tailed Student's t-test. \*  $p < 0.01$  compared to apoA-I.

## 2. Delivery of antagomiR-33a by DPPC:CE:LPC rHDL into foam cells in atherosclerosis plaque model

### 2.1. *Two-dimensional atherosclerosis plaque model set up*

A modular co-culture system, which facilitates the separation of each cellular compartment, was used to set up a three-cell 2D-atherosclerosis model. The system allows co-culturing ECs, VSMCs and macrophage-derived foam cells mimicking the vascular compartment thus facilitating the study of dynamics and interaction of rHDL with foam cells. A schematic illustration of the model is shown in **Figure 25A**. The use of  $0.4 \mu\text{m}$  pored transwell inserts allows separation of VSMCs and ECs by a thin transwell membrane. This avoids translayer contamination by the other cell types while at the same time allows to individually isolate each culture layer. Barrier

function was validated by determining transendothelial electrical resistance (TEER) of ECs. The calculated TEER value calculated by Ohm's law,  $24.6 \pm 1.2 \text{ } \Omega \cdot \text{cm}^2$  confirmed integrity and permeability of the in vitro barrier and are in agreement with values reported by others<sup>505,506</sup>.

As illustrated in **Figure 25B**, delivery of antagomiR-33a by DPPC:CE:LPC rHDL would promote miR-33a silencing and consequently upregulation of ABCA1 and ABCG1 transporters.

## *2.2. Uptake of DPPC:CE:LPC rHDL by ECs, VSMC and Foam Cells*

We next aimed to address the delivery of antagomiR-33a by rHDL through the 2D atheroma model and determined the efficiency of rHDL uptake by ECs, VSMCs and foam cells in confluent populations. To establish the optimal condition for efficient microRNA delivery, different concentrations of rHDL were used (0-100 µg/mL) (**Figure 25C**) and uptake of Dil-labelled DPPC:CE:LPC rHDL by the different cell types was assessed after 24 h by fluorescent microscopy and flow cytometry. As shown in **Figure 25**, foam cells were extremely avid internalizing DPPC:CE:LPC rHDL (**Figure 25C, lower panel**). On the other hand, VSMCs showed residual rHDL uptake (**Figure 25C, middle panel**) while ECs internalized rHDL in a moderate way (**Figure 25C, top panel**) compared to foam cells. To quantify rHDL uptake efficiency, cells from the different compartments were isolated after incubation with the nanoparticles and their uptake was analyzed by flow cytometry as described in Methods. As shown in **Figure 25D**, and confirming the results obtained by fluorescent microscopy, foam cells showed the highest ability in rHDL uptake, which resulted saturated at 50 µg/mL. Considering the fluorescence determined in foam cell uptake when treated with 100 µg/mL as 100%, rHDL uptake by ECs was 34% compared to foam cells while the uptake by VSMCs resulted residual (**Figure 25D**).

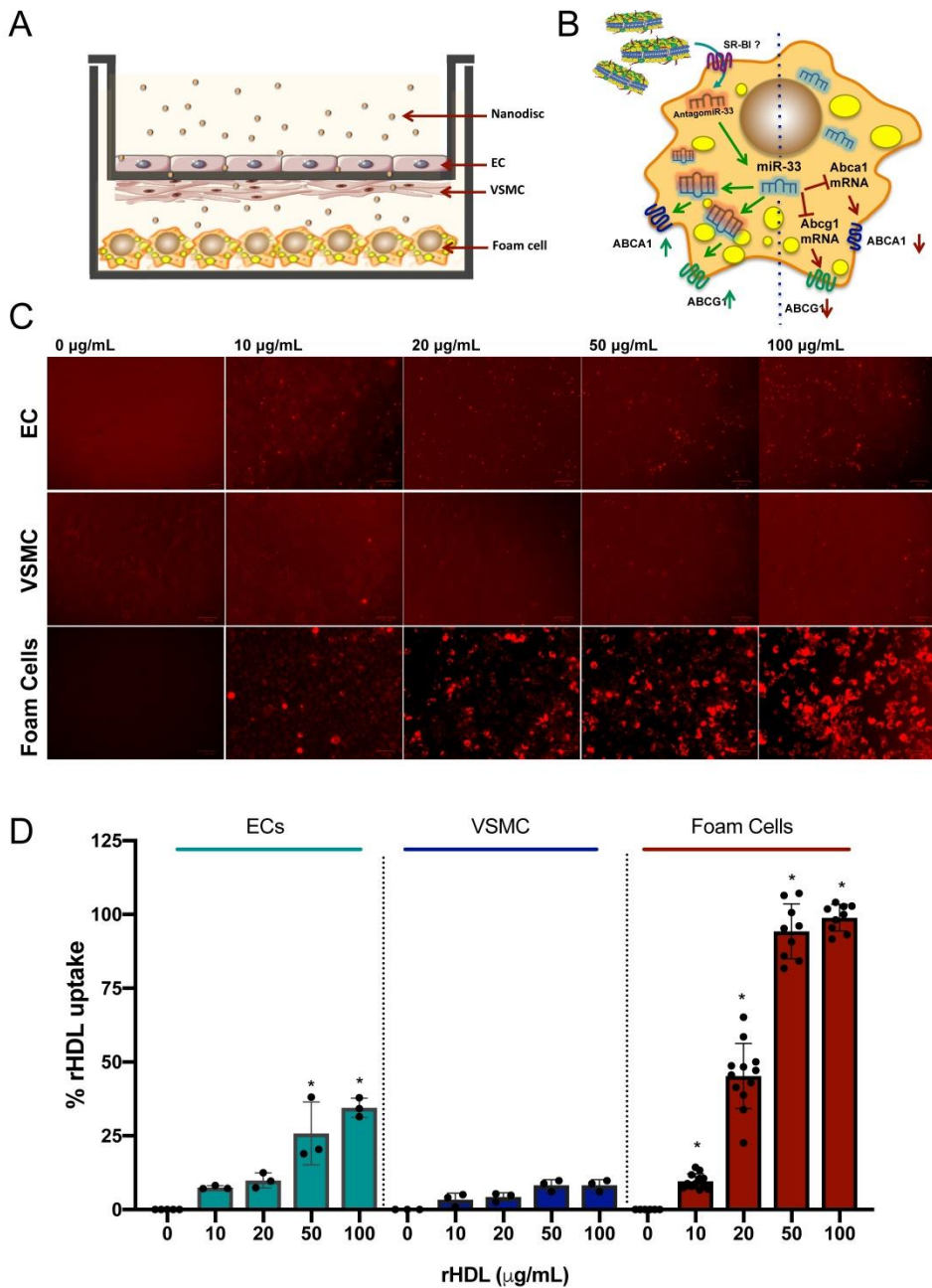


**Figure 25. DPPC:CE:LPC rHDL are efficiently delivered into foam cells in the 2D atheroma model.** **A.** A schematic illustration of the 2D atheroma model. The system allows co-culturing ECs, VSMCs and macrophage-derived foam cells mimicking the

vascular compartment. **B.** ABCA1 and ABCG1 upregulation in foam cells by the delivery of antagomiR-33a loaded rHDL, which promotes miR-33a silencing. **C.** Fluorescent micrographs showing rHDL uptake in ECs (top panel), VSMC (middle panel) and foam cells (lower panel) at different rHDL concentrations (0-100 µg/mL). **D.** Uptake of Dil-labelled DPPC:CE:LPC rHDL concentrations (0-100 µg/mL) by the different cell types assessed by flow cytometry. Data represent the mean ± S.D of at least three independent measurements. Levels of significance were determined by a two-tailed Student's t-test. \* p<0.01 compared to no rHDL addition (0 µg/mL). Scale bars 50 µm.

### *2.3. Delivery of antagomiR-33a by DPPC:CE:LPC rHDL to Foam Cells*

Intracellular delivery of miRNA by rHDL to foam cells was then assessed in the 2D atheroma model. First, delivery of cel-miR-67 (a microRNA that is naturally and specifically expressed in *C. elegans*) was used to set up validation. DPPC:CE:LPC rHDL particles loaded with cel-miR-67 at 1:1 mol:mol ratio were added in the ECs compartment at different concentrations (0-100 µg/mL rHDL) and miRNA incorporation into foam cells was determined after 24 h incubation with nanoparticles (**Figure 26A**). Total RNA was purified and intracellular cel-miR-67 levels were quantified as indicated in Methods. As shown in **Figure 26A**, delivery efficiency of miRNA reached maximum values at 100 µg/mL rHDL.

Similarly, a DPPC:CE:LPC rHDL dose-dependent (0-20 µg/mL rHDL) uptake assay was performed in macrophage-derived foam cells cultured alone in monolayer. In the absence of the vascular barrier simulated in the 2D atheroma model, the rHDL concentration required to achieve maximal delivery resulted five times lower (10 µg/mL rHDL) compared with the ones required in the 2D atheroma model (**Figure 27**).

We next examined the ability of silencing miR-33a by delivering antagomiR-33a in DPPC:CE:LPC rHDL in the 2D atheroma model. Therefore, nanoparticles were loaded with antagomiR-33a and then, 50 µg/mL rHDL-antagomiR-33a were added

into the ECs compartment and incubated for 48 h. Delivery of antagomiR-33a to foam cells by rHDL reduced  $\approx$ 4 times the levels of endogenous miR-33a compared with cells treated with nanodisc carrying control miRNA (**Figure 26B**). The extent of miR-33a silencing was also analyzed by determining the mRNA levels of ABCA1 and ABCG1, two known targets of miR-33a. As shown in **Figure 26C**, treatment with antagomiR-33a loaded rHDL resulted in  $\approx$ 2.5 and 2 fold higher levels of ABCA1 and ABCG1 compared to control cells (treated with control miRNA), respectively. Similarly, upregulation of ABCA1 and ABCG1 protein levels in foam cells by delivering antagomiR-33a in DPPC:CE:LPC rHDL was confirmed by Western blot **Figure 26D**. Expression levels of ABCA1 and ABCG1 determined by optical density were  $4.0 \pm 0.8$  and  $2.3 \pm 0.6$ , respectively (**Figure 26E**).

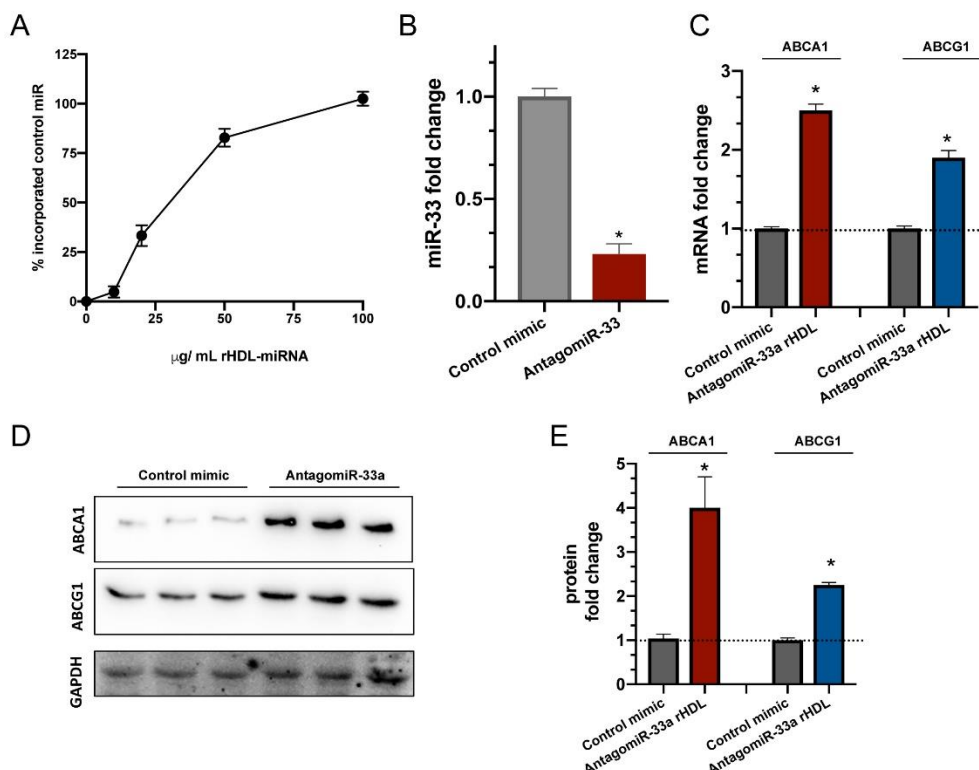


**Figure 26. miRNA transfer capacity, miR-33a downregulation and ABCA1/ABCG1 upregulation by miRNA delivery by DPPC:CE:LPC rHDL to foam cells.** rHDLs were added to the cells in Opti-MEM™ to allow miRNA delivery, mir-33a repression and protein upregulation. **A.** Intracellular delivery of miRNA by rHDL to foam cells assessed in the 2D atheroma model. DPPC:CE:LPC rHDL particles loaded with cel-miR-67 at 1:1 mol:mol ratio were added in the ECs compartment at different concentrations (0-100 µg/mL rHDL). **B.** miR-33a silencing by delivering antagomiR-33a in DPPC:CE:LPC rHDL (50 µg/mL) in the 2D atherosclerosis model. **C.** mRNA levels of ABCA1 and ABCG1 after delivery of antagomiR-33a by rHDL to foam cells. MiR-33a and mRNA levels were determined after incubation of rHDL with 2D atherosclerosis model foam cells during 48 h by qRT-PCR determined as described in Methods. **D.** Upregulation of ABCA1 and ABCG1 protein levels in foam cells by delivering antagomiR-33a in DPPC:CE:LPC rHDL. **E.** Expression levels of ABCA1 and ABCG1 determined by optical density. The data in A, B, C and E represent the mean ± S.D of at least three independent measurements. The data in D correspond to a representative western blot of n=3. Levels of significance were determined by a two-tailed Student's t-test. \*p<0.01 compared to control miRNA.

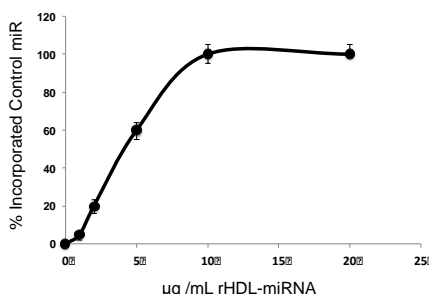


**Figure 27. miRNA transfer capacity by DPPC:CE:LPC rHDL to foam cells cultured in monolayer.** DPPC:CE:LPC rHDL particles loaded with cel-miR-67 (1:1 mol:mol ratio) were added at different concentrations (0-20 µg/mL rHDL) to the cells in Opti-MEM™ medium and incubated during 24 h to allow miRNA delivery. Intracellular delivery of miRNA by rHDL to foam cells was determined as described in Methods. The data represent the means ± S.D of at least three independent measurements.

### 3. Cholesterol efflux promoted in foam cells within the 2D atheroma model

Finally, the efficiency of cholesterol efflux induced by sequential administration of antagomiR-33a by DPPC:CE:LPC rHDL followed by DPPC rHDL was evaluated in macrophage-derived foam cells loaded with TopFluor® Cholesterol (**Figure 28A**)<sup>288</sup>. The efficiency of DPPC rHDL as cholesterol acceptor was compared with natural HDL (**Figure 28B**).

Additionally, a comparative study between cholesterol efflux in foam cells cultured in 1D and foam cells grown in the 2D atheroma model was performed. AntagomiR-33a-loaded DPPC:CE:LPC rHDL at 10 µg/mL was used in foam cells cultured alone and, 50 µg/mL in the 2D atheroma model. Nanoparticles were incubated for 48 h with the cells to allow cargo delivery and ABCA1/ABCG1 upregulation. After cholesterol loading, DPPC rHDL (10 µg/mL) or HDL (10 µg/mL) were administered and incubated for 6 h to allow cholesterol efflux (**Figure 28C**).

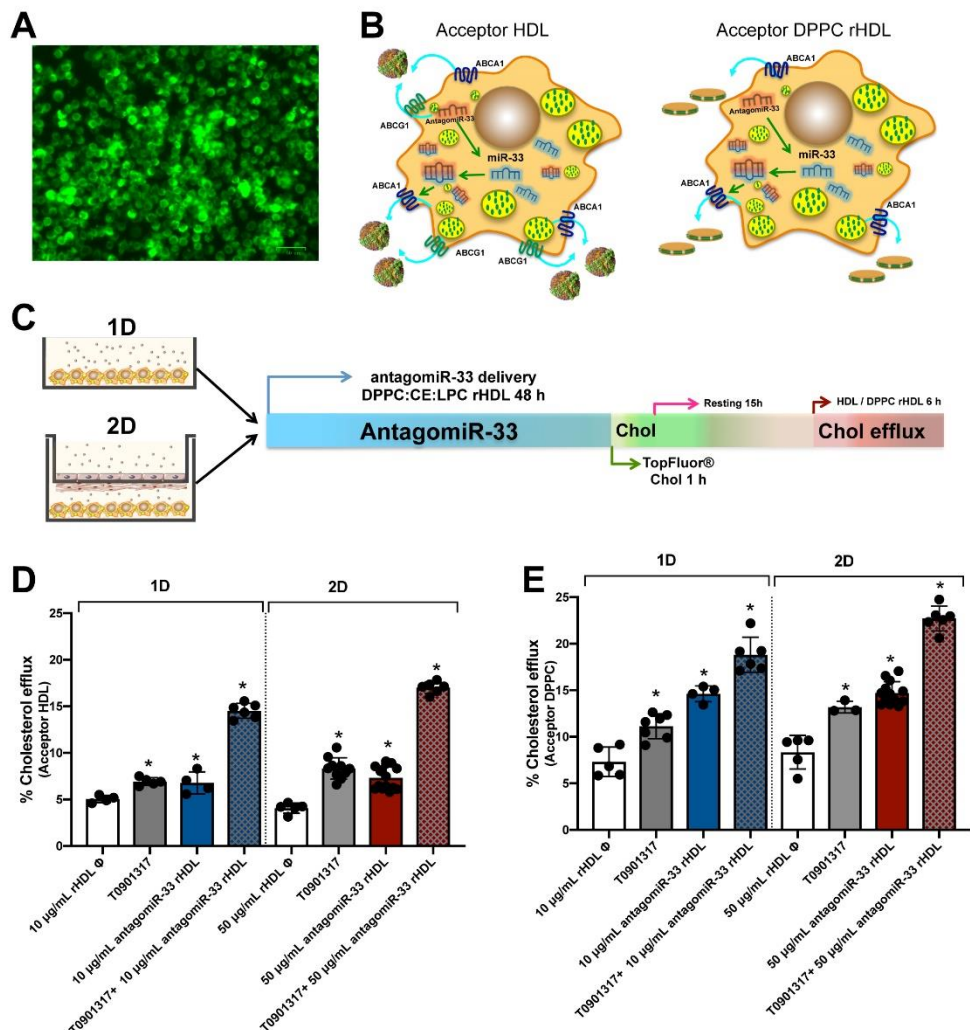


**Figure 28. Cholesterol efflux promoted in foam cells by sequential rHDL administration in a triple cell 2D atheroma model.** **A.** Macrophage-derived foam cells loaded with TopFluor® Cholesterol. **B.** Illustration of the acceptors used for cholesterol efflux. **C.** Schematic representation of time-course sequential administration of rHDL prior cholesterol efflux assay. **D.** Cholesterol efflux in 1D and 2D atheroma model cultured foam cells with HDL as acceptor. **E.** Cholesterol efflux in 1D and 2D atheroma model cultured foam cells with DPPC rHDL as acceptor. Cholesterol efflux was calculated as described in Methods. The data in D and E represent the mean  $\pm$  S.D of at least three independent measurements. Levels of significance were determined by ANOVA. \*  $p < 0.01$ .

### *3.1. HDL as cholesterol acceptor*

Incubation with miRNA-devoid rHDL (empty-rHDL) induced a cholesterol efflux to HDL of  $\approx$ 5% in both 1D and 2D atheroma model cultured foam cells (**Figure 28D**). The contribution of upregulating ABCA1 and ABCG1 to cholesterol efflux was assessed by incubating the cells with TO901317, a LXR agonist, as an internal control of the assay<sup>490</sup>. As shown in **Figure 28D**, TO901317 treatment increased significantly cholesterol efflux to HDL when compared to cells treated with empty-rHDL in both 1D and 2D cultured foam cells (**Figure 28D**). Similarly, upregulation of ABCA1 and ABCG1 by delivery of antagomiR-33a promoted a significant enhancement of cholesterol efflux to HDL. On the other hand, treatment with TO901317 and antagomiR-33a in combination caused a three times higher cholesterol efflux compared to cells treated with empty-rHDL (**Figure 28D**). Combination of TO901317 and antagomiR-33a-rHDL caused a synergistic upregulation of ABCA1 and ABCG1 protein levels in foam cells (**Figure 29**). The cholesterol efflux was paralleled by a similar reduction in the intracellular cholesterol content (**Figure 301**).

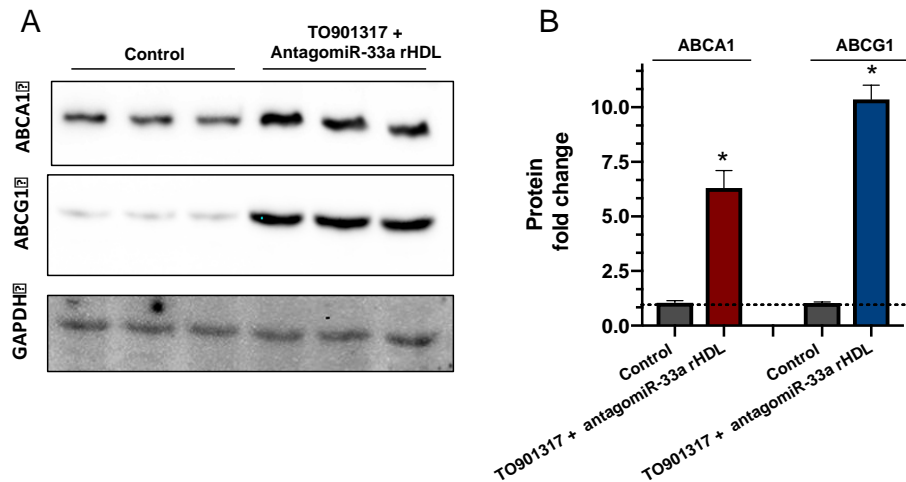


**Figure 29. Combination of TO901317 and antagomiR-33a-rHDL caused a synergistic upregulation of ABCA1 and ABCG1 protein levels in foam cells rHDLs** and TO901317 were added to the cells in Opti-MEM™ to allow miRNA delivery, mir-33a repression and LXR activation. **A.** Upregulation of ABCA1 and ABCG1 protein levels in foam cells by combined TO901317 treatment and delivery of antagomiR-33a in DPPC:CE:LPC rHDL. **B.** Expression levels of ABCA1 and ABCG1 determined by optical density. The data in A correspond to a representative western blot of n=3. The data in B and E represent the mean  $\pm$  S.D of three independent measurements. Levels of significance were determined by a two-tailed Student's t-test. \*p<0.01 compared to control miRNA.

### 3.2. DPPC rHDL as cholesterol acceptor

DPPC as cholesterol acceptor showed a higher efficiency in terms of cholesterol efflux compared to HDL (**Figure 28E**). Treatment with DPPC:CE:LPC rHDL without antagomiR-33a (10 µg/mL rHDL in 1D or 50 µg/mL rHDL in the 2D atheroma model) induced a cholesterol efflux of  $\approx$ 7.5% in both 1D cultured foam cells and 2D cultures (**Figure 28E**). Stimulation of LXR with TO901317 resulted in a significantly increased cholesterol efflux of 52 and 59% in 1D and 2D cultured foam cells, respectively, compared to cells treated with rHDL without antagomiR-33a ( $7.3 \pm 1.5$  vs.  $11.1 \pm 1.3$  and  $8.3 \pm 1.8$  vs.  $13.2 \pm 0.6$ , respectively) (**Figure 28E**). Delivery of antagomiR-

33a by DPPC:CE:LPC rHDL into foam cells (10 µg/mL rHDL in 1D or 50 µg/mL rHDL in the 2D atheroma model) increased cholesterol efflux by 100 and 77% in 1D and 2D cultured foam cells, respectively ( $7.3 \pm 1.5$  vs.  $14.6 \pm 0.8$  and  $8.3 \pm 1.8$  vs.  $14.7 \pm 1.2$ , respectively). On the other hand, treatment combination with TO901317 and antagomiR-33a also caused a higher effect on cholesterol efflux than cells treated with the agonist and antagomiR-33a alone (Figure 28E). The reduction in the intracellular cholesterol content when DPPC rHDL was used as cholesterol acceptor paralleled the cholesterol efflux to rHDL (Figure 301). In addition, data indicate that five times higher concentrations of antagomiR-33a loaded rHDL are required in foam cells grown in 2D atheroma model to achieve similar cholesterol efflux concentrations in those cultured in 1D.

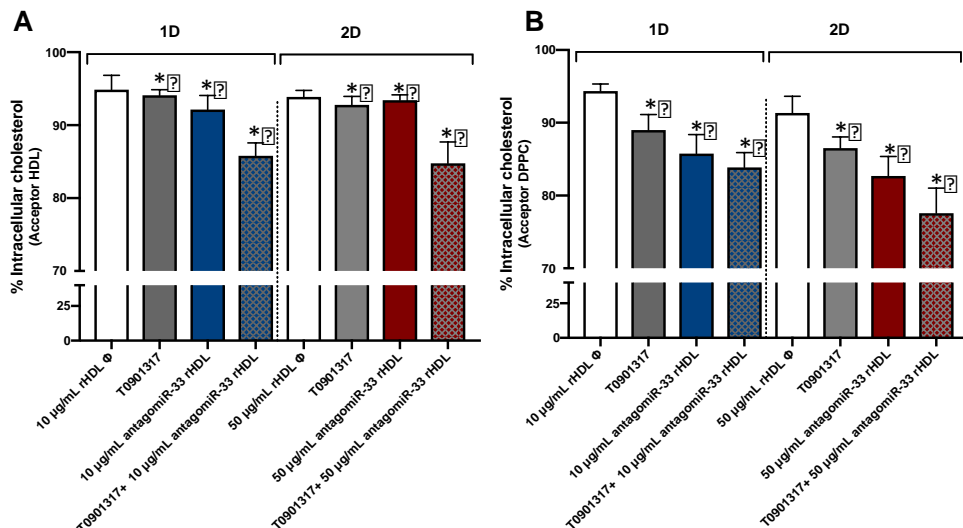


**Figure 301. Intracellular Cholesterol Levels in Foam Cells After TO901317 Treatment, AntagomiR-33a-rHDL Delivery or Combined Treatment of TO901317 and AntagomiR-33a-rHDL in 1D Grown Foam Cells or 2D Atheroma Model Foam Cells.** **A.** Intracellular cholesterol levels in 1D and 2D atheroma model cultured foam cells with HDL as acceptor. **B.** Intracellular cholesterol levels in 1D and 2D atheroma model cultured foam cells with DPPC rHDL as acceptor. Intracellular cholesterol levels were calculated as described in Methods. The data in A and B represent the mean  $\pm$  S.D of at least three

independent measurements. Levels of significance were determined by ANOVA. \* p<0.01.

Being lipid-poor apoA-I the most efficient acceptor of cholesterol from macrophages in the arterial wall via ABCA1 its effects as cholesterol acceptor was also determined. As shown in **Figure 312**, cholesterol efflux to apoA-I (10 µg/mL) in foam cells treated with empty-rHDL was 15.4 ±1.2%, in the presence of TO901317 was 21.5 ±2.1%, when cells were pre-treated with antagoniR-33a-loaded rHDL cholesterol efflux was 27.0 ±1.4%, and combination of TO901317 and antagoniR-33a-loaded rHDL caused a cholesterol efflux to apoA-I of 37.0 ±2.8%. These results support that antagoniR-33a-loaded rHDLs induce ABCA1 in functional level.

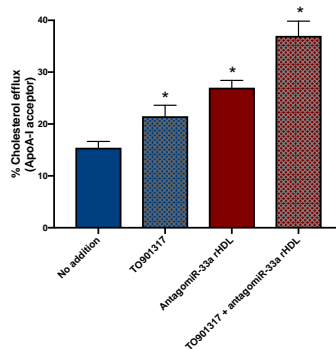


**Figure 31. Cholesterol efflux promoted in foam cells by sequential rHDL administration in a triple cell 2D atheroma model.** Cholesterol efflux with apoA-I as acceptor. Cholesterol efflux was calculated as described in Methods. The data represent the mean ± S.D of three independent measurements. Levels of significance were determined by ANOVA. \* p<0.01.

# **5. DISCUSSION**

## **EZTABaida**

Reverse cholesterol transport from peripheral tissues to the liver is a major atheroprotective event, with cholesterol efflux as a rate-limiting step<sup>507,508</sup>. Two principal transporters contribute to this process: ABCA1 and ABCG1<sup>509</sup>. ABCA1 results in the formation of discoidal HDL, while ABGC1 mediates cholesterol efflux through a diffusion mechanism that increases the pool of active cholesterol available for efflux<sup>510</sup>.

Although the exact mechanisms of cholesterol efflux mediated by the ABCA1 transporter are not known, a central feature of cholesterol transfer is apoA-I interaction with ABCA1, which stabilizes the transporter and induces bending of the plasma membrane bilayer. This process creates a high curvature site that allows apoA-I to solubilize lipids by binding to exovesiculated plasma membrane domains<sup>252,511</sup>. Although the structural and physical features of apoA-I variants and mimetic peptides that are important in the formation of HDL-like particles have been previously investigated<sup>512–515</sup>, the effect of the lipid content of rHDL has been less well characterized. Therefore, in this study, we sought to explore the effect of the lipid composition of rHDL on cholesterol efflux in macrophages, macrophage-derived foam cells unstimulated or stimulated with TO901317 and foam-VSMC unstimulated or stimulated with TO901317 to upregulate ABCA1 expression. Efficiency of cholesterol efflux mediated by DPPC, DPPC:Chol:LPC or DPPC:CE:LPC and Soy-PC rHDLs with similar sizes has been assessed. Here, we have used three lipid compositions resembling different maturation stages of natural HDLs in vivo and Soy-PC, which is the major lipid composition constituent used in rHDL that are being tested in clinical trials<sup>516</sup>. The rationale of this study relies on the information provided by previous studies using rHDLs with different lipid mixtures, which has already indicated that lipid composition plays a significant role in cholesterol efflux from macrophages<sup>517</sup>. According to the results obtained in this work, DPPC rHDLs, mimicking nascent HDL are the most effective particles in inducing cholesterol efflux in all the cellular models used. When compared to HDL-induced cholesterol

efflux, DPPC rHDLs were 20–40% more efficient depending on the cell culture tested (**Figure 23–Figure 14**). This effect can be attributed to the homogeneous composition of the DPPC rHDL as it has been previously shown that the phospholipid composition of HDL plays an important role in ABCA1-mediated cholesterol efflux and that enrichment of HDL with PC favors cholesterol efflux, in particular<sup>518,519</sup>. In addition, upregulation of ABCA1 with TO901317 favoured the cholesterol efflux induced by the nanoparticles, especially in macrophage derived foam cells (**Figure 13**).

Very interestingly, DPPC rHDLs also resulted in more efficiently favoring cholesterol efflux than Soy-PC, the lipid composition used in CSL-111 rHDLs and in the smaller CSL-112 nanoparticles currently being tested in humans. It has been described that rHDLs composed of saturated lipids exhibit greater cholesterol efflux from macrophages *in vitro* and cholesterol mobilization *in vivo*<sup>520,521</sup>. The more efficient cholesterol-efflux activity observed here with DPPC rHDL compared to Soy-PC rHDLs, can also be ascribed to the properties given by the different lipid composition of the nanodiscs. The main difference between Soy-PC and DPPC rHDL is that in the former, the existing 80% of PCs consist of a mixture of unsaturated fatty acids (C18:1, C18:2 and C18:3) and lyso-PC at 2.8% while composition in the latter is 100% DPPC. According to previously described data<sup>522,523</sup>, the increased cholesterol efflux induced by DPPC rHDLs may be attributed to the higher physical binding affinity to cholesterol of saturated phospholipids compared with Soy-PC, in which the majority of phospholipids are unsaturated. Similarly, and in agreement with this, the different lipid composition of *apoA-I Milano* rHDL (ETC-216) and ETC-642 rHDL could explain the differences among the cholesterol efflux induced by the particles because they are constituted by POPC (1-palmitoyl-2-oleoyl-sn-glycero-3-phosphocholine) or a mixture of DPPC and sphingomyelin, respectively<sup>451,524</sup>. In addition, differences in the protein moiety may also contribute. It has already been

shown that saturated long-chain-length phospholipids such as DPPC have higher physical binding affinity to cholesterol than POPC<sup>522</sup>. Additionally, the rigidifying effect of sphingomyelin present in ETC-642 rHDL can modify the physical properties of rHDLs resulting in a lower surface tension that could reduce the cholesterol exchange efficiency between membranes<sup>525</sup>.

One of the goals of this work was to study the cholesterol efflux efficiency among rHDL which simulate different maturation stages. To do so, we have compared the effects of DPPC rHDL, with DPPC:Chol:LPC and DPPC:CE:LPC that can be considered particles in a more mature stage. DPPC:Chol:LPC rHDL resembling nascent HDLs having incorporated free cholesterol, and DPPC:CE:LPC resembling those in which cholesterol is esterified by the effect of Lecithin–cholesterol acyltransferase (LCAT). As shown in Figures 3–5, DPPC rHDL were the most efficient particles in inducing cholesterol efflux, an effect that may be mediated by the physicochemical characteristics of the nanoparticles. The role of membrane lipid composition in cholesterol exchange between membranes is not well understood, however phospholipids and fatty acyl chains have been shown to influence the rate of cholesterol movement between membranes<sup>526–528</sup>. In addition, curvature of the lipid bilayer that is imposed by the overall geometry of lipids shows a physiological significance in cholesterol transfer<sup>529</sup>. Lipid geometry is defined by the ratio between the size of the polar head group and acyl chain saturation. PC is a cylindrical lipid that forms flat monolayers<sup>530</sup>. Conversely, the large head group to acyl chain ratio in lyso-PC confers an inverted conical shape to the lipids, thereby favoring a positive curvature of the membrane by bending the monolayer away from the head groups<sup>531–533</sup>. Addition of cholesterol increases the packing of conical lipids (such as LPC), and thus disfavors spontaneous curvature induced by the lysophospholipid<sup>534</sup> while the esterification of the 3' hydroxyl group of cholesteryl esters is structurally consistent with substantially increased positive

curvature<sup>535</sup>. Recent studies have shown that membrane curvature is an active driving force in many processes involving membrane remodelling and cholesterol exchange<sup>536</sup>. It has been shown that cholesterol transfer is about 10 times faster from donor bilayers with high positive curvatures and when the acceptor bilayer is planar<sup>529,537</sup>. Although the curvature of biological membranes is very low, the bending of the plasma membrane bilayer by ABCA1 creates a high curvature that can facilitate cholesterol transfer<sup>252,511</sup>. The cholesterol transfer will be favored thermodynamically from the high curvature promoted by ABCA1 in the cell membrane to DPPC rHDLs instead of DPPC:Chol:LPC and DPPC:CE:LPC, because the former are planar bilayers and the latter two have positive curvatures<sup>538</sup>.

The transfer of cholesterol between membranes is strongly dependent on temperature and is affected by the lipid composition, suggesting that membrane fluidity strongly influences the transfer rate<sup>526</sup>. In this work we have also assessed of thermotropic phase transition of HDL and rHDLs to compare their fluidity. Attending to the Tm of DPPC, DPPC:Chol:LPC and DPPC:CE:LPC rHDLs, the nanoparticles are more rigid as Chol, and CE are incorporated, DPPC < DPPC:Chol:LPC < DPPC:CE:LPC, showing a Tm increment of 1.7 and 4.1 °C compared to DPPC alone, respectively. This effect could indicate that particles with high transition temperatures could be less efficient in accommodating cholesterol from the plasma membrane due the intrinsic physical characteristics of the rHDL bilayer and that the higher Tm of rHDL, the lower the cholesterol efflux rate induced by the rHDL. However, attending to this hypothesis, Soy-PC would be the most efficient particles inducing cholesterol efflux followed by HDL, which show Tm below 0 °C and  $32.0 \pm 0.3$  °C, respectively. The lower capacity of promoting cholesterol efflux shown by HDL and Soy-PC indicates that rather than Tm, lipid composition favoring higher binding affinity of cholesterol (saturated acyl chains) and planar bilayer

geometries such as shown by DPPC rHDLs are more favorable to promote cholesterol efflux.

As indicated before, atherosclerotic plaque formation is a complex process in which macrophages play a key role in progression or regression of plaques<sup>539</sup>. During the last decades, disease management has improved significantly<sup>540</sup>, however research must now shift towards the necessity to develop new therapeutic strategies focused on accelerating atherosclerosis regression<sup>539</sup>. Although animal models provide essential information for atherosclerosis research, 2D culture and 3D multi-cellular atherosclerosis models allow mimicking in vivo-like conditions<sup>541,542</sup>, tackling the interaction between different cells in atherosclerotic plaques and, understanding the dynamics of new therapeutic approaches. Over the past five years, bio-nanomaterial-based strategies have emerged as therapeutic or theranostic agents for managing atherosclerosis<sup>543</sup>. Several nanoplatforms to direct delivery of pharmaceutical agents to atherosclerotic plaque-associated macrophages have shown to beneficially modulate disease process and improve outcomes. In example, core-shell nanoplatform composed of a poly(D,L-lactide-co-glycolide) (PLGA) efficiently deliver both siRNA against lectin-like oxidised low-density lipoprotein receptor-1 and atorvastatin to the atherosclerotic lesions and, exert a synergistic therapeutic effect on both endothelial cells and macrophages<sup>444</sup>. Similarly, mannose-functionalised dendimeric nanoparticle (mDNP)-based platforms have been successfully used for macrophage-specific delivery of LXR-L, leading to plaque attenuation and favourable modulation of plaque characteristics<sup>544</sup>. Moreover, mDNPs have also been proven to simultaneously deliver SR-A siRNA (to reduce LDL uptake) and LXR ligand (LXR-L, to stimulate cholesterol efflux) with significant regression of atherosclerotic lesions<sup>545</sup>.

In addition, nanoparticles have turned out to be powerful delivery vehicles for miRNA-based therapeutics through inhibition of targets that drive disease progression or overexpression of beneficial intermediates in CVD settings<sup>546–548</sup>.

In this work we sought to develop a targeted nanoparticle approach based in a staged administration of rHDL carrying antagoniR-33a to upregulate ABCA1 transporter followed by DPPC rHDL, which has been previously shown to be highly efficient removing cholesterol from foam cells<sup>549</sup>. We have investigated the efficiency of this strategy in a three-cell type 2D culture model mimicking the atheroma plaque microenvironment. A major challenge to realizing this goal has been an effective formulation and delivery of therapeutic miRNAs to the cytoplasm of foam cells in the atheroma context. A conceptual breakthrough to this problem is surpassed with the demonstration that natural HDL contain miRNAs and that these HDL-bound miRNAs have improved stability compared with naked miRNAs<sup>382</sup>. In addition, and taking the advantage that HDLs bind with their high-affinity receptor, scavenger receptor type B1 (SR-B1), we have developed functional HDL-like nanoparticles composed of DPPC:CE:LPC, which physically and chemically resemble to a natural mature HDLs; contain apoA-I, which is the main protein constituent of HDLs<sup>550</sup>, selectively target cells that express SR-B1<sup>551,552</sup>; and show no cytotoxicity (data not shown). Furthermore, HDL-mediated delivery of miRNAs to recipient cells was demonstrated to be dependent on SR-B1<sup>382</sup>. Purified DPPC:CE:LPC rHDLs showed an average diameter of ~10 nm as determined by DLS and NS-EM and high α-helical structure content determined by CD, indicating a correct reconstitution of rHDLs (**Figure 24**). In addition, they bound efficiently miRNA, reaching a maximum capacity at 1:1 mol:mol ratio and proved to be very avidly internalised by foam cells in the 2D atheroma model (**Figure 15–Figure 25**). It has been reported that HDL-miRNAs are taken up by HDL's receptor, SR-B1 and that transendothelial transport of HDL is actively regulated by a process that involves at least SR-B1, endothelial lipase and ABCG1<sup>382,553,554</sup>. Therefore, and using a transwell

system, we tested whether DPPC:CE:LPC rHDL are efficiently transported through EC/VSMC bilayer (**Figure 25C-D**). Using fluorescent microscopy, we found Dil-rHDL within the ECs and not between the intercellular spaces, confirming the results obtained by others<sup>555,556</sup>. VSMC showed residual intracellular uptake of Dil-labelled DPPC:CE:LPC rHDL while the uptake in macrophage-derived foam cells resulted to be highly efficient (**Figure 25C**), results that were further corroborated by flow cytometry (**Figure 25D**). We have also addressed the efficiency of nanoparticles reaching target cells in the 2D atheroma model and found that a five-fold higher concentration is required to achieve similar results than those observed in foam cells cultured alone in monolayer (**Figure 26A** and **Figure 27**).

We found that a simple treatment of DPPC:CE:LPC rHDL-antagomiR-33a for 48 h efficiently reduced intracellular miR-33 leading to upregulation of ABCA1 and ABCG1 transporters (**Figure 26**). Besides, our results confirm that miRNAs delivered via rHDL can escape the endosomal system and function in the RISC complex. Similar results have been shown using PEGylated chitosan nanoparticles delivering antagomiR-33 into the atheroma plaque<sup>557</sup>.

Once the first part of our goal proven to be effective, we further sought to improve the therapeutic relevance of our model by potentiating the extent of cholesterol efflux by a second-step administration of DPPC rHDL. We have previously shown that DPPC rHDL are more efficient favouring cholesterol efflux than CSL-112, nanoparticles composed of soy-PC, which are currently being tested in humans<sup>549,558</sup>. Therefore, and after inducing ABCA1 overexpression by DPPC:CE:LPC rHDL carrying antagomiR-33a, cells were loaded with fluorescent cholesterol and incubated with DPPC rHDL to promote cholesterol efflux (**Figure 28**). We used two cholesterol acceptors, HDL and DPPC rHDL and compared the efflux efficiency to each acceptor both in foam cells cultured alone and in those cultured in the 2D atheroma model. Cholesterol efflux into mature HDL particles is mainly mediated

by ABCG1 transporter while ABCA1 targets mainly lipid free apoA-1 or discoidal pre- $\beta$ -HDL (DPPC rHDL in our experimental conditions)<sup>343,549,559</sup>. We determined similar cholesterol efflux in the foam cells cultured in 1D or in the 2D atheroma model using 10 or 50  $\mu$ g/mL of antagomiR-33-loaded DPPC:CE:LPC rHDL, respectively. When HDL was used as cholesterol acceptor, both antagomiR-33a delivery and T0901317 promoted a significant enhanced cholesterol efflux compared to that of cells treated with empty DPPC:CE:LPC (**Figure 28D**). Being ABCG1 the transporter that mainly mediates cholesterol transport to assembled HDL<sup>263,560</sup>, the results presented here indicate that enhancing the in vitro expression of ABCG1 by delivery of antagomiR-33a is as effective as T0901317 in contributing to cholesterol efflux to HDL. The undesired side-effects of treatments with T0901317, which are associated with enhanced lipogenesis, resulting in elevated serum triglyceride levels and hepatic steatosis, highlights the potential of delivering antagomiR-33a to upregulate ABCG1 and potentiating cholesterol efflux without affecting cell citotoxicity<sup>561,562</sup>. As previously shown, DPPC rHDL-induced cholesterol efflux was more efficient than HDL<sup>549</sup>. Very interestingly, in 1D cultures, cholesterol efflux in cells pretreated with antagomiR-33a-loaded rHDL was two times higher than that in cells treated with empty DPPC:CE:LPC rHDL and slightly but significantly higher than cells treated with TO901317 (**Figure 28E**). Similarly, in 2D atheroma model, pretreatment with antagomiR-33a-loaded rHDL caused a 1.8 times higher cholesterol efflux compared to cells treated with empty rHDL and slightly higher than cells treated with TO901317 (**Figure 28E**). These results indicate that using rHDL as antagomiR-33a carrier is an efficient tool to upregulate ABCA1 and its potency is higher than that of T0901317. The higher efficacy of DPPC rHDL compared to natural HDL is in agreement with the study conducted by Adorni et al. showing that ABCA1 accounts for cholesterol efflux of 50%, while approximately 20% of the cholesterol efflux can be attributable to ABCG1<sup>343</sup>.

Notably, the results obtained in this proposed two-step atheroma plaque-targeting strategy highlights its use as a promising therapeutic intervention for favouring reverse cholesterol transport. It also can improve the overall targeted delivery efficiency of rHDL broadening potential applications in several diseases. Bringing the strategy of sequential administration of rHDL into in vivo usage is a challenge that requires further studies before clinical steps can be initiated. Systematic basic studies as those presented here concerning the mechanisms of nanoparticle transport, their interactions with cells and efficacy, improve the translation of basic research into developing and bringing novel nanomedical tools. This process involves multidisciplinary efforts and requires strong expertise in safety and healthcare issues. As mentioned above, a large number of studies have used rHDL as therapeutic agent addressing the central antiatherogenic and cardioprotective properties of HDL<sup>288,563</sup>. Inflammatory and atherogenic processes have been shown to be reduced by repeated infusion treatment with rHDL<sup>564</sup>. Therefore, sequential administration of antagomiR-33a-loaded rHDL followed by DPPC rHDL infusion could represent a good strategy to favour the reverse transport of cholesterol and contribute to the reduction of atheroma plaque. In any case, future in vivo studies in animal models will provide the necessary information to calculate the doses, the time interval between infusions and determine the antiatherogenic effects of the treatment strategy proposed in this work.

# **6. CONCLUSIONS**

## **6. ONDORIOAK**

Lan honetan, rHDLen konposizio lipidoak kolesterol kanporaketan duen eragina aztertu da hainbat zelula-eredutan, kolesterolaren kanporaketaren tasa maximoa lortzeko behar diren parametro optimoak zehazteko. Hiru lipido nahastura desberdin erabili ziren, HDL naturalen heldutasun etapa desberdinak imitatuz; eta Soy-PC, gaur egungo saiakuntza klinikoan erabiltzen diren rHDLen lipidoen osagaia. Horrez gain, ateroma modelo bidimentsionalak erabilita, lan honetan aurkeztutako datuek, funtzionalizatutako nanopartikulen administrazio sekuentzialak, zelula apartsuetatik kolesterol kanporaketa indartsua eragiten dutela demostratzen dute.

Lortutako emaitzen arabera, ondorengoa ondoriozta daiteke:

1. Lan honetan erabilitako metodologiak rHDL egonkorrik birsortzea ahalbidetzen du, HDL jaioberri naturalen antzeko ezaugarri eta propietate fisiko-kimikoak dituztenak.
2. Giza apoA-I eta DPPCrekin birsortutako rHDLak kolesterolaren kanporaketa eragiten duten partikula eraginkorrenak dira erabilitako zelula-eredu guztieta. Partikula horien erabilera, saiakuntza kliniko handietan ikusitako eraginkortasun eza gaindi dezake.
3. DPPC puruaren kate luzeko fosfolipido saturatuek kolesterolaren lotura fisiko handiagoa dute, eta, ondorioz, kolesterolaren kanporaketa sustatzeko gaitasun handiagoa ematen diote nanopartikulari.
4. DPPC rHDLen lipido bigeruzaren geometria lauak kolesterol-mintzetik nanopartikularako kolesterol-mugimendu tasa hobetzen du.
5. HDL jaioberrien antzeko lipidoen konposizioa eta ezaugarri fisiko-kimikoak dituzten rHDLak kontuan hartu behar dira rHDL eraginkorra diseinatzeko

eta kolesterolaren kanporaketa eta plakaren erregresioa sustatzeko tresna terapeutiko gisa erabili daitezen.

6. DPPC:CE:LPC (75:20:5 mol %) formulazio eraginkorra da miRNA terapeutikoak, kasu honetan antagomiR-33a, zelula apartsuen zitoplasmara garraiatzeko atheroma testuinguruan emateko.
7. DPPC:CE:LPC rHDLak 2D modeloaren zelula apartsuak dituzte itu gisa eta miRNAK a sistema endosomikotik ihes egiteko eta RISC konplexuan funtzionatzeko gai dira. Hori dela eta, DPPC:CE:LPC rHDL bidezko antagomiR-33a-aren garraioak, zelula barneko miR-33a modu eraginkorrean murrizten du, ABCA1 eta ABCG1 garraiatzaileen gainadierazpena eraginez.
8. Nanopartikulen administrazio sekuentzialak (lehena, antagomiR-33a-aren garraioa DPPC:CE:LPC rHDL bidez eta bigarrena, DPPC rHDL bidez) zelula apartsuetatik kolesterol kanporaketa indartsua eragiten du.
9. AntagomiR-33a-az kargatutako rHDL eta DPPC rHDLen administrazio sekuentzialak kolesterolaren alderantzizko garraio sinergikoa sustatzeko eta ateroma plaka murrizten laguntzeko estrategia potentzial bat da. Etorkizuneko animalia-ereduetako *in vivo* azterketek, dosiak, infusioen arteko denbora tartea eta efektu antiaterogenikoak zehazteko beharrezko informazioa emango dute.

## 7. REFERENCES

### 7. ERREFERENTZIAK

1. Rubanyi, G. M. The Role of Endothelium in Cardiovascular Homeostasis and Diseases: *Journal of Cardiovascular Pharmacology* **22**, S1–S14 (1993).
2. Vanhoutte, P. M. How to assess endothelial function in human blood vessels: *Journal of Hypertension* **17**, 1047–1058 (1999).
3. Shimokawa, H. Primary Endothelial Dysfunction: Atherosclerosis. *Journal of Molecular and Cellular Cardiology* **31**, 23–37 (1999).
4. Davies, P. F. Flow-mediated endothelial mechanotransduction. *Physiological Reviews* **75**, 519–560 (1995).
5. Jr, M. A. G. & García-Cardeña, G. Vascular endothelium, hemodynamics, and the pathobiology of atherosclerosis. **15** (2015).
6. Dewey, C. F., Bussolari, S. R., Gimbrone, M. A. & Davies, P. F. The Dynamic Response of Vascular Endothelial Cells to Fluid Shear Stress. *Journal of Biomechanical Engineering* **103**, 177–185 (1981).
7. Levesque, M. J., Liepsch, D., Moravec, S. & Nerem, R. M. Correlation of endothelial cell shape and wall shear stress in a stenosed dog aorta. *Arteriosclerosis* **6**, 220–229 (1986).
8. Levesque, M. J. & Nerem, R. M. The study of rheological effects on vascular endothelial cells in culture. *BIR* **26**, 345–357 (1989).
9. Favero, G., Paganelli, C., Buffoli, B., Rodella, L. F. & Rezzani, R. Endothelium and Its Alterations in Cardiovascular Diseases: Life Style Intervention. *BioMed Research International* **2014**, 1–28 (2014).
10. Aird, W. C. Phenotypic Heterogeneity of the Endothelium: I. Structure, Function, and Mechanisms. *Circulation Research* **100**, 158–173 (2007).
11. Passerini, A. G. *et al.* Coexisting proinflammatory and antioxidative endothelial transcription profiles in a disturbed flow region of the adult porcine aorta. *Proceedings of the National Academy of Sciences* **101**, 2482–2487 (2004).

12. Esper, R. J. *et al.* Endothelial dysfunction: a comprehensive appraisal. *Cardiovascular Diabetology* **18** (2006).
13. Natural history of aortic and coronary atherosclerotic lesions in youth. Findings from the PDAY Study. Pathobiological Determinants of Atherosclerosis in Youth (PDAY) Research Group. *Arterioscler Thromb* **13**, 1291–1298 (1993).
14. Davies, P. F. Hemodynamic shear stress and the endothelium in cardiovascular pathophysiology. *Nat Clin Pract Cardiovasc Med* **6**, 16–26 (2009).
15. Chiu, J.-J. & Chien, S. Effects of disturbed flow on vascular endothelium: pathophysiological basis and clinical perspectives. *Physiol Rev* **91**, 327–387 (2011).
16. Ross, R. The pathogenesis of atherosclerosis--an update. *N Engl J Med* **314**, 488–500 (1986).
17. Yu, X.-H., Fu, Y.-C., Zhang, D.-W., Yin, K. & Tang, C.-K. Foam cells in atherosclerosis. *Clin Chim Acta* **424**, 245–252 (2013).
18. Allahverdian, S., Chehroudi, A. C., McManus, B. M., Abraham, T. & Francis, G. A. Contribution of Intimal Smooth Muscle Cells to Cholesterol Accumulation and Macrophage-Like Cells in Human Atherosclerosis. *Circulation* **129**, 1551–1559 (2014).
19. Stary, H. C. *et al.* A definition of initial, fatty streak, and intermediate lesions of atherosclerosis. A report from the Committee on Vascular Lesions of the Council on Arteriosclerosis, American Heart Association. *Circulation* **89**, 2462–2478 (1994).
20. Kunsch, C. & Medford, R. M. Oxidative Stress as a Regulator of Gene Expression in the Vasculature. *Circulation Research* **85**, 753–766 (1999).
21. Verma, S. & Anderson, T. J. Fundamentals of Endothelial Function for the Clinical Cardiologist. *Circulation* **105**, 546–549 (2002).
22. Verma, S., Buchanan, M. R. & Anderson, T. J. Endothelial Function Testing as a Biomarker of Vascular Disease. *Circulation* **108**, 2054–2059 (2003).
23. Landmesser, U., Hornig, B. & Drexler, H. Endothelial Dysfunction in Hypercholesterolemia: Mechanisms, Pathophysiological Importance, and Therapeutic Interventions. *Semin Thromb Hemost* **26**, 529–538 (2000).

24. Gimbrone, M. A., Cybulsky, M. I., Kume, N., Collins, T. & Resnick, N. Vascular endothelium. An integrator of pathophysiological stimuli in atherogenesis. *Ann N Y Acad Sci* **748**, 122–131; discussion 131–132 (1995).
25. Gimbrone, M. A. & García-Cardeña, G. Endothelial Cell Dysfunction and the Pathobiology of Atherosclerosis. *Circ Res* **118**, 620–636 (2016).
26. Ross, R. & Glomset, J. A. The pathogenesis of atherosclerosis (first of two parts). *N Engl J Med* **295**, 369–377 (1976).
27. Caro, C. G., Fitz-Gerald, J. M. & Schroter, R. C. Atheroma and arterial wall shear. Observation, correlation and proposal of a shear dependent mass transfer mechanism for atherogenesis. *Proc R Soc Lond B Biol Sci* **177**, 109–159 (1971).
28. Atheroma and arterial wall shear - Observation, correlation and proposal of a shear dependent mass transfer mechanism for atherogenesis. *Proc. R. Soc. Lond. B.* **177**, 109–133 (1971).
29. Diamond, S. L. *et al.* Tissue plasminogen activator messenger RNA levels increase in cultured human endothelial cells exposed to laminar shear stress. *J Cell Physiol* **143**, 364–371 (1990).
30. Takada, Y. *et al.* Fluid Shear Stress Increases the Expression of Thrombomodulin by Cultured Human Endothelial Cells. *Biochemical and Biophysical Research Communications* **205**, 1345–1352 (1994).
31. Shyy, Y. J., Hsieh, H. J., Usami, S. & Chien, S. Fluid shear stress induces a biphasic response of human monocyte chemotactic protein 1 gene expression in vascular endothelium. *Proceedings of the National Academy of Sciences* **91**, 4678–4682 (1994).
32. Ohno, M., Cooke, J. P., Dzau, V. J. & Gibbons, G. H. Fluid shear stress induces endothelial transforming growth factor beta-1 transcription and production. Modulation by potassium channel blockade. *J Clin Invest* **95**, 1363–1369 (1995).
33. Lin, M. C. *et al.* Shear stress induction of the tissue factor gene. *J Clin Invest* **99**, 737–744 (1997).
34. Chien, S. & Shyy, J. Y. J. Effects of Hemodynamic Forces on Gene Expression and Signal Transduction in Endothelial Cells. *The Biological Bulletin* **194**, 390–393 (1998).

35. Gimbrone, M. A., Topper, J. N., Nagel, T., Anderson, K. R. & García-Cardeña, G. Endothelial Dysfunction, Hemodynamic Forces, and Atherogenesis. *Annals of the New York Academy of Sciences* **902**, 230–240 (2006).
36. Resnick, N. *et al.* Fluid shear stress and the vascular endothelium: for better and for worse. *Progress in Biophysics and Molecular Biology* **81**, 177–199 (2003).
37. Chiu, J.-J., Usami, S. & Chien, S. Vascular endothelial responses to altered shear stress: Pathologic implications for atherosclerosis. *Annals of Medicine* **41**, 19–28 (2009).
38. Chien, S. Role of shear stress direction in endothelial mechanotransduction. *Mol Cell Biomech* **5**, 1–8 (2008).
39. García-Cardeña, G. & Gimbrone, M. A. Biomechanical Modulation of Endothelial Phenotype: Implications for Health and Disease. in *The Vascular Endothelium II* (eds. Moncada, S. & Higgs, A.) vol. 176/II 79–95 (Springer Berlin Heidelberg, 2006).
40. Shyy, J. Y. *et al.* The cis-acting phorbol ester ‘12-O-tetradecanoylphorbol 13-acetate’-responsive element is involved in shear stress-induced monocyte chemotactic protein 1 gene expression. *Proceedings of the National Academy of Sciences* **92**, 8069–8073 (1995).
41. Hsiai, T. K. *et al.* Pulsatile flow regulates monocyte adhesion to oxidized lipid-induced endothelial cells. *Arterioscler Thromb Vasc Biol* **21**, 1770–1776 (2001).
42. Hsiai, T. K. *et al.* Monocyte recruitment to endothelial cells in response to oscillatory shear stress. *FASEB J* **17**, 1648–1657 (2003).
43. Kraiss, L. W. *et al.* Acute reductions in blood flow and shear stress induce platelet-derived growth factor-A expression in baboon prosthetic grafts. *Circ Res* **79**, 45–53 (1996).
44. Malek, A. M., Gibbons, G. H., Dzau, V. J. & Izumo, S. Fluid shear stress differentially modulates expression of genes encoding basic fibroblast growth factor and platelet-derived growth factor B chain in vascular endothelium. *J Clin Invest* **92**, 2013–2021 (1993).

45. Wilcox, J. N., Smith, K. M., Williams, L. T., Schwartz, S. M. & Gordon, D. Platelet-derived growth factor mRNA detection in human atherosclerotic plaques by *in situ* hybridization. *J Clin Invest* **82**, 1134–1143 (1988).
46. Silberman, M. *et al.* Shear stress-induced transcriptional regulation via hybrid promoters as a potential tool for promoting angiogenesis. *Angiogenesis* **12**, 231–242 (2009).
47. Davis, M. E., Grumbach, I. M., Fukai, T., Cutchins, A. & Harrison, D. G. Shear stress regulates endothelial nitric-oxide synthase promoter activity through nuclear factor kappaB binding. *J Biol Chem* **279**, 163–168 (2004).
48. Drummond, G. R., Cai, H., Davis, M. E., Ramasamy, S. & Harrison, D. G. Transcriptional and posttranscriptional regulation of endothelial nitric oxide synthase expression by hydrogen peroxide. *Circ Res* **86**, 347–354 (2000).
49. Almendro, N. *et al.* Cloning of the human platelet endothelial cell adhesion molecule-1 promoter and its tissue-specific expression. Structural and functional characterization. *J Immunol* **157**, 5411–5421 (1996).
50. Houston, P., White, B. P., Campbell, C. J. & Braddock, M. Delivery and Expression of Fluid Shear Stress-Inducible Promoters to the Vessel Wall: Applications for Cardiovascular Gene Therapy. *Human Gene Therapy* **10**, 3031–3044 (1999).
51. Gimbrone, M. A. & García-Cardeña, G. Vascular endothelium, hemodynamics, and the pathobiology of atherosclerosis. *Cardiovasc Pathol* **22**, 9–15 (2013).
52. Davies, P. F., Spaan, J. A. & Krams, R. Shear stress biology of the endothelium. *Ann Biomed Eng* **33**, 1714–1718 (2005).
53. Ludmer, P. L. *et al.* Paradoxical Vasoconstriction Induced by Acetylcholine in Atherosclerotic Coronary Arteries. *N Engl J Med* **315**, 1046–1051 (1986).
54. Loscalzo, J. & Welch, G. Nitric oxide and its role in the cardiovascular system. *Progress in Cardiovascular Diseases* **38**, 87–104 (1995).
55. Cooke, J. P. & Tsao, P. S. Is NO an endogenous antiatherogenic molecule? *Arterioscler Thromb* **14**, 653–655 (1994).
56. Libby, P. Current Concepts of the Pathogenesis of the Acute Coronary Syndromes. *Circulation* **104**, 365–372 (2001).

57. Marx, N., Sukhova, G. K., Collins, T., Libby, P. & Plutzky, J. PPAR $\alpha$  Activators Inhibit Cytokine-Induced Vascular Cell Adhesion Molecule-1 Expression in Human Endothelial Cells. *Circulation* **99**, 3125–3131 (1999).
58. Carlström, M. Nitric oxide signalling in kidney regulation and cardiometabolic health. *Nat Rev Nephrol* **17**, 575–590 (2021).
59. Biasucci, L. M. et al. Elevated Levels of Interleukin-6 in Unstable Angina. *Circulation* **94**, 874–877 (1996).
60. Kacimi, R., Long, C. S. & Karliner, J. S. Chronic Hypoxia Modulates the Interleukin-1 $\beta$ -Stimulated Inducible Nitric Oxide Synthase Pathway in Cardiac Myocytes. *Circulation* **96**, 1937–1943 (1997).
61. Torre-Amione, G. et al. Expression and Functional Significance of Tumor Necrosis Factor Receptors in Human Myocardium. *Circulation* **92**, 1487–1493 (1995).
62. Smith, S. C. & Allen, P. M. Neutralization of endogenous tumor necrosis factor ameliorates the severity of myosin-induced myocarditis. *Circ Res* **70**, 856–863 (1992).
63. Matsumori, A., Yamada, T., Suzuki, H., Matoba, Y. & Sasayama, S. Increased circulating cytokines in patients with myocarditis and cardiomyopathy. *Heart* **72**, 561–566 (1994).
64. Valen, G., Yan, Z. & Hansson, G. K. Nuclear factor kappa-B and the heart. *Journal of the American College of Cardiology* **38**, 307–314 (2001).
65. Casino, P. R., Kilcoyne, C. M., Quyyumi, A. A., Hoeg, J. M. & Panza, J. A. The role of nitric oxide in endothelium-dependent vasodilation of hypercholesterolemic patients. *Circulation* **88**, 2541–2547 (1993).
66. Panza, J. A., Casino, P. R., Kilcoyne, C. M. & Quyyumi, A. A. Role of endothelium-derived nitric oxide in the abnormal endothelium-dependent vascular relaxation of patients with essential hypertension. *Circulation* **87**, 1468–1474 (1993).
67. Alexander, R. W. Hypertension and the Pathogenesis of Atherosclerosis: Oxidative Stress and the Mediation of Arterial Inflammatory Response: A New Perspective. *Hypertension* **25**, 155–161 (1995).
68. Michel, C. C. & Curry, F. E. Microvascular permeability. *Physiol Rev* **79**, 703–761 (1999).

69. Rippe, B. & Haraldsson, B. Transport of macromolecules across microvascular walls: the two-pore theory. *Physiological Reviews* **74**, 163–219 (1994).
70. Rippe, B., Rosengren, B.-I., Carlsson, O. & Venturoli, D. Transendothelial Transport: The Vesicle Controversy. *J Vasc Res* **39**, 375–390 (2002).
71. Pappenheimer, J. R., Renkin, E. M. & Borrero, L. M. Filtration, diffusion and molecular sieving through peripheral capillary membranes; a contribution to the pore theory of capillary permeability. *Am J Physiol* **167**, 13–46 (1951).
72. Jang, E., Robert, J., Rohrer, L., von Eckardstein, A. & Lee, W. L. Transendothelial transport of lipoproteins. *Atherosclerosis* **315**, 111–125 (2020).
73. Zhang, X., Sessa, W. C. & Fernández-Hernando, C. Endothelial Transcytosis of Lipoproteins in Atherosclerosis. *Front. Cardiovasc. Med.* **5**, 130 (2018).
74. Goldstein, J. L. & Brown, M. S. The LDL Receptor. *ATVB* **29**, 431–438 (2009).
75. Kraehling, J. R. *et al.* Genome-wide RNAi screen reveals ALK1 mediates LDL uptake and transcytosis in endothelial cells. *Nat Commun* **7**, 13516 (2016).
76. Armstrong, S. M. *et al.* A novel assay uncovers an unexpected role for SR-BI in LDL transcytosis. *Cardiovasc Res* **108**, 268–277 (2015).
77. Huang, L. *et al.* SR-B1 drives endothelial cell LDL transcytosis via DOCK4 to promote atherosclerosis. *Nature* **569**, 565–569 (2019).
78. Dehouck, B. *et al.* A new function for the LDL receptor: transcytosis of LDL across the blood-brain barrier. *J Cell Biol* **138**, 877–889 (1997).
79. Babitt, J. *et al.* Murine SR-BI, a high density lipoprotein receptor that mediates selective lipid uptake, is N-glycosylated and fatty acylated and colocalizes with plasma membrane caveolae. *J Biol Chem* **272**, 13242–13249 (1997).
80. Santibanez, J. F. *et al.* Caveolin-1 interacts and cooperates with the transforming growth factor-beta type I receptor ALK1 in endothelial caveolae. *Cardiovasc Res* **77**, 791–799 (2008).
81. Rothberg, K. G. *et al.* Caveolin, a protein component of caveolae membrane coats. *Cell* **68**, 673–682 (1992).

82. Fernández-Hernando, C. *et al.* Genetic evidence supporting a critical role of endothelial caveolin-1 during the progression of atherosclerosis. *Cell Metab* **10**, 48–54 (2009).
83. Frank, P. G., Pavlides, S. & Lisanti, M. P. Caveolae and transcytosis in endothelial cells: role in atherosclerosis. *Cell Tissue Res* **335**, 41–47 (2009).
84. Wang, D.-X., Pan, Y.-Q., Liu, B. & Dai, L. Cav-1 promotes atherosclerosis by activating JNK-associated signaling. *Biochem Biophys Res Commun* **503**, 513–520 (2018).
85. Ramírez, C. M. *et al.* Caveolin-1 Regulates Atherogenesis by Attenuating Low-Density Lipoprotein Transcytosis and Vascular Inflammation Independently of Endothelial Nitric Oxide Synthase Activation. *Circulation* **140**, 225–239 (2019).
86. Zhang, X. & Fernández-Hernando, C. Transport of LDLs into the arterial wall: impact in atherosclerosis. *Curr Opin Lipidol* **31**, 279–285 (2020).
87. Yang, Y. & Schmidt, E. P. The endothelial glycocalyx: an important regulator of the pulmonary vascular barrier. *Tissue Barriers* **1**, 23494 (2013).
88. Ziegler, T., Abdel Rahman, F., Jurisch, V. & Kupatt, C. Atherosclerosis and the Capillary Network; Pathophysiology and Potential Therapeutic Strategies. *Cells* **9**, 50 (2019).
89. Skålén, K. *et al.* Subendothelial retention of atherogenic lipoproteins in early atherosclerosis. *Nature* **417**, 750–754 (2002).
90. Sprague, E. A., Steinbach, B. L., Nerem, R. M. & Schwartz, C. J. Influence of a laminar steady-state fluid-imposed wall shear stress on the binding, internalization, and degradation of low-density lipoproteins by cultured arterial endothelium. *Circulation* **76**, 648–656 (1987).
91. Carmena, R. *et al.* Effect of olive and sunflower oils on low density lipoprotein level, composition, size, oxidation and interaction with arterial proteoglycans. *Atherosclerosis* **125**, 243–255 (1996).
92. Levitan, I., Volkov, S. & Subbaiah, P. V. Oxidized LDL: Diversity, Patterns of Recognition, and Pathophysiology. *Antioxidants & Redox Signaling* **13**, 39–75 (2010).
93. Sheedy, F. J. *et al.* CD36 coordinates NLRP3 inflammasome activation by facilitating intracellular nucleation of soluble ligands into particulate ligands in sterile inflammation. *Nat Immunol* **14**, 812–820 (2013).

94. Witztum, J. L. & Steinberg, D. The oxidative modification hypothesis of atherosclerosis: does it hold for humans? *Trends Cardiovasc Med* **11**, 93–102 (2001).
95. Henriksen, T., Mahoney, E. M. & Steinberg, D. Enhanced macrophage degradation of biologically modified low density lipoprotein. *Arteriosclerosis* **3**, 149–159 (1983).
96. Heinecke, J. W., Baker, L., Rosen, H. & Chait, A. Superoxide-mediated modification of low density lipoprotein by arterial smooth muscle cells. *J Clin Invest* **77**, 757–761 (1986).
97. Steinbrecher, U. P. Role of superoxide in endothelial-cell modification of low-density lipoproteins. *Biochim Biophys Acta* **959**, 20–30 (1988).
98. Cathcart, M. K., Morel, D. W. & Chisolm, G. M. Monocytes and neutrophils oxidize low density lipoprotein making it cytotoxic. *J Leukoc Biol* **38**, 341–350 (1985).
99. Parthasarathy, S., Printz, D. J., Boyd, D., Joy, L. & Steinberg, D. Macrophage oxidation of low density lipoprotein generates a modified form recognized by the scavenger receptor. *Arteriosclerosis* **6**, 505–510 (1986).
100. Steinbrecher, U. P., Zhang, H. F. & Lougheed, M. Role of oxidatively modified LDL in atherosclerosis. *Free Radic Biol Med* **9**, 155–168 (1990).
101. Carr, A. C., McCall, M. R. & Frei, B. Oxidation of LDL by Myeloperoxidase and Reactive Nitrogen Species: Reaction Pathways and Antioxidant Protection. *ATVB* **20**, 1716–1723 (2000).
102. Nakajima, H. *et al.* Low-density lipoprotein is oxidized by phospholipase A2 and lipoxygenase in xanthoma lesions. *Eur. J. Lipid Sci. Technol.* **109**, 1053–1059 (2007).
103. Takahashi, Y., Zhu, H. & Yoshimoto, T. Essential roles of lipoxygenases in LDL oxidation and development of atherosclerosis. *Antioxid Redox Signal* **7**, 425–431 (2005).
104. Parthasarathy, S., Wieland, E. & Steinberg, D. A role for endothelial cell lipoxygenase in the oxidative modification of low density lipoprotein. *Proc Natl Acad Sci U S A* **86**, 1046–1050 (1989).
105. Esterbauer, H., Waeg, G., Puhl, H., Dieber-Rotheneder, M. & Tatzber, F. Inhibition of LDL oxidation by antioxidants. *EXS* **62**, 145–157 (1992).

106. Esterbauer, H., Jürgens, G., Quehenberger, O. & Koller, E. Autoxidation of human low density lipoprotein: loss of polyunsaturated fatty acids and vitamin E and generation of aldehydes. *J Lipid Res* **28**, 495–509 (1987).
107. Jialal, I., Norkus, E. P., Cristol, L. & Grundy, S. M. beta-Carotene inhibits the oxidative modification of low-density lipoprotein. *Biochim Biophys Acta* **1086**, 134–138 (1991).
108. Heinecke, J. W. Mechanisms of oxidative damage of low density lipoprotein in human atherosclerosis. *Curr Opin Lipidol* **8**, 268–274 (1997).
109. Berliner, J. A. *et al.* Atherosclerosis: basic mechanisms. Oxidation, inflammation, and genetics. *Circulation* **91**, 2488–2496 (1995).
110. Navab, M. *et al.* The Yin and Yang of oxidation in the development of the fatty streak. A review based on the 1994 George Lyman Duff Memorial Lecture. *Arterioscler Thromb Vasc Biol* **16**, 831–842 (1996).
111. Chistiakov, D. A., Bobryshev, Y. V. & Orekhov, A. N. Macrophage-mediated cholesterol handling in atherosclerosis. *J Cell Mol Med* **20**, 17–28 (2016).
112. Moore, K. J. & Freeman, M. W. Scavenger receptors in atherosclerosis: beyond lipid uptake. *Arterioscler Thromb Vasc Biol* **26**, 1702–1711 (2006).
113. Younis, N. *et al.* Glycation as an atherogenic modification of LDL. *Curr Opin Lipidol* **19**, 378–384 (2008).
114. Öörni, K., Pentikäinen, M. O., Annila, A. & Kovanen, P. T. Oxidation of Low Density Lipoprotein Particles Decreases Their Ability to Bind to Human Aortic Proteoglycans. *Journal of Biological Chemistry* **272**, 21303–21311 (1997).
115. Ling, W. *et al.* Oxidized or acetylated low density lipoproteins are rapidly cleared by the liver in mice with disruption of the scavenger receptor class A type I/II gene. *J Clin Invest* **100**, 244–252 (1997).
116. Lu, M. & Gursky, O. Aggregation and fusion of low-density lipoproteins in vivo and in vitro. *BioMolecular Concepts* **4**, 501–518 (2013).
117. Libby, P. The changing landscape of atherosclerosis. *Nature* **592**, 524–533 (2021).
118. Pober, J. S. & Cotran, R. S. THE ROLE OF ENDOTHELIAL CELLS IN INFLAMMATION: *Transplantation* **50**, 537–544 (1990).

119. Hunt, B. J. & Jurd, K. M. Endothelial cell activation. *BMJ* **316**, 1328–1329 (1998).
120. Pober, J. S. & Cotran, R. S. Cytokines and endothelial cell biology. *Physiological Reviews* **70**, 427–451 (1990).
121. Pober, J. S. & Sessa, W. C. Evolving functions of endothelial cells in inflammation. *Nat Rev Immunol* **7**, 803–815 (2007).
122. SenBanerjee, S. et al. KLF2 Is a Novel Transcriptional Regulator of Endothelial Proinflammatory Activation. *Journal of Experimental Medicine* **199**, 1305–1315 (2004).
123. Yurdagul, A. et al. Altered nitric oxide production mediates matrix-specific PAK2 and NF- $\kappa$ B activation by flow. *MBoC* **24**, 398–408 (2013).
124. Hamik, A. et al. Kruppel-like Factor 4 Regulates Endothelial Inflammation. *Journal of Biological Chemistry* **282**, 13769–13779 (2007).
125. Ley, K., Miller, Y. I. & Hedrick, C. C. Monocyte and Macrophage Dynamics During Atherogenesis. *Arterioscler Thromb Vasc Biol.* **31**, 1506–1516 (2011).
126. Gerrity, R. G. The role of the monocyte in atherogenesis: I. Transition of blood-borne monocytes into foam cells in fatty lesions. *Am J Pathol* **103**, 181–190 (1981).
127. Huo, Y., Hafezi-Moghadam, A. & Ley, K. Role of vascular cell adhesion molecule-1 and fibronectin connecting segment-1 in monocyte rolling and adhesion on early atherosclerotic lesions. *Circ Res* **87**, 153–159 (2000).
128. Ramos, C. L. et al. Direct demonstration of P-selectin- and VCAM-1-dependent mononuclear cell rolling in early atherosclerotic lesions of apolipoprotein E-deficient mice. *Circ Res* **84**, 1237–1244 (1999).
129. Ley, K., Laudanna, C., Cybulsky, M. I. & Nourshargh, S. Getting to the site of inflammation: the leukocyte adhesion cascade updated. *Nat Rev Immunol* **7**, 678–689 (2007).
130. Galkina, E. & Ley, K. Immune and Inflammatory Mechanisms of Atherosclerosis. *Annu. Rev. Immunol.* **27**, 165–197 (2009).
131. Campbell, J. J., Qin, S., Bacon, K. B., Mackay, C. R. & Butcher, E. C. Biology of chemokine and classical chemoattractant receptors: differential requirements

for adhesion-triggering versus chemotactic responses in lymphoid cells. *J Cell Biol* **134**, 255–266 (1996).

132. Campbell, J. J. Chemokines and the Arrest of Lymphocytes Rolling Under Flow Conditions. *Science* **279**, 381–384 (1998).

133. Springer, T. A. Traffic signals for lymphocyte recirculation and leukocyte emigration: the multistep paradigm. *Cell* **76**, 301–314 (1994).

134. Callewaere, C., Banisadr, G., Rostène, W. & Parsadaniantz, S. M. Chemokines and chemokine receptors in the brain: implication in neuroendocrine regulation. *J Mol Endocrinol* **38**, 355–363 (2007).

135. Sozzani, S. et al. Receptor-activated calcium influx in human monocytes exposed to monocyte chemotactic protein-1 and related cytokines. *J Immunol* **150**, 1544–1553 (1993).

136. Uggioni, M., D'Apuzzo, M., Loetscher, M., Dewald, B. & Baggioolini, M. Actions of the chemotactic cytokines MCP-1, MCP-2, MCP-3, RANTES, MIP-1 alpha and MIP-1 beta on human monocytes. *Eur J Immunol* **25**, 64–68 (1995).

137. Lin, J., Kakkar, V. & Lu, X. Impact of MCP-1 in atherosclerosis. *Curr Pharm Des* **20**, 4580–4588 (2014).

138. Allport, J. R., Muller, W. A. & Luscinskas, F. W. Monocytes induce reversible focal changes in vascular endothelial cadherin complex during transendothelial migration under flow. *J Cell Biol* **148**, 203–216 (2000).

139. Shaw, S. K., Bamba, P. S., Perkins, B. N. & Luscinskas, F. W. Real-time imaging of vascular endothelial-cadherin during leukocyte transmigration across endothelium. *J Immunol* **167**, 2323–2330 (2001).

140. Vestweber, D. Regulation of endothelial cell contacts during leukocyte extravasation. *Current Opinion in Cell Biology* **14**, 587–593 (2002).

141. Muller, W. A. Leukocyte-endothelial-cell interactions in leukocyte transmigration and the inflammatory response. *Trends Immunol* **24**, 327–334 (2003).

142. Engelhardt, B. & Wolburg, H. Mini-review: Transendothelial migration of leukocytes: through the front door or around the side of the house? *Eur J Immunol* **34**, 2955–2963 (2004).

143. Hallmann, R. *et al.* Expression and function of laminins in the embryonic and mature vasculature. *Physiol Rev* **85**, 979–1000 (2005).
144. Italiani, P. & Boraschi, D. From Monocytes to M1/M2 Macrophages: Phenotypical vs. Functional Differentiation. *Front. Immunol.* **5**, (2014).
145. Ferrante, C. J. & Leibovich, S. J. Regulation of Macrophage Polarization and Wound Healing. *Adv Wound Care (New Rochelle)* **1**, 10–16 (2012).
146. Ferrante, C. J. *et al.* The adenosine-dependent angiogenic switch of macrophages to an M2-like phenotype is independent of interleukin-4 receptor alpha (IL-4R $\alpha$ ) signaling. *Inflammation* **36**, 921–931 (2013).
147. De Paoli, F., Staels, B. & Chinetti-Gbaguidi, G. Macrophage phenotypes and their modulation in atherosclerosis. *Circ J* **78**, 1775–1781 (2014).
148. Peled, M. & Fisher, E. A. Dynamic Aspects of Macrophage Polarization during Atherosclerosis Progression and Regression. *Front Immunol* **5**, 579 (2014).
149. Bobryshev, Y. V. Monocyte recruitment and foam cell formation in atherosclerosis. *Micron* **37**, 208–222 (2006).
150. Wilfling, F. *et al.* Triacylglycerol synthesis enzymes mediate lipid droplet growth by relocalizing from the ER to lipid droplets. *Dev Cell* **24**, 384–399 (2013).
151. Chinetti-Gbaguidi, G. *et al.* Human atherosclerotic plaque alternative macrophages display low cholesterol handling but high phagocytosis because of distinct activities of the PPAR $\gamma$  and LXR $\alpha$  pathways. *Circ Res* **108**, 985–995 (2011).
152. Maitra, U., Parks, J. S. & Li, L. An innate immunity signaling process suppresses macrophage ABCA1 expression through IRAK-1-mediated downregulation of retinoic acid receptor alpha and NFATc2. *Mol Cell Biol* **29**, 5989–5997 (2009).
153. Kim, T. W. *et al.* The critical role of IL-1 receptor-associated kinase 4-mediated NF- $\kappa$ B activation in modified low-density lipoprotein-induced inflammatory gene expression and atherosclerosis. *J Immunol* **186**, 2871–2880 (2011).
154. Rekhter, M. *et al.* Genetic ablation of IRAK4 kinase activity inhibits vascular lesion formation. *Biochem Biophys Res Commun* **367**, 642–648 (2008).

155. Michelsen, K. S. *et al.* Lack of Toll-like receptor 4 or myeloid differentiation factor 88 reduces atherosclerosis and alters plaque phenotype in mice deficient in apolipoprotein E. *Proc Natl Acad Sci U S A* **101**, 10679–10684 (2004).
156. Björkbacka, H. *et al.* Reduced atherosclerosis in MyD88-null mice links elevated serum cholesterol levels to activation of innate immunity signaling pathways. *Nat Med* **10**, 416–421 (2004).
157. Nasiri, M. *et al.* Role of cholesterol crystals in atherosclerosis is unmasked by altering tissue preparation methods: Ethanol Dissolves Cholesterol Crystals in Plaques. *Microsc. Res. Tech.* **78**, 969–974 (2015).
158. Levene, C. I. The early lesions of atheroma in the coronary arteries. *J Pathol Bacteriol* **72**, 79–82 (1956).
159. Katz, S. S., Shipley, G. G. & Small, D. M. Physical chemistry of the lipids of human atherosclerotic lesions. Demonstration of a lesion intermediate between fatty streaks and advanced plaques. *J Clin Invest* **58**, 200–211 (1976).
160. Bogren, H. & Larsson, K. AN X-RAY-DIFFRACTION STUDY OF CRYSTALLINE CHOLESTEROL IN SOME PATHOLOGICAL DEPOSITS IN MAN. *Biochim Biophys Acta* **75**, 65–69 (1963).
161. Suhalim, J. L. *et al.* Characterization of cholesterol crystals in atherosclerotic plaques using stimulated Raman scattering and second-harmonic generation microscopy. *Biophys J* **102**, 1988–1995 (2012).
162. Baumer, Y., Mehta, N. N., Dey, A. K., Powell-Wiley, T. M. & Boisvert, W. A. Cholesterol crystals and atherosclerosis. *European Heart Journal* **41**, 2236–2239 (2020).
163. Abela, G. S. Cholesterol crystals piercing the arterial plaque and intima trigger local and systemic inflammation. *J Clin Lipidol* **4**, 156–164 (2010).
164. Guo, H., Callaway, J. B. & Ting, J. P.-Y. Inflammasomes: mechanism of action, role in disease, and therapeutics. *Nat Med* **21**, 677–687 (2015).
165. Hornung, V. *et al.* Silica crystals and aluminum salts activate the NALP3 inflammasome through phagosomal destabilization. *Nat Immunol* **9**, 847–856 (2008).
166. Zhou, R., Yazdi, A. S., Menu, P. & Tschopp, J. A role for mitochondria in NLRP3 inflammasome activation. *Nature* **469**, 221–225 (2011).

167. Mietus-Snyder, M., Gowri, M. S. & Pitas, R. E. Class A Scavenger Receptor Up-regulation in Smooth Muscle Cells by Oxidized Low Density Lipoprotein. *Journal of Biological Chemistry* **275**, 17661–17670 (2000).
168. Yan, P., Xia, C., Duan, C., Li, S. & Mei, Z. Biological characteristics of foam cell formation in smooth muscle cells derived from bone marrow stem cells. *Int J Biol Sci* **7**, 937–946 (2011).
169. Beyea, M. M. et al. The oxysterol 24(s),25-epoxycholesterol attenuates human smooth muscle-derived foam cell formation via reduced low-density lipoprotein uptake and enhanced cholesterol efflux. *J Am Heart Assoc* **1**, e000810 (2012).
170. Ricciarelli, R., Zingg, J.-M. & Azzi, A. Vitamin E Reduces the Uptake of Oxidized LDL by Inhibiting CD36 Scavenger Receptor Expression in Cultured Aortic Smooth Muscle Cells. *Circulation* **102**, 82–87 (2000).
171. Aoyama, T., Chen, M., Fujiwara, H., Masaki, T. & Sawamura, T. LOX-1 mediates lysophosphatidylcholine-induced oxidized LDL uptake in smooth muscle cells. *FEBS Letters* **467**, 217–220 (2000).
172. Choi, H. Y. et al. ATP-binding cassette transporter A1 expression and apolipoprotein A-I binding are impaired in intima-type arterial smooth muscle cells. *Circulation* **119**, 3223–3231 (2009).
173. Wang, Y. et al. Smooth Muscle Cells Contribute the Majority of Foam Cells in ApoE (Apolipoprotein E)-Deficient Mouse Atherosclerosis. *Arterioscler Thromb Vasc Biol* **39**, 876–887 (2019).
174. Lusis, A. J. Atherosclerosis. *Nature* **407**, 233–241 (2000).
175. Fisher, E. A., Feig, J. E., Hewing, B., Hazen, S. L. & Smith, J. D. High-density lipoprotein function, dysfunction, and reverse cholesterol transport. *Arterioscler Thromb Vasc Biol* **32**, 2813–2820 (2012).
176. Puri, R. et al. Factors underlying regression of coronary atheroma with potent statin therapy. *Eur Heart J* **34**, 1818–1825 (2013).
177. Chamié, D., Wang, Z., Bezerra, H., Rollins, A. M. & Costa, M. A. Optical Coherence Tomography and Fibrous Cap Characterization. *Curr Cardiovasc Imaging Rep* **4**, 276–283 (2011).
178. Schaper, W. & Ito, W. D. Molecular Mechanisms of Coronary Collateral Vessel Growth. *Circulation Research* **79**, 911–919 (1996).

179. Wolf, C. *et al.* Vascular remodeling and altered protein expression during growth of coronary collateral arteries. *J Mol Cell Cardiol* **30**, 2291–2305 (1998).
180. Zalewski, A., Shi, Y. & Johnson, A. G. Diverse Origin of Intimal Cells: Smooth Muscle Cells, Myofibroblasts, Fibroblasts, and Beyond? *Circulation Research* **91**, 652–655 (2002).
181. Louis, S. F. & Zahradka, P. Vascular smooth muscle cell motility: From migration to invasion. *Exp Clin Cardiol* **15**, e75-85 (2010).
182. Stiko-Rahm, A., Hultgårdh-Nilsson, A., Regnström, J., Hamsten, A. & Nilsson, J. Native and oxidized LDL enhances production of PDGF AA and the surface expression of PDGF receptors in cultured human smooth muscle cells. *Arterioscler Thromb* **12**, 1099–1109 (1992).
183. Kohno, M. *et al.* Induction by Lysophosphatidylcholine, a Major Phospholipid Component of Atherogenic Lipoproteins, of Human Coronary Artery Smooth Muscle Cell Migration. *Circulation* **98**, 353–359 (1998).
184. Raines, E. W., Dower, S. K. & Ross, R. Interleukin-1 mitogenic activity for fibroblasts and smooth muscle cells is due to PDGF-AA. *Science* **243**, 393–396 (1989).
185. Bentzon, J. F., Otsuka, F., Virmani, R. & Falk, E. Mechanisms of Plaque Formation and Rupture. *Circ Res* **114**, 1852–1866 (2014).
186. Shen, C. M., Mao, S. J., Huang, G. S., Yang, P. C. & Chu, R. M. Stimulation of smooth muscle cell proliferation by ox-LDL- and acetyl LDL-induced macrophage-derived foam cells. *Life Sci* **70**, 443–452 (2001).
187. Badimon, L., Padró, T. & Vilahur, G. Atherosclerosis, platelets and thrombosis in acute ischaemic heart disease. *European Heart Journal: Acute Cardiovascular Care* **1**, 60–74 (2012).
188. Ridley, A. J. *et al.* Cell migration: integrating signals from front to back. *Science* **302**, 1704–1709 (2003).
189. Richardson, P. D., Davies, M. J. & Born, G. V. Influence of plaque configuration and stress distribution on fissuring of coronary atherosclerotic plaques. *Lancet* **2**, 941–944 (1989).
190. Motoyama, S. *et al.* Computed Tomographic Angiography Characteristics of Atherosclerotic Plaques Subsequently Resulting in Acute Coronary Syndrome. *Journal of the American College of Cardiology* **54**, 49–57 (2009).

191. Visscher, M. *et al.* Data Processing Pipeline for Lipid Profiling of Carotid Atherosclerotic Plaque with Mass Spectrometry Imaging. *J. Am. Soc. Mass Spectrom.* **30**, 1790–1800 (2019).
192. Thim, T., Hagensen, M. K., Bentzon, J. F. & Falk, E. From vulnerable plaque to atherothrombosis. *J Intern Med* **263**, 506–516 (2008).
193. Linton, M. F. *et al.* Macrophage Apoptosis and Efferocytosis in the Pathogenesis of Atherosclerosis. *Circ J* **80**, 2259–2268 (2016).
194. Cabrera, J. T. O. & Makino, A. Efferocytosis of vascular cells in cardiovascular disease. *Pharmacology & Therapeutics* 107919 (2021) doi:10.1016/j.pharmthera.2021.107919.
195. Bäck, M., Yurdagul, A., Tabas, I., Öörni, K. & Kovanen, P. T. Inflammation and its resolution in atherosclerosis: mediators and therapeutic opportunities. *Nat Rev Cardiol* (2019) doi:10.1038/s41569-019-0169-2.
196. Gonzalez, L. & Trigatti, B. L. Macrophage Apoptosis and Necrotic Core Development in Atherosclerosis: A Rapidly Advancing Field with Clinical Relevance to Imaging and Therapy. *Canadian Journal of Cardiology* **33**, 303–312 (2017).
197. Coornaert, I. *et al.* Novel drug discovery strategies for atherosclerosis that target necrosis and necroptosis. *Expert Opinion on Drug Discovery* **13**, 477–488 (2018).
198. Wanke, F. *et al.* Ligand-dependent kinase activity of MERTK drives efferocytosis in human iPSC-derived macrophages. *Cell Death Dis* **12**, 538 (2021).
199. Quillard, T., Araújo, H. A., Franck, G., Tesmenitsky, Y. & Libby, P. Matrix metalloproteinase-13 predominates over matrix metalloproteinase-8 as the functional interstitial collagenase in mouse atheromata. *Arterioscler Thromb Vasc Biol* **34**, 1179–1186 (2014).
200. Galis, Z. S., Sukhova, G. K., Kranzhöfer, R., Clark, S. & Libby, P. Macrophage foam cells from experimental atheroma constitutively produce matrix-degrading proteinases. *Proc Natl Acad Sci U S A* **92**, 402–406 (1995).
201. Schneider, F. *et al.* Matrix Metalloproteinase-14 Deficiency in Bone Marrow-Derived Cells Promotes Collagen Accumulation in Mouse Atherosclerotic Plaques. *Circulation* **117**, 931–939 (2008).
202. Mulay, S. R. & Anders, H.-J. Crystallopathies. *N Engl J Med* **374**, 2465–2476 (2016).

203. Nidorf, S. M., Fiolet, A. & Abela, G. S. Viewing atherosclerosis through a crystal lens: How the evolving structure of cholesterol crystals in atherosclerotic plaque alters its stability. *Journal of Clinical Lipidology* **14**, 619–630 (2020).
204. Warnatsch, A., Ioannou, M., Wang, Q. & Papayannopoulos, V. Neutrophil extracellular traps license macrophages for cytokine production in atherosclerosis. *Science* **349**, 316–320 (2015).
205. Johnson, J. L. *et al.* Relationship of MMP-14 and TIMP-3 Expression with Macrophage Activation and Human Atherosclerotic Plaque Vulnerability. *Mediators of Inflammation* **2014**, 1–17 (2014).
206. García-García, H. M. *et al.* Relationship between cardiovascular risk factors and biomarkers with necrotic core and atheroma size: a serial intravascular ultrasound radiofrequency data analysis. *Int J Cardiovasc Imaging* **28**, 695–703 (2012).
207. Martinet, W., Schrijvers, D. M. & De Meyer, G. R. Y. Necrotic cell death in atherosclerosis. *Basic Res Cardiol* **106**, 749–760 (2011).
208. Steffel, J., Lüscher, T. F. & Tanner, F. C. Tissue Factor in Cardiovascular Diseases: Molecular Mechanisms and Clinical Implications. *Circulation* **113**, 722–731 (2006).
209. Nakahara, T. *et al.* Coronary Artery Calcification: From Mechanism to Molecular Imaging. *JACC Cardiovasc Imaging* **10**, 582–593 (2017).
210. Shi, X. *et al.* Calcification in Atherosclerotic Plaque Vulnerability: Friend or Foe? *Front. Physiol.* **11**, 56 (2020).
211. Wu, L. N. *et al.* Characterization of the nucleational core complex responsible for mineral induction by growth plate cartilage matrix vesicles. *J Biol Chem* **268**, 25084–25094 (1993).
212. Wiesmann, H. P., Meyer, U., Plate, U. & Höhling, H. J. Aspects of collagen mineralization in hard tissue formation. *Int Rev Cytol* **242**, 121–156 (2005).
213. Bobryshev, Y. V., Killingsworth, M. C., Lord, R. S. A. & Grabs, A. J. Matrix vesicles in the fibrous cap of atherosclerotic plaque: possible contribution to plaque rupture. *Journal of Cellular and Molecular Medicine* **12**, 2073–2082 (2008).
214. Anderson, H. C. Mechanisms of Pathologic Calcification. *Rheumatic Disease Clinics of North America* **14**, 303–319 (1988).

215. Kapustin, A. N. *et al.* Vascular Smooth Muscle Cell Calcification Is Mediated by Regulated Exosome Secretion. *Circ Res* **116**, 1312–1323 (2015).
216. New, S. E. P. *et al.* Macrophage-Derived Matrix Vesicles: An Alternative Novel Mechanism for Microcalcification in Atherosclerotic Plaques. *Circ Res* **113**, 72–77 (2013).
217. Canfield, A. E., Sutton, A. B., Hoyland, J. A. & Schor, A. M. Association of thrombospondin-1 with osteogenic differentiation of retinal pericytes in vitro. *J Cell Sci* **109** (Pt 2), 343–353 (1996).
218. Lomashvili, K. A., Cobbs, S., Hennigar, R. A., Hardcastle, K. I. & O'Neill, W. C. Phosphate-induced vascular calcification: role of pyrophosphate and osteopontin. *J Am Soc Nephrol* **15**, 1392–1401 (2004).
219. Otsuka, F., Sakakura, K., Yahagi, K., Joner, M. & Virmani, R. Has our understanding of calcification in human coronary atherosclerosis progressed? *Arterioscler Thromb Vasc Biol* **34**, 724–736 (2014).
220. Proudfoot, D., Skepper, J. N., Shanahan, C. M. & Weissberg, P. L. Calcification of Human Vascular Cells In Vitro Is Correlated With High Levels of Matrix Gla Protein and Low Levels of Osteopontin Expression. *ATVB* **18**, 379–388 (1998).
221. Demer, L. L. & Tintut, Y. Vascular Calcification: Pathobiology of a Multifaceted Disease. *Circulation* **117**, 2938–2948 (2008).
222. Reynolds, J. L. Human Vascular Smooth Muscle Cells Undergo Vesicle-Mediated Calcification in Response to Changes in Extracellular Calcium and Phosphate Concentrations: A Potential Mechanism for Accelerated Vascular Calcification in ESRD. *Journal of the American Society of Nephrology* **15**, 2857–2867 (2004).
223. Reith, S., Milzi, A., Dettori, R., Marx, N. & Burgmaier, M. Predictors for target lesion microcalcifications in patients with stable coronary artery disease: an optical coherence tomography study. *Clin Res Cardiol* **107**, 763–771 (2018).
224. Pugliese, G., Iacobini, C., Blasetti Fantauzzi, C. & Menini, S. The dark and bright side of atherosclerotic calcification. *Atherosclerosis* **238**, 220–230 (2015).
225. Asakura, T. & Karino, T. Flow patterns and spatial distribution of atherosclerotic lesions in human coronary arteries. *Circ Res* **66**, 1045–1066 (1990).

226. Malek, A. M., Alper, S. L. & Izumo, S. Hemodynamic shear stress and its role in atherosclerosis. *JAMA* **282**, 2035–2042 (1999).
227. Slager, C. *et al.* The role of shear stress in the generation of rupture-prone vulnerable plaques. *Nat Rev Cardiol* **2**, 401–407 (2005).
228. Stary, H. C. *et al.* A definition of the intima of human arteries and of its atherosclerosis-prone regions. A report from the Committee on Vascular Lesions of the Council on Arteriosclerosis, American Heart Association. *Circulation* **85**, 391–405 (1992).
229. Fuster, V., Moreno, P. R., Fayad, Z. A., Corti, R. & Badimon, J. J. Atherothrombosis and high-risk plaque: part I: evolving concepts. *J Am Coll Cardiol* **46**, 937–954 (2005).
230. Sodhi, N. & Brown, D. L. Pathophysiology of Acute Coronary Syndromes. in *Cardiac Intensive Care* 68–80.e2 (Elsevier, 2019). doi:10.1016/B978-0-323-52993-8.00007-2.
231. Libby, P. Inflammation in atherosclerosis. *Nature* **420**, 868–874 (2002).
232. Kovanen, P. T., Kaartinen, M. & Paavonen, T. Infiltrates of activated mast cells at the site of coronary atheromatous erosion or rupture in myocardial infarction. *Circulation* **92**, 1084–1088 (1995).
233. Sarén, P., Welgus, H. G. & Kovanen, P. T. TNF-alpha and IL-1beta selectively induce expression of 92-kDa gelatinase by human macrophages. *J Immunol* **157**, 4159–4165 (1996).
234. Pasterkamp, G. *et al.* Inflammation of the Atherosclerotic Cap and Shoulder of the Plaque Is a Common and Locally Observed Feature in Unruptured Plaques of Femoral and Coronary Arteries. *ATVB* **19**, 54–58 (1999).
235. Davì, G. & Patrono, C. Platelet activation and atherothrombosis. *N Engl J Med* **357**, 2482–2494 (2007).
236. Furie, B. & Furie, B. C. Mechanisms of Thrombus Formation. *N Engl J Med* **359**, 938–949 (2008).
237. Yun, S.-H., Sim, E.-H., Goh, R.-Y., Park, J.-I. & Han, J.-Y. Platelet Activation: The Mechanisms and Potential Biomarkers. *BioMed Research International* **2016**, 1–5 (2016).

238. Osaki, T. & Ichinose, A. [Current views of activating and regulatory mechanisms of blood coagulation]. *Nihon Rinsho* **72**, 1206–1211 (2014).
239. Mackman, N., Tilley, R. E. & Key, N. S. Role of the Extrinsic Pathway of Blood Coagulation in Hemostasis and Thrombosis. *ATVB* **27**, 1687–1693 (2007).
240. Grainger, D. J., Wakefield, L., Bethell, H. W., Farndale, R. W. & Metcalfe, J. C. Release and activation of platelet latent TGF-beta in blood clots during dissolution with plasmin. *Nat Med* **1**, 932–937 (1995).
241. Fuster, V., Badimon, L., Badimon, J. J. & Chesebro, J. H. The pathogenesis of coronary artery disease and the acute coronary syndromes (2). *N Engl J Med* **326**, 310–318 (1992).
242. Théroux, P. & Fuster, V. Acute Coronary Syndromes: Unstable Angina and Non-Q-Wave Myocardial Infarction. *Circulation* **97**, 1195–1206 (1998).
243. Thanvi, B. & Robinson, T. Complete occlusion of extracranial internal carotid artery: clinical features, pathophysiology, diagnosis and management. *Postgraduate Medical Journal* **83**, 95–99 (2007).
244. Lyaker, M. R., Tulman, D. B., Dimitrova, G. T., Pin, R. H. & Papadimos, T. J. Arterial embolism. *Int J Crit Illn Inj Sci* **3**, 77–87 (2013).
245. Trajkovska, K. T. High-density lipoprotein metabolism and reverse cholesterol transport: strategies for raising HDL cholesterol. *Anatol J Cardiol* (2017) doi:10.14744/AnatolJCardiol.2017.7608.
246. Ghosh, S. Early steps in reverse cholesterol transport: cholesteryl ester hydrolase and other hydrolases. *Curr Opin Endocrinol Diabetes Obes* **19**, 136–141 (2012).
247. Chistiakov, D. A., Bobryshev, Y. V. & Orekhov, A. N. Macrophage-mediated cholesterol handling in atherosclerosis. *J Cell Mol Med* **20**, 17–28 (2016).
248. Tall, A. R. An overview of reverse cholesterol transport. *Eur Heart J* **19 Suppl A**, A31-35 (1998).
249. Qian, H. *et al.* Structure of the Human Lipid Exporter ABCA1. *Cell* **169**, 1228-1239.e10 (2017).
250. Phillips, M. C. Is ABCA1 a lipid transfer protein? *Journal of Lipid Research* **59**, 749–763 (2018).

251. Arakawa, R. & Yokoyama, S. Helical apolipoproteins stabilize ATP-binding cassette transporter A1 by protecting it from thiol protease-mediated degradation. *J Biol Chem* **277**, 22426–22429 (2002).
252. Vedhachalam, C. *et al.* Mechanism of ATP-binding cassette transporter A1-mediated cellular lipid efflux to apolipoprotein A-I and formation of high density lipoprotein particles. *J Biol Chem* **282**, 25123–25130 (2007).
253. Fukuda, M. *et al.* Spontaneous reconstitution of discoidal HDL from sphingomyelin-containing model membranes by apolipoprotein A-I. *J Lipid Res* **48**, 882–889 (2007).
254. Gillotte, K. L. *et al.* Apolipoprotein-mediated Plasma Membrane Microsolubilization. *Journal of Biological Chemistry* **274**, 2021–2028 (1999).
255. Melchior, J. T. *et al.* A consensus model of human apolipoprotein A-I in its monomeric and lipid-free state. *Nat Struct Mol Biol* **24**, 1093–1099 (2017).
256. Linton, M. F. *et al.* The Role of Lipids and Lipoproteins in Atherosclerosis. in *Endotext* (eds. Feingold, K. R. *et al.*) (MDText.com, Inc., 2000).
257. Fielding, C. J. Mechanisms of action of lecithin-cholesterol acyltransferase. *Methods Enzymol* **129**, 783–790 (1986).
258. Cooke, A. L. *et al.* A thumbwheel mechanism for APOA1 activation of LCAT activity in HDL. *J Lipid Res* **59**, 1244–1255 (2018).
259. Jonas, A. Lecithin cholesterol acyltransferase. *Biochim Biophys Acta* **1529**, 245–256 (2000).
260. Rye, K. A., Clay, M. A. & Barter, P. J. Remodelling of high density lipoproteins by plasma factors. *Atherosclerosis* **145**, 227–238 (1999).
261. Ji, Y. *et al.* Scavenger receptor BI promotes high density lipoprotein-mediated cellular cholesterol efflux. *J Biol Chem* **272**, 20982–20985 (1997).
262. Jian, B. *et al.* Scavenger receptor class B type I as a mediator of cellular cholesterol efflux to lipoproteins and phospholipid acceptors. *J Biol Chem* **273**, 5599–5606 (1998).
263. Kennedy, M. A. *et al.* ABCG1 has a critical role in mediating cholesterol efflux to HDL and preventing cellular lipid accumulation. *Cell Metab* **1**, 121–131 (2005).

264. Frambach, S. J. C. M. *et al.* Brothers in Arms: ABCA1- and ABCG1-Mediated Cholesterol Efflux as Promising Targets in Cardiovascular Disease Treatment. *Pharmacol Rev* **72**, 152–190 (2020).
265. Luo, D., Cao, D., Xiong, Y., Peng, X. & Liao, D. A novel model of cholesterol efflux from lipid-loaded cells. *Acta Pharmacol Sin* **31**, 1243–1257 (2010).
266. de la Llera-Moya, M. *et al.* Scavenger receptor BI (SR-BI) mediates free cholesterol flux independently of HDL tethering to the cell surface. *J Lipid Res* **40**, 575–580 (1999).
267. Rhainds, D. & Brissette, L. The role of scavenger receptor class B type I (SR-BI) in lipid trafficking. *The International Journal of Biochemistry & Cell Biology* **36**, 39–77 (2004).
268. Baldán, A. *et al.* Deletion of the transmembrane transporter ABCG1 results in progressive pulmonary lipidosis. *J Biol Chem* **281**, 29401–29410 (2006).
269. Westerterp, M. *et al.* Deficiency of ATP-binding cassette transporters A1 and G1 in macrophages increases inflammation and accelerates atherosclerosis in mice. *Circ Res* **112**, 1456–1465 (2013).
270. Braun, A. *et al.* Loss of SR-BI expression leads to the early onset of occlusive atherosclerotic coronary artery disease, spontaneous myocardial infarctions, severe cardiac dysfunction, and premature death in apolipoprotein E-deficient mice. *Circ Res* **90**, 270–276 (2002).
271. Kleber, M. E., Grammer, T. B. & März, W. [High-density lipoprotein (HDL) and cholesteryl ester transfer protein (CETP): role in lipid metabolism and clinical meaning]. *MMW Fortschr Med* **152 Suppl 2**, 47–55 (2010).
272. Barter, P. & Rye, K. A. Cholesteryl ester transfer protein: its role in plasma lipid transport. *Clin Exp Pharmacol Physiol* **21**, 663–672 (1994).
273. Oliveira, H. C. F. & de Faria, E. C. Cholesteryl ester transfer protein: the controversial relation to atherosclerosis and emerging new biological roles. *IUBMB Life* **63**, 248–257 (2011).
274. Albers, J. J., Vuletic, S. & Cheung, M. C. Role of plasma phospholipid transfer protein in lipid and lipoprotein metabolism. *Biochim Biophys Acta* **1821**, 345–357 (2012).
275. Hegele, R. A. *et al.* Hepatic lipase deficiency. Clinical, biochemical, and molecular genetic characteristics. *Arterioscler Thromb* **13**, 720–728 (1993).

276. Connelly, P. W. The role of hepatic lipase in lipoprotein metabolism. *Clin Chim Acta* **286**, 243–255 (1999).
277. Shimizu, M. *et al.* Endothelial lipase gene polymorphism is associated with acute myocardial infarction, independently of high-density lipoprotein-cholesterol levels. *Circ J* **71**, 842–846 (2007).
278. Yang, H., Fogo, A. B. & Kon, V. Kidneys: key modulators of high-density lipoprotein levels and function. *Current Opinion in Nephrology and Hypertension* **25**, 174–179 (2016).
279. de Aguiar Vallim, T. Q., Tarling, E. J. & Edwards, P. A. Pleiotropic roles of bile acids in metabolism. *Cell Metab* **17**, 657–669 (2013).
280. Chiang, J. Y. L. Regulation of bile acid synthesis: pathways, nuclear receptors, and mechanisms. *Journal of Hepatology* **40**, 539–551 (2004).
281. Stieger, B. Recent insights into the function and regulation of the bile salt export pump (ABCB11). *Curr Opin Lipidol* **20**, 176–181 (2009).
282. Dikkers, A. & Tietge, U.-J. Biliary cholesterol secretion: more than a simple ABC. *World J Gastroenterol* **16**, 5936–5945 (2010).
283. Oude Elferink, R. P. & Groen, A. K. Mechanisms of biliary lipid secretion and their role in lipid homeostasis. *Semin Liver Dis* **20**, 293–305 (2000).
284. Hofmann, A. F. Bile Acids: The Good, the Bad, and the Ugly. *News Physiol Sci* **14**, 24–29 (1999).
285. Charach, G. *et al.* The association of bile acid excretion and atherosclerotic coronary artery disease. *Therap Adv Gastroenterol* **4**, 95–101 (2011).
286. White, R., Giordano, S. & Datta, G. Role of HDL-Associated Proteins and Lipids in the Regulation of Inflammation. in *Advances in Lipoprotein Research* (ed. Isbir, T.) (InTech, 2017). doi:10.5772/67141.
287. Marques, L. R. *et al.* Reverse Cholesterol Transport: Molecular Mechanisms and the Non-medical Approach to Enhance HDL Cholesterol. *Front. Physiol.* **9**, 526 (2018).
288. Uribe, B., Benito-Vicente, A., Martin, C., Blanco-Vaca, F. & Rotllan, N. (r)HDL in theranostics: how do we apply HDL's biology for precision medicine in atherosclerosis management? *Biomater. Sci.* **9**, 3185–3208 (2021).

289. Kontush, A., Lhomme, M. & Chapman, M. J. Unraveling the complexities of the HDL lipidome. *Journal of Lipid Research* **54**, 2950–2963 (2013).
290. Asztalos, B. F., Sloop, C. H., Wong, L. & Roheim, P. S. Two-dimensional electrophoresis of plasma lipoproteins: Recognition of new apo A-I-containing subpopulations. *Biochimica et Biophysica Acta (BBA) - Lipids and Lipid Metabolism* **1169**, 291–300 (1993).
291. Chistiakov, D. A., Orekhov, A. N. & Bobryshev, Y. V. ApoA1 and ApoA1-specific self-antibodies in cardiovascular disease. *Lab Invest* **96**, 708–718 (2016).
292. Puppione, D. L. *et al.* Mass spectral analyses of the two major apolipoproteins of great ape high density lipoproteins. *Comp Biochem Physiol Part D Genomics Proteomics* **4**, 305–309 (2009).
293. *High Density Lipoproteins: From Biological Understanding to Clinical Exploitation*. vol. 224 (Springer International Publishing, 2015).
294. Shao, B. & Heinecke, J. W. Quantifying HDL proteins by mass spectrometry: how many proteins are there and what are their functions? *Expert Review of Proteomics* **15**, 31–40 (2018).
295. Kontush, A. *et al.* Structure of HDL: particle subclasses and molecular components. *Handb Exp Pharmacol* **224**, 3–51 (2015).
296. Lhomme, M. C., Camont, L., Chapman, M. J. & Kontush, A. Lipidomics in Lipoprotein Biology. in *Lipidomics* (ed. Ekoos, K.) 197–217 (Wiley-VCH Verlag GmbH & Co. KGaA, 2012). doi:10.1002/9783527655946.ch10.
297. Wiesner, P., Leidl, K., Boettcher, A., Schmitz, G. & Liebisch, G. Lipid profiling of FPLC-separated lipoprotein fractions by electrospray ionization tandem mass spectrometry. *J Lipid Res* **50**, 574–585 (2009).
298. Kontush, A. *et al.* Preferential Sphingosine-1-Phosphate Enrichment and Sphingomyelin Depletion Are Key Features of Small Dense HDL3 Particles: Relevance to Antiapoptotic and Antioxidative Activities. *ATVB* **27**, 1843–1849 (2007).
299. Camont, L., Chapman, M. J. & Kontush, A. Biological activities of HDL subpopulations and their relevance to cardiovascular disease. *Trends Mol Med* **17**, 594–603 (2011).
300. *High-density lipoproteins: structure, metabolism, function, and therapeutics*. (John Wiley & Sons, Inc, 2012).

301. Ståhlman, M. *et al.* Dyslipidemia, but not hyperglycemia and insulin resistance, is associated with marked alterations in the HDL lipidome in type 2 diabetic subjects in the DIWA cohort: impact on small HDL particles. *Biochim Biophys Acta* **1831**, 1609–1617 (2013).
302. Camont, L. *et al.* Small, dense high-density lipoprotein-3 particles are enriched in negatively charged phospholipids: relevance to cellular cholesterol efflux, antioxidative, antithrombotic, anti-inflammatory, and antiapoptotic functionalities. *Arterioscler Thromb Vasc Biol* **33**, 2715–2723 (2013).
303. Asztalos, B. F., Tani, M. & Schaefer, E. J. Metabolic and functional relevance of HDL subspecies. *Curr Opin Lipidol* **22**, 176–185 (2011).
304. Brooks-Wilson, A. *et al.* Mutations in ABC1 in Tangier disease and familial high-density lipoprotein deficiency. *Nat Genet* **22**, 336–345 (1999).
305. Rust, S. *et al.* Tangier disease is caused by mutations in the gene encoding ATP-binding cassette transporter 1. *Nat Genet* **22**, 352–355 (1999).
306. Bodzioch, M. *et al.* The gene encoding ATP-binding cassette transporter 1 is mutated in Tangier disease. *Nat Genet* **22**, 347–351 (1999).
307. Fitzgerald, M. L., Mujawar, Z. & Tamehiro, N. ABC transporters, atherosclerosis and inflammation. *Atherosclerosis* **211**, 361–370 (2010).
308. Schaefer, E. J. Clinical, biochemical, and genetic features in familial disorders of high density lipoprotein deficiency. *Arteriosclerosis* **4**, 303–322 (1984).
309. Dean, M., Hamon, Y. & Chimini, G. The human ATP-binding cassette (ABC) transporter superfamily. *Journal of Lipid Research* **42**, 1007–1017 (2001).
310. Vasiliou, V., Vasiliou, K. & Nebert, D. W. Human ATP-binding cassette (ABC) transporter family. *Hum Genomics* **3**, 281–290 (2009).
311. Oram, J. F. & Lawn, R. M. ABCA1: the gatekeeper for eliminating excess tissue cholesterol. *Journal of Lipid Research* **42**, 1173–1179 (2001).
312. Smith, J. D. *et al.* ABCA1 mediates concurrent cholesterol and phospholipid efflux to apolipoprotein A-I. *Journal of Lipid Research* **45**, 635–644 (2004).
313. Lee, J.-Y. & Parks, J. S. ATP-binding cassette transporter AI and its role in HDL formation. *Curr Opin Lipidol* **16**, 19–25 (2005).

314. Fitzgerald, M. L. *et al.* Naturally occurring mutations in the largest extracellular loops of ABCA1 can disrupt its direct interaction with apolipoprotein A-I. *J Biol Chem* **277**, 33178–33187 (2002).
315. Mukhamedova, N., Fu, Y., Bukrinsky, M., Remaley, A. T. & Sviridov, D. The role of different regions of ATP-binding cassette transporter A1 in cholesterol efflux. *Biochemistry* **46**, 9388–9398 (2007).
316. Singaraja, R. R. *et al.* Palmitoylation of ATP-binding cassette transporter A1 is essential for its trafficking and function. *Circ Res* **105**, 138–147 (2009).
317. Denis, M. *et al.* Characterization of oligomeric human ATP binding cassette transporter A1. Potential implications for determining the structure of nascent high density lipoprotein particles. *J Biol Chem* **279**, 41529–41536 (2004).
318. Trompier, D. *et al.* Transition from dimers to higher oligomeric forms occurs during the ATPase cycle of the ABCA1 transporter. *J Biol Chem* **281**, 20283–20290 (2006).
319. Nagata, K. O., Nakada, C., Kasai, R. S., Kusumi, A. & Ueda, K. ABCA1 dimer-monomer interconversion during HDL generation revealed by single-molecule imaging. *Proc Natl Acad Sci U S A* **110**, 5034–5039 (2013).
320. Martinez, L. O., Agerholm-Larsen, B., Wang, N., Chen, W. & Tall, A. R. Phosphorylation of a pest sequence in ABCA1 promotes calpain degradation and is reversed by ApoA-I. *J Biol Chem* **278**, 37368–37374 (2003).
321. Vaughan, A. M. & Oram, J. F. ABCA1 redistributes membrane cholesterol independent of apolipoprotein interactions. *J Lipid Res* **44**, 1373–1380 (2003).
322. Prock, E., O'Mara, M. L., Bennett, W. F. D., Tielemans, D. P. & Gaudet, R. The mechanism of ABC transporters: general lessons from structural and functional studies of an antigenic peptide transporter. *FASEB J.* **23**, 1287–1302 (2009).
323. Quazi, F. & Molday, R. S. Differential phospholipid substrates and directional transport by ATP-binding cassette proteins ABCA1, ABCA7, and ABCA4 and disease-causing mutants. *J Biol Chem* **288**, 34414–34426 (2013).
324. Gogonea, V. Structural Insights into High Density Lipoprotein: Old Models and New Facts. *Front. Pharmacol.* **6**, (2016).

325. Fielding, P. E., Nagao, K., Hakamata, H., Chimini, G. & Fielding, C. J. A Two-Step Mechanism for Free Cholesterol and Phospholipid Efflux from Human Vascular Cells to Apolipoprotein A-1. *Biochemistry* **39**, 14113–14120 (2000).
326. Hassan, H. H. *et al.* Identification of an ABCA1-dependent phospholipid-rich plasma membrane apolipoprotein A-I binding site for nascent HDL formation: implications for current models of HDL biogenesis. *Journal of Lipid Research* **48**, 2428–2442 (2007).
327. Vedhachalam, C. *et al.* ABCA1-Induced Cell Surface Binding Sites for ApoA-I. *ATVB* **27**, 1603–1609 (2007).
328. Segrest, J. P. *et al.* Surface Density-Induced Pleating of a Lipid Monolayer Drives Nascent High-Density Lipoprotein Assembly. *Structure* **23**, 1214–1226 (2015).
329. Lin, G. & Oram, J. F. Apolipoprotein binding to protruding membrane domains during removal of excess cellular cholesterol. *Atherosclerosis* **149**, 359–370 (2000).
330. Wang, S., Gulshan, K., Brubaker, G., Hazen, S. L. & Smith, J. D. ABCA1 mediates unfolding of apolipoprotein AI N terminus on the cell surface before lipidation and release of nascent high-density lipoprotein. *Arterioscler Thromb Vasc Biol* **33**, 1197–1205 (2013).
331. Tontonoz, P. Transcriptional and posttranscriptional control of cholesterol homeostasis by liver X receptors. *Cold Spring Harb Symp Quant Biol* **76**, 129–137 (2011).
332. Venkateswaran, A. *et al.* Control of cellular cholesterol efflux by the nuclear oxysterol receptor LXR alpha. *Proc Natl Acad Sci U S A* **97**, 12097–12102 (2000).
333. Willy, P. J. *et al.* LXR, a nuclear receptor that defines a distinct retinoid response pathway. *Genes & Development* **9**, 1033–1045 (1995).
334. Zhu, R., Ou, Z., Ruan, X. & Gong, J. Role of liver X receptors in cholesterol efflux and inflammatory signaling (Review). *Molecular Medicine Reports* **5**, 895–900 (2012).
335. Luo, Y. & Tall, A. R. Sterol upregulation of human CETP expression in vitro and in transgenic mice by an LXR element. *J Clin Invest* **105**, 513–520 (2000).

336. Malerød, L., Juvet, L. K., Hanssen-Bauer, A., Eskild, W. & Berg, T. Oxysterol-activated LX $\alpha$ /RXR induces hSR-BI-promoter activity in hepatoma cells and preadipocytes. *Biochemical and Biophysical Research Communications* **299**, 916–923 (2002).
337. Rong, S. *et al.* Expression of SREBP-1c Requires SREBP-2-mediated Generation of a Sterol Ligand for LXR in Livers of Mice. *Elife* **6**, e25015 (2017).
338. Duong, P. T., Weibel, G. L., Lund-Katz, S., Rothblat, G. H. & Phillips, M. C. Characterization and properties of pre beta-HDL particles formed by ABCA1-mediated cellular lipid efflux to apoA-I. *J Lipid Res* **49**, 1006–1014 (2008).
339. Rye, K.-A. & Barter, P. J. Formation and Metabolism of Prebeta-Migrating, Lipid-Poor Apolipoprotein A-I. *ATVB* **24**, 421–428 (2004).
340. von Eckardstein, A., Huang, Y. & Assmann, G. Physiological role and clinical relevance of high-density lipoprotein subclasses. *Curr Opin Lipidol* **5**, 404–416 (1994).
341. Wang, X. & Rader, D. J. Molecular regulation of macrophage reverse cholesterol transport. *Curr Opin Cardiol* **22**, 368–372 (2007).
342. Van Eck, M. *et al.* Macrophage ATP-binding cassette transporter A1 overexpression inhibits atherosclerotic lesion progression in low-density lipoprotein receptor knockout mice. *Arterioscler Thromb Vasc Biol* **26**, 929–934 (2006).
343. Adorni, M. P. *et al.* The roles of different pathways in the release of cholesterol from macrophages. *J Lipid Res* **48**, 2453–2462 (2007).
344. Brewer, H. B., Lux, S. E., Ronan, R. & John, K. M. Amino acid sequence of human apoLp-Gln-II (apoA-II), an apolipoprotein isolated from the high-density lipoprotein complex. *Proc Natl Acad Sci U S A* **69**, 1304–1308 (1972).
345. Segrest, J. P., Jackson, R. L., Morrisett, J. D. & Gotto, A. M. A molecular theory of lipid-protein interactions in the plasma lipoproteins. *FEBS Lett* **38**, 247–258 (1974).
346. McLachlan, A. D. Repeated helical pattern in apolipoprotein-A-I. *Nature* **267**, 465–466 (1977).
347. Li, W. H., Tanimura, M., Luo, C. C., Datta, S. & Chan, L. The apolipoprotein multigene family: biosynthesis, structure, structure-function relationships, and evolution. *J Lipid Res* **29**, 245–271 (1988).

348. Segrest, J. P. *et al.* The amphipathic helix in the exchangeable apolipoproteins: a review of secondary structure and function. *J Lipid Res* **33**, 141–166 (1992).
349. Marcel, Y. L. *et al.* The epitopes of apolipoprotein A-I define distinct structural domains including a mobile middle region. *Journal of Biological Chemistry* **266**, 3644–3653 (1991).
350. Meng, Q. H., Calabresi, L., Fruchart, J. C. & Marcel, Y. L. Apolipoprotein A-I domains involved in the activation of lecithin:cholesterol acyltransferase. Importance of the central domain. *J Biol Chem* **268**, 16966–16973 (1993).
351. Sparks, D. L., Lund-Katz, S. & Phillips, M. C. The charge and structural stability of apolipoprotein A-I in discoidal and spherical recombinant high density lipoprotein particles. *Journal of Biological Chemistry* **267**, 25839–25847 (1992).
352. Phillips, M. C. New insights into the determination of HDL structure by apolipoproteins. *Journal of Lipid Research* **54**, 2034–2048 (2013).
353. Borhani, D. W., Rogers, D. P., Engler, J. A. & Brouillette, C. G. Crystal structure of truncated human apolipoprotein A-I suggests a lipid-bound conformation. *Proceedings of the National Academy of Sciences* **94**, 12291–12296 (1997).
354. Gursky, O. & Atkinson, D. Thermal unfolding of human high-density apolipoprotein A-1: implications for a lipid-free molten globular state. *Proc Natl Acad Sci U S A* **93**, 2991–2995 (1996).
355. Barbeau, D. L., Jonas, A., Teng, T. & Scanu, A. M. Asymmetry of apolipoprotein A-I in solution as assessed from ultracentrifugal, viscometric, and fluorescence polarization studies. *Biochemistry* **18**, 362–369 (1979).
356. Narayanaswami, V., Kiss, R. S. & Weers, P. M. M. The helix bundle: a reversible lipid binding motif. *Comp Biochem Physiol A Mol Integr Physiol* **155**, 123–133 (2010).
357. Saito, H. *et al.* Domain structure and lipid interaction in human apolipoproteins A-I and E, a general model. *J Biol Chem* **278**, 23227–23232 (2003).
358. Lund-Katz, S. *et al.* Surface plasmon resonance analysis of the mechanism of binding of apoA-I to high density lipoprotein particles. *J Lipid Res* **51**, 606–617 (2010).

359. Davidson, W. S. & Thompson, T. B. The structure of apolipoprotein A-I in high density lipoproteins. *J Biol Chem* **282**, 22249–22253 (2007).
360. Segrest, J. P. *et al.* A Detailed Molecular Belt Model for Apolipoprotein A-I in Discoidal High Density Lipoprotein. *Journal of Biological Chemistry* **274**, 31755–31758 (1999).
361. Sevugan Chetty, P. *et al.* Apolipoprotein A-I helical structure and stability in discoidal high-density lipoprotein (HDL) particles by hydrogen exchange and mass spectrometry. *Proceedings of the National Academy of Sciences* **109**, 11687–11692 (2012).
362. Zannis, V. I. *et al.* HDL biogenesis, remodeling, and catabolism. *Handb Exp Pharmacol* **224**, 53–111 (2015).
363. Ambros, V. The functions of animal microRNAs. *Nature* **431**, 350–355 (2004).
364. Bartel, D. P. MicroRNAs: genomics, biogenesis, mechanism, and function. *Cell* **116**, 281–297 (2004).
365. Bartel, D. P. MicroRNAs: target recognition and regulatory functions. *Cell* **136**, 215–233 (2009).
366. Filipowicz, W., Bhattacharyya, S. N. & Sonenberg, N. Mechanisms of post-transcriptional regulation by microRNAs: are the answers in sight? *Nat Rev Genet* **9**, 102–114 (2008).
367. Alles, J. *et al.* An estimate of the total number of true human miRNAs. *Nucleic Acids Research* **47**, 3353–3364 (2019).
368. Canfrán-Duque, A., Ramírez, C. M., Goedeke, L., Lin, C.-S. & Fernández-Hernando, C. microRNAs and HDL life cycle. *Cardiovasc Res* **103**, 414–422 (2014).
369. Kim, Y.-K. & Kim, V. N. Processing of intronic microRNAs. *EMBO J* **26**, 775–783 (2007).
370. The FANTOM Consortium *et al.* An integrated expression atlas of miRNAs and their promoters in human and mouse. *Nat Biotechnol* **35**, 872–878 (2017).
371. Denli, A. M., Tops, B. B. J., Plasterk, R. H. A., Ketting, R. F. & Hannon, G. J. Processing of primary microRNAs by the Microprocessor complex. *Nature* **432**, 231–235 (2004).

372. Han, J. The Drosha-DGCR8 complex in primary microRNA processing. *Genes & Development* **18**, 3016–3027 (2004).
373. Okada, C. *et al.* A High-Resolution Structure of the Pre-microRNA Nuclear Export Machinery. *Science* **326**, 1275–1279 (2009).
374. Zhang, H., Kolb, F. A., Jaskiewicz, L., Westhof, E. & Filipowicz, W. Single Processing Center Models for Human Dicer and Bacterial RNase III. *Cell* **118**, 57–68 (2004).
375. O'Brien, J., Hayder, H., Zayed, Y. & Peng, C. Overview of MicroRNA Biogenesis, Mechanisms of Actions, and Circulation. *Front. Endocrinol.* **9**, 402 (2018).
376. Miyoshi, K., Miyoshi, T. & Siomi, H. Many ways to generate microRNA-like small RNAs: non-canonical pathways for microRNA production. *Mol Genet Genomics* **284**, 95–103 (2010).
377. Jo, M. H. *et al.* Human Argonaute 2 Has Diverse Reaction Pathways on Target RNAs. *Molecular Cell* **59**, 117–124 (2015).
378. Jonas, S. & Izaurralde, E. Towards a molecular understanding of microRNA-mediated gene silencing. *Nat Rev Genet* **16**, 421–433 (2015).
379. Bofill-De Ros, X., Rovira-Rigau, M. & Fillat, C. Implications of MicroRNAs in Oncolytic Virotherapy. *Front. Oncol.* **7**, 142 (2017).
380. Rayner, K. J. & Moore, K. J. MicroRNA Control of High-Density Lipoprotein Metabolism and Function. *Circ Res* **114**, 183–192 (2014).
381. Michell, D. L. & Vickers, K. C. Lipoprotein carriers of microRNAs. *Biochim Biophys Acta* **1861**, 2069–2074 (2016).
382. Vickers, K. C., Palmisano, B. T., Shoucri, B. M., Shamburek, R. D. & Remaley, A. T. MicroRNAs are transported in plasma and delivered to recipient cells by high-density lipoproteins. *Nat Cell Biol* **13**, 423–433 (2011).
383. Wagner, J. *et al.* Characterization of levels and cellular transfer of circulating lipoprotein-bound microRNAs. *Arterioscler Thromb Vasc Biol* **33**, 1392–1400 (2013).
384. Kratzer, A., Giral, H. & Landmesser, U. High-density lipoproteins as modulators of endothelial cell functions: alterations in patients with coronary artery disease. *Cardiovasc Res* **103**, 350–361 (2014).

385. Tabet, F. *et al.* HDL-transferred microRNA-223 regulates ICAM-1 expression in endothelial cells. *Nat Commun* **5**, 3292 (2014).
386. Sedgeman, L. R. *et al.* Beta cell secretion of miR-375 to HDL is inversely associated with insulin secretion. *Sci Rep* **9**, 3803 (2019).
387. Cuesta Torres, L. F. *et al.* High-density lipoproteins induce miR-223-3p biogenesis and export from myeloid cells: Role of scavenger receptor BI-mediated lipid transfer. *Atherosclerosis* **286**, 20–29 (2019).
388. Veremeyko, T. *et al.* Neuronal extracellular microRNAs miR-124 and miR-9 mediate cell-cell communication between neurons and microglia. *J Neurosci Res* **97**, 162–184 (2019).
389. Vickers, K. C. & Michell, D. L. HDL-small RNA Export, Transport, and Functional Delivery in Atherosclerosis. *Curr Atheroscler Rep* **23**, 38 (2021).
390. Ben-Aicha Gonzalez, S. *et al.* Hyperlipidemia modifies HDL-mirna profile and enhances endothelial delivery of HDL- MIR126-3P/-5P through a SRB-1-dependent mechanism. *Atherosclerosis* **275**, e20–e21 (2018).
391. Hergenreider, E. *et al.* Atheroprotective communication between endothelial cells and smooth muscle cells through miRNAs. *Nat Cell Biol* **14**, 249–256 (2012).
392. Ben-Aicha, S. *et al.* High-density lipoprotein remodelled in hypercholesterolaemic blood induce epigenetically driven down-regulation of endothelial HIF-1 $\alpha$  expression in a preclinical animal model. *Cardiovasc Res* **116**, 1288–1299 (2020).
393. Devaux, Y. *et al.* Use of circulating microRNAs to diagnose acute myocardial infarction. *Clin Chem* **58**, 559–567 (2012).
394. Fiedler, J. & Thum, T. MicroRNAs in myocardial infarction. *Arterioscler Thromb Vasc Biol* **33**, 201–205 (2013).
395. Niculescu, L. S. *et al.* MiR-486 and miR-92a Identified in Circulating HDL Discriminate between Stable and Vulnerable Coronary Artery Disease Patients. *PLoS One* **10**, e0140958 (2015).
396. Eberlé, D., Hegarty, B., Bossard, P., Ferré, P. & Foufelle, F. SREBP transcription factors: master regulators of lipid homeostasis. *Biochimie* **86**, 839–848 (2004).

397. Horton, J. D., Goldstein, J. L. & Brown, M. S. SREBPs: activators of the complete program of cholesterol and fatty acid synthesis in the liver. *J Clin Invest* **109**, 1125–1131 (2002).
398. Hua, X., Wu, J., Goldstein, J. L., Brown, M. S. & Hobbs, H. H. Structure of the human gene encoding sterol regulatory element binding protein-1 (SREBF1) and localization of SREBF1 and SREBF2 to chromosomes 17p11.2 and 22q13. *Genomics* **25**, 667–673 (1995).
399. Miserez, A. R. *et al.* Sterol-regulatory element-binding protein (SREBP)-2 contributes to polygenic hypercholesterolaemia. *Atherosclerosis* **164**, 15–26 (2002).
400. Madison, B. B. Srebp2: A master regulator of sterol and fatty acid synthesis. *Journal of Lipid Research* **57**, 333–335 (2016).
401. Najafi-Shoushtari, S. H. *et al.* MicroRNA-33 and the SREBP host genes cooperate to control cholesterol homeostasis. *Science* **328**, 1566–1569 (2010).
402. Rottiers, V. & Näär, A. M. MicroRNAs in metabolism and metabolic disorders. *Nat Rev Mol Cell Biol* **13**, 239–250 (2012).
403. Gerin, I. *et al.* Expression of miR-33 from an SREBP2 intron inhibits cholesterol export and fatty acid oxidation. *J Biol Chem* **285**, 33652–33661 (2010).
404. Rayner, K. J. *et al.* MiR-33 Contributes to the Regulation of Cholesterol Homeostasis. *Science* **328**, 1570–1573 (2010).
405. Price, N. L. *et al.* Specific Disruption of Abca1 Targeting Largely Mimics the Effects of miR-33 Knockout on Macrophage Cholesterol Efflux and Atherosclerotic Plaque Development. *Circ Res* **124**, 874–880 (2019).
406. Price, N. L., Goedeke, L., Suárez, Y. & Fernández-Hernando, C. miR-33 in cardiometabolic diseases: lessons learned from novel animal models and approaches. *EMBO Mol Med* **13**, (2021).
407. Marquart, T. J., Allen, R. M., Ory, D. S. & Baldan, A. miR-33 links SREBP-2 induction to repression of sterol transporters. *Proceedings of the National Academy of Sciences* **107**, 12228–12232 (2010).
408. Horie, T. *et al.* MicroRNA-33 encoded by an intron of sterol regulatory element-binding protein 2 (Srebp2) regulates HDL in vivo. *Proc Natl Acad Sci U S A* **107**, 17321–17326 (2010).

409. Allen, R. M. *et al.* miR-33 controls the expression of biliary transporters, and mediates statin- and diet-induced hepatotoxicity. *EMBO Mol Med* **4**, 882–895 (2012).
410. Price, N. L. *et al.* Genetic Dissection of the Impact of miR-33a and miR-33b during the Progression of Atherosclerosis. *Cell Reports* **21**, 1317–1330 (2017).
411. Rayner, K. J. *et al.* Antagonism of miR-33 in mice promotes reverse cholesterol transport and regression of atherosclerosis. *J Clin Invest* **121**, 2921–2931 (2011).
412. Rotllan, N., Ramírez, C. M., Aryal, B., Esau, C. C. & Fernández-Hernando, C. Therapeutic silencing of microRNA-33 inhibits the progression of atherosclerosis in Ldlr<sup>-/-</sup> mice--brief report. *Arterioscler Thromb Vasc Biol* **33**, 1973–1977 (2013).
413. Rayner, K. J. *et al.* Inhibition of miR-33a/b in non-human primates raises plasma HDL and lowers VLDL triglycerides. *Nature* **478**, 404–407 (2011).
414. Rottiers, V. *et al.* Pharmacological inhibition of a microRNA family in nonhuman primates by a seed-targeting 8-mer antimicroRNA. *Sci Transl Med* **5**, 212ra162 (2013).
415. Price, N. L. *et al.* Loss of hepatic miR-33 improves metabolic homeostasis and liver function without altering body weight or atherosclerosis. *Proc Natl Acad Sci U S A* **118**, e2006478118 (2021).
416. Ouimet, M. *et al.* MicroRNA-33-dependent regulation of macrophage metabolism directs immune cell polarization in atherosclerosis. *J Clin Invest* **125**, 4334–4348 (2015).
417. Mineo, C., Deguchi, H., Griffin, J. H. & Shaul, P. W. Endothelial and Antithrombotic Actions of HDL. *Circulation Research* **98**, 1352–1364 (2006).
418. Brites, F., Martin, M., Guillas, I. & Kontush, A. Antioxidative activity of high-density lipoprotein (HDL): Mechanistic insights into potential clinical benefit. *BBA Clinical* **8**, 66–77 (2017).
419. Barter, P. J. *et al.* Antiinflammatory properties of HDL. *Circ Res* **95**, 764–772 (2004).
420. Gordon, T., Castelli, W. P., Hjortland, M. C., Kannel, W. B. & Dawber, T. R. High density lipoprotein as a protective factor against coronary heart disease. The Framingham Study. *Am J Med* **62**, 707–714 (1977).

421. Castelli, W. P. *et al.* Incidence of coronary heart disease and lipoprotein cholesterol levels. The Framingham Study. *JAMA* **256**, 2835–2838 (1986).
422. Frikke-Schmidt, R. *et al.* Association of loss-of-function mutations in the ABCA1 gene with high-density lipoprotein cholesterol levels and risk of ischemic heart disease. *JAMA* **299**, 2524–2532 (2008).
423. Zanoni, P. *et al.* Rare variant in scavenger receptor BI raises HDL cholesterol and increases risk of coronary heart disease. *Science* **351**, 1166–1171 (2016).
424. Voight, B. F. *et al.* Plasma HDL cholesterol and risk of myocardial infarction: a mendelian randomisation study. *The Lancet* **380**, 572–580 (2012).
425. Willer, C. J. *et al.* Discovery and refinement of loci associated with lipid levels. *Nat Genet* **45**, 1274–1283 (2013).
426. Rader, D. J. & Hovingh, G. K. HDL and cardiovascular disease. *The Lancet* **384**, 618–625 (2014).
427. Matz, C. E. & Jonas, A. Micellar complexes of human apolipoprotein A-I with phosphatidylcholines and cholesterol prepared from cholate-lipid dispersions. *J. Biol. Chem.* **257**, 4535–4540 (1982).
428. Schwendeman, A. *et al.* The effect of phospholipid composition of reconstituted HDL on its cholesterol efflux and anti-inflammatory properties. *Journal of Lipid Research* **56**, 1727–1737 (2015).
429. Kim, Y. *et al.* Single Step Reconstitution of Multifunctional High-Density Lipoprotein-Derived Nanomaterials Using Microfluidics. *ACS Nano* **7**, 9975–9983 (2013).
430. Kempen, H. J. *et al.* Incubation of MDCO-216 (ApoA-IMilano/POPC) with Human Serum Potentiates ABCA1-Mediated Cholesterol Efflux Capacity, Generates New Prebeta-1 HDL, and Causes an Increase in HDL Size. *Journal of Lipids* **2014**, 1–8 (2014).
431. Lerch, P. G., Förtsch, V., Hodler, G. & Bolli, R. Production and characterization of a reconstituted high density lipoprotein for therapeutic applications. *Vox Sang* **71**, 155–164 (1996).
432. Easton, R. *et al.* A multiple ascending dose study of CSL112, an infused formulation of ApoA-I. *J Clin Pharmacol* **54**, 301–310 (2014).

433. Tardif, J.-C. *et al.* Effects of the high-density lipoprotein mimetic agent CER-001 on coronary atherosclerosis in patients with acute coronary syndromes: a randomized trial. *Eur Heart J* **35**, 3277–3286 (2014).
434. Patel, H. *et al.* Characterization of apolipoprotein A-I peptide phospholipid interaction and its effect on HDL nanodisc assembly. *Int J Nanomedicine* **14**, 3069–3086 (2019).
435. Massey, J. B. & Pownall, H. J. Cholesterol is a determinant of the structures of discoidal high density lipoproteins formed by the solubilization of phospholipid membranes by apolipoprotein A-I. *Biochim Biophys Acta* **1781**, 245–253 (2008).
436. Duivenvoorden, R. *et al.* A statin-loaded reconstituted high-density lipoprotein nanoparticle inhibits atherosclerotic plaque inflammation. *Nat Commun* **5**, 3065 (2014).
437. Jiang, C. *et al.* Rational Design of Lovastatin-Loaded Spherical Reconstituted High Density Lipoprotein for Efficient and Safe Anti-Atherosclerotic Therapy. *Mol Pharm* **16**, 3284–3291 (2019).
438. Tang, J. *et al.* Immune cell screening of a nanoparticle library improves atherosclerosis therapy. *Proc Natl Acad Sci USA* **113**, E6731–E6740 (2016).
439. Guo, Y. *et al.* Synthetic High-Density Lipoprotein-Mediated Targeted Delivery of Liver X Receptors Agonist Promotes Atherosclerosis Regression. *EBioMedicine* **28**, 225–233 (2018).
440. Brulhart-Meynet, M.-C. *et al.* Improving Reconstituted HDL Composition for Efficient Post-Ischemic Reduction of Ischemia Reperfusion Injury. *PLoS ONE* **10**, e0119664 (2015).
441. Lameijer, M. *et al.* Efficacy and safety assessment of a TRAF6-targeted nanoimmunotherapy in atherosclerotic mice and non-human primates. *Nat Biomed Eng* **2**, 279–292 (2018).
442. Wolfrum, C. *et al.* Mechanisms and optimization of in vivo delivery of lipophilic siRNAs. *Nat Biotechnol* **25**, 1149–1157 (2007).
443. Nakayama, T. *et al.* Harnessing a Physiologic Mechanism for siRNA Delivery With Mimetic Lipoprotein Particles. *Molecular Therapy* **20**, 1582–1589 (2012).

444. Zhao, Y. *et al.* Co-delivery of LOX-1 siRNA and statin to endothelial cells and macrophages in the atherosclerotic lesions by a dual-targeting core-shell nanoplatform: A dual cell therapy to regress plaques. *J Control Release* **283**, 241–260 (2018).
445. Nissen, S. E. *et al.* Effect of Recombinant ApoA-I Milano on Coronary Atherosclerosis in Patients With Acute Coronary Syndromes: A Randomized Controlled Trial. *JAMA* **290**, 2292 (2003).
446. Tardif, J.-C. Effects of Reconstituted High-Density Lipoprotein Infusions on Coronary AtherosclerosisA Randomized Controlled Trial. *JAMA* **297**, 1675 (2007).
447. Newton, R. S. & Krause, B. R. HDL therapy for the acute treatment of atherosclerosis. *Atherosclerosis Supplements* **3**, 31–38 (2002).
448. Badimon, J. J., Badimon, L. & Fuster, V. Regression of atherosclerotic lesions by high density lipoprotein plasma fraction in the cholesterol-fed rabbit. *J. Clin. Invest.* **85**, 1234–1241 (1990).
449. Eriksson, M., Carlson, L. A., Miettinen, T. A. & Angelin, B. Stimulation of Fecal Steroid Excretion After Infusion of Recombinant Proapolipoprotein A-I: Potential Reverse Cholesterol Transport in Humans. *Circulation* **100**, 594–598 (1999).
450. Nanjee, M. N., Doran, J. E., Lerch, P. G. & Miller, N. E. Acute effects of intravenous infusion of ApoA1/phosphatidylcholine discs on plasma lipoproteins in humans. *Arterioscler Thromb Vasc Biol* **19**, 979–989 (1999).
451. Marchesi, M., Booth, E. A., Davis, T., Bisgaier, C. L. & Lucchesi, B. R. Apolipoprotein A-IMilano and 1-palmitoyl-2-oleoyl phosphatidylcholine complex (ETC-216) protects the in vivo rabbit heart from regional ischemia-reperfusion injury. *J Pharmacol Exp Ther* **311**, 1023–1031 (2004).
452. Hippalgaonkar, K., Majumdar, S. & Kansara, V. Injectable Lipid Emulsions—Advancements, Opportunities and Challenges. *AAPS PharmSciTech* **11**, 1526–1540 (2010).
453. Binderup, T. *et al.* Imaging-assisted nanoimmunotherapy for atherosclerosis in multiple species. *Sci Transl Med* **11**, eaaw7736 (2019).
454. Cormode, D. P. *et al.* Nanocrystal Core High-Density Lipoproteins: A Multimodality Contrast Agent Platform. *Nano Lett.* **8**, 3715–3723 (2008).

455. Libby, P. Changing concepts of atherogenesis. *J Intern Med* **247**, 349–358 (2000).
456. Gordon, D. J. *et al.* High-density lipoprotein cholesterol and cardiovascular disease. Four prospective American studies. *Circulation* **79**, 8–15 (1989).
457. Barter, P. *et al.* HDL Cholesterol, Very Low Levels of LDL Cholesterol, and Cardiovascular Events. *N Engl J Med* **357**, 1301–1310 (2007).
458. Chyu, K.-Y. & Shah, P. K. HDL/ApoA-1 infusion and ApoA-1 gene therapy in atherosclerosis. *Front. Pharmacol.* **6**, (2015).
459. Michael Gibson, C. *et al.* Safety and Tolerability of CSL112, a Reconstituted, Infusible, Plasma-Derived Apolipoprotein A-I, After Acute Myocardial Infarction: The AEGIS-I Trial (ApoA-I Event Reducing in Ischemic Syndromes I). *Circulation* **134**, 1918–1930 (2016).
460. Zhao, X.-Q. & Brown, B. G. ApoA-1 Milano/Phospholipid Complex. *Journal of the American College of Cardiology* **51**, 1110–1111 (2008).
461. Kallend, D. G. *et al.* A single infusion of MDCO-216 (ApoA-1 Milano/POPC) increases ABCA1-mediated cholesterol efflux and pre-beta 1 HDL in healthy volunteers and patients with stable coronary artery disease. *Eur Heart J Cardiovasc Pharmacother* **2**, 23–29 (2016).
462. Sirtori, C. R. *et al.* Cardiovascular Status of Carriers of the Apolipoprotein A-I Milano Mutant: The Limone sul Garda Study. *Circulation* **103**, 1949–1954 (2001).
463. Franceschini, G. *et al.* Relationship of the phenotypic expression of the A-IMilano apoprotein with plasma lipid and lipoprotein patterns. *Atherosclerosis* **58**, 159–174 (1985).
464. Nicholls, S. J. *et al.* Effect of Infusion of High-Density Lipoprotein Mimetic Containing Recombinant Apolipoprotein A-I Milano on Coronary Disease in Patients With an Acute Coronary Syndrome in the MILANO-PILOT Trial: A Randomized Clinical Trial. *JAMA Cardiol* **3**, 806 (2018).
465. Tardy, C. *et al.* HDL and CER-001 Inverse-Dose Dependent Inhibition of Atherosclerotic Plaque Formation in apoE-/ - Mice: Evidence of ABCA1 Down-Regulation. *PLoS ONE* **10**, e0137584 (2015).
466. Stukas, S. *et al.* Intravenously Injected Human Apolipoprotein A-I Rapidly Enters the Central Nervous System via the Choroid Plexus. *JAHA* **3**, (2014).

467. Bradford, M. M. A rapid and sensitive method for the quantitation of microgram quantities of protein utilizing the principle of protein-dye binding. *Anal Biochem* **72**, 248–254 (1976).
468. Mouritsen, O. G. Lipids, curvature, and nano-medicine. *Eur. J. Lipid Sci. Technol.* **113**, 1174–1187 (2011).
469. Urbani, A. & Warne, T. A colorimetric determination for glycosidic and bile salt-based detergents: applications in membrane protein research. *Analytical Biochemistry* **336**, 117–124 (2005).
470. Kelly, S. M., Jess, T. J. & Price, N. C. How to study proteins by circular dichroism. *Biochimica et Biophysica Acta (BBA) - Proteins and Proteomics* **1751**, 119–139 (2005).
471. Zhang, H., Wu, Q. & Berezin, M. Y. Fluorescence anisotropy (polarization): from drug screening to precision medicine. *Expert Opin Drug Discov* **10**, 1145–1161 (2015).
472. Van Blitterswijk, W. J., Van Hoeven, R. P. & Van der Meer, B. W. Lipid structural order parameters (reciprocal of fluidity) in biomembranes derived from steady-state fluorescence polarization measurements. *Biochim Biophys Acta* **644**, 323–332 (1981).
473. van der Meer, B. W., van Hoeven, R. P. & van Blitterswijk, W. J. Steady-state fluorescence polarization data in membranes. Resolution into physical parameters by an extended Perrin equation for restricted rotation of fluorophores. *Biochim Biophys Acta* **854**, 38–44 (1986).
474. Fiske, C. H. & Subbarow, Y. THE COLORIMETRIC DETERMINATION OF PHOSPHORUS. *Journal of Biological Chemistry* **66**, 375–400 (1925).
475. Bartlett, G. R. Phosphorus assay in column chromatography. *J Biol Chem* **234**, 466–468 (1959).
476. Sonn-Segev, A. *et al.* Quantifying the heterogeneity of macromolecular machines by mass photometry. *Nat Commun* **11**, 1772 (2020).
477. Malghani, M. S. & Yang, J. Stable Binding of DNA to Zwitterionic Lipid Bilayers in Aqueous Solutions. *J. Phys. Chem. B* **102**, 8930–8933 (1998).
478. Gromelski, S. & Brezesinski, G. DNA Condensation and Interaction with Zwitterionic Phospholipids Mediated by Divalent Cations. *Langmuir* **22**, 6293–6301 (2006).

479. Lu, D. & Rhodes, D. G. Binding of phosphorothioate oligonucleotides to zwitterionic liposomes. *Biochim Biophys Acta* **1563**, 45–52 (2002).
480. Janas, T., Janas, T. & Yarus, M. Specific RNA binding to ordered phospholipid bilayers. *Nucleic Acids Res* **34**, 2128–2136 (2006).
481. Berlot, P. E. & Locascio, G. A. Isopycnic ultracentrifugation: A simple and inexpensive demonstration of its principles. *J. Chem. Educ.* **67**, 627 (1990).
482. Basu, S. K., Goldstein, J. L., Anderson, G. W. & Brown, M. S. Degradation of cationized low density lipoprotein and regulation of cholesterol metabolism in homozygous familial hypercholesterolemia fibroblasts. *Proc Natl Acad Sci U S A* **73**, 3178–3182 (1976).
483. Feuer, H. *Solubilities of Inorganic and Organic Compounds: A Compilation of Solubility Data from the Periodical Literature*. Supplement to ed. 3. Atherton Seidell and William F. Linke. Van Nostrand, New York, 1952. 1254 pp. \$12.50. *Science* **119**, 902–902 (1954).
484. Srinivasan, B. *et al.* TEER Measurement Techniques for In Vitro Barrier Model Systems. *J Lab Autom.* **20**, 107–126 (2015).
485. Littlefield, M. J., Teboul, I., Voloshyna, I. & Reiss, A. B. Polarization of Human THP-1 Macrophages: Link between Adenosine Receptors, Inflammation and Lipid Accumulation. (2015) doi:10.13140/RG.2.1.4484.0485.
486. Das, R. *et al.* Macrophage Gene Expression and Foam Cell Formation Are Regulated by Plasminogen. *Circulation* **127**, 1209–1218 (2013).
487. Hayden, J. M. *et al.* Induction of monocyte differentiation and foam cell formation in vitro by 7-ketcholesterol. *Journal of Lipid Research* **43**, 26–35 (2002).
488. Banka, C. L., Black, A. S., Dyer, C. A. & Curtiss, L. K. THP-1 cells form foam cells in response to coculture with lipoproteins but not platelets. *J Lipid Res* **32**, 35–43 (1991).
489. Mehlem, A., Hagberg, C. E., Muhl, L., Eriksson, U. & Falkevall, A. Imaging of neutral lipids by oil red O for analyzing the metabolic status in health and disease. *Nat Protoc* **8**, 1149–1154 (2013).
490. Ramírez, C. M. *et al.* RNA binding protein HuR regulates the expression of ABCA1. *J Lipid Res* **55**, 1066–1076 (2014).

491. Ranganathan, S. & Kottke, B. A. Rapid regulation of apolipoprotein A-I secretion in HepG2 cells by a factor associated with bovine high-density lipoproteins. *Biochimica et Biophysica Acta (BBA) - Lipids and Lipid Metabolism* **1046**, 223–228 (1990).
492. Vado, Y. *et al.* Design and Validation of a Process Based on Cationic Niosomes for Gene Delivery into Novel Urine-Derived Mesenchymal Stem Cells. *Pharmaceutics* **13**, 696 (2021).
493. Cavigiolio, G. *et al.* The Interplay between Size, Morphology, Stability, and Functionality of High-Density Lipoprotein Subclasses. *Biochemistry* **47**, 4770–4779 (2008).
494. Andrews, P. The gel-filtration behaviour of proteins related to their molecular weights over a wide range. *Biochem J* **96**, 595–606 (1965).
495. Erickson, H. P. Size and Shape of Protein Molecules at the Nanometer Level Determined by Sedimentation, Gel Filtration, and Electron Microscopy. *Biol Proced Online* **11**, 32–51 (2009).
496. Rumsey, S. C., Galeano, N. F., Arad, Y. & Deckelbaum, R. J. Cryopreservation with sucrose maintains normal physical and biological properties of human plasma low density lipoproteins. *J Lipid Res* **33**, 1551–1561 (1992).
497. Holzer, M., Kern, S., Trieb, M., Trakaki, A. & Marsche, G. HDL structure and function is profoundly affected when stored frozen in the absence of cryoprotectants. *Journal of Lipid Research* **58**, 2220–2228 (2017).
498. Lakowicz, J. R., Prendergast, F. G. & Hogen, D. Fluorescence anisotropy measurements under oxygen quenching conditions as a method to quantify the depolarizing rotations of fluorophores. Application to diphenylhexatriene in isotropic solvents and in lipid bilayers. *Biochemistry* **18**, 520–527 (1979).
499. Halling, K. K., Ramstedt, B., Nyström, J. H., Slotte, J. P. & Nyholm, T. K. M. Cholesterol interactions with fluid-phase phospholipids: effect on the lateral organization of the bilayer. *Biophys J* **95**, 3861–3871 (2008).
500. Shaw, A. W., McLean, M. A. & Sligar, S. G. Phospholipid phase transitions in homogeneous nanometer scale bilayer discs. *FEBS Letters* **556**, 260–264 (2004).
501. Prassl, R. *et al.* Low Density Lipoproteins as Circulating Fast Temperature Sensors. *PLoS ONE* **3**, e4079 (2008).

502. O'neill, S. D. & Leopold, A. C. An assessment of phase transitions in soybean membranes. *Plant Physiol* **70**, 1405–1409 (1982).
503. Chistiakov, D. A., Melnichenko, A. A., Myasoedova, V. A., Grechko, A. V. & Orekhov, A. N. Mechanisms of foam cell formation in atherosclerosis. *J Mol Med* **95**, 1153–1165 (2017).
504. Goikuria, H. *et al.* Characterization of Carotid Smooth Muscle Cells during Phenotypic Transition. *Cells* **7**, E23 (2018).
505. Kim, D., Eom, S., Park, S. M., Hong, H. & Kim, D. S. A collagen gel-coated, aligned nanofiber membrane for enhanced endothelial barrier function. *Sci Rep* **9**, 14915 (2019).
506. Tschugguel, W. *et al.* High precision measurement of electrical resistance across endothelial cell monolayers. *Pflügers Arch - Eur J Physiol* **430**, 145–147 (1995).
507. Dergunov, A. D., Garaeva, E. A., Savushkin, E. V. & Litvinov, D. Y. Significance of Lipid-Free and Lipid-Associated ApoA-I in Cellular Cho-esterol Efflux. *Curr Protein Pept Sci* **18**, 92–99 (2017).
508. Litvinov, D. Y., Savushkin, E. V., Garaeva, E. A. & Dergunov, A. D. Cholesterol Efflux and Reverse Cholesterol Transport: Experimental Approaches. *Curr Med Chem* **23**, 3883–3908 (2016).
509. Phillips, M. C. Molecular Mechanisms of Cellular Cholesterol Efflux. *Journal of Biological Chemistry* **289**, 24020–24029 (2014).
510. Yvan-Charvet, L., Wang, N. & Tall, A. R. Role of HDL, ABCA1, and ABCG1 transporters in cholesterol efflux and immune responses. *Arterioscler Thromb Vasc Biol* **30**, 139–143 (2010).
511. Vedhachalam, C. *et al.* Influence of Apolipoprotein (Apo) A-I Structure on Nascent High Density Lipoprotein (HDL) Particle Size Distribution. *Journal of Biological Chemistry* **285**, 31965–31973 (2010).
512. Anantharamaiah, G. M. *et al.* Studies of synthetic peptide analogs of the amphipathic helix. Structure of complexes with dimyristoyl phosphatidylcholine. *J Biol Chem* **260**, 10248–10255 (1985).
513. Bielicki, J. K. *et al.* A new HDL mimetic peptide that stimulates cellular cholesterol efflux with high efficiency greatly reduces atherosclerosis in mice. *J Lipid Res* **51**, 1496–1503 (2010).

514. Bloedon, L. T. *et al.* Safety, pharmacokinetics, and pharmacodynamics of oral apoA-I mimetic peptide D-4F in high-risk cardiovascular patients. *J Lipid Res* **49**, 1344–1352 (2008).
515. Khan, M., Lalwani, N. D., Drake, S. L., Crockatt, J. G. & Dasseux, J. Luis. H. Single-dose intravenous infusion of etc-642, a 22-mer apoa-i analogue and phospholipids complex, elevates hdl-c in atherosclerosis patients. *Circulation* 563–563 (2003).
516. Yang, N. *et al.* Reverse-D-4F improves endothelial progenitor cell function and attenuates LPS-induced acute lung injury. *Respir Res* **20**, 131 (2019).
517. Getz, G. S. & Reardon, C. A. Apoprotein E and Reverse Cholesterol Transport. *Int J Mol Sci* **19**, E3479 (2018).
518. Marais, A. D. Apolipoprotein E in lipoprotein metabolism, health and cardiovascular disease. *Pathology* **51**, 165–176 (2019).
519. Mahley, R. W., Weisgraber, K. H. & Huang, Y. Apolipoprotein E: structure determines function, from atherosclerosis to Alzheimer's disease to AIDS. *J Lipid Res* **50 Suppl**, S183-188 (2009).
520. Ma, C.-I. J. *et al.* Tweaking the cholesterol efflux capacity of reconstituted HDL. *Biochem. Cell Biol.* **90**, 636–645 (2012).
521. Marmillot, P., Patel, S. & Lakshman, M. R. Reverse cholesterol transport is regulated by varying fatty acyl chain saturation and sphingomyelin content in reconstituted high-density lipoproteins. *Metabolism* **56**, 251–259 (2007).
522. Ramstedt, B. & Slotte, J. P. Interaction of cholesterol with sphingomyelins and acyl-chain-matched phosphatidylcholines: a comparative study of the effect of the chain length. *Biophys J* **76**, 908–915 (1999).
523. Ohvo-Rekilä, H., Ramstedt, B., Leppimäki, P. & Slotte, J. P. Cholesterol interactions with phospholipids in membranes. *Prog Lipid Res* **41**, 66–97 (2002).
524. Di Bartolo, B. A. *et al.* The apolipoprotein A-I mimetic peptide ETC-642 exhibits anti-inflammatory properties that are comparable to high density lipoproteins. *Atherosclerosis* **217**, 395–400 (2011).
525. Montalvo, G., Pons, R., Zhang, G., Díaz, M. & Valiente, M. Structure and Phase Equilibria of the Soybean Lecithin/PEG 40 Monostearate/Water System. *Langmuir* **29**, 14369–14379 (2013).

526. Nakagawa, Y., Inoue, K. & Nojima, S. Transfer of cholesterol between liposomal membranes. *Biochim Biophys Acta* **553**, 307–319 (1979).
527. Fugler, L., Clejan, S. & Bittman, R. Movement of cholesterol between vesicles prepared with different phospholipids or sizes. *J Biol Chem* **260**, 4098–4102 (1985).
528. Yeagle, P. L. Cholesterol and the cell membrane. *Biochim Biophys Acta* **822**, 267–287 (1985).
529. McLean, L. R. & Phillips, M. C. Cholesterol transfer from small and large unilamellar vesicles. *Biochim Biophys Acta* **776**, 21–26 (1984).
530. Frolov, V. A., Shnyrova, A. V. & Zimmerberg, J. Lipid polymorphisms and membrane shape. *Cold Spring Harb Perspect Biol* **3**, a004747 (2011).
531. Vanni, S., Hirose, H., Barelli, H., Antonny, B. & Gautier, R. A sub-nanometre view of how membrane curvature and composition modulate lipid packing and protein recruitment. *Nat Commun* **5**, 4916 (2014).
532. Pinot, M. *et al.* Lipid cell biology. Polyunsaturated phospholipids facilitate membrane deformation and fission by endocytic proteins. *Science* **345**, 693–697 (2014).
533. Chernomordik, L. V. & Kozlov, M. M. Protein-lipid interplay in fusion and fission of biological membranes. *Annu Rev Biochem* **72**, 175–207 (2003).
534. Ikonen, E. Cellular cholesterol trafficking and compartmentalization. *Nat Rev Mol Cell Biol* **9**, 125–138 (2008).
535. Churchward, M. A. *et al.* Specific Lipids Supply Critical Negative Spontaneous Curvature—An Essential Component of Native Ca<sup>2+</sup>-Triggered Membrane Fusion. *Biophysical Journal* **94**, 3976–3986 (2008).
536. McMahon, H. T. & Gallop, J. L. Membrane curvature and mechanisms of dynamic cell membrane remodelling. *Nature* **438**, 590–596 (2005).
537. McLean, L. R. & Phillips, M. C. Mechanism of cholesterol and phosphatidylcholine exchange or transfer between unilamellar vesicles. *Biochemistry* **20**, 2893–2900 (1981).
538. Thomas, P. D. & Poznansky, M. J. Effect of surface curvature on the rate of cholesterol transfer between lipid vesicles. *Biochem J* **254**, 155–160 (1988).

539. World Health Organization. <https://www.who.int/health-topics/cardiovascular-diseases>.
540. Libby, P. *et al.* Atherosclerosis. *Nat Rev Dis Primers* **5**, 56 (2019).
541. Noonan, J. *et al.* A Novel Triple-Cell Two-Dimensional Model to Study Immune-Vascular Interplay in Atherosclerosis. *Front. Immunol.* **10**, 849 (2019).
542. Gualtero, D. F., Lafaurie, G. I. & Fontanilla, M. R. Two-dimensional and three-dimensional models for studying atherosclerosis pathogenesis induced by periodontopathogenic microorganisms. *Mol Oral Microbiol* **33**, 29–37 (2018).
543. Chan, C. K. W. *et al.* Recent Advances in Managing Atherosclerosis via Nanomedicine. *Small* **14**, 1702793 (2018).
544. He, H. *et al.* Development of mannose functionalized dendrimeric nanoparticles for targeted delivery to macrophages: use of this platform to modulate atherosclerosis. *Translational Research* **193**, 13–30 (2018).
545. He, H. *et al.* Nanoparticle-based “Two-pronged” approach to regress atherosclerosis by simultaneous modulation of cholesterol influx and efflux. *Biomaterials* **260**, 120333 (2020).
546. Dahlman, J. E. *et al.* In vivo endothelial siRNA delivery using polymeric nanoparticles with low molecular weight. *Nature Nanotech* **9**, 648–655 (2014).
547. Yin, H. *et al.* Non-viral vectors for gene-based therapy. *Nat Rev Genet* **15**, 541–555 (2014).
548. Khan, O. F. *et al.* Endothelial siRNA delivery in nonhuman primates using ionizable low-molecular weight polymeric nanoparticles. *Sci. Adv.* **4**, eaar8409 (2018).
549. Jebari-Benslaiman, S. *et al.* Cholesterol Efflux Efficiency of Reconstituted HDL Is Affected by Nanoparticle Lipid Composition. *Biomedicines* **8**, 373 (2020).
550. Thaxton, C. S., Rink, J. S., Naha, P. C. & Cormode, D. P. Lipoproteins and lipoprotein mimetics for imaging and drug delivery. *Advanced Drug Delivery Reviews* **106**, 116–131 (2016).
551. Rink, J. S. *et al.* Rational Targeting of Cellular Cholesterol in Diffuse Large B-Cell Lymphoma (DLBCL) Enabled by Functional Lipoprotein Nanoparticles: A Therapeutic Strategy Dependent on Cell of Origin. *Mol. Pharmaceutics* **14**, 4042–4051 (2017).

552. Yang, S. *et al.* Biomimetic, synthetic HDL nanostructures for lymphoma. *Proceedings of the National Academy of Sciences* **110**, 2511–2516 (2013).
553. Robert, J. *et al.* Interleukin 6 Stimulates Endothelial Binding and Transport of High-Density Lipoprotein Through Induction of Endothelial Lipase. *Arterioscler Thromb Vasc Biol.* **33**, 2699–2706 (2013).
554. Rohrer, L. *et al.* High-Density Lipoprotein Transport Through Aortic Endothelial Cells Involves Scavenger Receptor BI and ATP-Binding Cassette Transporter G1. *Circulation Research* **104**, 1142–1150 (2009).
555. Perisa, D., Rohrer, L., Kaech, A. & von Eckardstein, A. Itinerary of high density lipoproteins in endothelial cells. *Biochimica et Biophysica Acta (BBA) - Molecular and Cell Biology of Lipids* **1861**, 98–107 (2016).
556. Fung, K. Y. *et al.* SR-BI Mediated Transcytosis of HDL in Brain Microvascular Endothelial Cells Is Independent of Caveolin, Clathrin, and PDZK1. *Front. Physiol.* **8**, 841 (2017).
557. Nguyen, M.-A. *et al.* Delivery of MicroRNAs by Chitosan Nanoparticles to Functionally Alter Macrophage Cholesterol Efflux *in Vitro* and *in Vivo*. *ACS Nano* **13**, 6491–6505 (2019).
558. Sankaranarayanan, S. *et al.* Effects of acceptor composition and mechanism of ABCG1-mediated cellular free cholesterol efflux. *Journal of Lipid Research* **50**, 275–284 (2009).
559. Tall, A. R. Cholesterol efflux pathways and other potential mechanisms involved in the athero-protective effect of high density lipoproteins. *J Intern Med* **263**, 256–273 (2008).
560. Nakamura, K. *et al.* Expression and Regulation of Multiple Murine ATP-binding Cassette Transporter G1 mRNAs/Isoforms That Stimulate Cellular Cholesterol Efflux to High Density Lipoprotein. *Journal of Biological Chemistry* **279**, 45980–45989 (2004).
561. Repa, J. J. *et al.* Regulation of mouse sterol regulatory element-binding protein-1c gene (SREBP-1c) by oxysterol receptors, LXR $\alpha$  and LXR $\beta$ . *Genes Dev.* **14**, 2819–2830 (2000).
562. Liang, G. *et al.* Diminished Hepatic Response to Fasting/Refeeding and Liver X Receptor Agonists in Mice with Selective Deficiency of Sterol Regulatory

Element-binding Protein-1c. *Journal of Biological Chemistry* **277**, 9520–9528 (2002).

563. Sirtori, C. R., Calabresi, L. & Franceschini, G. Recombinant apolipoproteins for the treatment of vascular diseases. *Atherosclerosis* **142**, 29–40 (1999).

564. Murphy, A. J., Chin-Dusting, J. & Sviridov, D. Reconstituted HDL: a therapy for atherosclerosis and beyond. *Clinical Lipidology* **4**, 731–739 (2009).

## **ANNEX I:** Functional characterization of LDLR and PCSK9 variants

**The results presented in this section have been published at:**

1. Mutation type classification and pathogenicity assignment of sixteen missense variants located in the EGF-precursor homology domain of the LDLR. Galicia-Garcia U, Benito-Vicente A, Uribe KB, **Jebari S**, Larrea-Sebal A, Alonso-Estrada R, Aguiló-Arce J, Ostolaza H, Palacios L, Martín C. Sci Rep. 2020 Feb 3;10(1):1727. doi:10.1038/s41598-020-58734-
2. The Arg499His gain-of-function mutation in the C-terminal domain of PCSK9. Sánchez-Hernández RM, Di Taranto MD, Benito-Vicente A, Uribe KB, Lamiquiz-Moneo I, Larrea-Sebal A, **Jebari S**, Galicia-Garcia U, Nóvoa FJ, Boronat M, Wägner AM, Civeira F, Martín C, Fortunato G. Atherosclerosis. 2019 Oct;289:162-172. doi:10.1016/j.atherosclerosis.2019.08.020.
3. Validation of LDLr Activity as a Tool to Improve Genetic Diagnosis of Familial Hypercholesterolemia: A Retrospective on Functional Characterization of LDLr Variants. Benito-Vicente A, Uribe KB, **Jebari S**, Galicia-Garcia U, Ostolaza H, Martín C. Int J Mol Sci. 2018 Jun 5;19(6):1676. doi: 10.3390/ijms19061676.
4. Familial Hypercholesterolemia: The Most Frequent Cholesterol Metabolism Disorder Caused Disease. Benito-Vicente A, Uribe KB, **Jebari S**, Galicia-Garcia U, Ostolaza H, Martín C. Int J Mol Sci. 2018 Nov 1;19(11):3426. doi: 10.3390/ijms19113426.
5. Leu22\_Leu23 duplication at the signal peptide of PCSK9 promotes intracellular degradation of LDLr and autosomal dominant hypercholesterolemia. Asier Benito-Vivente, Kepa Uribe, Asier Larrea-Sebal, Lourdes Palacios, Cenarro Ana, Xabier Calle, Unai Galicia-Garcia, **Shifa Jebari**, Rosa Sánchez-Hernández, Marianne Stef, Gilles Lambert, Fernando Civeira, and Cesar Martín (*under review.*)
6. MLb-LDLr: A Machine Learning Model for Predicting the Pathogenicity of *LDLr* Missense Variants. Larrea-Sebal A, Benito-Vicente A, Fernandez-Higuero JA, **Jebari-Benslaiman S**, Galicia-Garcia U, Uribe KB, Cenarro A, Ostolaza H, Civeira F, Arrasate S, González-Díaz H, Martín C. JACC Basic Transl Sci. 2021 Nov 22;6(11):815-827. doi: 10.1016/j.jacbts.2021.08.009.

## 1. Familial Hypercholesterolemia (FH)

Familial hypercholesterolemia (FH) is one of the most frequent dyslipidaemias characterized by high concentrations of total and LDL cholesterol (LDL-c) leading to accelerated atherosclerosis and premature coronary heart disease (CHD)<sup>1,2</sup>. FH is an autosomal monogenic disorder and, with a frequency estimated between 1:200–1:250, constitutes one of the most serious commonly inherited metabolic diseases. Despite its high prevalence, FH is still severely underdiagnosed and undertreated. Autosomal dominant mutations in *LDLR* (encoding the LDL receptor), *APOB* (encoding apolipoprotein B100 (apoB100)), and *PCSK9* (encoding proprotein convertase subtilisin/kexin type 9) genes account for most cases of FH<sup>3–6</sup>. Most individuals with FH are heterozygous for mutations in one of these genes and, therefore, have heterozygous FH. Being its penetrance almost 100%, half of the offspring (mean prevalence) of an affected parent have a severely increased plasma cholesterol level from birth onwards. Mutations in *LDLR* are the main genetic cause of FH<sup>7,8</sup> constituting more than 90% of the mutations found in FH patients, with more than 2000 *LDLR* genetic variants submitted so far to the Human Gene Mutation Database (HGMD).

### 1.1. Genetics of FH

Cholesterol metabolism and its distribution is a complex system in which many proteins and pathways are involved. LDL catabolism is one of the key points in this process and any defect in its function by any of the proteins taking part on it can generate FH. The major determinants in that system are *LDLR*, accounting for 80–85% of FH cases, *apoB100*, causing 5–10% of the cases, *PCSK9* 2% of the cases and *LDL receptor adaptor protein 1 (LDLRAP1)* accounting for less than 1% of the cases (Figure 1)<sup>9</sup>. Mutations in *APOE*<sup>10</sup>, *signal transducing adaptor family member*

*1 (STAP1)<sup>11</sup>, lysosomal acid lipase (LIPA)<sup>12</sup>, ABCG5 or ABCG8<sup>13</sup>* genes can also generate a FH like phenotype, but its frequency is very low in all of the cases.

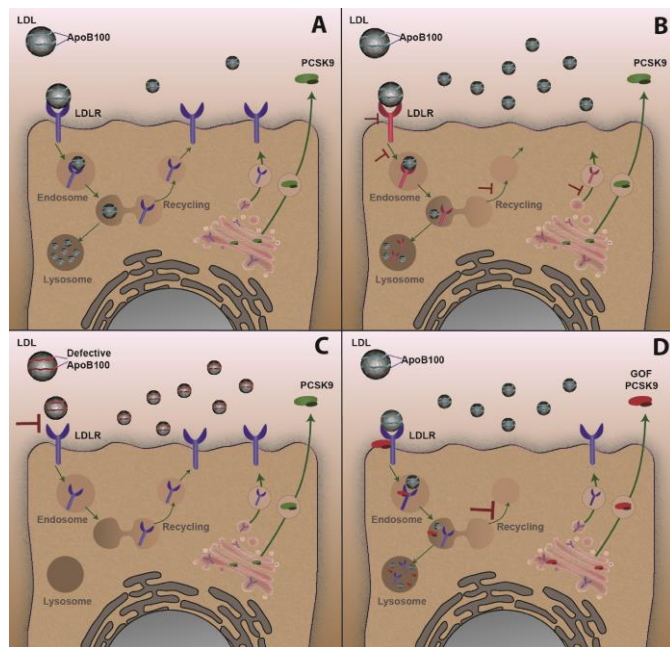


**Figure 1: Most frequent LDL catabolism defects.** (A) physiological LDL uptake process by LDLR; (B) defective LDLR derived impaired LDL uptake; (C) defective ApoB100 derived impaired LDL uptake; (D) GOF PCSK9-mediated , impaired LDL uptake.

## 1.2. LDLR

*LDLR* with more than 3000 variants already reported (Clin Var database<sup>14</sup>) is one of the key genes responsible of FH development<sup>15</sup>. LDLR removes LDL from plasma circulation (**Figure 2A**) and malfunctioning of LDLR is commonly associated with high levels of circulating LDL-C. Many different *LDLR* variants have been described as pathogenic, including large-scale DNA copy number variation (CNV), insertion and deletions, nonsense and missense mutations and splicing mutations<sup>9,1516</sup>. CNV, nonsense and splicing mutations are commonly associated with higher LDL-C levels

than missense mutations. LDLR mutations can affect at different steps of the LDL uptake system and thus can be classified depending on their phenotypic behavior as: Class 1 mutants are characterized by a null protein synthesis; class 2 mutants are partially or completely retained in the endoplasmic reticulum (**Figure 2B**); class 3 mutants have a binding defect and are not able to properly interact with apoB apolipoprotein (**Figure 2C**); class 4 mutants have an impaired endocytosis (**Figure 2D**) and finally class 5 mutants affect the recycle mechanism and LDLR cannot be recycle back to the membrane (**Figure 2E**).

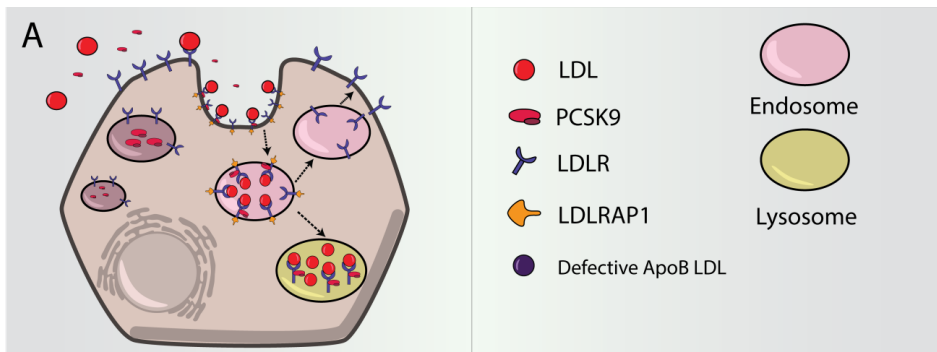
### 1.3 APOB

Mutations in *APOB* are a second cause of FH with a phenotype known as familial defective APOB<sup>9</sup>. Mutations in *APOB* gene were first detected in the highly conserved receptor binding-site (exons 26 and 29)<sup>17</sup> leading to deficient binding to LDLR. Recently some studies have also described new variants out from the consensus binding site of the *APOB*<sup>18</sup>, these variants have been functionally characterized and classified as pathogenic indicating that LDLR-LDL binding could be more dynamic than expected . *APOB* pathogenic variants are associated with lower LDL-C levels than those observed with *LDLR* pathogenic variants (**Figure 2F**).

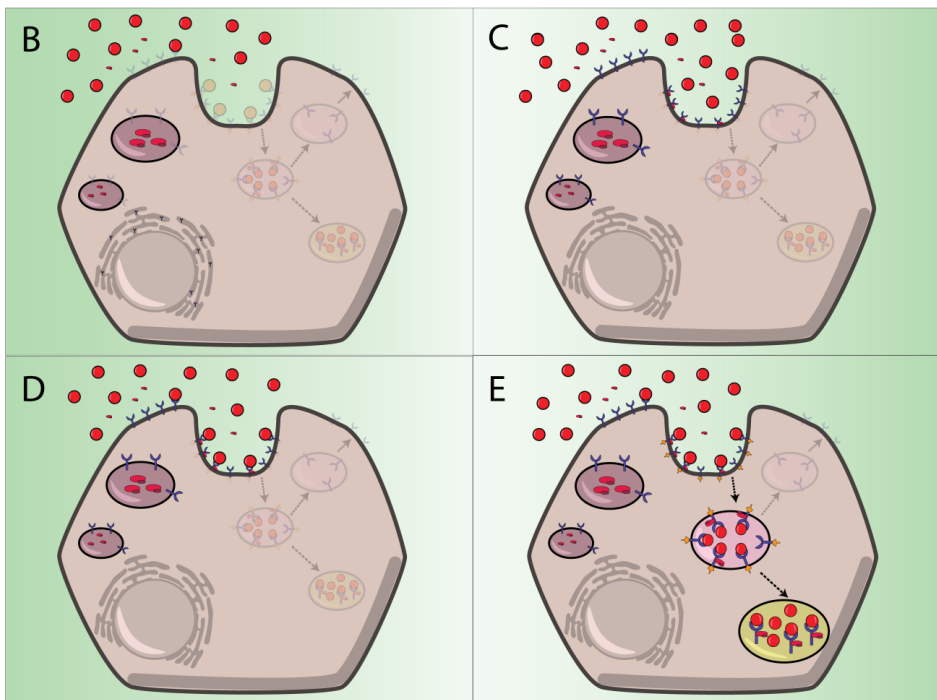
### 1.4. PCSK9

*PCSK9* variants started to be described in the early 2000s when *PCSK9* locus was mapped<sup>19</sup>. These variants can either be loss of function (LOF) variants, generating less functional proteins or gain of function variants (GOF) producing more active proteins<sup>20</sup>. GOF variants are associated with increased LDL-C levels as they enhances degradation of LDLR extracellularly, due to increased affinity (**Figure 2G**) or intracellularly while it is been transported to the membrane<sup>21</sup>. Both mechanisms lead to a reduced expression of LDLR resulting in plasma LDL accumulation. To date,

more than 30 GOF PCSK9 variants have been reported; most of them missense mutations located all around the 3 domains of PCSK9<sup>20</sup>. Different mechanisms underlying the increased activity, including increased transcription, altered autocatalysis or enhanced binding ability for the receptor have been described<sup>20</sup>. LOF mutations are less common than GOF mutations and are associated with lower LDL-C levels and reduced cardiovascular disease<sup>22</sup>.



LDLR defect



ApoB100 defect

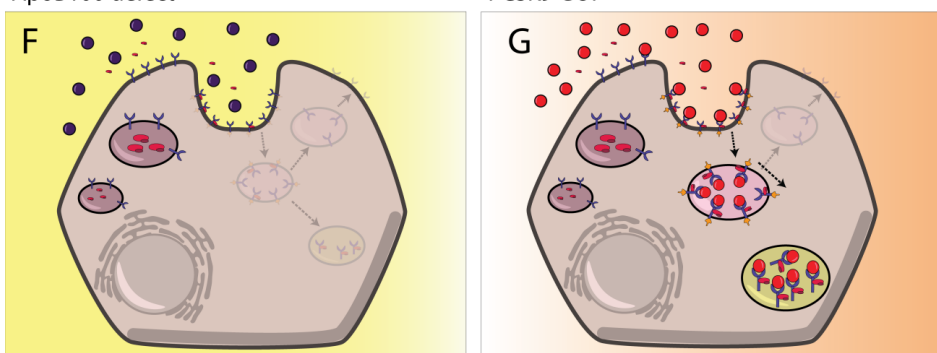


**Figure 2. Most frequent LDL catabolism defects.** (A) LDL uptake process by LDLR; (B) class 2 LDLR mutants, LDLR retention in the endoplasmic reticulum; (C) Class 3 mutants, no LDL-LDLR binding; (D) class 4 mutants, impaired LDL-LDLR complex internalization; (E) class 5 mutants, recycling defect; (F) defective ApoB-100 derived impaired LDL-LDLR binding; (G) PCSK9 gain of function.

## 2. Determining the Pathogenicity of LDLr Variants

The majority of FH patients with positive genetic testing results have rare pathogenic variants in LDLr [45], which comprise 60% of the ~2000 LDLr genetic variants that have been submitted to the HGMD. Determining pathogenicity of LDLr is a key challenge in genomic medicine; Functional assays are a direct method to determine whether the activity of a mutant protein is altered by taking into account all the involved biological mechanisms. To date, functional studies of LDLr variants have been conducted using two major approaches: 1. *ex vivo* methods, using cells from FH patients; 2. *in vitro* methods using cell lines transfected with the LDLR mutant (**Figure 3**).

# LDLr functional validation

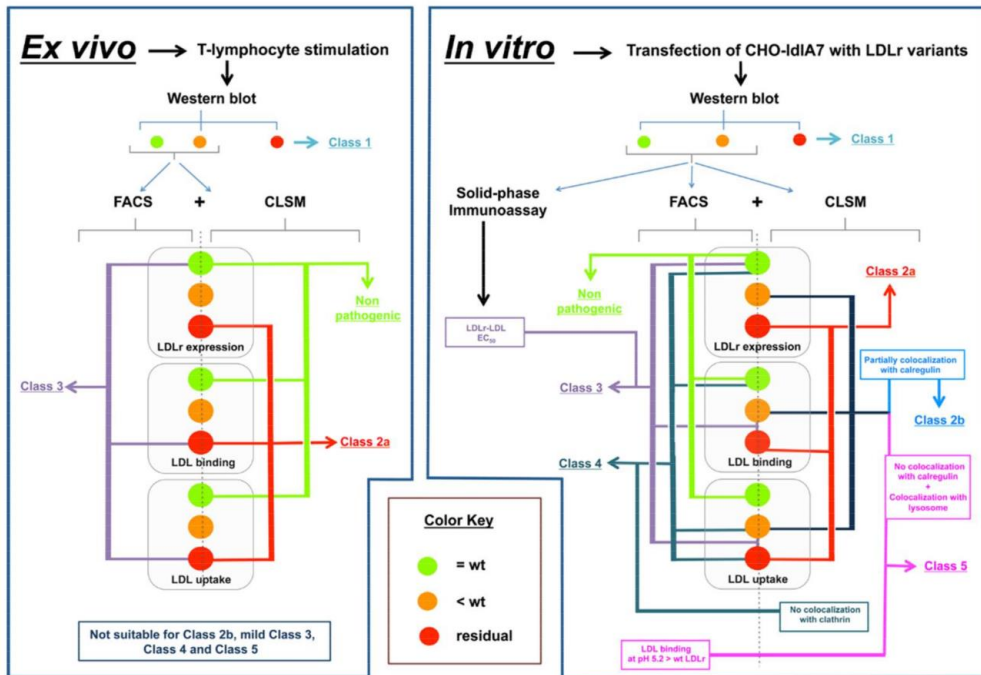


**Figure 3. Flowchart of the used methodologies to functionally characterize LDLr variants *ex vivo* and *in vitro*.** Functional studies of LDLr variants are mainly conducted using two major approaches: 1. *ex vivo* methods, using cells from Familial Hypercholesterolemia (FH) patients (left-hand panel); 2. *in vitro* methods using cell lines transfected with the LDLr variant (right-hand panel). LDLr activity determination is based in combination of different methodologies: Western blot to analyse LDLr expression followed by fluorescence-activated cell sorting (FACS) and Confocal Laser Scanning Microscopy (CLSM) that allow assessment of Class type mutation. The *ex vivo* approach is adequate for Class 1, Class 2a and Class 3 LDLr variants. In *vitro* characterization allows identification of Class 2b mutations by colocalizing the LDLr variants in the ER with calregulin; using a solid-phase immunoassay it is possible to determine LDLr-LDL EC<sub>50</sub> values for Class 3 mutations which is important to understand mild pathogenic variants; Class 4 variants are classified by complementing CLSM with a colocalization assay with clathrin and, identification of Class 5 mutants is performed by absence of LDLr colocalization with calregulin, LDLr colocalization with a lysosome marker complemented by a FACS analysis of LDL binding to LDLr at different pH (7.4–5.2).

### 3. Determining the Pathogenicity PCSK9 Variants

PCSK9 GOF mutations are usually missense defects, located in any exon, except exon 3<sup>20</sup>. Functional studies on human GOF variants show different mechanism to achieve the enhanced degradation of LDLr. Some mutations affecting the prodomain region result in an increase in internal and external LDLr degradation<sup>23,24</sup>. Variants that affect catalytic domain and prodomain share very similar mechanisms and effects<sup>25</sup>. The best characterized PCSK9 GOF mutation is p.(Asp374Tyr) which produces a ten-fold increase in LDLr degradation<sup>26</sup> by increasing the binding affinity of PCSK9 to the epidermal growth factor-like domain of LDLr<sup>27,28</sup>.

## 4. Materials and Methods

### 4.1. LDLR variant selection

In order to select variants in the EGF-precursor homology domain of the LDLR that could have an impact in the activity of the receptor, we used the ClinVar database (<https://clinvarminer.genetics.utah.edu>) and selected the following ones: p.(Cys46Gly), p.(Asp47Asn), p.(Thr62Met), p.(Trp305Ser), p.(Leu371Pro), p.(Gly373Ala), p.(Gln378Pro), p.(Ala399Thr), p.(Thr413Met), p.(Ile473Asn), p.(Val578Ile), p.(Ala606Ser), p.(Met652Thr), p.(Asp638His), p.His656Asn) and p.(Thr659Asn). These LDLR variants were selected because they have been described in FH patients, their clinical interpretation was not previously assessed and we did not find any study that had functionally characterized them. All these variants have also been found by the LIPOchip® platform and/or by the SEQPRO LIPO S® platform from Progenika Biopharma (Derio, Spain), both having the CE mark.

## 4.2. Construction of LDLR variants carrying plasmids

Plasmids containing the LDLR variants were designed by Innoprot (Derio, Spain). Using the QuickChange Lightning mutagenesis kit (Agilent). The mammalian expression vector pcDNA3 was used to introduce the variants into the human LDLR cDNA (NM\_000527.4) under control of a SV40 promoter by oligonucleotide site-directed mutagenesis and according to manufacturer's instructions. In order to generate the plasmids carrying the LDLR variants, oligonucleotides were synthesized in vitro and subcloned using SacII and EcoRI restriction enzymes. The presence of the desired nucleotide alteration was confirmed by PCR and restriction enzyme digestion of the appropriate fragments, while direct sequence analysis was used to verify the integrity of the remaining LDLR cDNA sequence of the construct.

## 4.3. LDL isolation and labelling

Blood plasma was collected from healthy individuals after 30 min centrifugation at 2,000 × g at 4 °C. In order to isolate LDL (1.019–1.050 g/mL) by a sequential ultracentrifugation, plasma density was adjusted to 1.21 g/mL adding KBr. Afterwards, a second ice-cold PBS buffer was slowly added at the top of the solution generating a two phase gradient. Ultracentrifugation was carried out in a SW28.1 rotor (Beckman Coulter, USA) at 27,000 rpm for 22 h at 4 °C. Then, the band corresponding to LDL was collected and stored at 4 °C. LDL was used within 2–3 days after purification. LDL was fluorescently labelled with fluorescein isothiocyanate (FITC) as described previously<sup>24</sup>. Briefly, LDL was incubated with 10 µL/mL FITC in 0.1 M NaHCO<sub>3</sub> (pH 9.0) at room temperature under slight agitation for 2 h. Once incubation was completed, the non-bounded FITC was removed by washing the lipoprotein solution in a previously PBS EDTA-free balanced Sephadex G-25 column. Protein concentration was determined in all fractions using BSA as standard (Pierce BCA protein assay, Pierce). This study was

approved by the Research Ethics Committee of the University of the Basque Country (Comité de Ética en la investigación y la práctica docente de la Universidad del País Vasco/Euskal Herriko Unibertsitatea; CEIAB/186/2014/MARTÍN PLÁGARO). Methods were carried out according to the approved guidelines. All participants signed the written informed consent. All experiments were carried out according to relevant guidelines and regulations.

#### 4.4. Analysis of LDLR expression by FACS

LDLR expression at the cell membrane was assessed in a FACScalibur using Mouse anti-human-LDLR (1:100; 2.5 mg/L; Progen Biotechnik GmbH) and Alexa Fluor 488-conjugated goat anti-mouse IgG (1:100; Molecular Probes) primary and secondary antibodies, respectively. Immunostaining was performed as previously described<sup>25</sup>. Each sample was performed in triplicate and 10,000 events were acquired for data analysis.

#### 4.5. Analysis of LDLR activity by FACS

Cells were transfected as described above and, 48 h after transfection, FITC-LDL (20 µg/mL) was added to the cell culture medium. Cells were incubated during 2 h at 4 °C or 4 h at 37 °C in order to determine LDL binding and uptake, respectively. Then, cells were washed out with PBS-1% BSA, fixed in 4% paraformaldehyde for 10 minutes at room temperature and rinsed again to eliminate the surplus fixative. Trypan blue solution (0.2% final concentration, Sigma-Aldrich, Steinheim, Germany) was added to the samples to determine LDL uptake, allowing the quenching of the extracellular FITC signal coming from the non-internalized LDL–LDLR complexes. Geometric mean fluorescence intensity (GMFI) of each sample was determined in a FACScalibur Flow cytometer following the manufacturer's instructions. GMFI of

10,000 events was obtained for each sample and every assay determination was performed at least three times.

#### 4.6. Analysis of PCSK9-LDLR EC50 by Solid-Phase Immunoassay

Purified ED-LDLR diluted in working buffer (10 mM Tris-HCl, pH 7.4, 50 mM NaCl, 2 mM CaCl<sub>2</sub>) was used to coat 96-well microtiter plates at a fixed concentration by incubation overnight at 4 °C. Plates were blocked and incubated with a serial dilution of each of the PCSK9 variants diluted in working buffer (pH 7.4) for 2 h at room temperature. Plates were washed thoroughly with working buffer containing 0.1% Tween 20 (Merck, Sigma-Aldrich, Steinheim am Albuch, Germany). Rat monoclonal anti-DYKDDDDK tag (clone L5) (Cat. No.: MA1-142; Thermo Fisher Scientific, Carlsbad, CA, USA) and peroxidase-conjugated goat anti-rat (Cat. No.: 7077S; Cell Signalling Technology® Inc., Danvers, MA, USA) antibodies were used for detection [21]. 2,2'-Azino-bis (3-ethylbenzothiazoline-6-sulfonic acid) substrate solution (Merck, Sigma-Aldrich, Steinheim am Albuch, Germany) was used as a substrate, and absorbance was determined at 405 nm. All absorbance values were corrected for unspecific binding relative to maximum absorbance, and EC50 values were extracted from curves after fitting the data to 5-parameter logistic (5-PL) equation (SigmaPlot 13.0, Systat Software Inc., San Jose, CA, USA).

### 5. Results

#### 5.1. Characterization of LDLr variants

Expression of the LDLR variants was analysed by flow cytometry in CHO-IdIA7 transfected cells as described in Materials and Methods. Two variants were used as internal-method controls, p.(Trp87)\* (a null allele mutant) and, Ex3\_4del LDLR variant that is expressed at similar extent than wt LDLR but it is a class 3 variant with 100% impaired binding activity<sup>24</sup>. According to the obtained results,

expression of the assessed variants can be classified into two categories, those with similar activity than wt and those with lower activity than wt.. As shown in table 1, activity of p.(Asp47Asn), p.(Thr62Met), p.(Trp305Ser), p.(Leu371Pro), p.(Gly373Ala), p.(Gln378Pro), p.(Ala399Thr), p.(Thr413Met), p.(Val578Ile), p.(Ala606Ser), p.(His656Asn) and p.(Thr659Asn) LDLR variants is similar than wt. On the other hand p.(Cys46Gly), p.(Ile473Asn), p.(Met652Thr) and p.(Asp638His) showed reduced activity than wt LDLR thus can be consideres as pathogenic variants.

**Table 1. LDLR variants characterized by Flow Cytometry.**

LDLR variant	% LDLr expression	LDL uptake
wt	100 ± 5	100 ± 2
Ex3_4del	98 ± 4	10 ± 5
p.(Trp87*)	5 ± 5	5 ± 5
p.(Cys46Gly)	100 ± 3	60 ± 7
p.(Asp47Asn)	98 ± 6	99 ± 5
p.(Thr62Met)	97 ± 4	103 ± 6
p.(Trp305Ser)	N.A.	6 ± 5
p.(Leu371Pro)	N.A.	9 ± 5
p.(Gly373Ala)	N.A.	25 ± 10
p.(Gln378Pro)	101 ± 4	81 ± 4
p.(Ala399Thr)	97 ± 3	92 ± 6
p.(Thr413Met)	81 ± 7	90 ± 3

p.(Ile473Asn)	N.A.	$27 \pm 9$
p.(Val578Ile)	N.A.	$105 \pm 15$
p.(Ala606Ser)	$99 \pm 5$	$89 \pm 7$
p.(Met652Thr)	N.A.	$40 \pm 9$
p.(Asp638His)	N.A.	$15 \pm 5$
p.His656Asn)	$101 \pm 8$	$95 \pm 5$
p.(Thr659Asn)	$103 \pm 3$	$102 \pm 5$

## 5.2. Characterization of PCSK9 variants

We assessed the affinity of PCSK9 variants toward the LDLR. Binding affinities were determined by solid-phase immunoassay. As shown in table 2, p.(Arg499His), L8 (Leu23del) and L11 (Leu22\_Leu23) PCSK9 variants showed similar affinity for the LDLR than that of wild-type PCSK9.

**Table 2. EC50 values representing the binding affinity of PCSK9 variants to the LDLR determined by solid-phase immunoassay at pH 7.4.**

PCSK9 variant	EC <sub>50</sub> (mean ± S.D.)
wt	$112.2 \pm 17$
p.(Asp374Tyr)	$19.3 \pm 9.5$
p.(Arg499His)	$95 \pm 5$
p.(Cys46Gly)	$110.6 \pm 33.5$

L8 (Leu23del)	$84.9 \pm 5.9$
L11 (Leu22_Leu23)	$94.6 \pm 10.6$

## REFERENCES

1. Hopkins, P. N., Toth, P. P., Ballantyne, C. M., Rader, D. J., & National Lipid Association Expert Panel on Familial Hypercholesterolemia. Familial hypercholesterolemias: prevalence, genetics, diagnosis and screening recommendations from the National Lipid Association Expert Panel on Familial Hypercholesterolemia. *J Clin Lipidol* **5**, S9-17 (2011).
2. Talmud, P. J., Futema, M. & Humphries, S. E. The genetic architecture of the familial hyperlipidaemia syndromes: rare mutations and common variants in multiple genes. *Current Opinion in Lipidology* **25**, 274–281 (2014).
3. Brown, M. S. & Goldstein, J. L. A receptor-mediated pathway for cholesterol homeostasis. *Science* **232**, 34–47 (1986).
4. Damgaard, D. *et al.* No genetic linkage or molecular evidence for involvement of the PCSK9, ARH or CYP7A1 genes in the Familial Hypercholesterolemia phenotype in a sample of Danish families without pathogenic mutations in the LDL receptor and apoB genes. *Atherosclerosis* **177**, 415–422 (2004).
5. Graham, C. A. *et al.* Genetic screening protocol for familial hypercholesterolemia which includes splicing defects gives an improved mutation detection rate. *Atherosclerosis* **182**, 331–340 (2005).
6. Rader, D. J., Cohen, J. & Hobbs, H. H. Monogenic hypercholesterolemia: new insights in pathogenesis and treatment. *J Clin Invest* **111**, 1795–1803 (2003).
7. Fouchier, S. W., Kastelein, J. J. P. & Defesche, J. C. Update of the molecular basis of familial hypercholesterolemia in The Netherlands. *Hum Mutat* **26**, 550–556 (2005).
8. Soutar, A. K. Intracellular transport of the low-density lipoprotein receptor. *Biochem Soc Trans* **24**, 547–552 (1996).

9. Nordestgaard, B. G. *et al.* Familial hypercholesterolaemia is underdiagnosed and undertreated in the general population: guidance for clinicians to prevent coronary heart disease: consensus statement of the European Atherosclerosis Society. *Eur Heart J* **34**, 3478–3490a (2013).
10. Cenarro, A. *et al.* The p.Leu167del Mutation in APOE Gene Causes Autosomal Dominant Hypercholesterolemia by Down-regulation of LDL Receptor Expression in Hepatocytes. *J Clin Endocrinol Metab* **101**, 2113–2121 (2016).
11. Fouchier, S. W. *et al.* Mutations in STAP1 are associated with autosomal dominant hypercholesterolemia. *Circ Res* **115**, 552–555 (2014).
12. Reiner, Ž. *et al.* Lysosomal acid lipase deficiency--an under-recognized cause of dyslipidaemia and liver dysfunction. *Atherosclerosis* **235**, 21–30 (2014).
13. Rios, J., Stein, E., Shendure, J., Hobbs, H. H. & Cohen, J. C. Identification by whole-genome resequencing of gene defect responsible for severe hypercholesterolemia. *Hum Mol Genet* **19**, 4313–4318 (2010).
14. Landrum, M. J. *et al.* ClinVar: public archive of interpretations of clinically relevant variants. *Nucleic Acids Res* **44**, D862-868 (2016).
15. Etxebarria, A. *et al.* Functional characterization and classification of frequent low-density lipoprotein receptor variants. *Hum Mutat* **36**, 129–141 (2015).
16. Defesche, J. C. *et al.* Familial hypercholesterolaemia. *Nat Rev Dis Primers* **3**, 17093 (2017).
17. Alves, A. C. *et al.* Further evidence of novel APOB mutations as a cause of familial hypercholesterolaemia. *Atherosclerosis* **277**, 448–456 (2018).
18. Alves, A. C., Etxebarria, A., Soutar, A. K., Martin, C. & Bourbon, M. Novel functional APOB mutations outside LDL-binding region causing familial hypercholesterolaemia. *Hum Mol Genet* **23**, 1817–1828 (2014).
19. Abifadel, M. *et al.* Mutations in PCSK9 cause autosomal dominant hypercholesterolemia. *Nat Genet* **34**, 154–156 (2003).
20. Dron, J. S. & Hegele, R. A. Complexity of mechanisms among human proprotein convertase subtilisin-kexin type 9 variants. *Curr Opin Lipidol* **28**, 161–169 (2017).

21. Mousavi, S. A., Berge, K. E. & Leren, T. P. The unique role of proprotein convertase subtilisin/kexin 9 in cholesterol homeostasis. *J Intern Med* **266**, 507–519 (2009).
22. Cohen, J. C., Boerwinkle, E., Mosley, T. H. & Hobbs, H. H. Sequence Variations in PCSK9, Low LDL, and Protection against Coronary Heart Disease. *N Engl J Med* **354**, 1264–1272 (2006).
23. Abifadel, M. *et al.* Identification and characterization of new gain-of-function mutations in the PCSK9 gene responsible for autosomal dominant hypercholesterolemia. *Atherosclerosis* **223**, 394–400 (2012).
24. Cameron, J. *et al.* Effect of mutations in the PCSK9 gene on the cell surface LDL receptors. *Hum Mol Genet* **15**, 1551–1558 (2006).
25. Lipari, M. T. *et al.* Furin-cleaved proprotein convertase subtilisin/kexin type 9 (PCSK9) is active and modulates low density lipoprotein receptor and serum cholesterol levels. *J Biol Chem* **287**, 43482–43491 (2012).
26. Poirier, S., Mamarbachi, M., Chen, W.-T., Lee, A. S. & Mayer, G. GRP94 Regulates Circulating Cholesterol Levels through Blockade of PCSK9-Induced LDLR Degradation. *Cell Rep* **13**, 2064–2071 (2015).
27. Bottomley, M. J. *et al.* Structural and biochemical characterization of the wild type PCSK9-EGF(AB) complex and natural familial hypercholesterolemia mutants. *J Biol Chem* **284**, 1313–1323 (2009).
28. Geschwindner, S. *et al.* Characterisation of de novo mutations in the C-terminal domain of proprotein convertase subtilisin/kexin type 9. *Protein Engineering Design and Selection* **28**, 117–125 (2015).

## **ANNEX II: An atlas of O-linked glycosylation on peptide hormones reveals diverse biological roles**

**The results presented in this section have been published at:**

- An atlas of O-linked glycosylation on peptide hormones reveals diverse biological roles.Madsen TD, Hansen LH, Hintze J, Ye Z, Jebari S, Andersen DB, Joshi HJ, Ju T, Goetze JP, Martin C, Rosenkilde MM, Holst JJ, Kuhre RE, Goth CK, Vakhrushev SY, Schjoldager KT. Nat Commun. 2020 Aug 20;11(1):4033. doi: 10.1038/s41467-020-17473-1.

## 1. Introduction

In this work it is shown that O-glycans positioned within the receptor binding motifs of members of the neuropeptide Y (NPY) family modulate receptor activation properties and substantially extend peptide half-lives<sup>1</sup>. The alpha-helix is important for receptor recognition and activation, and specifically for NPY, the alpha-helix is suggested to play a crucial role in prompting a two-step receptor-binding mechanism<sup>2,3</sup>. To explore the potential structural impact of O-glycans on NPY, we measured mature NPY in solution without and with O-glycans at Thr32: NPY Tn, NPY T and NPY ST which contains one, two or three sugars, respectively.

## 2. Methods

Circular dichroism was used to analyse the effect of sugars in the structure of NPY. CD spectra of 20 µM NPY or NPY glycovariants were obtained in 15 mM sodium phosphate buffer (pH 7) at 25 °C between 200 and 260 nm at a scan rate of 50 nm/min. Each spectrum was obtained as an average of 15 accumulations corrected by subtracting the measurements in 15 mM phosphate buffer alone. Measurements were performed in a Jasco-810 spectropolarimeter equipped with Peltier temperature control, using a quartz cuvette of 0.1 cm path length. Alpha-helical content was calculated by the mean residue molar ellipticity at 222 nm as  $[(-[\theta]_{222} + 3000)/(36,000 + 3000)] \times 100^4$ .

## 3. Results

As shown in **Figure 1**, NPY present a typical spectra of alpha helix (negative bands at 208 and 222 nm). NPY showed 33% alpha-helical content in line with previous studies, whereas NPY Thr32 glycovariants with O-glycans in the alpha-helical

interface decreased the alpha-helical content to 23–26%, seen as an increase in ellipticity at 222 nm.

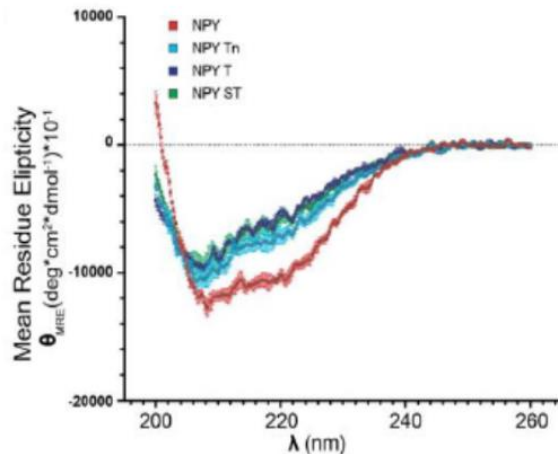


**Figure 1. CD spectroscopy of NPY or different glycovariants of NPY at 25°C pH 7 in aqueous solution.** The rise in ellipticity at 222 nm reflect disruption of the alpha-helix. Ellipticity is expressed as the mean-residue molar ellipticity. Mean +/- S.E.M. is shown (n=4 for non-glyc., T and ST; n=3 for Tn).

## REFERENCES

1. Tian, E. *et al.* Galnt11 regulates kidney function by glycosylating the endocytosis receptor megalin to modulate ligand binding. *Proc Natl Acad Sci U S A* **116**, 25196–25202 (2019).
2. Bader, R. & Zerbe, O. Are hormones from the neuropeptide Y family recognized by their receptors from the membrane-bound state? *Chembiochem* **6**, 1520–1534 (2005).
3. Sargent, D. F. & Schwyzer, R. Membrane lipid phase as catalyst for peptide-receptor interactions. *Proc Natl Acad Sci U S A* **83**, 5774–5778 (1986).
4. Horn, M. & Neundorf, I. Design of a novel cell-permeable chimeric peptide to promote wound healing. *Sci Rep* **8**, 16279 (2018).

## **ANNEX III:** Design and Validation of a Process Based on Cationic Niosomes for Gene Delivery into Novel Urine-Derived Mesenchymal Stem Cells

**The results presented in this section have been published at:**

- Design and Validation of a Process Based on Cationic Niosomes for Gene Delivery into Novel Urine-Derived Mesenchymal Stem Cells. Vado Y, Puras G, Rosique M, Martin C, Pedraz JL, **Jebari-Benslaiman S**, de Pancorbo MM, Zarate J, Perez de Nanclares G. *Pharmaceutics*. 2021 May 11;13(5):696. doi: 10.3390/pharmaceutics13050696.

#### **4. Introduction**

Mesenchymal stem cells (MSCs) are a pool of multipotent adult stem cells present in a variety of niches that can differentiate into mesoderm-derived cells, such as osteocytes or adipocytes<sup>1</sup>. Several studies have shown that MSCs can also differentiate into cells of endodermal or ectodermal origin<sup>2</sup>. In addition to in vitro differentiation into osteocytes, adipocytes, and chondrocytes, MSCs in culture can attach to plastic and grow under standard culture conditions. Moreover, these cells must present CD73, CD90, and CD105 surface antigens and lack expression of CD14, CD34, and CD45<sup>3</sup>. The isolation of urine-derived mesenchymal stem cells (hUSCs) was recently described. hUSCs present additional benefits in the fact that they can be easily obtained noninvasively. Regarding gene delivery, nonviral vectors based on cationic niosomes have been used and are more stable and have lower immunogenicity than viral vectors. However, their transfection efficiency is low and in need of improvement.

#### **5. Methods**

I participated in the characterization of the hUSC cells. hUSCs were isolated from urine and for cell characterization, cell surface markers were analyzed by flow cytometry. Briefly, 50,000 cells were grown in 24-well culture plates. For this assay, commercial mesenchymal stem cells (PCS-500-011™, ATCC, Manassas, VA, USA) were used as a positive control while HEK293 cells (ATCC) were used as a negative

control. When cell confluence was approximately 80%, cells were fixed with 200 µL paraformaldehyde (PFA; PanReac AppliChem, Barcelona, Spain) for 10 min. Once fixed, cells were scraped and centrifuged at 3000 rpm for 5 min. The supernatant was discarded, and the pellet was resuspended in 50 µL blocking solution, PBS with 5% of inactive FBS (Gibco-Thermo Fisher Scientific, Waltham, MA, USA). Cells were kept in this solution for 30 min at room temperature. Then, fluorescent antibodies were added at a final dilution of 1/100, and cells were incubated for 45 min at room temperature in the dark. The antibodies and their fluorophores are listed below, all of which were acquired from Sigma- Aldrich (Saint Louis, MO, USA):

- Surface markers specific for mesenchymal stem cells: antiCD73-AlexaFluor488, antiCD90-APC, and antiCD105-PE;
- Surface markers that are absent in mesenchymal stem cells: antiCD14-FITC, antiCD34-APC, and antiCD45-PE.

For verifying the binding specificity of the antibodies, isotype controls for each fluorophore

were also used. As the isotypes do not recognize any protein, every signal obtained from them would be due to unspecific binding. This way, background staining levels can be determined<sup>4</sup>. Once the incubation was completed, unbound antibody was removed by centrifugation of cells at 3000 rpm for 5 min, and the supernatant was discarded. The pellet was resuspended in 200 µL of PBS and the sample was introduced to a CytoFLEX (Beckman Coulter, Brea, CA, USA) flow cytometer. The results were analysed using CytExpert software (Beckman Coulter, v. 2.3.0.84, Brea, CA, USA). These cells were then used to analyse transfection efficiency of cationic niosomes.

## 6. Results

Cell populations analyzed by flow cytometry showed the surface antigen expression pattern described in **Table 1**. On the one hand, for the three markers that should be present (CD73, CD90, and CD105), cells showed high fluorescence levels. On the other hand, for those that should be absent (CD14, CD34, and CD105), there was no observable signal due to the corresponding antibodies. It must be highlighted that the antiCD45-PE antibody displayed more fluorescence than expected. Nevertheless, it did not reach the values of the positive antigens. As suspected, HEK293 cells were not positive for MSC markers. Compared to the reference values proposed by the International Society for Cellular Therapy (ISCT)<sup>3</sup>, this culture did not fulfil the hallmarks. However, this is not surprising as, in the literature, it has been demonstrated that conclusive characterization of this cell type requires more in-depth analysis. Moreover, results obtained from different groups are not concordant, and the expression levels established by the ISCT are not always obtained<sup>5</sup>. Moreover, commercial cells, which are supposed to meet quality criteria, did not reach the minimum required either, and their percentages were similar to those of hUSCs.

**Table 1. Percentage of positive cells for each cell surface marker studied by flow cytometry.**

Cell Type	CD73-AlexaFluor488	CD90-APC	CD105-PE	CD14-FITC	CD34-APC	CD45-PE
Commercial mesenchymal stem cells	63.4%	81.7%	70.1%	0.8%	1.3%	20.5%
hUSCs	78.6%	86.4%	66.1%	6.8%	13.4%	52.4%
HEK293	36.5%	0.9%	3.5%	2.8%	0.8%	11.3%

CD73, CD90, and CD105 correspond to antigens that are present specifically in mesenchymal stem cells. However, CD14, CD34, and CD45 are absent in MSCs. The different fluorophores used were FITC, APC, PE, and AlexaFluor488

## REFERENCES

1. Friedenstein, A. J. *et al.* Precursors for fibroblasts in different populations of hematopoietic cells as detected by the in vitro colony assay method. *Exp Hematol* **2**, 83–92 (1974).
2. Jeon, B.-G. *et al.* Differentiation potential of mesenchymal stem cells isolated from human dental tissues into non-mesodermal lineage. *Animal Cells and Systems* **19**, 321–331 (2015).
3. Dominici, M. *et al.* Minimal criteria for defining multipotent mesenchymal stromal cells. The International Society for Cellular Therapy position statement. *Cytotherapy* **8**, 315–317 (2006).
4. Hulspas, R., O'Gorman, M. R. G., Wood, B. L., Gratama, J. W. & Sutherland, D. R. Considerations for the control of background fluorescence in clinical flow cytometry. *Cytometry* **76B**, 355–364 (2009).
5. Bento, G. *et al.* Urine-Derived Stem Cells: Applications in Regenerative and Predictive Medicine. *Cells* **9**, 573 (2020).

## **ANNEX IV: Statin-induced type 2 diabetes mellitus by upregulation of mir-27b**

**The results presented in this section have been published at:**

- Pathophysiology of Type 2 Diabetes Mellitus. Galicia-Garcia U, Benito-Vicente A, **Jebari S**, Larrea-Sebal A, Siddiqi H, Uribe KB, Ostolaza H, Martín C. Int J Mol Sci. 2020 Aug 30;21(17):6275. doi: 10.3390/ijms21176275.
- Statin Treatment-Induced Development of Type 2 Diabetes: From Clinical Evidence to Mechanistic Insights. Galicia-Garcia U, **Jebari S**, Larrea-Sebal A, Uribe KB, Siddiqi H, Ostolaza H, Benito-Vicente A, Martín C. Int J Mol Sci. 2020 Jul 2;21(13):4725. doi: 10.3390/ijms21134725.
- miR-27b Modulates Insulin Signaling in Hepatocytes by Regulating Insulin Receptor Expression. Benito-Vicente A, Uribe KB, Rotllan N, Ramírez CM, **Jebari-Benslaiman S**, Goedeke L, Canfrán-Duque A, Galicia-García U, Saenz De Urturi D, Aspichueta P, Suárez Y, Fernández-Hernando C, Martín C. Int J Mol Sci. 2020 Nov 17;21(22):8675. doi: 10.3390/ijms21228675.
- Molecular mechanisms of lipotoxicity-induced pancreatic β-cell dysfunction. Benito-Vicente A, **Jebari-Benslaiman S**, Galicia-García U, Larrea-Sebal A, Uribe KB, Martin C. Int Rev Cell Mol Biol. 2021;359:357-402. doi: 10.1016/bs.ircmb.2021.02.013.

## 1. Type 2 Diabetes Mellitus and liver

Type 2 Diabetes Mellitus (T2DM) is one of the most common metabolic disorders worldwide and its development is primarily caused by a combination of two main factors: defective insulin secretion by pancreatic  $\beta$ -cells and the inability of insulin-sensitive tissues to respond to insulin<sup>1</sup>. Insulin release and action have to precisely meet the metabolic demand; hence, the molecular mechanisms involved in the synthesis and release of insulin, as well as the insulin response in tissues must be tightly regulated. Therefore, defects in any of the mechanisms involved can lead to a metabolic imbalance that leads to the pathogenesis of T2DM.

In the liver, insulin does not only regulate glucose production/utilization but also affects lipid metabolism more broadly. When circulating glucose levels increase and insulin is secreted by pancreatic  $\beta$ -cells, insulin binding to liver INSR induces autophosphorylation of the receptor. Consequently, insulin receptor substrates (IRSs) are recruited and phosphorylated. In turn, IRSs activate PI3K, which phosphorylates phosphatidylinositol (4,5)-bisphosphate (PIP2), generating phosphatidylinositol (3,4,5)-triphosphate (PIP3). PIP3 then activates PDK1, which phosphorylates AKT. In addition, AKT is phosphorylated by mTORC2. Once AKT is fully activated, it participates in several downstream pathways that regulate multiple metabolic processes including glycogen synthesis, gluconeogenesis, glycolysis and lipid synthesis<sup>2</sup>.

In physiological states, the combined action of glucagon and insulin allows the precise regulation of hepatic glucose output. While glucagon induces hepatic glucose production, insulin acts as a potent inhibitor of glucose production when its concentration in the blood is elevated<sup>3</sup>. The effect of insulin on hepatic glucose production is due to both direct and indirect mechanisms. However, the relative importance of each of these mechanisms remains unclear<sup>4</sup>.

In addition to inducing glycogen synthesis, insulin also inhibits hepatic glucose production by activating FOXO1, resulting in a reduction of hepatic glucose release. FOXO1 is a transcription factor that belongs to a subclass of the forkhead family of transcription factors that possess a forkhead box-type DNA binding domain. FOXO1 recognizes a specific regulatory element termed the insulin response element (IRE) on the promoters of glucose-6-phosphatase (G6Pase) and phosphoenolpyruvate carboxykinase (PEPCK) genes, both of which play important roles in maintaining glucose level in states of starvation<sup>5–7</sup>. Thus, through inhibition of FOXO1, insulin promotes glucose storage as glycogen and inhibits glucose synthesis and hepatic glucose output<sup>8</sup> (**Figure 1**).

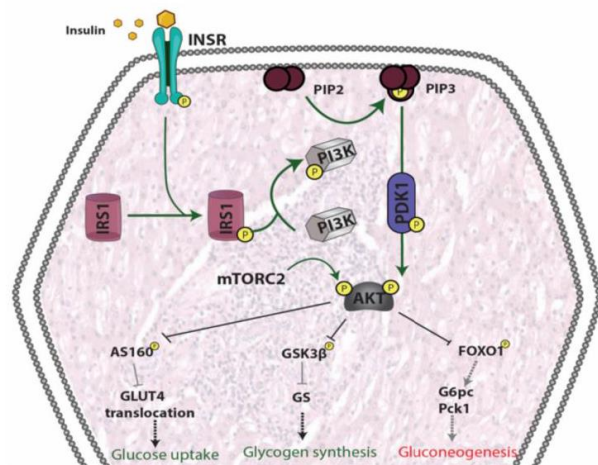


**Figure 1.** Signaling pathways involved in insulin signaling in hepatocytes. Binding of insulin to INSR induces IRSs recruitment and phosphorylation. Phosphorylated IRSs activate PI3K, generating PIP3 which activates PDK resulting in AKT phosphorylation. AKT is fully activated by further mTORC2 phosphorylation and participates in several downstream pathways that regulate multiple metabolic processes including glycogen synthesis, gluconeogenesis, glycolysis and lipid synthesis. INSR: insulin receptor; PIP2: inositol 1,3-bisphosphate; PIP3: inositol 1,4,5-trisphosphate; IRS1: insulin receptor substrate 1; PI3K: phosphoinositide 3 kinase; mTORC2: mammalian target of rapamycin complex 2; PDK1: Phosphoinositide-dependent kinase-1; AKT: protein kinase B; AS160: Akt substrate of 160 kDa; GLUT4: glucose transporter 4; GSk3 $\beta$ : Glycogen Synthase Kinase 3 Beta; GS: Glycogen synthase; FOXO1: Forkhead box protein O1; G6pc:Glucose 6 phosphate; Pck1: Phosphoenolpyruvate Carboxykinase 1.

## 2. Statin Treatment-Induced Development of Type 2 Diabetes

Statins are a guideline-directed, first line therapy for prevention of primary and secondary cardiovascular disease (CVD), which is the leading cause of mortality worldwide<sup>9,10</sup>. Although the principal mechanism of the action of statins is inhibition of 3-hydroxy-3-methyl-glutaryl coenzyme-A (HMG-CoA) reductase, statins have been implicated in several other beneficial pleiotropic effects including improving endothelial function, stabilization of atherosclerotic plaques and anti-inflammatory activities<sup>11</sup>. Despite the safety and relative tolerability of statins, observational studies<sup>12–14</sup>, clinical trials<sup>15,16</sup> and meta-analyses<sup>17–19</sup> have found that statins can increase the risk of new-onset type 2 diabetes mellitus (T2DM). These studies implicated statins in negatively impacting insulin sensitivity, decreasing secretion by pancreatic  $\beta$ -cells and increasing insulin resistance<sup>20,21</sup>. While the lipid-lowering mechanism of statins is relatively well understood, the mechanisms underlying statin-induced T2DM development seem to be multifactorial and remain unclear. Among experimental studies, multiple works have indicated that statins diminish pancreatic  $\beta$ -cell function via Ca<sup>2+</sup> signaling

pathways impairment<sup>22,23</sup>, compromise insulin signaling and down-regulate the insulin-responsive glucose transporter 4 (GLUT-4)<sup>24,25</sup>. In addition, it has also been described that statins impact on epigenetics may also contribute to statin-induced T2DM via differential expression of microRNAs<sup>26</sup>.

### 2.1. Primary Action of Statins: Cholesterol Biosynthetic Pathway

Statins are reversible and competitive inhibitors of HMG-CoA reductase, which is the rate-determining enzyme in the cholesterol biosynthetic pathway<sup>27</sup>. The HMG-like portion of statins, which is a modified 3,5-dihydroxyglutaric acid moiety, is structurally similar to HMG-CoA and causes the inhibition of HMG-CoA reduction reactions<sup>28</sup>. Through this mechanism, the mevalonate pathway is inhibited along with a consequent decrease in downstream products and cholesterol synthesis (**Figure 2A**). In addition, this statin-mediated decrease in intracellular cholesterol content leads to up-regulation of the LDL receptor (LDLR) in the liver and peripheral tissues, resulting in decreased blood LDL cholesterol (LDL-C)<sup>29</sup>. LDLR is the primary route by which LDL-C is removed from circulation, and its synthesis has been shown to be inversely correlated to the amount of cholesterol synthesized by a cell<sup>30</sup>. Through the action of statins, the cellular cholesterol concentration decreases, stimulating production of more LDLR and promoting LDL-C removal from the bloodstream, ultimately reducing CVD risk<sup>30</sup>.

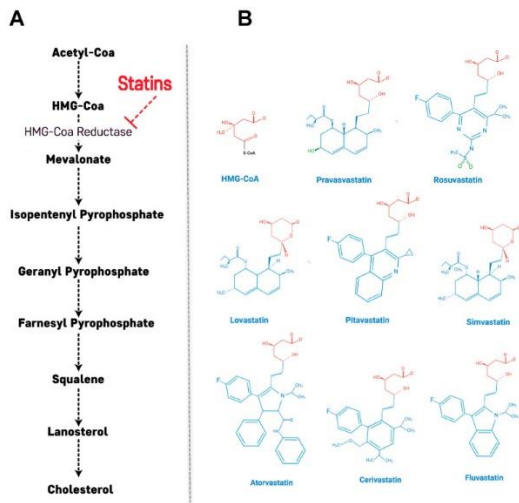


**Figure 2. Statin-induced inhibition of the mevalonate pathway and structure of statins.** (A) Inhibition of HMG-CoA reductase significantly blocks the production of mevalonate, a necessary precursor for cholesterol synthesis. Mevalonate is the building block for a variety of other compounds. (B) Structural formulas of statins and HMG-CoA. The HMG-like moiety (in red) is conserved in all statins. The polar substituents responsible of pravastatin and rosuvastatin are colored in green.

Statins are classified according to their hydrophobicity into hydrophilic statins (pravastatin and rosuvastatin) and lipophilic statins (atorvastatin, cerivastatin, fluvastatin, lovastatin, pitavastatin and simvastatin)<sup>31,32</sup>. The solubility and pharmacological properties of statins are determined by the substituents on the ring attached to the active moiety<sup>32</sup>. Hydrophilicity originates from polar substituents added to the active site while the addition of nonpolar substituents leads to lipophilicity<sup>28,32</sup> (**Figure 2B**). Although the target of both types of statins is HMG-CoA reductase, the inhibitory mechanisms are distinct. Hydrophilic statins target the liver more efficiently because their uptake is carrier-mediated, while lipophilic statins passively diffuse through the hepatocellular membrane and similarly are also able to diffuse in extrahepatic tissues, thus showing reduced hepatoselectivity<sup>32,33</sup>. Their diffuse influence on extrahepatic tissues may explain the higher incidence of adverse effects observed with lipophilic statins. The notable

exception to this is rosuvastatin, which is a hydrophilic statin but has a similar activity profile to lipophilic statins<sup>34</sup>.

## 2.2. MicroRNAs and Impact of Statin Therapy on microRNA Expression Profile

MicroRNAs (miRs) are small (22 nucleotide) noncoding regulatory RNAs, which act as post-transcriptional regulators of gene expression<sup>35,36</sup>. miRs usually silence gene expression through mRNA degradation or sequestration of the target mRNA from translation machinery<sup>37</sup>. It has been shown that miRs are involved in many biological processes including insulin expression, skeletal muscle adaptation to elevated glucose, insulin sensitivity and glucose stimulated insulin secretion (GSIS)<sup>38</sup>. It has been shown that miRs likely mediate the pleiotropic effects of statins via modulation of lipid metabolism, enhancement of endothelial function, inhibition of inflammation, improvement of plaque stability and immune regulation. More specifically, miRs appear to regulate the fine-tuning of cellular phenotypes rather than serving as molecular on-off switches<sup>39</sup>.

Statin therapy has been found to affect the expression of several miRs, which play a central role in the regulation of lipid and glucose metabolism<sup>40</sup> and that are associated with development of T2DM. Recently, the miR-27 family (miR-27a and miR-27b) has emerged as a new key regulator of cholesterol and lipid homeostasis<sup>41-43</sup>. Interestingly, the miR-27 family has been shown to be upregulated in a dose-dependent manner by simvastatin in HepG2 cells. Alvarez et al. demonstrated that miR-27a directly decreases both LDLR RNA and protein levels by binding to the 3'UTR of the *LDLR* mRNA<sup>44</sup>.

### 3. MiR-27b modulates insulin signaling in hepatocytes

With more than 1.9 billion overweight adults and 650 million obese people in 2016, obesity has become a global epidemic that has nearly tripled since 1975. Obesity is associated with increased risk for cardiovascular disease, type 2 diabetes mellitus (T2DM), hypertension and coronary heart disease. In particular, obesity-related T2DM is expected to double in prevalence to 300 million by 2025<sup>45</sup>. Although the molecular mechanisms leading to obesity-related T2DM remain unclear, common features in obese individuals with T2DM include elevation of triglycerides (TG), reduction in high-density lipoprotein (HDL)-C, increased concentration of ApoB-100, small dense low-density lipoprotein (LDL) and HDL.

Obesity leads to increased circulating lipids (cholesterol and TG) that may promote excess lipid deposition in the heart, muscle, pancreas or liver<sup>46</sup>. In the liver, the imbalance among lipid synthesis, uptake, secretion and oxidation results in deleterious lipid accumulation, which results in non-alcoholic fatty liver disease (NAFLD)<sup>47</sup>. Hepatocyte lipotoxicity can activate cell death and endoplasmic reticulum stress response pathway, thereby inducing activation of Kupffer cells and recruitment of extra-hepatic monocytes/macrophages, leading to hepatic inflammation. Eventually, liver lipid overload and increased inflammation promote liver insulin resistance (IR)<sup>48</sup>, characterized by impaired insulin signaling. Under these circumstances, insulin exerts a lower biological effect than the expected<sup>49</sup> and consequently IR constitutes one of the major factors for developing T2DM. Furthermore, IR is commonly associated with NAFLD or cardiovascular disease (CVD)<sup>49</sup>, which in turn have been associated with changes in lipid and lipoprotein metabolism that could promote both pathogenic situations<sup>50</sup>.

To date, multiple key processes underlying the molecular mechanism leading to IR, which include polymorphisms in insulin cascade-related genes, have been

identified<sup>51</sup>. However, post-transcriptional mechanisms and their role in IR pathogenesis remain less well characterized. Recently, a major focus of interest has emerged on the role of microRNAs (miRNAs) as regulators of the pathophysiology of multiple cardiometabolic pathologies, including obesity, IR, atherosclerosis and heart failure<sup>52-54</sup>. There is evidence that the coordinated action of multiple miRNAs regulates multiple pathways that may converge to promote development of IR<sup>55,56</sup>, T2DM and CVD<sup>57,58</sup>. Therefore, gaining insight into miRNA-mediated IR development may provide enormous potential in the prevention and early diagnosis of disease. Upregulation of several miRNAs has been associated with both obesity and IR, including miR-27b which has been shown to be overexpressed in the liver of obese people<sup>43,59</sup>. miR-27b controls the expression of genes regulating hepatic lipid metabolism including angiopoietin-like 3 (ANGPTL3) and glycerol-3-phosphate acyltransferase 1, mitochondrial (GPAM)<sup>43,59</sup>. While the role of miR-27b in lipid metabolism is well established, its contribution in regulating insulin signaling in hepatocytes is not known. The high expression levels of miR-27b in the liver, its role in regulation of lipid metabolism and its ~3-fold upregulation determined in liver of mice on a high-fat diet<sup>43</sup> highlight the importance of determining the impact of miR-27b on development IR through hepatic tissue. In addition, given that lipid metabolism alteration is closely related to IR, studying the role of miR-27b in hepatocytes is particularly relevant. In this study, we elucidated how miR-27 expression affects insulin signaling in the liver and its contribution to the development of hepatic insulin resistance in high lipid concentration environments. Notably, we found that miR-27b levels in human hepatoma cell, Huh7, influence the expression of numerous components of the insulin signaling pathways including the INSR and insulin receptor substrate 1 (IRS1). These results were further confirmed *in vivo* showing that overexpression and inhibition of hepatic miR-27 enhances and suppresses INSR expression in the liver, respectively. Together, this study identified a novel role for miR-27 in regulating insulin signaling and these

findings suggest that targeting of miR-27 may be a potential approach to increase insulin sensitivity in obese people in prediabetes stage.

### 3.1. MiR-27b Controls the Expression INSR and IRS1 Expression

To assess the role of miR-27b in regulating *INSR*, *AKT2*, *FOXO1* *IRS1* and *GSK3B* expression in hepatocytes, we overexpressed or inhibited miR-27 levels in Huh7 cells using miRNA mimics and inhibitors, respectively. Transfection of Huh7 cells with miR-27b mimic and inhibitor markedly increased and decreased miR-27b levels, respectively (**Figure 3A,B**). Overexpression of miR-27b reduced INSR and IRS1 mRNA levels (**Figure 3C**). Conversely, miR-27b inhibition enhanced the expression of INSR and IRS1 (**Figure 3D**), indicating a physiological role of miR-27 expression levels in regulating components of insulin signaling pathway. As expected by our previous results, ATP-binding cassette transporter ABCA1 (ABCA1) expression was suppressed and upregulated in Huh7 cells transfected with miR-27b mimics and inhibitors, respectively (**Figure 3C**). Other predicted target genes associated to insulin signaling such as AKT2, FOXO1 or GSK3 $\beta$  were not affected by miR-27b mimic or inhibitor transfection, suggesting that, in these conditions, they are not regulated by miR-27b in Huh7 cells (**Figure 3C**).

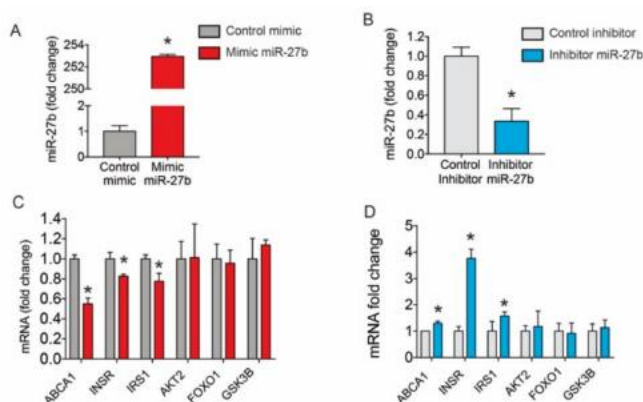


**Figure 3. miR-27b modulation affects insulin signaling in Huh7 cell line:** (A,B) miR-27b levels in Huh7 cells transfected with (A) 40 nM control mimic and mimic miR-27b or (B) 40 nM control inhibitor and inhibitor miR-27b; (C,D) mRNA expression of *ABCA1*, *INSR*, *IRS1*, *AKT2*, *FOXO1* and *GSK3 $\beta$*  in Huh7 cells transfected with (C) 40 nM control mimic and mimic miR-27b or (D) 40 nM control inhibitor and inhibitor miR-27b.

#### 4. Molecular mechanisms of lipotoxicity-induced pancreatic $\beta$ -cell dysfunction

In this book chapter different molecular mechanisms of lipotoxicity that induce pancreatic  $\beta$ -cell dysfunction were exposed. Among these mechanisms Lipid signaling pathways involved in the free fatty acid modulation of glucose-stimulated insulin secretion (GSIS) were explained, like GPR 40-mediated GSIS potentiation.

Several reports have shown the involvement of different pathways in GPR40-mediated GSIS potentiation. GPR40 is activated by mediumand long-chain FFAs (especially, eicosatrienoic acid (C20:3)) and facilitates GSIS in pancreatic  $\beta$ -cells<sup>60,61</sup> presumably to promote uptake of carbohydrate- and fat-derived-energy-rich molecules after a meal by liver and adipose tissue. Ligand binding to GPR40 activates G $\alpha$  subunit by GDP/GTP exchange and thus dissociates from the trimeric G-protein. As a result, phospholipase C (PLC) is activated, and thereby the intracellular concentration of inositol triphosphate (IP3) and diacylglycerol (DAG) increases with the consequent hydrolysis of phosphatidylinositol 4,5-bisphosphate (PIP2)<sup>60,62-64</sup>. It has been demonstrated that DAG activates protein kinase D (PKD) 1 and promotes actin depolymerization, which subsequently increases insulin secretion<sup>65</sup> (**Figure 4**). Simultaneously, the increased IP3 levels promote the release of Ca2+ from the endoplasmic reticulum (ER) and potentiate GSIS in MIN6 cells<sup>66</sup>. However, the mechanism by which ER Ca2+ release leads to GSIS potentiation remains unknown.

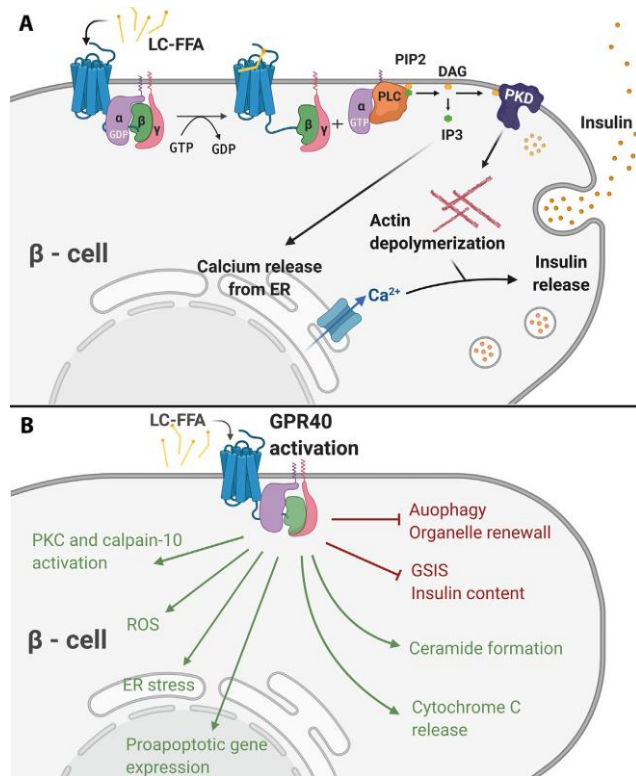


**Figure 4. Involvement of long-chain FA in GPR40-mediated insulin release in physiological and detrimental condition.** (A) Physiological conditions: ligand binding to GPR40 activates G $\alpha$  subunit and dissociates from the trimeric G-protein activating PLC. As a consequence intracellular concentration of IP3 and DAG increases with the consequent hydrolysis of PIP2. DAG activates PKD1 and promotes actin depolymerization leading to insulin secretion. Simultaneously, IP3 promotes Ca $^{2+}$  release from the ER and potentiate GSIS. (B) Detrimental conditions: long-term exposure to LC-FFA inhibits autophagy, GSIS response and insulin content. On the other hand, ceramide formation is increased, Cytochrome c release and ER stress are induced, PCK and calpain-10 are activated, ROS are produced and proapoptotic gene expression is upregulated.

## REFERENCES

1. Roden, M. & Shulman, G. I. The integrative biology of type 2 diabetes. *Nature* **576**, 51–60 (2019).
2. Titchenell, P. M., Lazar, M. A. & Birnbaum, M. J. Unraveling the Regulation of Hepatic Metabolism by Insulin. *Trends in Endocrinology & Metabolism* **28**, 497–505 (2017).
3. Cherrington, A. D., Moore, M. C., Sindelar, D. K. & Edgerton, D. S. Insulin action on the liver *in vivo*. *Biochemical Society Transactions* **35**, 1171–1174 (2007).
4. Edgerton, D. S. Insulin’s direct effects on the liver dominate the control of hepatic glucose production. *Journal of Clinical Investigation* **116**, 521–527 (2006).
5. van SCHAFTINGEN, E. & Gerin, I. The glucose-6-phosphatase system. *Biochemical Journal* **362**, 513–532 (2002).
6. Oh, K.-J., Han, H.-S., Kim, M.-J. & Koo, S.-H. CREB and FoxO1: two transcription factors for the regulation of hepatic gluconeogenesis. *BMB Reports* **46**, 567–574 (2013).
7. Montal, E. D. *et al.* PEPCK Coordinates the Regulation of Central Carbon Metabolism to Promote Cancer Cell Growth. *Molecular Cell* **60**, 571–583 (2015).
8. Leclercq, I. A., Da Silva Morais, A., Schroyen, B., Van Hul, N. & Geerts, A. Insulin resistance in hepatocytes and sinusoidal liver cells: Mechanisms and consequences. *Journal of Hepatology* **47**, 142–156 (2007).
9. Cholesterol Treatment Trialists’ (CTT) Collaborators. Efficacy and safety of cholesterol-lowering treatment: prospective meta-analysis of data from 90 056 participants in 14 randomised trials of statins. *The Lancet* **366**, 1267–1278 (2005).
10. Colhoun, H. M. *et al.* Primary prevention of cardiovascular disease with atorvastatin in type 2 diabetes in the Collaborative Atorvastatin Diabetes Study (CARDS): multicentre randomised placebo-controlled trial. *The Lancet* **364**, 685–696 (2004).
11. Mihos, C. G., Pineda, A. M. & Santana, O. Cardiovascular effects of statins, beyond lipid-lowering properties. *Pharmacological Research* **88**, 12–19 (2014).
12. Casula, M. *et al.* Statin use and risk of new-onset diabetes: A meta-analysis of observational studies. *Nutrition, Metabolism and Cardiovascular Diseases* **27**, 396–406 (2017).

13. Cederberg, H. *et al.* Increased risk of diabetes with statin treatment is associated with impaired insulin sensitivity and insulin secretion: a 6 year follow-up study of the METSIM cohort. *Diabetologia* **58**, 1109–1117 (2015).
14. Jones, M., Tett, S., Peeters, G. M. E. E., Mishra, G. D. & Dobson, A. New-Onset Diabetes After Statin Exposure in Elderly Women: The Australian Longitudinal Study on Women's Health. *Drugs Aging* **34**, 203–209 (2017).
15. Crandall JP. Correction: Statin use and risk of developing diabetes: results from the Diabetes Prevention Program. *BMJ Open Diab Res Care* **5**, bmjdrc-2017-000438corr1 (2017).
16. Ridker, P. M., Pradhan, A., MacFadyen, J. G., Libby, P. & Glynn, R. J. Cardiovascular benefits and diabetes risks of statin therapy in primary prevention: an analysis from the JUPITER trial. *The Lancet* **380**, 565–571 (2012).
17. Agarwala, A., Kulkarni, S. & Maddox, T. The Association of Statin Therapy with Incident Diabetes: Evidence, Mechanisms, and Recommendations. *Curr Cardiol Rep* **20**, 50 (2018).
18. Alberton, M., Wu, P., Druyts, E., Briel, M. & Mills, E. J. Adverse events associated with individual statin treatments for cardiovascular disease: an indirect comparison meta-analysis. *QJM: An International Journal of Medicine* **105**, 145–157 (2012).
19. Mills, E. J. *et al.* Efficacy and safety of statin treatment for cardiovascular disease: a network meta-analysis of 170 255 patients from 76 randomized trials. *QJM* **104**, 109–124 (2011).
20. Betteridge, D. J. & Carmena, R. The diabetogenic action of statins — mechanisms and clinical implications. *Nat Rev Endocrinol* **12**, 99–110 (2016).
21. Shetty, G. K., Economides, P. A., Horton, E. S., Mantzoros, C. S. & Veves, A. Circulating Adiponectin and Resistin Levels in Relation to Metabolic Factors, Inflammatory Markers, and Vascular Reactivity in Diabetic Patients and Subjects at Risk for Diabetes. *Diabetes Care* **27**, 2450–2457 (2004).
22. Kruit, J. K., Brunham, L. R., Verchere, C. B. & Hayden, M. R. HDL and LDL cholesterol significantly influence β-cell function in type 2 diabetes mellitus: *Current Opinion in Lipidology* **21**, 178–185 (2010).
23. Kruit, J. K. *et al.* Cholesterol efflux via ATP-binding cassette transporter A1 (ABCA1) and cholesterol uptake via the LDL receptor influences cholesterol-

- induced impairment of beta cell function in mice. *Diabetologia* **53**, 1110–1119 (2010).
24. Chamberlain, L. H. Inhibition of isoprenoid biosynthesis causes insulin resistance in 3T3-L1 adipocytes. *FEBS Letters* **507**, 357–361 (2001).
25. Nakata, M. *et al.* Effects of statins on the adipocyte maturation and expression of glucose transporter 4 (SLC2A4): implications in glycaemic control. *Diabetologia* **49**, 1881–1892 (2006).
26. Paseban, M., Butler, A. E. & Sahebkar, A. Mechanisms of statin-induced new-onset diabetes. *J Cell Physiol* **234**, 12551–12561 (2019).
27. Endo, A. A gift from nature: the birth of the statins. *Nat Med* **14**, 1050–1052 (2008).
28. Fong, C. W. Statins in therapy: Understanding their hydrophilicity, lipophilicity, binding to 3-hydroxy-3-methylglutaryl-CoA reductase, ability to cross the blood brain barrier and metabolic stability based on electrostatic molecular orbital studies. *European Journal of Medicinal Chemistry* **85**, 661–674 (2014).
29. Endo, A. A historical perspective on the discovery of statins. *Proc. Jpn. Acad., Ser. B* **86**, 484–493 (2010).
30. Goldstein, L. J. & Brown, S. M. The Low-Density Lipoprotein Pathway and its Relation to Atherosclerosis. *Annu. Rev. Biochem.* **46**, 897–930 (1977).
31. Mason, R. P., Walter, M. F., Day, C. A. & Jacob, R. F. Intermolecular Differences of 3-Hydroxy-3-Methylglutaryl Coenzyme A Reductase Inhibitors Contribute to Distinct Pharmacologic and Pleiotropic Actions. *The American Journal of Cardiology* **96**, 11–23 (2005).
32. Schachter, M. Chemical, pharmacokinetic and pharmacodynamic properties of statins: an update. *Fundam Clin Pharmacol* **19**, 117–125 (2005).
33. Shitara, Y. & Sugiyama, Y. Pharmacokinetic and pharmacodynamic alterations of 3-hydroxy-3-methylglutaryl coenzyme A (HMG-CoA) reductase inhibitors: Drug–drug interactions and interindividual differences in transporter and metabolic enzyme functions. *Pharmacology & Therapeutics* **112**, 71–105 (2006).
34. Davidson, M. H. Rosuvastatin: a highly efficacious statin for the treatment of dyslipidaemia. *Expert Opinion on Investigational Drugs* **11**, 125–141 (2002).

35. Bartel, D. P. MicroRNAs: target recognition and regulatory functions. *Cell* **136**, 215–233 (2009).
36. Friedman, R. C., Farh, K. K.-H., Burge, C. B. & Bartel, D. P. Most mammalian mRNAs are conserved targets of microRNAs. *Genome Res.* **19**, 92–105 (2009).
37. Filipowicz, W., Bhattacharyya, S. N. & Sonenberg, N. Mechanisms of post-transcriptional regulation by microRNAs: are the answers in sight? *Nat Rev Genet* **9**, 102–114 (2008).
38. Williams, M. D. & Mitchell, G. M. MicroRNAs in Insulin Resistance and Obesity. *Experimental Diabetes Research* **2012**, 1–8 (2012).
39. Ambros, V. MicroRNA Pathways in Flies and Worms. *Cell* **113**, 673–676 (2003).
40. Fernández-Hernando, C., Ramírez, C. M., Goedeke, L. & Suárez, Y. MicroRNAs in Metabolic Disease. *ATVB* **33**, 178–185 (2013).
41. Zhang, M. *et al.* MicroRNA-27a/b regulates cellular cholesterol efflux, influx and esterification/hydrolysis in THP-1 macrophages. *Atherosclerosis* **234**, 54–64 (2014).
42. Chen, W.-J., Yin, K., Zhao, G.-J., Fu, Y.-C. & Tang, C.-K. The magic and mystery of MicroRNA-27 in atherosclerosis. *Atherosclerosis* **222**, 314–323 (2012).
43. Vickers, K. C. *et al.* MicroRNA-27b is a regulatory hub in lipid metabolism and is altered in dyslipidemia. *Hepatology* **57**, 533–542 (2013).
44. Alvarez, M. L., Khosroheidari, M., Eddy, E. & Done, S. C. MicroRNA-27a decreases the level and efficiency of the LDL receptor and contributes to the dysregulation of cholesterol homeostasis. *Atherosclerosis* **242**, 595–604 (2015).
45. Dyson, P. A. The therapeutics of lifestyle management on obesity. *Diabetes, Obesity and Metabolism* **12**, 941–946 (2010).
46. Dirkx, E., Schwenk, R. W., Glatz, J. F. C., Luiken, J. J. F. P. & van Eys, G. J. J. M. High fat diet induced diabetic cardiomyopathy. *Prostaglandins, Leukotrienes and Essential Fatty Acids (PLEFA)* **85**, 219–225 (2011).
47. Tarantino, G. Hepatic steatosis, low-grade chronic inflammation and hormone/growth factor/adipokine imbalance. *WJG* **16**, 4773 (2010).

48. Koyama, Y. & Brenner, D. A. Liver inflammation and fibrosis. *Journal of Clinical Investigation* **127**, 55–64 (2017).
49. Ormazabal, V. *et al.* Association between insulin resistance and the development of cardiovascular disease. *Cardiovasc Diabetol* **17**, 122 (2018).
50. Grundy, S. M. Small LDL, Atherogenic Dyslipidemia, and the Metabolic Syndrome. *Circulation* **95**, 1–4 (1997).
51. Petersen, M. C. *et al.* Insulin receptor Thr1160 phosphorylation mediates lipid-induced hepatic insulin resistance. *Journal of Clinical Investigation* **126**, 4361–4371 (2016).
52. Vegter, E. L., van der Meer, P., de Windt, L. J., Pinto, Y. M. & Voors, A. A. MicroRNAs in heart failure: from biomarker to target for therapy. *Eur J Heart Fail* **18**, 457–468 (2016).
53. Fernández-Hernando, C. & Moore, K. J. MicroRNA Modulation of Cholesterol Homeostasis. *ATVB* **31**, 2378–2382 (2011).
54. Fernández-Hernando, C., Suárez, Y., Rayner, K. J. & Moore, K. J. MicroRNAs in lipid metabolism: *Current Opinion in Lipidology* **22**, 86–92 (2011).
55. Liu, H., Ren, G., Zhu, L., Liu, X. & He, X. The upregulation of miRNA-146a inhibited biological behaviors of ESCC through inhibition of IRS2. *Tumor Biol.* **37**, 4641–4647 (2016).
56. Landgraf, P. *et al.* A Mammalian microRNA Expression Atlas Based on Small RNA Library Sequencing. *Cell* **129**, 1401–1414 (2007).
57. Melkman-Zehavi, T. *et al.* miRNAs control insulin content in pancreatic β-cells via downregulation of transcriptional repressors: miRNA control insulin content in pancreatic β-cells. *The EMBO Journal* **30**, 835–845 (2011).
58. Zhou, K. *et al.* Interpreting the various associations of MiRNA polymorphisms with susceptibilities of cardiovascular diseases: Current evidence based on a systematic review and meta-analysis. *Medicine* **97**, e10712 (2018).
59. Fernández-Hernando, C. Emerging role of MicroRNAs in the regulation of lipid metabolism. *Hepatology* **57**, 432–434 (2013).
60. Itoh, Y. *et al.* Free fatty acids regulate insulin secretion from pancreatic beta cells through GPR40. *Nature* **422**, 173–176 (2003).

61. Miyauchi, S., Hirasawa, A., Ichimura, A., Hara, T. & Tsujimoto, G. New Frontiers in Gut Nutrient Sensor Research: Free Fatty Acid Sensing in the Gastrointestinal Tract. *J Pharmacol Sci* **112**, 19–24 (2010).
62. Alquier, T. *et al.* Deletion of GPR40 impairs glucose-induced insulin secretion in vivo in mice without affecting intracellular fuel metabolism in islets. *Diabetes* **58**, 2607–2615 (2009).
63. Shapiro, H., Shachar, S., Sekler, I., Hershfinkel, M. & Walker, M. D. Role of GPR40 in fatty acid action on the  $\beta$  cell line INS-1E. *Biochemical and Biophysical Research Communications* **335**, 97–104 (2005).
64. Salehi, A. *et al.* Free fatty acid receptor 1 (FFA1R/GPR40) and its involvement in fatty-acid-stimulated insulin secretion. *Cell Tissue Res* **322**, 207–215 (2005).
65. Ferdaoussi, M. *et al.* G protein-coupled receptor (GPR)40-dependent potentiation of insulin secretion in mouse islets is mediated by protein kinase D1. *Diabetologia* **55**, 2682–2692 (2012).
66. Sakuma, K. *et al.* Fasiglifam (TAK-875) has dual potentiating mechanisms via G $\alpha$ q-GPR40/FFAR1 signaling branches on glucose-dependent insulin secretion. *Pharmacol Res Perspect* **4**, e00237 (2016).